VERTICAL SIDEWALL BOUNDARY LAYERS IN COMBINED WAVES AND CURRENTS

by

ALI PARSADOUST

A thesis submitted for the degree of Doctor of Philosophy

in the University of London

Department of Civil and Environmental Engineering

University College London

September 1995

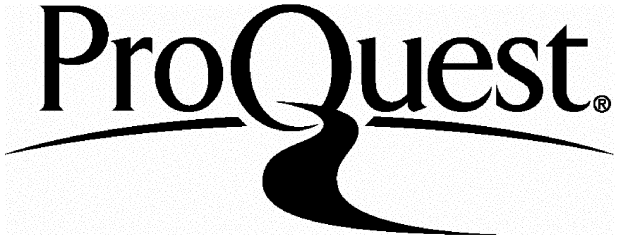

ABSTRACT

This thesis describes a theoretical and experimental investigation into the effects of flume sidewalls on wave damping in combined flows. It proposes two different theoretical models, namely the "modified Hunt formula" (for laminar flows) and the "wave attenuation equation" (for turbulent flows). Both models account for the separate contribution of bed and sidewall boundaries. They allow researchers to successfully predict wave height attenuation after the addition of following or opposing currents, in wave dominated or current dominated flows, and near smooth or rough boundaries.

To test the validity of the derived theories, experiments with parameters ranging from near deep to near shallow water waves and from wave dominated to current dominated flows were carried out. Measurements were also performed in channels with extremely low aspect ratios to isolate the rate of wave attenuation attributable to sidewalls alone. The present study is among the first to make detailed measurements (using Laser Doppler Anemometry) of orbital and steady velocity profiles near a vertical boundary for interacting waves and steady currents.

The results confirmed the theoretical approach adopted to describe the flow behaviour near a sidewall. The comparison between the predictions of the developed theories and experimental data showed the ability of the two solutions to account for both the bed and sidewall contributions to wave height attenuation. These findings are projected to provide a guide to wave damping in a wide range of flow condition and environments both in still water and combined flows.

to my parents

Mahin and Fereidoun

ACKNOWLEDGMENTS

The author above all owes a great debt to Dr. R.R. Simons for his enthuasiastic supervision and advice throughout the course of this research. The conclusion of this study would not have been possible without his sympathetic understanding of the author's outside commitments and his patient encouragement. The author is also indebted to Prof. A.J. Grass who, in the first instance, encouraged him to undertake this research and consistently provided him with generous advice and helpful ideas.

The author is particularly grateful to Steve Tidmarsh, Bill Fairman, and Keith Harvey for their dedicated technical support and good company; to Les Smith, Jack Jackson and John Ford for their valuable assistance; and to the members of the fluid group - Mehrdad Mansour Tehrani, Sandra Paskin, Achilleas Kalopedis, Ali Husseinzadeh, Wamid Saleh and Ruairi MacIver - for their constructive discussions and friendship. The author must also thank Dr. Peter Domon for his assistance; Professors K.J. Ives and J. Croll for their permission to undertake this research in the Dept. of Civil and Environmental Engineering; and the Science and Engineering Research Council for their financial support.

The enthusiastic support of many friends and family members has been a perpetual source of encouragement. Special thanks must go to Mairi Johnson. Of her many selfless contributions, proofreading this thesis was only the most obvious. Gratitude should also be extended to every one involved with Victoria and Gilan, who helped make this project financially possible and win a Royal award. But above all, the author is indebted to Mahin, Fereidoun, and Azin Parsadoust, simply the best family for which one could wish.

CONTENTS

CONTENTS

page

Lists of Figures and Tables

LIST OF FIGURES

Figure 6.12 Variation in wave attenuation with aspect ratio; T=1.0s; H=40mm, Uc=0mm/s. Modified Hunt Formula.

Figure 6.14 Variation in wave attenuation with wave period; B/D=3.3, H=40mm, Uc=0mm/s. Modified Hunt Theory ,

Figure 6.15 Variation in wave attenuation with steady current. B/D=3.3, H=40mm, T=1.0s. The vertical dotted line separates the current dominated flow.

LIST OF TABLES

NOMENCLATURE

a	Wave amplitude
a_0	Horizontal orbital amplitude
B	Channel Width
C	Phase speed of waves
C_r	Relative phase speed of waves
C_g	Group velocity of waves
C_{ga}	Absolute group velocity
C_{gr}	Relative group velocity
E	Wave energy
E_f	Energy flux
f	Friction factor
g	Gravitational acceleration
H	Wave height
H_0	Initial wave height
h	Flow depth
k	Wave number, $2\pi/L$
k_s	Equivalent sand roughness
L	Wavelength
P	Pressure
R	Reynolds number, $U_c h/\upsilon$
RE	Amplitude Reynolds number, $u_0^2 /\omega\upsilon$
S_{xx}	Radiation stress in the horizontal direction
T	Wave Period
t	Time
U	Local horizontal current velocity
U_c	Depth averaged current velocity
U^*	Current shear velocity, $\sqrt{(\tau_c/\rho)}$
u	Instantaneous horizontal orbital velocity
u_0	Amplitude of the horizontal orbital velocity just outside wave boundary

u_m	Mass transport velocity
u^*	Wave shear velocity in the horizontal direction, $\sqrt{(\tau_w/\rho)}$
V	Spanwise current velocity
v	Spanwise orbital velocity
w	Vertical component of the orbital velocity
w_0	Amplitude of the vertical orbital velocity just outside wave boundary layer
w^*	Wave shear velocity in the vertical direction, $\sqrt{(\tau_{wz}/\rho)}$
x	Streamwise distance
y	Transverse distance
z	Vertical distance
z_0	Roughness length
z_{0a}	Apparent roughness length
α	Wave attenuation coefficient
Γ	Energy dissipation
δ	boundary layer thickness
ϵ	Eddy viscosity
κ	Karman's constant
μ	Fluid viscosity
ν	Kinematic viscosity of water
β	$\sqrt{(2\omega/\nu)}$
π	3.1412
ρ	Density of water
ϕ	Velocity potential
ω	Wave frequency
σ	Ratio of shear stresses between the current and wave components of combined flows

subscripts

b	at the bed
c	current component of the combined flow
cw	combined waves and current flow
c0	current only flow
s	at the sidewall
T	Total
t	instantaneous
w	wave component of the combined flow
w0	waves only flow
x	in the horizontal direction (streamwise)
y	in the transverse direction
z	in the vertical direction

CHAPTER 1

INTRODUCTION AND LITERATURE SURVEY

1. INTRODUCTION

Knowledge of wave heights is of fundamental importance to engineers designing and maintaining coastal, offshore and sub-sea structures. The common source of this information is measurements usually taken not on site, but a considerable distance away in deep water. However, as waves propagate towards the shore they encounter changing environments that can transform their properties. Such transformations commonly occur as waves are superimposed on tidal currents, or when they travel over shallow waters and experience an irreversible reduction in height due to the frictional dissipation of energy at the bed. Wave damping and the interaction of waves and current, with their significant engineering consequences, have been the subject of a large number of studies.

Most of the research has involved flows in laboratory flumes which, unlike the prototype conditions at sea, are affected by additional solid boundaries at channel walls. A boundary layer develops at the sidewall in the same way as it does over the bed, and forms an integral part of a three dimensional flow distribution in flumes. Thus, depending on the aspect ratio of the flow, a very significant amount of damping can occur in laboratory experiments due to the influence of the sidewall. However, only a very limited number of studies aiming to identify the contribution of channel walls to the overall wave attenuation has been carried out. In addition, the overwhelming number of these studies has been concerned with wave only regimes and have ignored the interaction of waves and currents.

This project follows a continuing research programme within the fluid mechanics group

at University College London. The programme's main area of interest has been the study of wave and current interactions, with authors such as Kemp, Grass, Simons and Kyriacou accomplishing significant work in the last two decades. More recently, the problems associated with wave height attenuation have become a primary subject of research within the group. Simons, Grass and Kyriacou (1988) published a paper entitled "The influence of current on wave attenuation" which reported on their most recent findings and identified the need for further research on the effect of sidewalls on wave damping in a flume. Consequently, the present research investigated wave height attenuation in laboratory channels in both waves only and combined waves and current flows. It carried out measurements of wave damping in a variety of laboratory environments and documented in detail the steady and orbital velocity distributions near a vertical boundary. Based on this empirical work, a theoretical approach was developed to enable researchers to account for the influence of sidewalls on wave height attenuation in combined flows.

This chapter introduces the relevant background literature. A large amount of work has been done on boundary layers in combined flows. The first part of this literature survey only refers to the publications and/or studies that were considered directly during the course of this research. This is followed by a brief review of the studies published on wave height attenuation. It concludes with an outline of the limited number of papers that report on investigations into the effect of sidewalls on wave height attenuation in a flume. Chapter two of this thesis summarises the basic theories concerned with waves, currents and combined flows. It describes the existing models predicting wave height attenuation on still water and derives two different solutions - the "modified Hunt formula" and the "wave attenuation equation" - for wave damping in combined flows.

In the course of this project, detailed tests were carried out in extremely narrow channels to assess the rate of wave attenuation attributable to sidewalls alone. Laser Doppler Anemometry was used in a wider flume, in which both the sidewalls and bed induce energy losses. Quantitative measurements were made within the sidewall boundary layer and on the water surface for various interacting waves and steady currents. Chapter three describes the experimental apparatus used during this project and gives details of the Channels employed. It discusses the L.D.A. system devised and provides a description of the data analysis system including the computer hardware and software. The experimental parameters, programme and procedure are explained in Chapter four and the test results are presented in Chapter five.

Since the present study is among the first to make detailed measurements of a flow near a sidewall, Chapter six draws some conclusions with respect to vertical boundaries that are already well established for flow over a horizontal bed. It then compares the measured wave height attenuation with those predicted by the two approaches proposed in Chapter two. Finally, Chapter six projects the findings to conclude how a change in various properties of the flow will affect wave damping in combined waves and currents.

1.2 LITERATURE SURVEY

1.2.1 Boundary Layers in Combined Flows

When studying boundary layers, it is important to determine whether the flow is laminar or turbulent and at what stage the transition from one to the other occurs. Many researchers, while studying the interaction of waves and current, pay little or no attention to laminar flows. This is because steady currents in the sea are almost always turbulent as Reynolds numbers based on depth are usually very large. However, it should be noted that when steady currents are very small, wave induced flows may remain laminar over a wide range of conditions. Even where the steady component of a combined flow is not negligible but the flow is dominated by waves, laminar flow results could still provide a good first approximation in the vicinity of smooth boundaries.

In view of the above argument, in laminar regimes, attention should be restricted to wave induced flows. At very low values of the Amplitude Reynolds number, the flow near a smooth boundary is laminar throughout the cycle of the oscillation. Here the Amplitude Reynolds number is defined as $u_0 a/\upsilon$, where "a" is the orbital amplitude of the fluid. Lamb (1932) obtained the now classic shear wave solution, deriving the following first approximation for waves over a flat bed:

$$u = u_0[\cos(kx-\omega t) - e^{-\beta z}\cos(kx-\beta z-\omega t)] \qquad \text{(Eq. 1.1)}$$

where u_0 is the amplitude orbital velocity just outside the wave boundary layer and

$\beta=\sqrt{(\omega/2\upsilon)}$. The above relationship has been verified experimentally by Sleath (1968). Longuet-Higgins (1953) obtained a second approximation which considered the wave induced mean velocity. He presented the following solution for "the mass transport" in progressive waves:

$$u_{mt}=\frac{u_0 k}{4\omega}(5-8e^{\beta y}\cos\beta y+3e^{-2\beta y}) \qquad \text{(Eq.. 1.2)}$$

Isaacson (1976) derived higher order terms to overcome the discrepancy in high flow rates with test data obtained by Collins (1963).

Hino, Sawamato, and Takasu (1976) carried out tests to investigate the transition from laminar to turbulent flow. They observed that as the periodic velocity increases in a laminar flow, a short burst of turbulence occurs during the decelerating phase of the flow cycle, while the flow remains laminar at other phases of the cycle. At higher Reynolds numbers, the length of time for which the flow is turbulent increases. The first signs of instability occurring at $Re=1.6x10^4$. However, significant changes took place at $Re = 1.6 \times 10^5$. Hino et al. found that even at values of Re as high as 1.7×10^6 the flow still remained laminar for a considerable part of the oscillation cycle, but they did not establish any limits for fully developed turbulence over a smooth boundary. Tanaka and Shuto (1984) carried out tests in a wind tunnel to study the transition for combined flows. Their experimental results were in general agreement with Hino et al.(1976) showing a similar disappearance of turbulent fluctuation during the accelerating phase of the flow cycle.

However, as mentioned earlier, in the sea or river environment combined waves and current flows are almost always turbulent. A complication with turbulent combined flows is that the turbulence generated by either flow component will affect the velocity distribution of the other. Thus, the assumption made by Lighthill (1954) for laminar coexistent flows, which suggested that the combined flow is the arithmetic sum of the two independent components of the velocity, does not remain valid. It is also important to note that the relative strengths of the wave and steady current change with the distance from the solid boundary. It is usually assumed that the waves are dominant in the region close to the wall and the steady current dominates further out.

If the non-linear terms other than the Reynolds stress are neglected, the governing linearised equation of motion for turbulent boundary layer over a horizontal bed reduces to:

$$\frac{\partial u}{\partial t} = -\frac{1}{\rho}\frac{\partial P}{\partial x} + \frac{1}{\rho}\frac{\partial \tau}{\partial z} \qquad \text{(Eq..1.3)}$$

Equation 1.3 cannot be solved without further assumptions. This has lead researchers to adopt a number of different approaches to the problem.. The method favoured by many authors involves the use of an eddy viscosity. Sleath (1984) published a survey of the models presented for turbulent oscillatory flows, while a similar though more extensive list is provided by Kyriacou (1988). Grant and Madsen (1986) and Sleath (1990) both published comprehensive reviews of eddy viscosity models encompassing wave only and combined wave and current flows.

Any review of eddy viscosity models will reveal differences in their assumptions and

definitions of eddy viscosity, boundary layer thickness and shear stress. A comparison between the models presented by Grant and Madsen (1979), Christoffersen and Jonsson (1985), and Myrhaug (1989) reveals the extent of disagreement between them on the definition of boundary layer thickness and shear stress. For instance, Christoffersen and Jonsson's definition of boundary layer thickness is 5.4 times smaller than Grant and Madsen's and 2.7 times smaller than that of Myrhaug.

There is also a more general criticism of eddy viscosity models. While these, by and large, simple models can be calibrated to produce good results when sufficient data exist and under limited conditions, they cannot be easily applied to complicated problems faced in sea and river environments. The dynamics of boundary layers in offshore, coastal and river waters are extremely complex because of the coexistence of many competing mechanisms in turbulent flows, such as wave current interaction, non-linearity, and the presence of intricate structures or bed forms. Hence, some researchers argue that any model that attempts to provide a physical insight and to solve practical engineering problems cannot be simple.

Many alternative approaches to semi-empirical eddy viscosity models have been proposed. Some researchers, for example Asano, Nakagawa, and Iwagaki (1986), have taken a purely experimental approach to describe the distribution of velocity near a solid boundary. Others, such as Davies, Soulsby, and King (1988) have used the K-ϵ method which has been widely employed in steady flow, for combined waves and currents. These models do not assume the eddy viscosity to be independent of time. Instead of employing arbitrary assumptions, they obtain a shear stress and velocity gradient from the turbulent

energy equation. Other authors such as Thomas (1981, 1990) prefer to use increasingly powerful computers to solve the Navier Stokes equation and simulate turbulent boundary layers. A good reference for various available exact solutions is a review paper published by Wang (1991). Second order closure models are another approach favoured by some researchers. Sheng (1986) succeeded in deriving a model to solve a complete hierarchy of turbulent boundary layers. However, even the simplest of these models, such as Brink-Kjær and Jonsson (1976) are cumbersome to work with.

The nature of engineering practice is as such that many of the eddy viscosity models, in some instances in combination with other approximations, should prove acceptable for most engineers. One such model was derived by Myrhaug and Slaattelid (1990), and gives wave-current friction coefficients and the phase lead of the bottom shear stress over the free stream oscillatory velocity for smooth, rough and transition turbulent flows. Diagrams illustrate the variation of friction factors and the phase lead with Reynolds number. In the case of the smooth boundary, these show the phase lead and the friction coefficient at the bed for combined wave and current motion to increase with decreasing Re. They also show that increasing the ratio of steady current velocity over maximum orbital velocity leads to increasing friction factor while decreasing the phase lead. By disregarding the phase lead, Myrhaug and Slaatelid derived a simpler approximation for the friction coefficient, and concluded that all flow conditions that are not smooth turbulent should be considered rough turbulent.

The above model takes its basic definition from Christoffersen (1982) using the same eddy viscosity model inside the wave boundary layer for both current and waves. Some writers,

including Coffey and Nielsen (1986), argue against this assumption, and find it is necessary to investigate differences between the current eddy viscosity ϵ_c and the wave eddy viscosity ϵ_w. You, Wilkinson, and Nielson (1991) used the Navier-Stokes equation to derive ϵ_c and ϵ_w in the combined flow and demonstrate the differences between the two eddy viscosity coefficients. Their derivation shows that for the current component, the eddy viscosity is time invariant, while for waves it may be time variant. It also shows a change in dominant factors influencing the current and wave eddy viscosities with distance from the solid boundary. Thus, You et al suggest a three layer distribution for current eddy viscosity, while proposing a two layer distribution for wave eddy viscosity. They employed their eddy viscosity assumptions to develop a model to predict velocity profiles in the combined wave and current flows near a fixed bed. The predictions of their model proved to be in good agreement with experimental data from Jonsson and Carlsen (1976), Van Doorn (1981, 1982) and Jensen (1989). This provides more weight for the time invariant wave eddy viscosity assumption.

Soulsby et al.(1993) reviewed the state-of-the-art in semi empirical approaches to wave-current interaction, and found considerable variations between the models' output. While they concluded that the general forms of the models' predictions of mean and maximum shear stress were broadly similar, they found discrepancies of up to 30% in predicting the maximum shear stress and up to a factor of 4 in mean shear stress between the models.

1.2.2 Wave Height Attenuation

The energy dissipation in the boundary layers leads to wave height attenuation. By equating the mean energy dissipation at the bed with the rate of energy flux derived from first order wave theory, Biesel (1949) obtained a first approximation for wave height attenuation coefficient due to the energy dissipation at the bed:

$$\alpha_b = \frac{k^2}{\beta(2kh + \sinh 2kh)} \qquad \text{(Eq.. 1.4)}$$

Biesel's doubt about his own solution encouraged Carry (1956) to obtain an expression which took account of the energy dissipation in the body of the fluid and the change in wave length and wave height as waves advance towards the coast. Ignoring third order terms in k/β, where $k=2\pi/L$ and $\beta=\sqrt{(\omega/2\nu)}$, Carry derived the following expression for wave height attenuation coefficient:

$$\alpha = \frac{k^2}{\beta(2kh + \sinh 2kh)}\left[1 + \frac{2k}{\beta}\left(\sinh 2kh + \frac{8kh + 6\sinh 2kh + \sinh 4kh}{4(2kh + \sinh 2kh)^2}\right)\right]$$

(Eq.. 1.5)

Since k/β is in most situations of practical importance less than 10^{-3}, the contribution to wave height attenuation from the body of the fluid is very small except for very large depths. For laboratory tests, the contribution of the energy dissipation in the body of the fluid to wave height attenuation would be negligible.

A limited number of studies has been carried out to evaluate the wave height attenuation in combined flow (a review was published by Kyriacou - 1988). Sarpkaya (1955) was one of the first researchers to study wave height stability in combined flows. He suggested that when separate current and waves are combined, the resultant flow would acquire a completely different energy balance. He argued that waves can only remain stable if the energy dissipated by them is balanced by the energy added by the steady current, and that any surplus energy is used either to amplify or attenuate the waves. Sarpkaya concluded that for any given flow there is only one stable wave.

Jonsson (1966) attempted to determine the wave-current friction factor from wave height attenuation and/or the rate of change of water level. However, his derivations were based on the assumption of the linear superposition of the periodic and steady components of the velocity, which is only true in the absence of turbulence. To simplify his calculations, Jonsson also assumed a steady uniform current profile and a time invariant friction factor. Sleath (1984) compared the friction factor obtained from the model and the experimental data of Inman and Bowen (1963), Brevic and Aas (1980) and Brevic (1981). His results showed good agreement while the effect of current was very small but very large discrepancies when combined flows included stronger steady current.

Brevik and Aas (1980) and Brevik (1981) extending Jonsson's work, adopted a frame of reference moving with the current. They employed a relative angular frequency in the calculations to overcome the restriction of a weak wave-current system. Brevic noted that the agreement was still not very good, especially for the tests with longer wave periods. He argued that the discrepancy was due to experimental errors and to the

sidewall correction.

Kamphuis (1975) carried out an extensive study (though limited to waves on still water) of wave height attenuation in an oscillating flow water tunnel. An important conclusion of his work was that small imperfections in an otherwise smooth bed lead to non-laminar flow with higher wave height attenuation.

Kyriacou (1988) performed a theoretical and experimental study to investigate the rate of wave-height attenuation of gravity waves superimposed on a following unidirectional turbulent current over both hydraulically smooth and rough beds. He measured the surface profile along the length of the channel to obtain the wave attenuation coefficient on the basis of an exponential decay, and employed a laser Doppler anemometer to record profiles of the mean and periodic component of velocity at one central section of the channel. Kyriacou's measurements agreed with those of Brevic and Aas (1980) and Kemp and Simons (1982) in showing a reduction of wave attenuation - by as much as 70% for deeper waves and 20% for intermediate depth waves - for waves propagating over a following current. He also showed that the effect of wave-current interactions on bed shear stress is greatest when the steady current is of the same magnitude as the periodic motion. Kyriacou presented time averaged equations for the conservation of momentum and conservation of energy, and a wave energy equation to predict the wave height attenuation in combined flow. Due to difficulty in measuring the water level slope he was unable to employ the conservation of momentum or energy equations to predict the attenuation coefficient. However his Wave Energy equation suggested the same trend for wave damping with superimposed current as that observed in the laboratory tests.

Kyriacou concluded that wave attenuation in large scale combined wave-current flows can be predicted by his wave energy equation together with the eddy viscosity model proposed by Christoffersen and Jonsson (1985).

1.2.3 Waves Attenuation due to the Sidewall Boundary Layer

The present project concentrates on the sidewall's contribution to the overall wave attenuation in a laboratory flume. In the last 40 years, very few papers addressed this subject. Most of the research has been concerned with waves in still water and has relied on the first order solution of small amplitude theory to suggest approximations for predicting the sidewall effects.

Hunt (1952) proposed an amendment to Biesel's (1949) expression to take account of the wave attenuation due to sidewalls in a laboratory channel. He assumed a two dimensional laminar wave regime and employed small amplitude theory to estimate the attenuation coefficient. His approach was based on equating the rate of dissipation of energy at the bed and sidewalls inside a control volume with the energy transmitted across that volume. The derivation of Hunt's formula is detailed in the next chapter, but the following expression was proposed by him for wave height attenuation in a finite width laboratory flume:

$$\alpha = \frac{2k}{b}\sqrt{\frac{\nu}{2\sigma}\left(\frac{kb + \sinh 2kh}{2kh + \sinh 2kh}\right)} \qquad \text{(Eq.. 1.6)}$$

This expression reduces to the principal term given by Biesel when the width of the

channel becomes very large. Later tests showed that although Hunt's derivation tends to underestimate wave damping, it does provide a good first approximation.

Treloar and Brebner (1970) tested Hunt's formulation by directly measuring the sidewall and bottom rates of energy dissipation in laminar wave only boundary layers. They measured wave height attenuation in two identical flumes of different widths and used their results to separate the bed and sidewall energy losses. Further, they employed these separated energy losses to modify Hunt's expression. They based their approach on the notion that the spatial rate of change of average wave power per unit area is equivalent to the sum of the time-average rates of energy dissipation per unit plan area on the bed and sidewalls. They suggested that by employing two flumes which are identical except for their width, it is possible to create two simultaneous equations that can be solved for the rate of energy losses at the bed and sidewalls separately. Treloar and Brebner then used a dimensional analysis of energy dissipation to solve the equations. They carried out a total of nine tests with varying wave periods and water depths and obtained empirical correction factors to make the following amendment to the Hunt's formula:

$$\alpha = \frac{2k}{b}\sqrt{\frac{\nu}{2\sigma}\left(\frac{Akb + B\sinh 2kh}{2kh + \sinh 2kh}\right)}$$

For energy losses at the bed they suggested a factor A of 1.45 ± 0.15, and for sidewalls a factor B of 0.94 ± 0.09.

Fredsoe (1984) published a theoretical paper to investigate the turbulent boundary layer

which develops along both rough and smooth vertical plates placed in deep water waves. The intention was to estimate drift and damping forces on moored ships and flow resistance to ship motions. The potential flow outside the boundary layer along a vertical plate has a circular orbit for deep water waves and an elliptical orbit in case of shallow water waves. While the latter case is more general, Fredsoe chose the circular orbit for study because of its simplicity. The elliptic orbit involves unsteadiness in both boundary layer thickness and the shear stress direction, whereas in circular orbits, only the shear stress changes its direction and the boundary layer thickness remains constant. Fredsoe presented a table of results and a graphical comparison between the friction factor and boundary layer thickness for the two and three dimensional case. He concluded that the boundary layer thickness decreases by nearly a factor two compared with the two dimensional wave boundary layer while the friction factor is slightly increased. In the case of combined wave and current flow, Fredsoe derived the mean value of the shear stress on a vertical wall and concluded that shear stress is greater on the vertical part than on the horizontal part and the mean friction on a vertical plate is 30-40% higher compared to mean friction on a horizontal plate.

Kyriacou (1988) attempted to evaluate the effect of sidewall boundary layers in his study of wave attenuation in combined flows. Adopting the laminar theory presented by Hunt (1952) for sidewall correction, Kyriacou performed a series of tests in order to check the correction term. The tests were carried out in very narrow channels (of 10 and 20 mm width) to achieve very low aspect ratios and thus maximise the effect of the sidewalls on wave attenuation. A 300 mm water depth and 1.0 second and 0.7 second waves were employed for the tests. Kyriacou concluded that the sidewall boundary layer is a

significant energy sink in laboratory tests at small aspect ratios. He suggested that in the case of waves propagating in still water, although Hunt's formula tends to underpredict the laboratory measured attenuation coefficient, it can be used to predict the sidewall dissipation to within 15%. However, he also found that Hunt's formula can produce a discrepancy of as much as 30% in the case of deeper water waves. In the case of combined wave and current flow, Kyriacou carried out additional measurements of velocity profile away from the sidewalls using a propeller meter. The transverse velocity measurements near the sidewalls revealed a significant increase in the combined wave-current velocities over that of the current only and a reduction of sidewall boundary layer thickness (up to 35% in the upper region, thus confirming the smooth bed results of Kemp and Simons (1983). Kyriacou suggested that a redistribution of transverse velocity occurs leading to velocity reduction in other regions of the channel to counter this near wall velocity increase. His experimental results suggest that wave attenuation due to sidewall dissipation in combined wave and current flows reduces from that in wave only regimes in a similar way to bed induced attenuation.

CHAPTER 2

THEORY

BASIC CURRENT AND WAVE THEORY

The aim of sections 2.1 to 2.3 of this chapter is to summarise the basic theories concerned with waves only, current only, and combined waves and current flows. The formulae mainly follow those presented in the Shore Protection Manual (1984), Sleath (1984), Christoffersen and Jonsson (1985), and Myrhaug and Slaattelid (1990). Only those results that are directly employed in the theoretical development of this thesis are presented here.

2.1. Steady Currents Over a Solid Boundary

2.1.1. Laminar Flow

When a steady current flows over a stationary solid boundary, the fluid in immediate contact with the boundary is stationary. The fluid velocity gradually increases away from the boundary until it reaches the value U_m at a distance not affected by the solid boundary. The region in which the current velocity grows from zero to U_m is called the boundary layer. If a boundary layer fills the whole depth of the flow, the flow is known as "fully developed", and results in a velocity profile that remains constant with downstream distance, provided that conditions are unchanged.

It is useful to identify Reynolds numbers below which the flow remains laminar, and above which small disturbances to the laminar flow are turned into turbulence. By referring to other researchers, Sleath (1990) provided the following limits for laminar and turbulent flows:

R < 890 Flow is laminar
R > 5000 Flow is turbulent

(Eq. 2.1)

Here the Reynolds number is defined as

$$R = U_c \frac{h}{\nu} \qquad \text{(Eq. 2.2)}$$

where U_c is the mean current velocity integrated over a vertical plane, and υ is the kinematic viscosity of water. It is clear from the equation 2.2 that laminar flow will only occur for extremely weak currents. The relationship between the shear stress and the mean velocity is given by:

$$\tau = \mu \frac{\partial U}{\partial z} \qquad \text{(Eq. 2.3)}$$

while the shear velocity is defined as:

$$U_c^* = \sqrt{\frac{\tau_0}{\rho}} \qquad \text{(Eq. 2.4)}$$

2.1.2. Turbulent Flow

There have been many attempts to obtain analytical expressions for the velocity distribution in turbulent flows. A principal difficulty is to obtain a relationship between the shear stress and the mean velocity. One approach is to assume this relationship remains the same as laminar flow except that kinematic viscosity υ is replaced by an eddy viscosity ϵ. It is convenient to divide the flow within a boundary layer into three regions: the viscous sublayer or inner layer, the logarithmic layer or overlap layer, and the outer layer.

For smooth boundaries the inner layer is sometimes referred to as the laminar sublayer since in the immediate vicinity of the boundary, turbulent eddies are inhibited by the presence of the solid boundary. As viscous stresses dominate the motion in this layer equation 2.4. still applies. The thickness of the viscous sublayer is usually taken to be:

$$\delta = 11.6\frac{\nu}{U^*} \qquad \text{(Eq. 2.5)}$$

For the overlap layer the relationship between the shear stress and mean velocity is:

$$\frac{U}{U^*} = \frac{1}{\kappa}\ln\left(\frac{z}{z_0}\right) \qquad \text{(Eq. 2.6)}$$

where κ is normally taken as 0.4, and z_0 is the boundary roughness constant which must be determined experimentally. The magnitude of z_0 is related to the size of the equivalent sand roughness of the boundary, k_s, compared with the thickness δ of the inner layer. According to Sleath (1984):

$$z_0 = \frac{k_s}{30}\left[1 - \exp\left(-\frac{k_s U^*}{27\nu}\right)\right] + \frac{\nu}{9U^*} \qquad \text{(Eq. 2.7)}$$

For hydraulically smooth boundaries, where $U^*k_s/\upsilon < 5$, the second term of equation 2.8 dominates its right hand side. For hydraulically rough boundaries, however, where $U^* k_s/\upsilon > 70$, z_0 is approximately given by $k_s/30$.

As we shall see later, it is also necessary to define a pure current friction factor in the following way:

$$\tau_{c0} = \frac{1}{2} f_{co}\ \rho U_c^2 \qquad \text{(Eq. 2.8)}$$

2.2. Basic Wave Theory

Because of their apparent random behaviour, non linearity, and three-dimensional characteristics, actual water waves are rather difficult to describe mathematically. As exact numerical solutions of the governing equations require significant computing resources, most of the available solutions are based on approximations and are valid only over a limited range of conditions. Dean (1970) and Le Mehaute (1976) produce a figure suggesting the limits of validity of various wave theories. The figure was updated by Sleath (1984) to take account of the work by Cokelet (1977). According to Sleath's plot, the waves employed for the present study are best described by Stokes 2nd order theory. However there are many references to and applications of first order small amplitude theory throughout this study. The following section will accordingly discuss both first and second order small amplitude theories.

2.2.1. Definitions and Assumptions

Developed originally by Airy, this is the most elementary wave theory. The Airy theory is a first mathematical approximation of a complete theoretical description of wave behaviour. Higher orders of approximation are usually called "Stokes waves". They attempt to obtain a better description of waves using successive terms in a series expansion, where each additional term to the series is a correction to the preceding terms. Among many authors who presented the derivation of the linear wave theory in detail is Lamb(1932). "The Shore Protection Manual" (US army Corps of Engineers) provides a guide to this and various other wave theories.

Any description of a wave should include both its surface form and the fluid motion. Small amplitude wave theory describes a simple sinusoidal periodic wave by its length, height and period for a particular water depth. The wave length (L) is defined as the horizontal distance between corresponding points on two successive waves, wave height (H) as the vertical distance between a crest and a trough, period (T) as the time it takes a wave to pass a given point, and depth (h) as the distance between the bed and the still water level.

Several assumptions are commonly made in developing Small Amplitude theory:

A. The bed is horizontal, fixed and impermeable ,

B. The fluid is incompressible and homogeneous.

C. The flow is irrotational and viscous effects are neglected.

D. The flow is two dimensional .

E. The wave height is small compared with both the water depth and the wavelength.

F. The wave does not interact with any other water motion.

G. Surface tension is neglected.

H. Coriolis effects are neglected.

I. Surface pressure is uniform and constant.

2.2.2. The First Order Solution

Here only those results that are directly employed in the theoretical developments of this thesis are presented. Small amplitude wave theory is developed by the introduction of a velocity potential ϕ which satisfies both the irrotationality and the incompressibility

assumptions. The first order solution that satisfies the boundary conditions is

$$\phi = \frac{H}{2}\frac{gT}{2\pi}\frac{\cosh(kz)}{\cosh(kh)}.\sin(kx-\omega t) \qquad \text{(Eq. 2.9)}$$

where z is the height above the bed, ω is the wave frequency, defined as $2\pi/T$, and k is the wave number, $2\pi/L$. The horizontal and vertical wave velocity components are respectively given as:

$$u = \frac{\partial \phi}{\partial x} = \frac{H}{2}\frac{gT}{L}\frac{\cosh(kz)}{\cosh(kh)}\cos(kx-\omega t) \qquad \text{(Eq. 2.10)}$$

$$w = \frac{\partial \phi}{\partial z} = \frac{H}{2}\frac{gT}{L}\frac{\sinh(kz)}{\cosh(kh)}\sin(kx-\omega t) \qquad \text{(Eq. 2.11)}$$

Wave celerity is the speed at which a waveform propagates and can be calculated from the following relationships:

$$C = \frac{L}{T} = \sqrt{\frac{gL}{2\pi}\tanh(kh)} = \frac{gT}{2\pi}\tanh(kh) \qquad \text{(Eq. 2.12)}$$

An expression for the wavelength as a function of depth and wave period can be obtained from the above equations:

$$L = \frac{gT^2}{2\pi}\tanh(kh) \qquad \text{(Eq. 2.13)}$$

The solution of this expression can only be achieved by iteration or use of special tables since the unknown wavelength appears on both sides of the equation. The free surface profile is described by:

$$\eta = \frac{H}{2}\cos(kx - \omega t) \qquad \text{(Eq. 2.14)}$$

The mean wave energy per unit area is given as:

$$E = \frac{\rho g H^2}{8} \qquad \text{(Eq. 2.15)}$$

The group velocity which is also the speed at which the wave energy is carried along can be obtained from

$$C_g = \frac{C}{2}\left(1 + \frac{2kh}{\sinh(2kh)}\right) \qquad \text{(Eq. 2.16)}$$

2.2.4. The Second Order Solution

Although the linear solution produces a first approximation of wave characteristics, it can be improved considerably by including higher order terms. In addition, the higher order solutions can explain phenomena such as mass transport that cannot be described by the linear theory. In general, linear theory is best applied to a wave that is symmetrical about the still water level and has water particles that move in closed orbits. The second order solution, however, predicts a waveform that is asymmetrical about the still water level but

symmetrical about a vertical line through the crest and has water particle orbits that are open.

The second order solution for the velocity potential is quoted by Sleath (1984) as

$$\phi = \frac{H}{2}\frac{gT}{2\pi}\frac{\cosh(kz)}{\cosh(kh)}\sin(kx-\omega t) - \frac{3H^2\omega\cosh(kz)\sin 2(\omega t-kx)}{32\sinh^4(kh)}$$

(Eq . 2 .17)

The expressions for wave celerity and wavelength in the second order theory are identical to those obtained from the linear theory. The second order solutions for the horizontal and vertical components of orbital velocity are:

$$u = \frac{H}{2}\frac{gT}{L}\frac{\cosh(kz)}{\cosh(kh)}\cos(kx-\omega t) + \frac{3}{4}\left(\frac{\pi H}{L}\right)^2 C\frac{\cosh(2kz)}{\sinh^4(kh)}\cos(2kx-2\omega t)$$

(Eq. 2 .18)

and

$$w = \frac{H}{2}\frac{gT}{L}\frac{\sinh(kz)}{\cosh(kh)}\sin(kx-\omega t) + \frac{3}{4}\left(\frac{\pi H}{L}\right)^2 C\frac{\sinh(2kz)}{\sinh^4(kh)}\sin(2kx-2\omega t)$$

(Eq. 2 . 19)

where C is the wave celerity given by equation 2.12.

It can be shown that during each wave cycle a particle in the flow is displaced irrespective of its periodic movement. The distance a particle is displaced during one wave period when divided by the wave period gives a mean drift velocity u_m, called the mass transport velocity.

$$u_m = \frac{gH^2}{8hC_r} \qquad \text{(Eq. 2.20)}$$

where $C_r = L / T$.

It will also be necessary for the later section of this chapter to define a friction factor for pure waves:

$$\tau_{wo} = \frac{1}{2} f_{wo} \rho u_0^2 \qquad \text{(Eq. 2.21)}$$

2.3. Combined Waves And Currents

For laminar flow, Lighthill (1954) concluded that a reasonable approximation to the velocity distribution in combined waves and currents is provided by the assumption that the periodic and steady components of the flow are unaffected by each other. Unless the steady current is extremely weak, however, almost always a combined flow is turbulent. In a turbulent combined flow there is an interaction between the steady and oscillatory components, with the turbulence generated by one affecting the velocity distribution of the other.

Many researchers (see Chapter 1) have suggested basic formulae to predict the behaviour of a turbulent combined flow. It was decided that the formulae proposed by Christoffersen and Jonsson (1985), and later used in a different form by Myrhaug and Slaattelid (1990), are most suited for the purposes of this study. This was done due both to the simplicity of their approach and the fact that so many researchers today refer to their work.

The relationship between velocity distribution and shear stress in a combined flow is given below. In the following expression the streamwise and transverse vectors are separated by the ",".

$$\tau_{bcw}=\frac{1}{2}\rho f_{bcw}|u_0|^2[(\sigma\cos\chi+\cos(\theta+\phi_b)),\sigma\sin\chi] \qquad \text{(Eq. 2.22)}$$

where f_{bcw} is a bed friction factor for combined flows, χ is the angle between the current and wave propagation, θ is the phase function ($kx-\omega_a t$), ϕ_b is the phase lead of the shear stress over the wave induced velocity, and σ is the ratio of shear stresses between the current and wave components of combined flows,

$$\sigma=\frac{f_{bc}}{f_{bcw}}\left(\frac{U_c}{u_0}\right)^2 \qquad \text{(Eq. 2.23)}$$

f_{bc} is the bed friction factor of the current component of the combined flow, and f_{bcw} is the bed friction factor for the waves in combined flows. It follows from the above relationships that the magnitude of the maximum bed shear stress is given by:

$$\tau_{bcw}=\frac{1}{2}\rho f_{bcw} m |u_0|^2 \qquad \text{(Eq. 2.24)}$$

where

$$m=\sqrt{1+2\sigma\cos\chi+\sigma^2} \qquad \text{(Eq. 2.25)}$$

Myrhaug and Slaattelid(1990) derived a combined waves and currents friction factor for rough and smooth boundaries. According to their derivation, the combined friction factor is defined:

for smooth boundaries as

$$\frac{\kappa^2}{f_{cw}/2m}=[\ln(4.5\ c\ Re\ m\ f_{cw})]^2+b^2 \qquad \text{(Eq. 2.2}$$

and for rough boundaries as

$$\frac{\kappa^2}{f_{cw}/2m}=[\ln(30c\frac{|u_0|}{\omega_a k_b}\sqrt{\frac{m f_{cw}}{2}})]^2+b^2 \qquad \text{(Eq. 2.27)}$$

where f_{cw} is the wave friction factor in the combined flow, b and c are constants, and

$$Re=\frac{|u_0|^2}{\omega_a \nu} \qquad \text{(Eq. 2.28)}$$

For both waves only motion and the combined flow, the suggested values for b and c are 1.28 and 0.30 respectively. Equations 2.26. and 2.27. are implicit equations for the determination of f_{cw} and can be solved by iteration. However, as can be seen from

equation 2.23 which considers the bed boundary (thus subscript "b") the friction factor associated with the current in a combined flow, f_c , is also required to solve the problem. The value of f_c can be obtained from the following expression provided by Myrhaug and Slaattelid (1990):

$$\sqrt{\frac{2}{f_c}} = \sqrt{\frac{2}{f_{c0}}} - \frac{1}{\kappa}\ln\left(\frac{z_{0a}}{z_0}\right) \qquad \text{(Eq.2.29)}$$

where f_{c0} is the friction factor associated with the pure current flow, and z_{0a} is the apparent boundary roughness. These two values are computed from the following relationships respectively (Myrhaug and Slaattelid -1990):

$$\sqrt{\frac{2}{f_{c0}}} = \frac{1}{\kappa}\ln\left(\frac{h}{ez_0}\right) \qquad \text{(Eq. 2.30)}$$

and

$$z_{0a} = z_0\left(\frac{\delta_w}{z_0}\right)^{\left(1-\sqrt{\frac{\sigma}{m}}\right)} \qquad \text{(Eq. 2.31)}$$

where δ_w is the thickness of the wave boundary layer given by

$$\delta_w = c\frac{u^*_{cwm}}{\omega_a} \qquad \text{(Eq. 2.32)}$$

u^*_{cwm} is the combined flow shear velocity associated with the maximum shear stress at the boundary and is defined by:

$$u^*_{cwm} = \sqrt{\frac{\tau_m}{\rho}} = \sqrt{(\frac{1}{2} f_{cw\ m})|u_0|} \qquad \text{(Eq. 2.33)}$$

The shear velocity associated with the current both in the combined flow and the current only flow can be obtained from the following expressions respectively:

$$u^*_c = \sqrt{\frac{\tau_c}{\rho}} = \sqrt{(\frac{1}{2} f_c) U_c} \qquad \text{(Eq. 2.34)}$$

and

$$u^*_{c0} = \sqrt{\frac{\tau_{c0}}{\rho}} = \sqrt{(\frac{1}{2} f_{c0}) U_c} \qquad \text{(Eq. 2.35)}$$

An approximate estimate of the maximum orbital velocity can be obtained from the simple linear theory modified to account for the presence of a steady current. The maximum wave velocity can be estimated from:

$$|u_0| = a_0 \omega_r \qquad \text{(Eq. 2.36.)}$$

where a_0 is the amplitude of the orbital motion near the boundary and ω_r is the relative wave frequency. a_0 is given by:

$$a_0 = \frac{H}{2\sinh(kh)} \qquad \text{(Eq. 2.37.)}$$

and ω_r is obtained from:

$$\omega_r = \sqrt{g.k.\tanh(kh)} = \omega_a - kU_c \qquad \text{(Eq. 2.38)}$$

WAVE ATTENUATION DUE TO VISCOSITY

* Please see the addition overleaf.

This section starts by presenting the works of Lamb (1932), Biesel (1949) and Hunt (1952) who employed linear small amplitude theory to develop a prediction of wave height attenuation on still water. It then proceeds to develop solutions for wave height attenuation when a current is superimposed, both for laminar and turbulent regimes.

2.4. Waves On Still Water

2.4.1. Internal Dissipation Due To Viscous Stresses

In the following the same assumptions as those described for the linear wave theory are made. The coordinates are chosen such that OX axis is along the length of the channel, the OZ axis is vertically upward, and the OY axis is across the width of the channel, with the OY-OZ origin at the intersection of the bed and a sidewall.

Lamb (1932) was the first to study the relationship between viscosity and wave height attenuation. He showed that the mean rate of work done by water surface forces on the fluid is given by $2\mu k^3 C^2 H^2$, where μ is water viscosity, k is wave number, C is wave celerity, and H is wave height. This he argued should equate to the rate of change of

Page 52, add after the title : Wave Attenuation Due to Viscosity

As waves propagate towards the shore, they suffer attenuation due to three main processes of energy dissipation. These are internal dissipation due to viscous stresses acting throughout the depth of the flow, surface dissipation associated with surface tension, and the frictional dissipation caused by a solid boundary. In a laboratory flume, where the water depth is usually less than the wavelength and the aspect ratio is relatively small, solid boundary friction is the most important source of energy dissipation. The viscous retarding force applied by the solid boundary reduces the pressure gradient that drives the oscillatory velocity of the waves. This leads to a reduction in the kinetic energy, which in turn results in the fall of the potential wave energy. The wave heights, dependent on the potential energy, consequently suffer attenuation.

energy, where the mean energy density is given by:

$$\frac{1}{2}\rho g H^2 = \frac{1}{2}\rho H^2 \left(\frac{2\pi L}{T^2}\right) = \frac{1}{2}\rho \frac{2\pi}{L}\frac{L^2}{T^2} H^2 = \frac{1}{2}\rho k C^2 H^2$$

Thus, in deep water:

$$\frac{d\left(\frac{1}{2}\rho k C^2 H^2\right)}{dt} = -2\mu k^3 C^2 H^2 \qquad \text{(Eq. 2.39)}$$

which can be rearranged as:

$$\frac{1}{2}\frac{1}{H^2}\frac{d(H^2)}{dt} = -2\nu k^2 \qquad \text{(Eq. 2.40)}$$

Changing the differentiation variable to H, will lead to:

$$\frac{1}{2}\frac{1}{H^2}\frac{2H\, d(H)}{dt} = -2\nu k^2 \qquad \text{(Eq. 2.41)}$$

It follows that

$$\int \frac{1}{H} dH = \int -2\nu k^2 dt \qquad \text{(Eq. 2.42)}$$

which when integrated results in

$$\ln H - \ln H_o = -2\nu k^2 t$$

therefore

$$H = H_0 e^{-2\nu k^2 t}$$

or

$$H=H_0 e^{-\alpha t} \quad \text{with} \quad \alpha = 2\,\nu k^2$$

(Eq. 2. 43)

If a constant phase speed is assumed, and a coordinate transformation is made with d/dx=(1/c)d/dt, the attenuation coefficient can be obtained in terms of propagation distance, x.

Thus,

$$H = H_0 e^{-2\nu k^2 x/c}$$

or

$$\alpha = 2\,\nu k^2/c \qquad \text{(Eq. 2.44)}$$

2.4.2. The Effect of the Bottom Boundary

Later laboratory experiments showed that this formula greatly underestimated the wave height damping. Biesel (1949) argued that the rate of change of energy should be balanced by a more significant factor in shallow water, that is the energy dissipation due to the solid boundary at the bed. Lamb (1932) had showed that the rate of dissipation of mechanical energy per unit time in an incompressible fluid is given by:

$$\Gamma=\nu\rho\iiint(E)dxdzdy \qquad \text{(Eq. 2.45)}$$

where

$$E=2(\frac{du}{dx})^2+2(\frac{dw}{dz})^2+2(\frac{dv}{dy})^2+(\frac{dv}{dz}+\frac{dw}{dy})^2+(\frac{du}{dy}+\frac{dv}{dx})^2+(\frac{dw}{dx}+\frac{du}{dz})^2$$

(Eq. 2. 46)

The principal term in equation 2.45 is:

$$\Gamma=\nu\rho\int\int\int_{\frac{1}{2}}(\frac{du}{dz})^2 dxdzdy \qquad \text{(Eq. 2.47)}$$

The equation of motion can be simplified for laminar flow to take the form:

$$\frac{\partial u}{\partial t}=-\frac{1}{\rho}\frac{\partial p}{\partial x}+g\frac{\partial z}{\partial x}+\nu\frac{\partial^2 u}{\partial z^2} \qquad \text{(Eq. 2.48)}$$

Assuming the bed is flat, and the rate of change of pressure with x is negligible within the viscous sublayer, the above equation reduces to:

$$\frac{\partial u}{\partial t}=\nu\frac{\partial^2 u}{\partial z^2} \qquad \text{(Eq. 2.49)}$$

The solution is:

$$u=-u_0 e^{\sqrt{\frac{z\omega}{2\nu}}} \qquad \text{(Eq. 2.50)}$$

differentiating equation 2.50 with respect to z and substituting into equation 2.47, the dissipation of energy at the boundary layer near the bed in time T (=$2\pi/\omega$) is given by:

$$\Gamma_b = \pi \rho \sqrt{(\frac{\nu}{2\omega})} \int\int (u_0^2) dx dy \qquad \text{(Eq.2.51)}$$

Substituting from linear wave theory , for the amplitude of the orbital velocity near the bed, and evaluating the integral, the dissipation of energy at the bed per unit length of the channel, in time T, and through the width of the flume is

$$\Gamma_b = \pi \rho \sqrt{(\frac{\nu}{2\omega})} \frac{\omega^2 H^2 B}{4\sinh^2(kh)} \qquad \text{(Eq.2.52)}$$

The energy transmitted across a vertical plane (x = constant) in one wave period is:

$$E_f = \int\int (EC_g) dy dt \qquad \text{(Eq. 2.53)}$$

Substitution from equations 2.15 and 2.16, and evaluation of the integral gives

$$E_f = \frac{2\pi}{\omega} . B . \frac{\rho g H^2 \omega}{8\sinh^2(kh)} . \frac{2kh + \sinh(2kh)}{2k}$$

which (with ω^2 = gk tanh kh) can be rewritten in a more commonly used form as:

$$E_f = \frac{\pi \rho \omega^2 B H^2}{8k\sinh^2(kh)} . \frac{2kh + \sinh(2kh)}{2k} \qquad \text{(Eq. 2.54)}$$

Balancing the energy dissipated at the bed with the rate of change of wave energy transmission along the channel

$$\frac{d(E_f)}{dx} = -\Gamma_b \qquad \text{(Eq. 2.55)}$$

results in

$$\frac{\partial}{\partial x}\left[\frac{\pi \rho \omega^2 B H^2}{8k\sinh^2(kh)} \cdot \frac{2kh+\sinh(2kh)}{2k}\right] = \pi \rho \sqrt{\frac{\nu}{2\omega}} \frac{\omega^2 H^2 B}{4\sinh^2(kh)}$$

The above relationship reduces to

$$\frac{1}{H^2}\frac{d(H^2)}{dx} = \sqrt{\frac{\nu}{2\omega}}\left(\frac{4k^2}{2kh+\sinh 2kh}\right)$$

Changing the variable in the integration ($dH^2 = 2H\, dH$) results in,

$$\int \frac{1}{H} dH = \int \left[\sqrt{\frac{\nu}{2\omega}}\left(\frac{2k^2}{2kh+\sinh 2kh}\right)\right] dx$$

which can be solved as:

$$H = H_0 e^{-\alpha x}$$

where

$$\alpha = \sqrt{\frac{\nu}{2\omega}}\left(\frac{2k^2}{2kh+\sinh 2kh}\right) \qquad \text{(Eq. 2.56)}$$

This can be rewritten in the format presented by Sleath (1984)

$$\alpha = \frac{k^2}{\beta(2kh + \sinh 2kh)}$$

where

$$\beta = \sqrt{\frac{\omega}{2\nu}}$$

Equation 2.56, was also presented by Biesel (1949) to predict the wave height attenuation in a viscous flow.

2.4.3 The Effect of the Sidewall Boundary

Biesel' s formula still underestimated the wave damping measured in laboratory flumes. Hunt (1952) argued that for laboratory measurements it is necessary also to know the effect of energy dissipation due to the friction on the sidewalls. He suggested that equation 2.55 should be amended accordingly, and rewritten as:

$$\frac{d(E_p)}{dx} = -\Gamma_b - 2\Gamma_s \qquad \text{(Eq. 2.57)}$$

where Γ_b and Γ_s are respectively the energy dissipated per unit length in one wave period at the bed and the sidewall. To obtain the energy dissipated at the sidewall, Hunt argued that the principal terms in equation 2.45 at the sidewall boundary are

$$\Gamma_s = \rho \int\int\int [(\frac{\partial u}{\partial y})^2 + (\frac{\partial w}{\partial y})^2] dx dz dy$$

which in a similar manner to the steps taken between equations 2.48. and 2.51. can be shown to be:

$$\Gamma_s = \pi \rho \sqrt{\frac{\nu}{2\omega}} \iint (u_0^2 + w_0^2) dx dz$$

where u_0 and w_0 at the sidewall boundary can be estimated from linear wave theory.

$$u_0 = \omega \frac{H}{2} \frac{\cosh(kz)}{\sinh(kh)} \qquad \text{(Eq. 2.58)}$$

and

$$w_0 = \omega \frac{H}{2} \frac{\sinh(kz)}{\sinh(kh)} \qquad \text{(Eq. 2.59)}$$

Substitution and evaluation of the integral gives the dissipation of energy at the sidewall per unit length of the channel, and through the depth, in time T as:

$$\Gamma_s = \pi \rho \sqrt{(\frac{\nu}{2\omega})(\frac{\omega^2 H^2}{4\sinh^2(kh)})(\frac{\sinh(2kh)}{kB})} \qquad \text{(Eq. 2.60)}$$

And now balancing the energy dissipated at the bed and sidewalls with the rate of change of energy transmission along the channel, the wave height attenuation coefficient becomes:

$$\alpha = \frac{k^2}{\beta (2kh + \sinh 2kh)} (1 + \frac{\sinh(kh)}{kB}) \qquad \text{(Eq. 2.61)}$$

For the case of a channel of infinite width, the above equation reduces to that presented

by Biesel (1949). In spite of ignoring the effect of energy dissipation in the body and surface of the fluid, mass transport, radiation stress, and change of water level along the channel, Hunt's formula provides a good approximation for wave height attenuation in a viscous flow.

2.5 Waves In Combined Flows

2.5.1 The Modified Hunt's Theory

Lighthill (1954) studied the laminar combination of steady and periodic flows. He concluded that if the oscillatory boundary layer is thin in comparison with the steady flow length scale, a reasonable approximation to the velocity distribution is provided by the assumption that the periodic and steady currents are unaffected by each other. In the combined flows of the order under study in this project, this condition is well satisfied as the wave boundary layer is only a few millimetres thick while the steady current boundary layer nearly covers the depth of the water. In such conditions, since the energy balance of the waves is influenced only negligibly by the addition of the steady current, Hunt's (1952) formula could continue to be employed, albeit with a moving frame of reference, to provide a reasonable first approximation. The usual irrotational dispersion relationship presented in equation 2.38, modified for the superimposed current, could be used to obtain the wave number, k, needed to evaluate equation 2.60.

The use of an irrotational theory, which is the basis for Hunt's formula, was shown to be reasonable under certain conditions in combined flow by Thomas (1981). He concluded

that irrotational theory can be employed successfully for combined flow if the mean velocity profiles are approximately uniform over most of the depth, in spite of the existence of strong narrow shear layers near the channel bed and free surface.

As noted in the preceding literature survey, the periodic component of the combined flow remains laminar through a considerable phase of the oscillation, even in combination with a relatively strong current, and especially over smooth boundaries. Thus, the following modified version of Hunt's theory, employing a moving frame of reference, can serve as a first approximation for wave height attenuation in combined flows:

$$\alpha = \frac{k'^2}{\beta(2k'h+\sinh 2k'h)}\left(1+\frac{\sinh(k'h)}{k'B}\right) \qquad \text{(Eq. 2.61.)}$$

where k' = 2π/L', and L' is the transformed wavelength after the addition of the current to the wavetrain given by:

$$L = \frac{gT^2}{2\pi}\tanh(k'h)$$

2.5.2 Turbulent Flow Equations

In the case of combined turbulent flow there is an interaction between the steady and oscillatory components, with the turbulence generated by one affecting the velocity distribution of the other. This results in a dynamic and kinematic transformation of both components creating a steady current with altered boundary layer profile, velocity and

energy level, and a wavetrain with altered wavelength, wave height, velocities and wave energy. It is the transformation in the characteristics of the periodic component which has an important influence on wave height attenuation.

When there is a superimposed mean current the calculation is considerably more complicated than that of waves on still water. The energy dissipated within the turbulent inner layer cannot be calculated analytically and assumptions involving the use of eddy viscosities and friction factors are necessary. In addition, the analysis of the rate of change of energy transmission along the channel cannot be restricted to the wave energy flux, although it will be shown later that this remains the dominant term. It should also include terms relating to mass transport, radiation stress, and kinetic energy. Further, the change in mean water level cannot be ignored.

Below, an approach to the problem is outlined, encompassing the factors mentioned above. The result is an equation predicting wave height attenuation in turbulent flows. The expression can also be used for the case of turbulent waves alone as this represents the special condition of $U_c = 0$.

The derivation is similar to that outlined for waves on still water. The energy dissipation at bed and sidewalls within the inner layers is calculated by employing a semi empirical approach. The energy dissipation is then balanced against the rate of change of energy transmission along the channel. It is not possible to obtain an exponential attenuation coefficient for turbulent flow. Instead the rate of change of wave height along the channel is computed directly. The dissipation of energy at the surface and in the body of the fluid

is once again ignored as it was by Biesel and Hunt. A considerable advantage of the present approach is that the derivation can be readily amended to be compatible with many of the existing wave-current models that propose a relationship between flow velocities and shear stresses.

The total instantaneous bed shear stress in a combined flow is given by equation 2.22. At the sidewalls, however, the relationship is somewhat different. The expression needs to be modified to accommodate the vertical component of the orbital velocity and take into consideration the fact that the angle between the waves and the current is zero at the sidewall ($\cos\chi=1$). Thus, the horizontal instantaneous shear stress at the sidewall associated with the wave motion in a combined flow can be shown to be:

$$\tau_{scwx}=\frac{1}{2}\rho f_{scw} u_{0s}^2[\sigma+\cos(\theta+\phi_s)] \qquad \text{(eq. 2.62)}$$

Similarly, the vertical wave instantaneous shear stress at the sidewall is:

$$\tau_{swz}=\frac{1}{2}\rho f_{swz} w_{0z}^2 \sin(\theta+\phi_s) \qquad \text{(eq. 2.63)}$$

where ϕ is the phase lead of the shear stress over the wave velocity, and θ is the phase function ($\omega_r t$-kx). The subscript "s" attributes the value to the sidewall, and subscript "z" denotes the vertical direction. Thus, f_{cwz} is the friction factor at the sidewall due to the waves only motion in the vertical direction. Similarly, u_{0s} and w_{0z} are the amplitudes of the

horizontal and vertical components of the orbital velocity at the sidewall. It should be noted that these values are clearly different from those associated with the bed boundary.

To evaluate the combined flow energy dissipation, Christoffersen and Jonsson (1985) used an approach similar to that by Kajiura (1968), who considered pure wave motions. They argued that the instantaneous total energy dissipated at a boundary can be determined from the following relationship:

$$\Gamma_{tb} = \int \tau \frac{\partial U_T}{\partial z}\, dz \qquad \text{(eq. 2.64)}$$

where U_T is the instantaneous total velocity given by:

$$U_T = U + u_t = U_c + u_0 \cos\theta \qquad \text{(eq. 2.65)}$$

Subscript "t"denotes instantaneous and subscript "T" is associated with the total velocity.

After a series of calculations, Christoffersen and Jonsson (1985) show that equation 2.64 can be written as the sum of the wave dissipation and the current dissipation.

$$\Gamma_t = \tau_{wt} u_0 \cos\theta + \tau_{ct} U_c \qquad \text{(Eq. 2.66)}$$

where τ_{wt} and τ_{ct} are the instantaneous shear stresses associated with the wave and current motion in the combined flow respectively. It should be stressed that τ_c and τ_w cannot be calculated from the pure current and pure wave motions as in a combined flow the two

components are dependent on each other. The current shear stress is given by the mean value of the shear stress, i.e.

$$\tau_c = < \tau > \qquad \text{(eq. 2.67)}$$

Thus, equation 2.66 can be written as

$$\Gamma = < \tau > .U_c + <\tau_w .u_0 \cos \theta>$$

or

$$\Gamma_w = \Gamma - < \tau > .U_c \qquad (2.68)$$

Assuming that the flow is collinear ($\cos\chi=1$), and substituting for the shear stress and the total velocity in equation 2.65, the instantaneous total energy dissipated at the bed is:

$$\Gamma_{tbcw} = \frac{1}{2}\rho f_{bcw} u_{0b}^2 .\cos(\theta + \phi_b).(u_o \cos\theta) + \frac{1}{2}\rho f_{bc} U_c^3$$

(Eq. 2.69)

Similarly, the instantaneous total energy dissipated at the sidewall can be obtained by resolving it into horizontal and vertical components first, and then as energy is not a directional vector, adding the two up to give the total value. Thus, the horizontal component of the energy dissipated at the sidewall is:

$$\Gamma_{scwx} = \frac{1}{2}\rho f_{scw} u_{0s}^2 \cos(\theta + \phi_s).(u_{0s} .\cos\theta) + \frac{1}{2}\rho f_{sc} U_c^3$$

(Eq. 2. 70)

While the vertical component is given by:

$$\Gamma_{swz} = \frac{1}{2}\rho f_{swz} w_{0s}^2 [\sin(\theta + \phi_s)].(w_{0S} \sin\theta)$$

(Eq. 2. 71)

A computer programme is written as part of this project to evaluate energy dissipation at the bed and sidewalls, and is discussed in Chapter 6. Neglecting the loss of energy in the body and at the surface of the fluid, the dissipation of energy at the two boundaries under consideration is balanced by the rate of change of energy flux along the channel. Thus,

$$\frac{d}{dx}(\int E_f dy) = - (\int \Gamma_b dy + 2 \int \Gamma_s dz) \qquad \text{(Eq. 2.72)}$$

As mentioned earlier, when a steady current is superimposed onto a wave train, the analysis of energy flux cannot be restricted to the wave energy contribution only. It should also include terms accounting for mass transport, radiation stress, the kinetic energy, and the potential energy. Thus, following Van Hoften and Karaki (1976), the equation for energy flux at a vertical plane x of the channel can be written as,

$$\mathbf{E_f = E.C_{gr} + E.U_m + S_{xx}\, U_m + (1/2)\,h\rho.U_m^3 + \frac{1}{2}\rho.g.h^2.U_m}$$

(Eq. 2. 73)

where the first term on the right hand side of the equation is the same as that described in the section for waves on still water. C_{gr} is the relative group velocity of the waves described in equation 2.17.

The second term accounts for the transmission of the wave energy by the total mass transport velocity , U_m. It is defined as the linear superposition of the steady current and the wave mass transport velocities in order to make readily apparent the contribution made by each component to the final assessment of the energy flux. Thus,

$$U_m = U_c + u_m = U_c + \frac{gH^2}{8hC_r} \qquad \text{(eq. 2.74)}$$

where u_m is the wave mass transport velocity, defined in equation 2.21. In the following derivation U_c is taken as uniform with depth in the evaluation of the rate of energy flux to simplify the calculation. This assumption, although not strictly true, will have a marginal effect on the final outcome, with the exception of very shallow flows. In the case of the present evaluation, velocity measurements have shown that the steady component of the flow retains a relatively uniform profile for over 90% of the depth.

The third term in equation 2.70. accounts for the radiation stress, a concept introduced by Longuet-Higgins and Stewart (1960). It is defined as the excess flow of momentum due to the presence of waves, and can be determined from the integration of the total momentum flux of wave and current minus the momentum flux of current alone. The radiation stress can be expressed as a two dimensional tensor, S_{ij}, Following Van Hoften and Karaki (1976):

$$S_{IJ} = E \begin{vmatrix} \frac{2kh}{\sinh(2kh)} + \frac{1}{2} & 0 \\ 0 & \frac{kh}{\sinh(2kh)} \end{vmatrix} \qquad \text{(eq. 2.75)}$$

The component of interest in the present analysis is the term S_{xx}=E{2kh/sinh2kh)+1/2},

which acts in the "x" direction.

The fourth and fifth terms on the right hand side of equation 2.70 account for the contribution of total kinetic energy of the steady flow and potential energy respectively.

Substitution into equation 2.70. and expansion of the terms, will give a basic expression for the rate of energy transfer through the width of the channel, similar to that given by Kyriacou (1988):

$$\frac{d}{dx}\left(\int E_f\, dy\right) = B.\left[\frac{1}{8}\rho g C_{gr}\frac{\partial(H^2)}{\partial x}\right.$$
$$+\frac{1}{8}\rho g.\left(U_c\frac{\partial(H^2)}{\partial x} + \frac{g}{8C_r}\frac{\partial(H^2)}{\partial x}\frac{1}{\partial h/\partial x}\right)$$
$$+\frac{1}{8}\rho g\left(U_c G\frac{\partial(H^2)}{\partial x} + \frac{\rho g^2 G}{64C_r}\frac{\partial(H^4)}{\partial x}\frac{1}{\partial h/\partial x}\right)$$
$$+\frac{1}{2}\rho\frac{\partial h}{\partial x}.\left(U_C^3 + \frac{3}{8}U_C^2\frac{g}{C_r}\frac{\partial(H^2)}{\partial x}.\frac{1}{\partial h/\partial x}\right.$$
$$+\frac{3}{64}U_c\left(\frac{g}{C_r}\right)^2\left[\frac{\partial(H^2)}{\partial x}.\frac{1}{\partial h/\partial x}\right]^2$$
$$\left.+\frac{1}{512}\left(\frac{g}{C_r}\right)^3\left[\frac{\partial(H^2)}{\partial x}.\frac{1}{\partial h/\partial x}\right]^3\right)$$
$$\left.+\frac{1}{2}\rho g\frac{\partial(h^2)}{\partial x}\left(U_c + \frac{1}{8}\frac{g}{C_r}\frac{\partial(H^2)}{\partial x}.\frac{1}{\partial h/\partial x}\right)\right]$$

(Eq. 2.76)

where G = (4kh + sinh 2kh) /2 sinh 2kh= $\frac{c\,C_{gr}}{C_r} - \frac{1}{2}$

Terms containing the cross correlation $\partial(H^2)/\partial x.(1/(\partial h/\partial x)$ and terms with powers of H larger than 2 are too small to have any significant effect on the outcome of the formula and are neglected. The full equation thus simplifies to:

$$\frac{d}{dx}(\int E_f\, dydt) = B.[\frac{1}{8}\rho g C_{gr}(2H)\frac{\partial H}{\partial x} + \frac{1}{8}\rho g.U_c(2H)\frac{\partial H}{\partial x} + \frac{1}{8}\rho g U_c G(2H)\frac{\partial H}{\partial x} + \frac{1}{2}\rho\frac{\partial h}{\partial x}U_C^3 + \frac{3}{16}U_C^2\frac{g}{C_r}(2H)\frac{\partial H}{\partial x} + \rho g U_c 2\frac{\partial h}{\partial x}]$$

(Eq. 2.77)

Rearranging equation 2.74, and substitution into equation 2.69 results in a general relationship that can predict the behaviour of the combined turbulent flow along a laboratory channel. Thus, assuming the rate of loss of energy flux is equal to the rate of dissipation of energy at the boundaries, the following relationship should hold:

$$B.[2\rho gH\frac{dH}{dx}(\frac{1}{8}C_{gr}+\frac{1}{8}U_c+\frac{1}{8}U_c G+\frac{3}{16}\frac{U_c^2}{C_r}) + \rho\frac{dh}{dx}(\frac{1}{2}U_c^3+ ghU)] = -B\Gamma_b - 2h\Gamma_s$$

(Eq. 2.78)

Expanding the right hand side of the above equation by substituting from equations 2.67. and 2.68., gives a more general expression that depends only on the basic properties of a flow for its inputs:

$$B.[2\rho gH\frac{dH}{dx}(\frac{1}{8}C_{gr}+\frac{1}{8}U_c+\frac{1}{8}U_cG+\frac{3}{16}\frac{U_c^2}{C_r}) + \rho\frac{dh}{dx}(\frac{1}{2}U_c^3+ ghU)]$$
$$=-B.\{(\frac{1}{2}\rho f_{bcw}u_{0b}^2\cos(\theta+\phi_b).(u_{0b}\cos\theta) + (\frac{1}{2}\rho f_{bc}U_c^3)\}$$
$$-2h.\{(\frac{1}{2}\rho f_{scw}u_{0s}^2.\cos(\theta+\phi_s)].(u_{0s}\cos\theta) + (\frac{1}{2}\rho f_{sc}U_c^3)$$
$$+(\frac{1}{2}\rho f_{swz}w_{0s}^2[\sin(\theta+\phi_s)].(w_{0S}\sin\theta)\}$$

(Eq. 2.79)

A computer programme is written to evaluate the terms in the above equation at each phase of the wave cycle and then integrate the results through the cycle. Alternatively, equation 2.76 can be evaluated according to the energy dissipation equations given by Christoffersen and Jonsson (1985):

$$B.[\frac{1}{4}\rho gH\frac{dH}{dx}(C_{gr}+U_c+U_cG+\frac{3}{2}\frac{U_c^2}{C_r}) + \rho\frac{dh}{dx}(\frac{1}{2}U_c^3+ ghU)]]$$
$$=-B.[(\frac{1}{4}\rho f_{bcw}\cos\phi_b u_{0b}^3 + \frac{1}{2}\rho f_{bc}U_c^3]$$
$$-2h.[(\frac{1}{4}\rho f_{scw}\cos\phi_s u_{0s}^3 + \frac{1}{2}\rho f_{sc}.U_c^3 + \frac{1}{4}\rho f_{swz}\sin\phi_s w_{0s}^3)]$$

(Eq. 2.80)

For further simplicity of calculation Christoffersen and Jonsson (1985) argued that the phase shift between the shear stress and orbital velocity can be approximated by $8/3\pi$. Any discrepancy which results from this approximation will be small since $8/3\pi=0.84$ and $0.71<\cos\phi<1.0$ or $45°>\phi>0°$ degree. Thus, energy dissipation at the bed boundary is given by:

$$\Gamma_b = \frac{2}{3\pi}\rho f_{bcw}\, u_{0b}^3 + \frac{1}{2}\rho f_{bc} U_c^3 \qquad \text{(Eq. 2.81)}$$

and for the sidewall,

$$\Gamma_s = \frac{2}{3\pi}\rho f_{scw} u_{0s}^3 + \frac{1}{2}\rho f_{sc} U_c^3 + \frac{2}{3\pi}\rho f_{swz} w_{0s}^3$$

(Eq. 2.82)

Using the above approximations, equation 2.80 can be simplified to :

$$B.[\frac{1}{4}\rho g H \frac{dH}{dx}(C_{gr} + U_c + U_c G + \frac{3}{2}\frac{U_c^2}{C_r}) + \rho\frac{dh}{dx}(\frac{1}{2}U_c^3 + ghU)]$$
$$= -B.[\frac{2}{3\pi}\rho f_{bcw} u_{0b}^3 + \frac{1}{2}\rho f_{bc} U_c^3]$$
$$2h.[\frac{2}{3\pi}\rho f_{scw} u_{0s}^3 + \frac{1}{2}\rho f_{bc} U_c^3 + \frac{4}{3\pi}\rho f_{swz} w_{0s}^3]$$

(Eq. 2.83)

For the special case of turbulent waves on still water, where $U_c = 0$, equation 2.79 reduces to :

$$B[\frac{1}{4}\rho g H \frac{dH}{dx} C_{ga}\ ] =$$
$$-B.\{\frac{1}{2}\rho f_{bw0} u_{0b}^2 . \cos(\theta + \phi_b).(u_{0b} . \cos\theta)\}$$
$$-2h.\{[\frac{1}{2}\rho f_{sw0} u_{0s}^2 . \cos(\theta + \phi_s).(u_{0s} . \cos\theta)]$$
$$+[\frac{1}{2}\rho f_{swz} w_{0s}^2 . \sin(\theta + \phi_s).(w_{0S} . \sin\theta)]\}\ ]$$

(Eq. 2.84)

In a similar manner, equation 2.83 can be reduced for the turbulent waves only case to :

$$\frac{1}{4}B.\rho gHC_{ga}\frac{dH}{dx} = -B.\frac{2}{3\pi}\rho f_{bw0}u_{0b}^{3} - 2h.[\frac{2}{3\pi}\rho f_{sw0}u_{0s}^{3} + \frac{2}{3\pi}\rho f_{sws}w_{0s}^{3}]$$

(Eq. 2.85)

In the above equation for turbulent waves alone, wave height attenuation -dH/dx- is obtained from dividing the energy loss at the solid boundaries by the rate of transmission of energy through the body of the fluid, which is similar to Hunt's formula for laminar flows.

2.5.3 The Wave Attenuation Equation

There exists a practical difficulty in evaluating any of the equations for turbulent flow given above. The model is highly dependent on the slope of the mean water level which in practice is very difficult to measure. Thus, it would be desirable to devise a model that does not require this slope as an input. Jonsson (1968) suggested that equations of conservation of momentum and conservation of energy can be combined to eliminate the slope of the mean water level. He wrote the equation of conservation of momentum as:

$$B\{\frac{d}{dx}(\rho hU_{m}^{2})+\frac{d}{dx}S_{xx}+\frac{d}{dx}(\frac{1}{2}\rho gh^{2})\}=-B\tau_{b}-2h\tau_{s} \qquad \text{(Eq. 2.86)}$$

where

$$U_m^2 = U_c^2 + \frac{2U_c g H^2}{8C_r h} + \frac{g^2 H^4}{64 C_r^2 h^2}$$

Expanding the equation of conservation of momentum, and ignoring terms of higher order than H^4, the following relationship is obtained:

$$B.\{\frac{1}{4}\rho g H \frac{dH}{dx}[\frac{2U_C}{C_r} + G] + \frac{dh}{dx}[\rho U_c^2 + \rho g h]\} = B\tau_{bcw} + 2h\tau_{scw}$$

(Eq. 2. 87)

The following substitutions are made in the conservation of momentum and energy equations:

$$\frac{1}{4}\rho g H \frac{dH}{dx} = Q_1$$

$$\rho\ gh = Q_2$$

$$U_c / C_r = Q_3$$

$$\Gamma_T = B\ \Gamma_b + 2h\ \Gamma_s$$

$$\tau_T = B\ \tau_b + 2h\ \tau_s$$

The equation of conservation of energy can then be rewritten as:

$$-\Gamma_T = B.\{Q_1(C_{gr} + U_c + U_c G + \frac{3}{2}U_c Q_3) + \frac{dh}{dx}(\frac{1}{2}\rho U_c^3 + Q_2 U_c)\} \qquad \text{(Eq. 2. 88)}$$

The equation of conservation of momentum is rewritten as

$$-\tau_T = Q_1(2Q_3+G)+\frac{dh}{dx}(\rho U_C^2+Q_2)$$

Rearranging the above equation gives:

$$\frac{dh}{dx} = \frac{-\tau_T - Q_1(2Q_3+G)}{(\rho U_C^2+Q_2)}$$

This relationship can be used to eliminate the water surface slope from equation 2.88:

$$-\Gamma_T = B.\{Q_1(C_{gr}+U_c+U_cG+\frac{3}{2}U_cQ_3)+[\frac{-\tau_T-Q_1(2Q_3+G)}{\rho U_c^2+Q_2}].(\frac{1}{2}\rho U_c^3+Q_2U_c)\}$$

Multiplying both sides of the equation by $\rho\ U_c^2 + Q_2$ and expanding the terms result in:

$$-\Gamma_T(\rho U_c^2+Q_2)=$$
$$B.\{\ Q_1(C_{gr}\rho U_c^2+\rho U_c^3+\rho U_c^3G+\frac{3}{2}\rho U_c^3Q_3+C_{gr}Q_2+U_cQ_2+U_cGQ_2+\frac{3}{2}U_cQ_3Q_2)$$
$$-\frac{1}{2}\rho U_c^3\tau_T-U_cQ_2\tau_T-\frac{1}{2}\rho U_c^3Q_1(2Q_3)-2U_cQ_1Q_2Q_3-\frac{1}{2}\rho U_c^3GQ_1-Q_2U_cQ_1G\ \}$$

The above equation can be reduced by collecting terms:

$$-\Gamma_T(\rho U_c^2+Q_2)=B.\{\ Q_1(C_{gr}\rho U_c^2+\rho U_c^3+\frac{1}{2}\rho U_c^3G+\frac{1}{2}\rho U_c^3Q_3+C_{gr}Q_2+U_cQ_2-\frac{1}{2}U_cQ_3Q_2)$$
$$-\ \tau_T(\frac{1}{2}\rho U_c^3+U_cQ_2)\ \}$$

Replacing the substitutions for Q_1, Q_2, Q_3, Γ_T, and τ_T will result in :

$$B.[\frac{1}{4}\rho gH\frac{dH}{dx}(\rho U_c^2 C_{gr}+\rho U_c^3+\frac{1}{2}\rho U_c^3 G+\frac{1}{2}\rho U_c^3(\frac{U_c}{C_r})+ C_{gr}\rho gh+ U_c\rho gh-\rho gh\frac{U_c^2}{C_r})$$
$$+(\tau_b+\frac{2h}{B}\tau_s)(\frac{1}{2}\rho U_c^3+\rho ghU_c)]= -(B\Gamma_b+2h\Gamma_s)(\rho gh+\rho U_c^2)$$

Dividing both sides of the above equation by $2\rho gh$, and noting that $C_{ga}=C_{gr}+U_c$ will result in a simpler format. Below, the energy dissipation and shear stress terms are collected in one side of the equation:

$$B.\{\frac{1}{4}\rho gH\frac{dH}{dx}(\frac{1}{gh}U_c^2 C_{ga}+\frac{1}{2gh}U_c^3 G+\frac{1}{2gh}\frac{U_c^4}{C_r})+C_{ga}-\frac{1}{2}\frac{U_c^2}{C_r})\}$$
$$=-(B\Gamma_b+2h\Gamma_s)(1+\frac{1}{2gh}U_c^2)+(B\tau_b+2h\tau_s)(\frac{1}{gh}U_c^3+U_c)$$

Expanding the right hand side of the equation and taking the common factors out, we find:

$$B.\{\frac{1}{4}\rho gH\frac{dH}{dx}\ .\ [C_{ga}-\frac{1}{2}\frac{U_c^2}{C_r}+\frac{U_c^2}{gh}.(C_{ga}+\frac{1}{2}U_c G+\frac{1}{2}\frac{U_c^2}{C_r})]\}$$
$$=B.(-\Gamma_b+U_c\tau_b)+2h.(-\Gamma_s+U_c\tau_s)+\frac{U_c^2}{gh}.[B(-\Gamma_b+\frac{1}{2}U_c\tau_b)+2h(-\Gamma_s+\frac{1}{2}U_c\tau_s)]$$

Substituting from eq.2.68 and solving the above equation for dH/dx will provide an expression for the rate of wave height attenuation in combined waves and current flows:

$$\frac{dH}{dx} = -\frac{1}{\frac{1}{4}\rho g H B} \cdot \frac{B.\Gamma_{wb} + 2h.\Gamma_{ws} + \frac{U_c^2}{gh}.[B(\Gamma_b - \frac{1}{2}U_c\tau_b) + 2h(\Gamma_s - \frac{1}{2}U_c\tau_s)]}{C_{ga} - \frac{1}{2}\frac{U_c^2}{C_r} + \frac{U_c^2}{gh}.(C_{ga} + \frac{1}{2}U_c G + \frac{1}{2}\frac{U_c^2}{C_r})}$$

(Eq. 2. 89)

The separate contribution of the bed and sidewall boundaries to wave height attenuation can be determined from the above equation. Thus, the wave damping due to the bed boundary is given by:

$$(\frac{dH}{dx})_b = -\frac{1}{\frac{1}{4}\rho g H} \cdot \frac{\Gamma_{wb} + \frac{U_c^2}{gh}(\Gamma_b - \frac{1}{2}U_c\tau_b)}{C_{ga} - \frac{1}{2}\frac{U_c^2}{C_r} + \frac{U_c^2}{gh}.(C_{ga} + \frac{1}{2}U_c G + \frac{1}{2}\frac{U_c^2}{C_r})}$$

(Eq. 2.90)

Similarly the wave attenuation caused by the presence of the sidewalls is given by:

$$(\frac{dH}{dx})_s = \frac{-1}{\frac{1}{4}\rho g H} \cdot \frac{2h}{B} \cdot \frac{\Gamma_{ws} + \frac{U_c^2}{gh}(\Gamma_s - \frac{1}{2}U_c\tau_s)}{C_{ga} - \frac{1}{2}\frac{U_c^2}{C_r} + \frac{U_c^2}{gh}.(C_{ga} + \frac{1}{2}U_c G + \frac{1}{2}\frac{U_c^2}{C_r})}$$

(Eq. 2.91)

Neglecting wave mass transport and assuming small Froude numbers, equation 2.89 can be approximated to a simpler form which agrees with the derivation of Kyriacou (1988):

$$\frac{dH}{dx} = -\frac{1}{\frac{1}{4}\rho g H B} \frac{B.\Gamma_{wb}+2h.\Gamma_{ws}}{C_{ga}}$$

(Eq. 2.92)

which is similar in form to the familiar Hunt formula.

The above equations together provide a tool to evaluate wave height attenuation in turbulent combined waves and current flows. A computer programme has been written to evaluate equation 2.89. The outline of the programme is summarised below to provide a guide to how the equation is solved.

The software's inputs are the channel breadth, water depth, wave period, wave height, maximum steady current velocity, water temperature and the boundary roughnesses. From these, the programme computes the kinematic viscosity of water and the wavelength and wave height after the addition of steady current. It also calculates the maximum orbital velocities near the two boundaries. It uses the waves only and current only friction factors as the starting point to solve Myrhaug and Slaattelid's (1990) equations for waves and current friction factors in a combined flow. Two separate processes are employed for smooth and rough boundaries. Values of the current and waves shear stress and energy dissipation are then computed at one degree intervals for each boundary, and the averaged

value is obtained. Other terms of the wave attenuation equation related to energy flux in the body of the fluid are calculated and finally the rate of wave damping is computed. The outputs of the software are compared with test results in Chapter six.

CHAPTER 3

EXPERIMENTAL APPARATUS

3.1 Test Flume

A channel 14.5 metres long, 455mm wide, and 690 mm deep was used for the tests. The sidewalls were constructed of 10 mm thick plate glass, and the bed of 1.83m long cast aluminium sections, coated with marine quality paint. At the measuring position, a section of the bed was cut out and replaced by a 210x290x10mm glass plate in order to allow the passage of laser beams from below the bed. The flume was supported along its full length by an old iron channel, with U shaped cast aluminium sections providing support at 915 mm intervals.

The water was supplied to the flume from storage tanks 16 metres above laboratory level, with the level in the tanks varying, on average, 1% of the total head during the pumping cycle. A 150 mm diameter supply pipe connected the storage tanks to the inlet end of the channel. Two steel gate valves and a diaphragm valve were used to set the flow rate, and a manometer was connected to a 56 mm diameter Venturi-meter in the main supply pipe to monitor it.

To reduce any turbulent mixing immediately in front of the wave generator, the current was introduced into the main 10.79 metre long horizontal section of the channel through a pipe situated below the bed. This was made possible by constructing a 12 degree sloping bed at the inlet end of the flume, and using a false bed sloping upwards at 7.5 degrees for 1.52 metres.

To minimise the effects of wave reflections, a sheet of Scotch Brite Gold matting was

used to construct a sloping beach at the outlet. Water was withdrawn from the channel via a steel water tank fixed to the beach end, and by two 75 mm diameter pipes with adjustable inlets set to control the flow. A wall of ballatini and a section of 10mm honeycomb flow straightener separated these pipes from a fared inlet section. Although not utilised in the present tests, the generation of a current in the opposite direction was possible since a 100 mm inlet pipe connected the outlet tank to a constant head inlet tank overhead. The waves were generated by a wave paddle, allowing the wave height and period to be preset.

During the course of the preliminary "narrow channel" tests, the flume was partitioned into two sections, with one very narrow, starting 0.9 metres from the start of the horizontal section. The division was created by fixing a 10 mm thick and 6 metres long wall of plate glass at a constant distance from one of the sidewalls. The width of the narrow section of the channel was set at 10mm, 20mm or 30mm for different tests. To facilitate the smooth flow of water into the narrow section, the leading edge of the dividing glass plate was given a sharp edge, and a 0.15 metre high curved perspex vane was fixed to it to maintain a strong current.

3.2 Laser Doppler Anemometer (L.D.A.)

3.2.1 Introduction

Laser Doppler Anemometry allows measurement of the velocity of tracer particles present as seeding in the water without disturbing the flow. As the research project required the determination of mean and periodic velocity profiles in the immediate vicinity of the boundaries, it was decided to employ this non-intrusive optical technique. Simons (1980)

designed an L.D.A. system which both he and later Kyriacou (1988) have used successfully at UCL. However, certain modifications were made to allow velocity measurements within the thin viscous layer near the sidewalls. Both Simons (1980) and Kyriacou(1988) have assessed the capabilities, limitations, and operating modes of the adopted system and described its different components in detail. To avoid repetition, this section only includes a brief description of the main concepts and components of the system and the modifications made to original arrangements.

The basic principle of the L.D.A. involves the measurement of the transit time of a particle across a known number of interference fringes formed by the intersection of two coherent light beams. Durst, Melling and Whitelaw (1976) described this principle in detail and various methods available to form the interference pattern. For the present project, the optical arrangement employed a dual beam system, using two intersecting light beams of equal intensity to produce an interference pattern within their volume of intersection. As each particle crosses the interference fringes the intensity of light scattered and collected by a photomultiplier rises and falls at a rate directly proportional to the velocity. The photomultiplier converts the light to a voltage whose frequency varies with the scattered light intensity. From this frequency, the velocity of the fluid particles, which is assumed to be the same as the fluid itself can be calculated. In order to establish the direction of the measured velocity, an optical frequency shifting device was used to alter the relative frequency of the two beams. This means that the Doppler frequency corresponding to zero velocity was displaced to a finite positive value greater than any expected negative velocities.

3.2.2. System Components

A resume of the main component parts of the system is given below and illustrated in figure 3.1.

1. The light source of the L.D.A. system was a Spectra-Physics Model 120 5 mW Helium Neon Laser, generating a 0.65 mm diameter beam of laser light with a wavelength of 632.8 x 10^{-9} m. The generator was driven by a Spectra-Physics 256 Exciter and supported on two Ealing Beck traverse devices providing horizontal and vertical adjustment.

2. A Malvern Instruments RF307 was attached to the outlet of the laser. The unit performed as a combined polariser and beam splitter, allowing an adjustable beam separation. During the course of the tests, the beams were set parallel and 20 mm apart.

3. To create a frequency shift between the two beams, a Malvern K9023 Electro-optic phase modulator was used. A converging lens of either 200 mm or 300 mm focal length was attached in front of the modulator arrangement to focus the two beams together at the measuring point in the channel. The unit was mounted on a Malvern tilt and rotate RR126 unit.

4. A corresponding Malvern K9023 drive unit was used to control the phase modulator. It was set at 200 KHz to produce an apparent zero velocity reading far greater

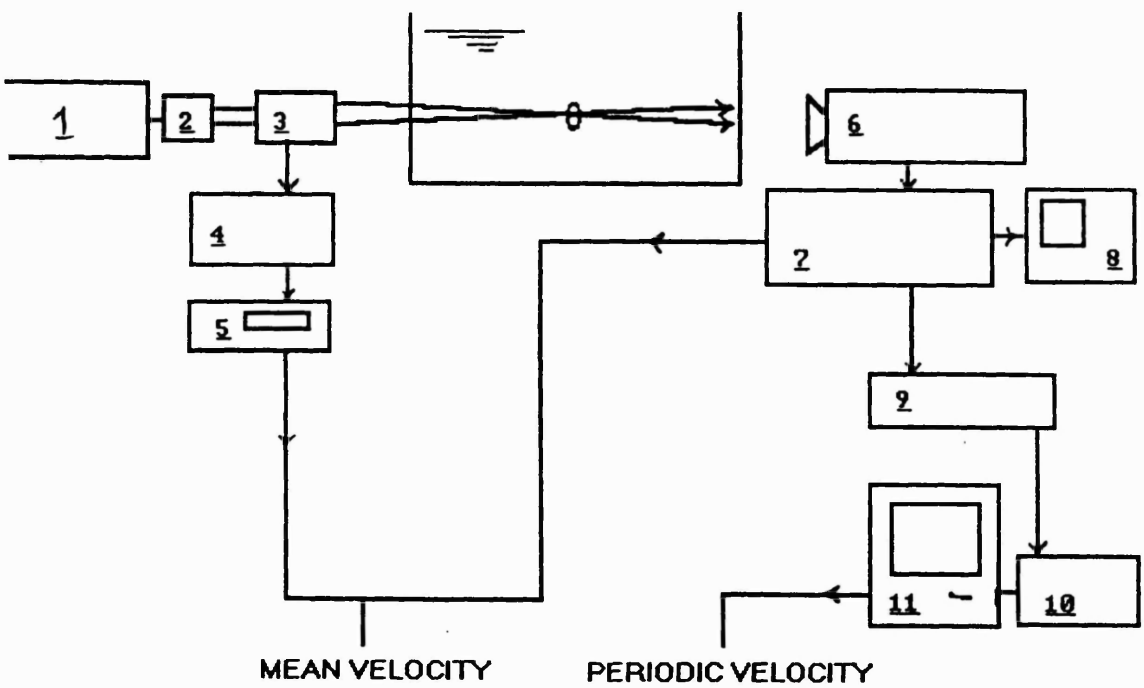

Figure 3.1 Components of the L.D.A system

than that arising from the maximum wave orbital motion. The drive unit applied a saw tooth voltage to the two electro-optic crystals, advancing or retarding the phase of the two laser beams relative to each other.

5. A Bradley Electronics Counter-Timer 234 set on a short display time was connected to the drive unit of the phase modulator to monitor and display its frequency output.

6. A Centronix photomultiplier tube fitted with a Pentacon Auto F1.8-50 mm adjustable lens and a 25μm pinhole was focused on the control volume to detect the change in light intensity. A V.G stabilised High Voltage Supply Unit running at 1.4 KV was used to drive the unit.

7. A Cambridge Consultants Laser Doppler Velocimeter with a total of five frequency settings covering from 100 Hz to 10 MHz was used for "tracking" the Doppler frequency (i.e. determining the frequency of the photomultiplier output). During the course of the tests the frequency range was set between 100 KHz - 1MHz, to correspond with the value of the expected velocities plus the superimposed frequency shift. In addition, the band width was set at 3%, the ramp scan was turned off, the tracking rate was set at the slow position, the "dropout protect" facility was activated, and the normalise switch was set at peak position.

Raven (1974), Simons (1980), Stuart (1984), and Kyriacou (1988) have previously reported on the use of the same model and discussed the reasons for the above settings.

8. The quality of the output signal from the photomultiplier and tracker was monitored by an Advance Instruments OS 3000 oscilloscope, which included features such as dual input mixing, fast time base speeds and high sensitivity.

9. A Krohn-Hite model 3750 electronic filter was employed to remove the d.c. signal resulting from the frequency shift and the steady current in the coexistent wave current flows, or the mass transport in the wave alone experiments. The filter was set at bandpass function, with the cutoff slope at 24 db. The high pass cut off was set at its lowest possible value of 0.02 Hz and the low pass cut off chosen was 50 Hz to remove noise and high frequency turbulence.

10 . The computer is discussed later on in this chapter.

3.2.3 L.D.A. Arrangements

During the different stages of the experiments the laser Doppler anemometry system arrangements were modified to suit the test objectives. For the tests measuring the velocity profiles away from the bed, the same optical arrangement as that designed by Simons (1980) was used. The same arrangement was also used to carry out a full set of preliminary tests to measure the velocity profiles away from the sidewall at various heights. This time, however, as the measured velocities were being averaged across the longer diameter of the control volume (approximately 1.5mm), the system was unable to produce any sensible data for the local velocities within the thin viscous layer in the immediate vicinity of the sidewall. This was because the dimension of the measuring

volume was longer than the thickness of the viscous sublayer and therefore made any reasonable measurements within the inner layer impossible. In general, the velocity measurement for positions in the immediate vicinity of the side-walls could not be considered accurate as the measurement distances were smaller than the diameter of the control volume.

To overcome this problem, the bed of the flume at the laser position was replaced by a glass plate to enable the laser beams to be both turned by 90 degrees with the use of a silver faced mirror, and shone into the channel from under its bed. This shifted the orientation of the laser crossing volume by a corresponding 90 degrees, allowing the system to measure the local streamwise velocity averaged across the shorter diameter of the control volume (approximately 200μm). However, since light waves vibrate with various degrees of strength in different directions, the beams in their new position could not be seen from the location of the photomultiplier.

Thus, the position of the detector had to be changed to improve its view of the beams. Visual inspection showed that the beams could be viewed reasonably well from a position on the same side of the channel as the laser generator, looking down at the cross volume with an angle of less than 30 degrees to the vertical. An adjustable support unit was built and the photomultiplier was mounted on it to look at the control volume with an angle as close to the vertical as possible but still through the sidewall and at a position below the water surface. In practice, this arrangement did not prove effective since although the beams could be seen with the naked eye from that position, the intensity was not enough for the detector to get more than a very faint image of the cross volume.

Viewing the beams from different angles with protected eyes showed that visibility was at its strongest when looking down the line between the two incident laser beams. This meant positioning the photomultiplier above the water surface, which presented another obvious difficulty. With waves propagating along the flume, refraction by the curved water surface caused the beams to come out of the water at various directions depending on their continually changing angle of incidence with the wave surface, thus making it impossible for a stationary detector to get a constant view of the control volume. To avoid surface interference, an extension was attached to the lens of the photomultiplier and inserted through the surface of the water (Figure 3.2). This simple device enabled the detector to obtain a constant view of the measuring volume at an angle which allowed the formation of a strong image. The extension was made out of a plastic tube 10 mm in diameter closed on one end with a thin plate of glass (to avoid water entering), and the other an interconnecting piece fixing it to the photomultiplier lens. The small diameter of the intrusive device, combined with the fact that its lowest end was always kept at least 80 mm from the control volume ensured negligible interference with the flow at the measurement position. * (Please see the addition overleaf)

Very near to the sidewall, the reflection of the beams (and other light) by the sidewall glass made a clear image of the crossing volume extremely difficult to obtain. To overcome this, a narrow strip on the wall was painted matt black to stop reflection. The paint was sprayed on the wall to ensure its thickness did not exceed a few microns, thus not disturbing the smoothness of the surface and causing any change in the dynamics of the flow.

Page 88, add to the end of paragraph 1:

Section 5.5.1 of this thesis reports on a series of tests that were performed to confirm the reliability of this arrangement. The tests demonstrated that the intrusion made by the extension did not produce any significant interference in the velocity profile of the steady flow. Similarly, as the diameter of the extension was less that 1% of the wavelength and its distance from the measuring position was at least twice the wave heights, it was assumed that the intrusion will have similar negligible effect on the wave flow field.

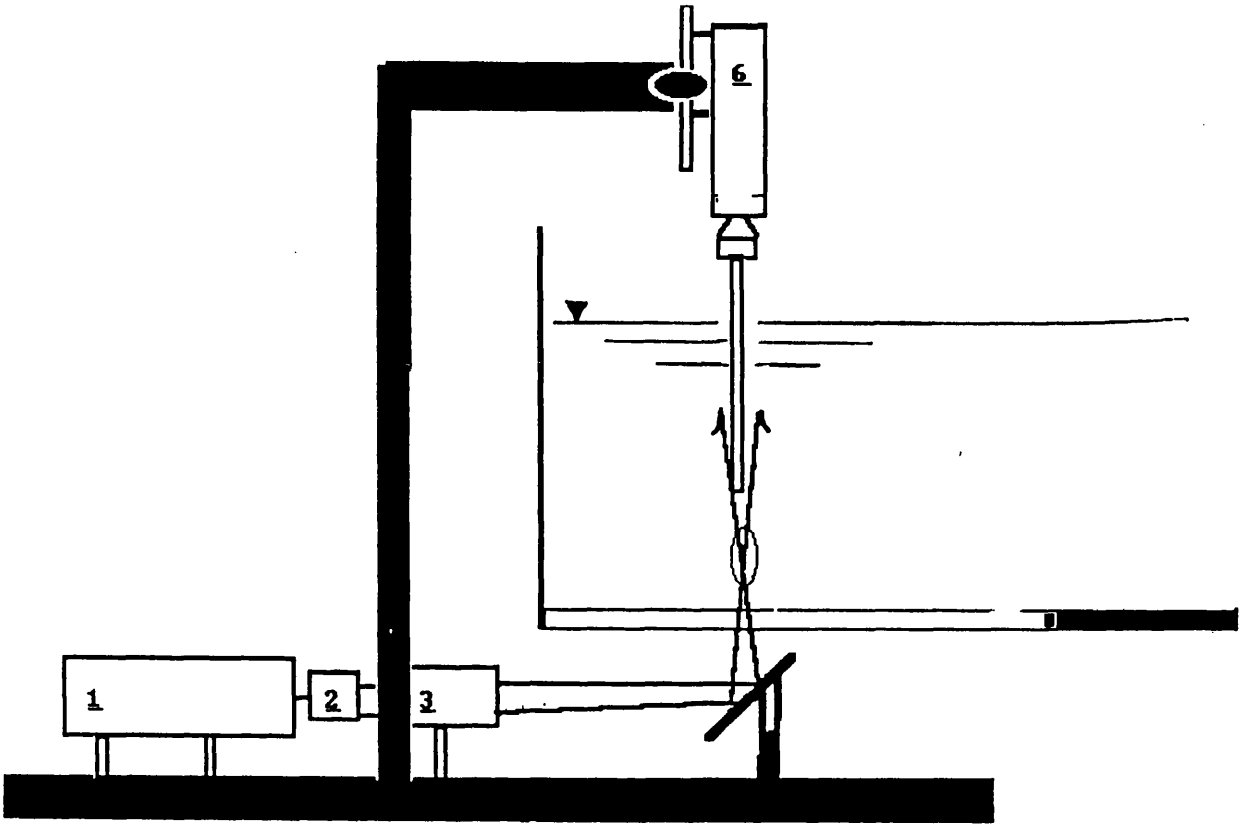

Figure 3.2 L.D.A System Arrangement C

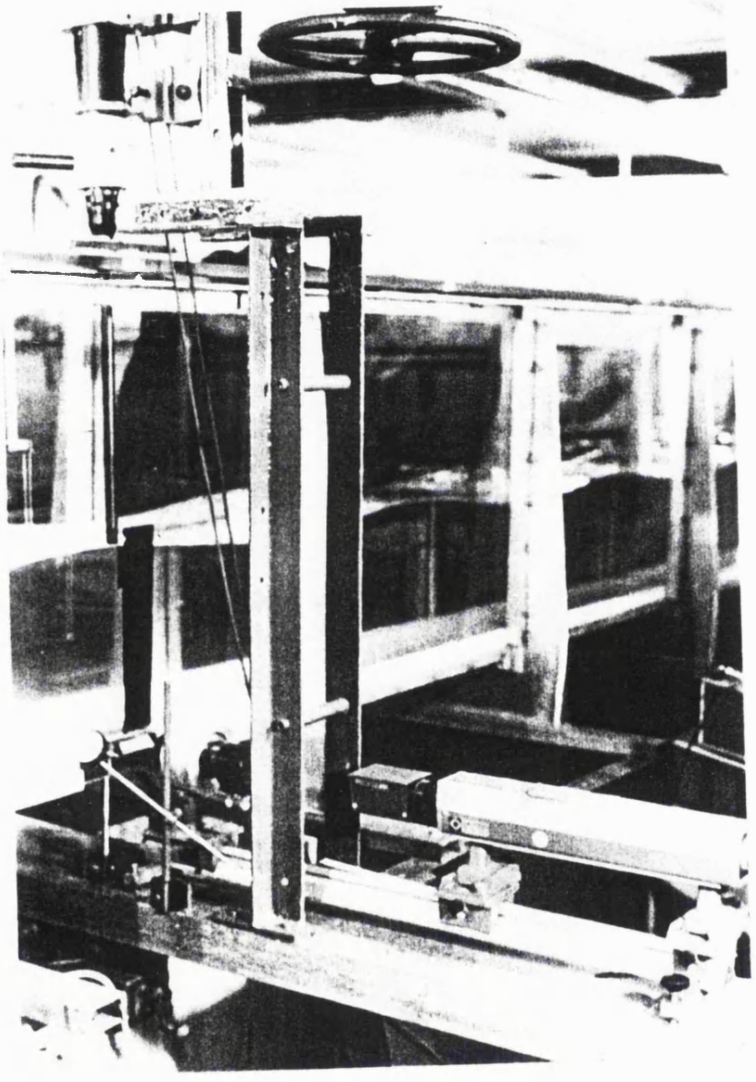

Figure 3.3 A view of the L.D.A. system arrangement

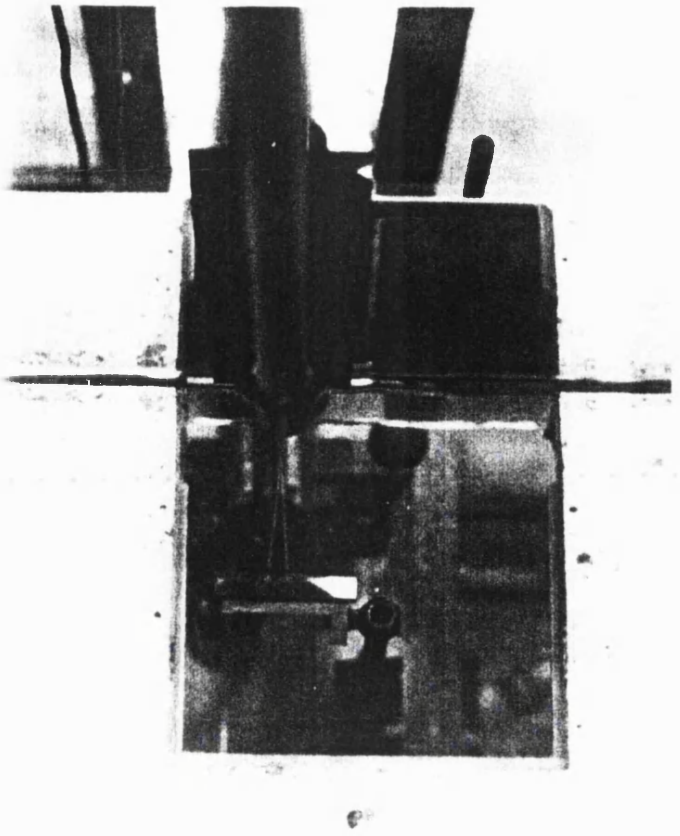

Figure 3.4.

A view from the top of the channel, looking down at the laser beams entering from the glass bed.

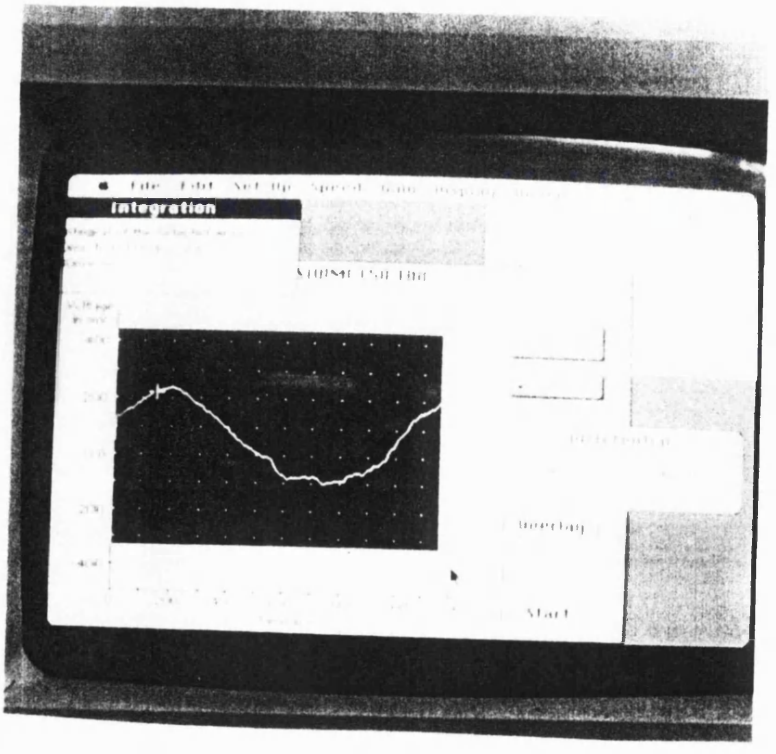

Figure 3.5.

The screen output of the on line computer analysis.

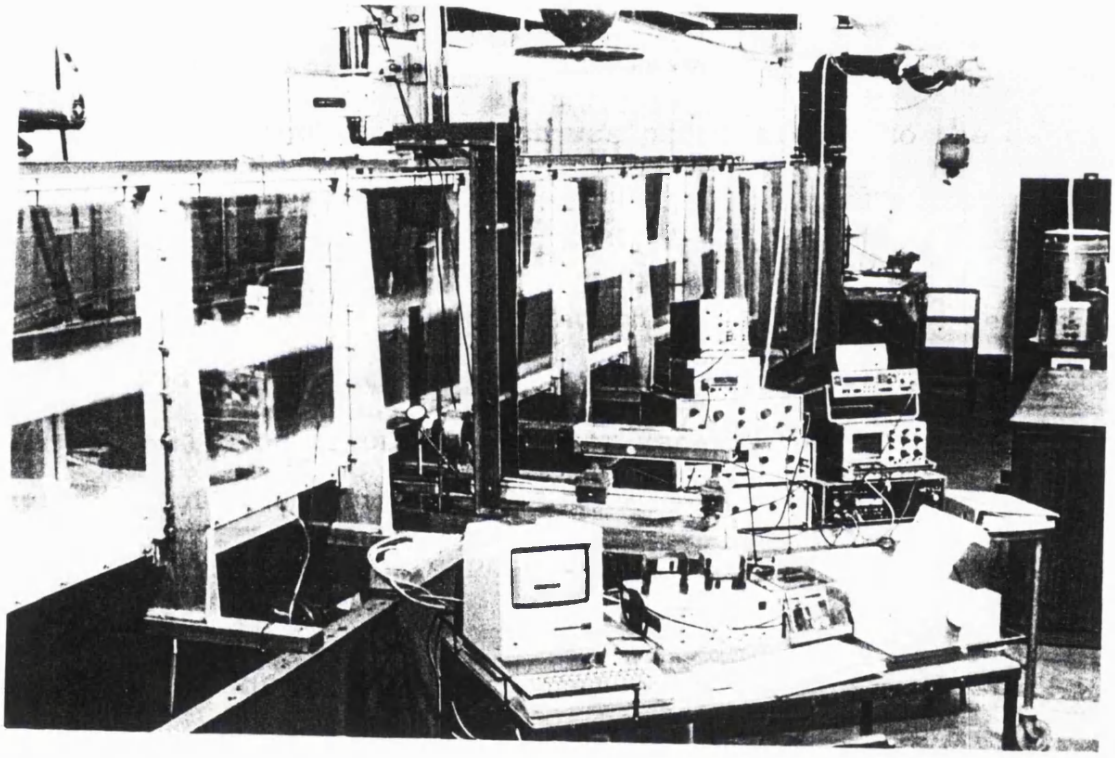

Figure 3.6. The laboratory flume, and the measurement and analysis apparatus.

3.3. Water Surface Monitor

A resistance type probe was used in conjunction with a Churchill two channel wave monitor module to measure the amplitude and profile of surface waves. The resistance wires on the wave probe were 1.5 mm in diameter, 300 mm in length, and approximately 12 mm apart. A special assembly with accurately spaced positioning holes at 10 mm intervals supported the wave probe, and a 15 metre long cable connected it to the control module.

The electronic circuit in the Churchill module could detect the resistance and convert it to an output voltage. This voltage was adjustable to obtain greater sensitivity according to the amplitude of the waves. Following a simple calibration, the output voltage could be expressed in terms of wave height.

In the case of the preliminary tests, in the "narrow channel" wave heights could not be measured by resistance probes since the width of the channel was of the same order as the distance between the wires. Thus wave heights were measured by a translucent plastic ruler positioned vertically on lines drawn at successive 100mm intervals on the side of the channel. In order to make the measurement of the moving heights possible, the narrow section of the channel was isolated and darkened with the use of blackboards, and a spot light was shone on the water surface to visually determine its position.

3.4 Data Analysis System

3.4.1 Introduction

The two sets of tests, performed during the course of this project relied on fundamentally different methods of data collection and averaging. The measurements in the narrow channel tests were all performed with the most basic of equipment and techniques, involving reading from a ruler with the naked eye. The tests in the wide channel, in contrast, employed laser Doppler anemometer combined with an analogue to digital signal converter and a data analysis system to produce on line ensemble averaged presentation.

The on line data collection and analysis technique had obvious advantages over the manual method used for the narrow channel tests. Most importantly, the extremely short time span between data collection and analysis allowed prompt assessment of the incoming data from the on-screen graphical displays of the ensemble averaged velocities. This made it possible to repeat the test under the same flow conditions, in case the data collected originally proved erroneous.

3.4.2. Computer Hardware

3.4.2.1 The Narrow Channel Tests

An IBM-AT compatible DELL System 200 computer was used for data storage and analysis. The system unit specifications were as follows.

Microprocessor	80286
Processor Speed	selectable 6.25 MHz/12.5 MHz
I/O bus speed	6.25 MHz/8.33 MHz
Data bus	16 bit
Direct Memory Access channel	7
Interrupt levels	15
Programmable timer channels	3
Installed Ram	640 - KB Dynamic RAM
Memory Access Time	120 ns (1 wait state)

As indicated above, there were two drives available. A 40-MB Winchester hard disk provided high speed, high capacity storage for programs and information. In addition, a 5.25 inch, double-sided, double-density "Reflex" MD2DD (96TPI) floppy disk drive was also used.

3.4.2.2 The Wide Channel Tests

An Apple Macintosh II personal computer (PC), together with a MacLab analogue to digital converter was used for data acquisition and analysis during the course of the wide channel tests. The processing speed of the Apple Macintosh II is 8 MHz. As the unit had no hard disk, a system disk was provided to boot the computer and perform various operating procedures.

The MacLab Hardware unit contained 4 differential high gain input amplifiers, a fast 12

bit analogue to digital converter running at a maximum of 40 KHz and a microprocessor with 16K of memory. It also contained a digital to analogue converter with a variable gain output amplifier, and an internal expansion converter. The 4 analogue inputs were designed to accept up to + or - 10 V, and the output amplifier could deliver up to 200 m A. An external trigger device allowed an analogue input to be used for synchronizing sampling to external devices. The limits on this input were + or - 12 V. A 7 segment LED display provided a check on the status of the MacLab unit.

3.4.3. Computer Software

A whole series of commercial and user written programmes was employed at different stages of the project. An important part of this research project was concerned with developing and programming a mathematical model to predict the rate of wave height attenuation. The resulting "wave attenuation software" (WAS) does much more than just the above task; it evaluates a large number of flow characteristics such as friction factors, shear stresses and energy dissipation at both the bed and sidewall boundaries. This programme is described and presented in detail in section 6.5 and the Appendix A of the thesis and is not discussed here. As mentioned above, however, apart from the main programme written by the author, other software were employed during the course of this research. Below, is a brief introduction to these programmes.

3.4.3.1 The Narrow Channel Tests

The overall system management of the DELL System 200 microcomputer was undertaken by MS-DOS operating system. GW-BASIC programming language was employed for programming. All together three categories of programmes were written; for data storage, data analysis, and data presentation .

The data storage category mainly included the "DATIN", and the "DATA.IN" programmes. Both were very simple programmes, taking the experimental data as input and filing them in the format necessary for future use. These programmes created some 61 data files, stored simply under the serial name "TEST ...".

The data analysis category included programmes such as the "P..." series, "TH.CAL", "AC.DIF", "AC.PER", and a part of the "PLOT" series. Using a curve fit procedure and Hunt's formula, the "P..." series computed the wave attenuation coefficient and the initial wave height for each test. One version of the programme provided the option to change the starting position in the channel, and ignore any chosen point of the initial data. The "TH.CAL" programme subsequently used the calculated values of the attenuation coefficient and the initial wave height to work out the coordinates of a curve to represent wave attenuation along the channel. Parts of the "PLOT" series of programmes were employed to compute the wave length and the theoretical values of wave attenuation coefficient for each test. The programme also worked out and filed the coordinates of a curve to represent the theoretically predicted wave attenuation along the channel. The "AC.DIF" and "AC.PER" programmes were written to compute, respectively, the actual

and percentage difference between the empirically and theoretically obtained values of attenuation coefficients, and to file them away for later presentation use.

The third category of programmes, for data representation, included the "GEN.RES" series, the "PLOT" series, and the "GRAPH" series. The "GEN.RES" series of programmes created a file of all necessary data and values for each test, and presented them in the form of a table. The "PLOT" series of programmes, apart from the tasks mentioned above, used the available data to plot profiles of both empirical and theoretical wave attenuation along the channel. The programme also made it possible for the graphs to show all the measurements, and present the required test parameters. The "GRAPH" series of programmes produced a graphical representation of both actual and percentage differences between the empirical and theoretical wave attenuation coefficients, for each series of tests.

At a later stage, two new larger programmes were written to carry out most of the tasks outlined above. They were named "PROG" and "PROT". They both took test measurements as the input, calculated empirical and theoretical wave attenuation coefficients, initial wave height and length, worked out co-ordinates for wave attenuation profile curves, and stored the computed results in different files. In addition, the "PROG" programme calculated the actual and percentage difference between the theoretical and empirical wave attenuation coefficients, and presented all the results plus test parameters in a table. In comparison, the "PROT" programme plotted the wave attenuation profile curves, showed the observed measurements and presented some of the calculation results and test parameters on the graph.

3.4.3.2 The Wide Channel Tests

The necessary "windows" based software was supplied with the Macintosh computer hardware to allow instant on-line analysis. Two software packages were provided. The first - Scope - enabled the Macintosh to emulate a single channel storage oscilloscope, while the second - Chart - performed the task of a 4 channel chart recorder. Both packages were designed for simplicity of use and the system was set up and run using the mouse. For the greater part of the tests the Scope package was employed to provide an immediate graphical presentation of the ensemble averaged measurements on the screen.

CHAPTER 4

LABORATORY TESTS

4.1 Test Parameters

The main test parameters for the present experiments are the water depth, the mean current, the wave period and wave height. Below is a summary of the factors considered in choosing the values of these parameters.

4.1.1 Aspect Ratio

The aspect ratio, defined as the ratio between the channel width and the depth of the flow, should be high enough to ensure the central part of the flow is unaffected by the sidewalls. At the same time, the water level should be large enough to allow measurements at a distance away from the bed where the flow is only slightly affected by it. Further, the water depth should allow the required value of wave height.

In two projects preceding this one, Simons (1980) and Kyriacou (1988) chose a water level of 200 mm for their tests. However, for the present test it was decided to use a 300 mm depth to allow measurements in flow regions that are not dominated by bottom effects. As the width of the channel is 457 mm, the aspect ratio for the main body of the tests in this project was approximately 1.5.

For the narrow channel tests, the objective was to minimise the effect of the bed on wave height attenuation. Calculations based on the formula proposed by Hunt (1952) showed that it would be possible to achieve over 99% wave attenuation due to the sidewalls if the aspect ratio was kept below 0.1. With the water level kept at 300 mm, 3 different values

were chosen for the channel width. These were 10 mm, 20 mm, and 30 mm, giving aspect ratios of 0.022, 0.066, and 0.1 respectively.

4.1.2 Current

The value of the steady current was chosen such that the flow would cover both a wave dominated regime, where $U_c/(u_0+U_c)<0.5$, and a current dominated regime, where $U_c/(u_0+U_c)>0.5$. For reasons that will be discussed later, a single wave height was employed, leading to a small range of u_0. Simple first order calculations showed that the maximum orbital velocities near the boundaries were expected to range between 50 mm/s to 100 mm/s.

It was therefore decided to use a nominal 50 mm/s (weak) current to create a wave dominated regime. To create a current dominated regime, it was necessary to use as large a mean current as possible. After testing the capabilities of the water supply system at the UCL flume, it was proposed that a nominal 140 mm/s (strong) mean current be used. This ensured a u_b/U of well below 1. Considering the range of periodic bed velocities used in the tests, a nominal 90 mm/s (intermediate) mean current was employed to cover the flow range between the wave and current dominated regimes.

For the narrow flume tests, it was impossible to reach a steady velocity of 140mm/s in channels with widths of 30mm or less. However, tests were performed with 50 mm/s and 90 mm/s steady current.

4.1.3 Wave Period

For the purposes of consistency and comparison, the same wave periods as those used by Kyriacou were used; namely 0.7 s, 1 s, and 1.2 s. As the water depth was different in the present tests, a number of checks were carried out to ensure that these wave periods did not cause any difficulties from secondary effects. The presentation of detailed calculations is omitted below and only the conclusions drawn from it are mentioned.

In order to avoid secondary crests, Machemehl and Hebrich (1971) suggested that the ratio of water depth over wave length should be greater than 0.09. Thus with a water depth of 300 mm, the wave lengths should not be larger than 3.3 m.

Similarly, Hansen et. al. (1975) proposed that, to obtain the least distortion of the wave surface profile, the ratio of water depth over wave length should equal 0.15. This can be achieved with a wave period of 1.3 s. To use 0.7s, 1s, and 1.2s periods could result in a ratio of 0.4, 0.29, and 0.17, respectively which observations have shown will not result in any significant distortion of the wave profile. To avoid cross channel effects, wave length should not be equal to twice the channel width or any multiples of it divisible by two. This condition did not create any problem with wave periods of 0.7s, 1.0s, and 1.2s.

From the above considerations it became clear that the wave periods already employed in previous studies could continue to be used for both the narrow and wide channel tests.

4.1.4 Wave Height

The choice of wave height is affected by two limits. On the one hand if the waves are too steep, they will not remain sinusoidal and can break. On the other hand, low waves will be more liable to reflection and reduce the relative sensitivity of the measurements.

The following factors were considered in determining the wave heights. With respect to wave reflections from the beach, Miche suggested, in order to limit the reflection coefficient to below 10%, for a beach slope of 6.2 degrees, the deep water wave steepness should be greater than 9.7×10^{-3}. Stoke's criterion for breaking waves is that the ratio of wave height over wave length should be smaller than 0.143. The limiting value here is given by the shortest wave period and calculations based on that show the wave height should be smaller than 107 mm. Furthermore, Madsen et al. (1970) proposed that the Ursell number ($U_r=HL^2/h^3$) should be less than five to ensure a sinusoidal wave form. Here the largest limit of wave height is given by the longest wave period and consequently, wave height should be smaller than 46 mm.

From the above considerations, it was concluded that a wave height within the range of 2.6 mm to 45 mm would be satisfactory for the purpose of these experiments. For the narrow channel tests the values of 20 mm, 35 mm, and 45 mm were chosen. However the results of these tests in conjunction with those carried out earlier by Simons and Kyriacou showed that it would not be necessary to use more than one wave height for any one wave period for the wide channel tests. Consequently, it was decided to employ only the 40mm wave height for the main set of experiments.

4.2 Experimental Programme

4.2.1 Narrow Flume Tests

All together, some 57 tests were carried out to investigate the effect of sidewalls on wave attenuation, both in the case of waves in still water and current and waves combined. The objective was to obtain wave height attenuation predominantly due to the sidewalls, by keeping the aspect ratio extremely low.

Three different widths for the narrow channel were employed: 10 mm, 20 mm, and 30 mm. For each flume width, wave attenuation was measured for 0.7 and 1.2 second waves, with three different current strengths: 0 mm/s, 50 mm/s, and 100 mm/s. For each combination of waves and current, three tests were performed with approximately 20 mm, 35 mm, and 45 mm average initial wave height.

Below is a full list of all the tests performed in this section of the project.

TEST	Channel Width (mm)	Mean Current Strength (mm/s)	Wave Period (second)	Wave Height (mm)
ADW10.20	10	0	0.7	20
ADW10.35	10	0	0.7	35
ADW10.45	10	0	0.7	45
ASW10.20	10	0	1.2	20
ASW10.35	10	0	1.2	35
ASW10.45	10	0	1.2	45

TEST	Channel Width (mm)	Mean Current Strength (mm/s)	Wave Period (second)	Wave Height (mm)
ADWWC10.20	10	50	0.7	20
ADWWC10.35	10	50	0.7	35
ADWWC10.45	10	50	0.7	45
ASWWC10.20	10	50	1.2	20
ASWWC10.35	10	50	1.2	35
ASWWC10.45	10	50	1.2	45
ADWMC10.20	10	90	0.7	20
ADWMC10.35	10	90	0.7	35
ADWMC10.45	10	90	0.7	45
ASWMC10.20	10	90	1.2	20
ASWMC10.35	10	90	1.2	35
ASWMC10.45	10	90	1.2	45
ADW20.20	20	0	0.7	20
ADW20.35	20	0	0.7	35
ADW20.45	20	0	0.7	45
ASW20.20	20	0	1.2	20
ASW20.35	20	0	1.2	35
ASW20.45	20	0	1.2	45
ADWWC20.20	20	50	0.7	20
ADWWC20.35	20	50	0.7	35
ADWWC20.45	20	50	0.7	45
ASWWC20.20	20	50	1.2	20
ASWWC20.35	20	50	1.2	35
ASWWC20.45	20	50	1.2	45
ADWMC20.20	20	90	0.7	20
ADWMC20.35	20	90	0.7	35
ADWMC20.45	20	90	0.7	45
ASWMC20.20	20	90	1.2	20
ASWMC20.35	20	90	1.2	35
ASWMC20.45	20	90	1.2	45

TEST	Channel Width (mm)	Mean Current Strength (mm/s)	Wave Period (second)	Wave Height (mm)
ADW30.20	30	0	0.7	20
ADW30.35	30	0	0.7	35
ADW30.45	30	0	0.7	45
ASW30.20	30	0	1.2	20
ASW30.35	30	0	1.2	35
ASW30.45	30	0	1.2	45
ADWWC30.20	30	50	0.7	20
ADWWC30.35	30	50	0.7	35
ADWWC30.45	30	50	0.7	45
ASWWC30.20	30	50	1.2	20
ASWWC30.35	30	50	1.2	35
ASWWC30.45	30	50	1.2	45
ADWMC30.20	30	90	0.7	20
ADWMC30.35	30	90	0.7	35
ADWMC30.45	30	90	0.7	45
ASWMC30.20	30	90	1.2	20
ASWMC30.35	30	90	1.2	35
ASWMC30.45	30	90	1.2	45

In the above, the following codes have been used: A for narrow channel tests, DW for deep water waves, SW for shallow waves, WC for weak current, and MC for medium current. Thus, ASWMC30.45 denotes the narrow channel test with shallow waves and medium current which took place in 30 mm wide flume and employing 45 mm initial wave height.

4.2.2 Contamination Tests In the Narrow Channel

In order to investigate the effect of water surface contamination on wave attenuation, tests were performed in the 20 mm wide channel. Altogether four tests were carried out in the closed flume employing deep water waves only. The water in the channel remained the same during the course of these experiments. The first test was done with the channel filled with fresh water. The second test was performed a day later, with the water left in the channel overnight. After 3 days the third test was carried out with the water surface being visibly very "dirty." The fourth test was done immediately afterward, using a wetting agent to "clear" the water surface. The results of these tests are presented in Chapter 5.

4.2.3 Wide Channel Preliminary Tests

A number of preliminary tests was performed in the wide channel in order to familiarise the author with the techniques involved in laser Doppler anemometry.

Following these, two sets of preliminary tests employing the same L.D.A. arrangements as Simons (1980) and Kyriacou (1988) were performed. One measured velocity profiles away from the bed and the other measured velocity profiles away from the sidewall.

4.2.3.1 Velocity Profiles Away From the Bed

Tests were performed on the 100 mm/s unidirectional current to measure velocity profiles at 6 different points across the channel. The purpose of these experiments was to confirm flow symmetry and establish a preliminary understanding of velocity profiles away from the centre of the channel. Measurements were taken at 43 points on a vertical line from the bed through the bottom 200 mm of flow, and at the following distances from the sidewall: 25mm, 72mm, 150mm, 222mm, 290mm, and 330mm. These experiments were, respectively, named, B-BMC25, B-BMC72, B-BMC150, and so on.

4.2.3.2 Velocity Profiles Away from the Sidewall

Again using the same L.D.A. arrangements as Simons (1980) and Kyriacou (1988), a set of 21 tests was performed to measure velocity profiles away from the sidewall at 7 different heights from the bed. The purpose of these experiments was to confirm the results obtained in the previous set, and more importantly, to establish a better understanding of velocity profiles away from the sidewall in wave only, current only and coexistent wave and current regimes. The following table lists the various experiments carried out.

Test	Current Strength (mm/s)	Wave Period (s)	Wave Height (mm)	Distance From Bed (mm)
B-SMC.150	90	0	0	150
B-SMC.75	90	0	0	75
B-SMC.50	90	0	0	50
B-SMC.25	90	0	0	25
B-SMC.10	90	0	0	10
B-SMC.5	90	0	0	5
B-SMC.1	90	0	0	1
B-SIW.150	0	1	35	150
B-SIW.75	0	1	35	75
B-SIW.50	0	1	35	50
B-SIW.25	0	1	35	25
B-SIW.10	0	1	35	10
B-SIW.5	0	1	35	5
B-SIW.1	0	1	35	1
B-SIWMC.150	90	1	35	150
B-SIWMC.75	90	1	35	75
B-SIWMC.50	90	1	35	50
B-SIWMC.25	90	1	35	25
B-SIWMC.10	90	1	35	10
B-SIWMC.5	90	1	35	5
B-SIWMC.1	90	1	35	1

In the above list the following notation is employed: B for L.D.A. beams horizontal, S for tests measuring velocity profiles away from the side wall, MC for medium current, IW for intermediate waves, and the figure after the dot for the measuring distance away from the bed.

4.2.4 Main Test Programme in the Wide Channel

As the L.D.A. arrangement used for the tests described in section 4.2.3 was designed for velocity profile measurements away from the bed of the flume, it was unable to obtain any meaningful readings in the viscous sublayer close to the sidewall of the channel. Thus, the L.D.A. arrangement had to be redesigned as described in chapter 3 to obtain readings in the immediate vicinity of the sidewall.

Tests listed in the above section were repeated for the new system. This confirmed that the new arrangement was working satisfactorily, by validating data against the previous results and ensuring that the two systems were compatible. In practice it was found that the new arrangement could not obtain any accurate readings within the bottom 15 mm layer of the flume.

It was clear that a significant section of the sidewall boundary layer in any flow is influenced by the proximity of the bed. Thus, it was necessary to establish an understanding of the interaction of sidewall and bottom boundary layers. To achieve this, a detailed experimental study of the effect of the height above the bed on the development of the sidewall boundary layer was required. Thus, the following test plan, which concentrated on a limited but representative number of experiments, was adopted:

Test	Wave Period (s)	Current Strength (mm/s)	Wave Height (mm)	Distance From Bed (mm)
C-SWC.20	0	50	0	20
C-SWC.50	0	50	0	50
C-SWC.150	0	50	0	150
C-SMC.25	0	90	0	25
C-SMC.50	0	90	0	50
C-SMC.75	0	90	0	75
C-SMC.150	0	90	0	150
C-SSC.20	0	140	0	20
C-SSC.50	0	140	0	50
C-SSC.150	0	140	0	150
C-SDW.20	0.7	0	40	20
C-SDW.50	0.7	0	40	50
C-SDW.150	0.7	0	40	150
C-SDWWC.20	0.7	50	39	20
C-SDWWC.50	0.7	50	39	50
C-SDWWC.150	0.7	50	39	150
C-SDWMC.20	0.7	90	35	20
C-SDWMC.50	0.7	90	35	50
C-SDWMC.150	0.7	90	35	150
C-SDWSC.20	0.7	140	33	20
C-SDWSC.50	0.7	140	33	50
C-SDWSC.150	0.7	140	33	150
C-SIW.25	1	0	40	25
C-SIW.50	1	0	40	50
C-SIW.75	1	0	40	75
C-SIW.150	1	0	40	150
C-SIWWC.20	1	50	39	20
C-SIWWC.50	1	50	39	50
C-SIWWC.150	1	50	39	150
C-SIWMC.25	1	90	35	25
C-SIWMC.50	1	90	35	50
C-SIWMC.75	1	90	35	75
C-SIWMC.150	1	90	35	150

Test	Wave Period (s)	Current Strength (mm/s)	Wave Height (mm)	Distance From Bed (mm)
C-SIWSC.20	1	140	33	20
C-SIWSC.50	1	140	33	50
C-SIWSC.150	1	140	33	150
C-SSW.20	1.2	0	40	20
C-SSW.50	1.2	0	40	50
C-SSW.150	1.2	0	40	150
C-SSWWC.20	1.2	50	39	20
C-SSWWC.50	1.2	50	39	50
C-SSWWC.150	1.2	50	39	150
C-SSWMC.20	1.2	90	35	20
C-SSWMC.50	1.2	90	35	50
C-SSWMC.150	1.2	90	35	150
C-SSWSC.20	1.2	140	33	20
C-SSWSC.50	1.2	140	33	50
C-SSWSC.150	1.2	140	33	150

Tests with the intermediate waves and medium currents were performed first. On the evidence of the results from these tests, measurements at 75 mm above the bed were omitted from the remaining experiments as it was shown that the form and magnitude of velocities at this height are not significantly different from the ones obtained at 150mm depth tests. For each of the above experiments, the following measurements were made: water level, water temperature, surface velocity, wave period, wave length, wave height at the laser position and along the channel for each wave condition, instantaneous periodic velocity, and mean velocity.

4.2.5 Wave Attenuation Tests

The wave attenuation along the channel was measured for the wave only and the combined wave and current flows in the above tests. Measurements were taken at 100 mm intervals in the following 3 regions along the channel: 1-2 metres (inlet), 3-4 metres (laser), and 7-8 metres (beach).

4.3 Test Procedures

4.3.1 Narrow Flume Tests

As the experiment depended on the reproducibility of the flow conditions, it was necessary to both employ a methodical and reliable laboratory technique, and keep the test environment stable. Thus, the channel sidewalls were regularly cleaned since accumulating dirt would have increased the boundary roughness and resulted in an increase in damping of the waves. The current and wave generating facilities, and the resulting flow were monitored continuously by measuring the initial wave height and current strength at regular time intervals.

To set the water level for the wave only tests, the two outlet pipes were closed, and the required amount of water was supplied through the main inlet valve. Any excess water was drained away. In the case of the combined waves and current tests, the water level was set by using a combination of inlet pipe valve control and lowering or raising bellmouth attachments fitted to the two outlet pipes. In all cases the level was set at the

laser position.

To obtain the true wave height, a computer programme was employed to remove the reflected wave component from the measured wave heights, by fitting a "least square" regression curve through the data. The success of this method depended on taking measurements of the wave heights at closely spaced, regular intervals along the length of the channel, in order to avoid any bias towards the higher or lower values in the curve fitting process.

Wave heights were measured at intervals of 100 mm along the channel, starting from the inlet of the partitioned channel, and ending approximately 2 metres upstream of the beach, thus minimising local reflection effects. As the narrow width of the channel did not allow the use of resistance probes, the measurements were taken manually using a metric scale ruler. Each reading was repeated 3 times and the average value of wave height was noted. The maximum velocity was measured by introducing dye into the flow in the narrow channel, and using a stop watch to find the time the most forward traces of the dye took to travel over a fixed distance.

4.3.2 L.D.A. Tests

The same procedure as that outlined in section 4.3.1 was used to set the current strength and the output of the wave generator. In the course of these experiments, however, the on-line data collection and analysis technique allowed the computer to monitor the output of the wave generator to an accuracy of 10^{-6} V and 10^{-3} s , and to ensure a precise

repetition of test parameters.

The experimental procedure for the measurement of fluid velocities using the present laser anemometer system has been refined over the years by researchers such as Raven (1977), Simons (1980), Stuart (1984), and Kyriacou (1988). They have all described, in great detail, the preliminary checks necessary to ensure that the LDA system was functioning correctly, and the procedure for tuning, focusing, optimizing and obtaining a high quality signal. The same procedures as those outlined by these authors were employed for the present tests and the reader is referred to the papers cited above.

The following measurements were taken for each test:

A. Water Level:

This was measured with a ruler at the laser position. The accuracy of this measurement was +/-0.5 mm.

B. Water Temperature:

This was measured, both before and after each test, with a thermometer with an accuracy of 0.5 degrees centigrade.

C. Surface Velocity:

This was measured by placing a small floating object on the water surface and calculating the time it takes to travel a distance of 5 m along the channel. The velocity was averaged over 3 experiments.

D. Wave Heights:

This was measured by using the resistance probes at the laser position, and analysing the ensemble averaged data on line with the computer system. The probes were calibrated every few days.

E. Wave Period:

This was measured in two ways: first, by monitoring the output of the wave generator with the on line computer system and, second, by analysing the output of the A.D. converter which registers the data collected by the wave probe at the laser position.

F. Velocity measurements within the flow with the L.D.A.:

Measurements were taken at the following distances away from the particular boundary for both bed and sidewall tests:

0.2mm,	0.3mm,	0.4mm,	0.6mm,	0.8mm,	1.0mm,
1.2mm,	1.4mm,	1.6mm,	1.8mm,	2.0mm,	2.3mm,
2.6mm,	3.0mm,	3.5mm,	4.0mm,	4.5mm,	5.0mm,
6.0mm,	7.0mm,	8.0mm,	9.0mm,	10mm,	12mm,
14mm,	16mm,	18mm,	20mm,	22.5mm,	25mm,
30mm,	35mm,	40mm,	50mm,	60mm,	80mm,
100mm,	125mm,	150mm,	175mm,	and 200mm.	

CHAPTER 5

PRESENTATION OF RESULTS

Introduction

This chapter is divided into two sections. The first presents the results of the measurements carried out on the surface of the flow. It provides details of the wave lengths and wave heights measured for each wave condition and compares them with theoretical predictions. It finds the wave height attenuation for each flow condition and establishes the effect of superimposing currents with varying degrees of strengths on the waves. The results of wave height attenuation measurements performed in very narrow channels, are also presented in this part to study the predominant effect of sidewalls. The second section provides details of the L.D.A. velocity profile measurements carried out in current only, waves only and combined flows. It demonstrates the behaviour of the flow motion near and away from both a horizontal (channel bed) and a vertical (sidewall) boundary, and investigates their interaction.

Wherever in this chapter it was necessary to compare the results of an experiment with theoretical predictions, the limits proposed by Le Mehaute (1976) were considered in choosing the valid wave theory. As discussed in chapter four, the waves in the present tests are best described by the Stoke's second order theory according to range of the parameter H/gT^2 and h/gT^2. However, in order to keep the theoretical calculations as simple as possible, it was decided that the flow properties should also be adequately approximated by the linear theory. Thus, in the following all data comparisons are made with the predictions of the first order theory, unless stated otherwise.

The reader should be reminded that although in this chapter the three waves used for the

experiments are consistently referred to as deep, intermediate and shallow water waves, this description is strictly speaking not correct. For the 0.7 second waves, the working range was $0.326<h/L<0.405$, for the 1.0 second waves the range was $0.180<h/L<0.231$, and for the 1.2 second waves the range was $0.148<h/L<0.176$. Thus, all the tests were within the range of $0.05<h/L<0.5$, and should have been classified as intermediate depth waves. However, as the aim of this research was to make further progress on the investigation carried out by Kemp and Simons (1982) and Simons, Grass and Kyriacou (1988), it was important to employ the same wave periods as they had chosen for their experiments. Consequently, it was decided to accept their argument that tests in the upper and lower bounds of the programme had approached deep and shallow water conditions respectively.

In order to be able to carry out comparisons between different test conditions, it was necessary to be consistent throughout this study. Thus, in this chapter a number of common reference parameters are used depending on which results are being described. For instance, although the wave lengths and wave heights changed according to the strength of the superimposed currents, the energy input of each category of waves (0.7s, 1.0s, or 1.2s) remained constant. This was achieved by keeping the paddle excursion amplitude and rate constant throughout the tests for each wave period, for respective waves alone and combined flows.

SURFACE MEASUREMENTS

5.1 Wave length And Wave Height Measurements

Wave lengths and wave heights were measured for all the waves only and combined waves and current test conditions. The method employed was described in detail in chapter four. For each experiment, wave length measurements were taken along the length of usually three waves, centred about the laser position, to obtain an average value. The wave heights were recorded through the passage of 100 waves at the laser position only.

Many researchers in the past have demonstrated the stretching effect of increasing steady current on the waves. Thus, here the figures related to this effect are included briefly simply to present the results of this study.

Table 5.1. presents the measured wave lengths for all the flow conditions used during this study. It also shows a value predicted by the first order theory and computed by a user written software. The software employed a simple iteration technique to solve the dispersion relation. For combined flows, it used a frame of reference moving with the current and a relative angular frequency to calculate the wave length. The last column of the table shows the percentage discrepancy between the experimentally obtained wave lengths and those predicted from the linear wave theory. As can be seen, the difference between the two values is negligible. In general however, the theoretical predictions of wave lengths for waves alone compared better with the measured value than in the case of the combined flows. The percentage increase in wave length due to the addition of a current does not become more prominent with the increase in the wave period.

	Steady Current (nominal, mean) mm/s	Wavelength measured mm	Wavelength predicted mm	Discrepancy %
0.7s waves	0	740	755	2%
	50	780	816	4%
	90	820	852	4%
	140	915	898	-2%
1.0s waves	0	1300	1320	2%
	50	1370	1443	5%
	90	1450	1478	2%
	140	1650	1541	-7%
1.2s waves	0	1700	1718	1%
	50	1800	1837	2%
	90	1820	1884	3%
	140	2030	1971	-3%

Table 5.1 Comparison between measured wavelengths and those predicted by the linear theory.

During the test programme, the amplitude of the waves reduced with increasing current strength. Table 5.2. shows the measured wave heights for each test condition, and demonstrates the percentage reduction in the wave heights due to the addition of the currents. It is clear from the data presented in the table that the larger the wave period, the smaller is the reduction in the wave height with increasing strength of the current. This is illustrated in figure 5.1 which plots the ratio of wave heights in combined flows over that in still water against the maximum steady current for the three wave periods.

Kemp and Simons (1982) carried out a series of tests which measured lengths of waves of equal period but varying wave height. They observed that the length of the waves increased with wave height. The tendency was not noticeable in the present study as the superimposition of stronger currents reduced the wave height and increased the wave length at the same time, by "stretching" the waves. In any case, the linear theory used for computations in this investigation would not have been able to predict the increase in wave length observed by Simons. Stokes' third order theory does account for such a trend, but it was thought that the phenomenon is not significant enough to justify over-complicating the calculation procedures by employing a third order solution.

5.2 Mean Water Surface Slope Measurements

The slope of the mean water surface was obtained for each wave condition in the following manner. In the process of recording the wave height attenuation along the length of the channel, resistance probes measured the movement of the water level at intervals of

	Steady Current mm/s	Wave-Height mm	Reduction %
0.7s waves	0	40	0%
	50	39	-3%
	90	35	-13%
	140	30	-25%
1.0s waves	0	40	0%
	50	38	-5%
	90	36	-10%
	140	33	-18%
1.2s waves	0	40	0%
	50	39	-3%
	90	35	-13%
	140	34	-15%

Table 5.2 Measured wave height for all test conditions and the percentage reduction due to the addition of currents; B=457mm.

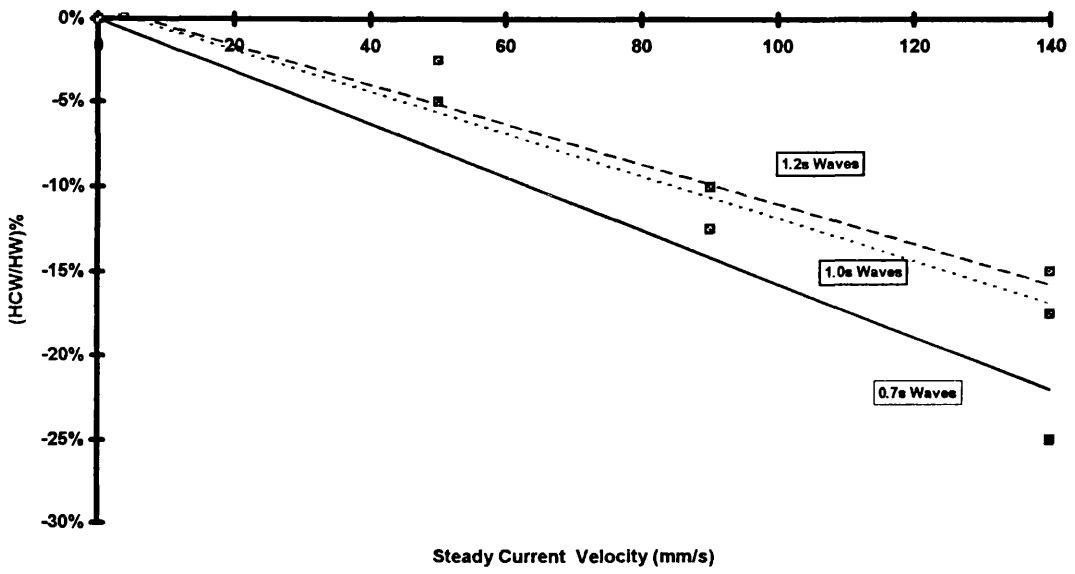

Figure 5.1 The effect of current on the ratio of wave heights in the combined flows over that in still water, for the three waves; B=457mm

100 mm along three different regions of the channel. Consequently, the computer software calculated the mean water level at each measuring position from the collected data. The measurement system was calibrated to take account of the imperfections of the channel by measuring the mean water level in still water, and employing the result as a calibrating factor for each measurement position. Figure 5.2. shows how the true mean water level was obtained by subtracting the measurements in the still water from those in the flow. A straight decay line was fitted through the mean water levels obtained along the channel, and the slope of the line was calculated by the software.

Figure 5.3. compares the gradient of the water surface in closed channel and in flows of varying strength for the 0.7 second waves. Figures 5.4. and 5.5. present the results for the intermediate and shallow water waves respectively. Table 5.3. presents the gradient of the mean water level for all the test conditions. The results however, should be treated with caution. As can be seen from the table and the graphs, the change in mean water level was at most a few millimetres along a working span of over 8 metres, which made measurements with the available instruments difficult. Due to this limitation, each test was repeated a number of times to minimise the uncertainties involved in the measurements. Figure 5.6. shows the trend in the gradient of the water surface with increasing steady current strength for the 0.7s, 1.0s, and 1.2 s waves.

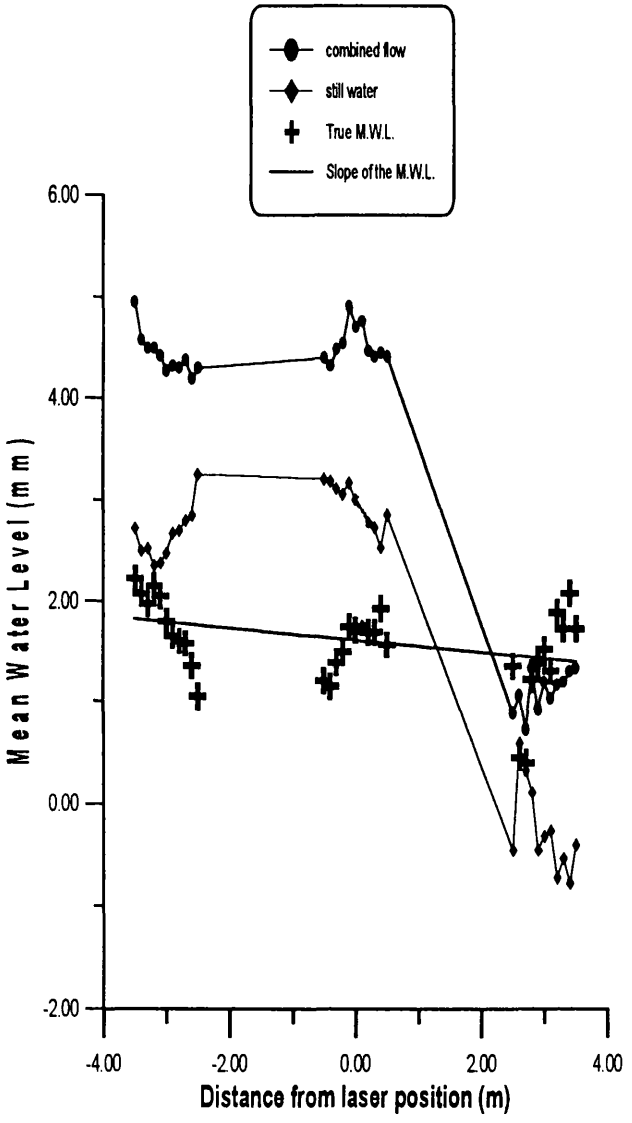

Figure 5.2 Mean water level calibration by subtracting the MWL measured in the still water from that in the flow.

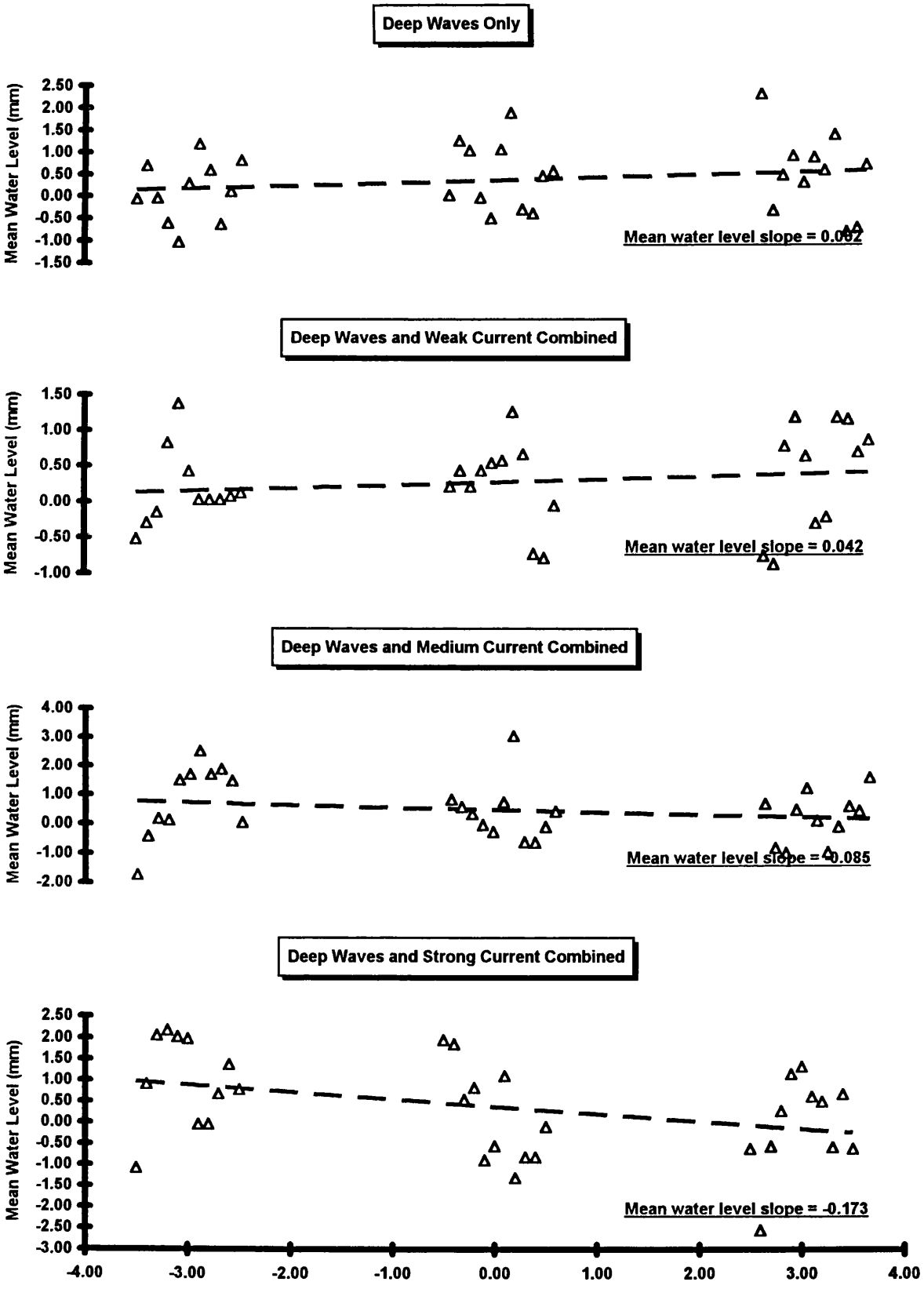

Figure 5.3 The slope of the mean water level along the channel for waves in still water and combined flows; T = 0.7s

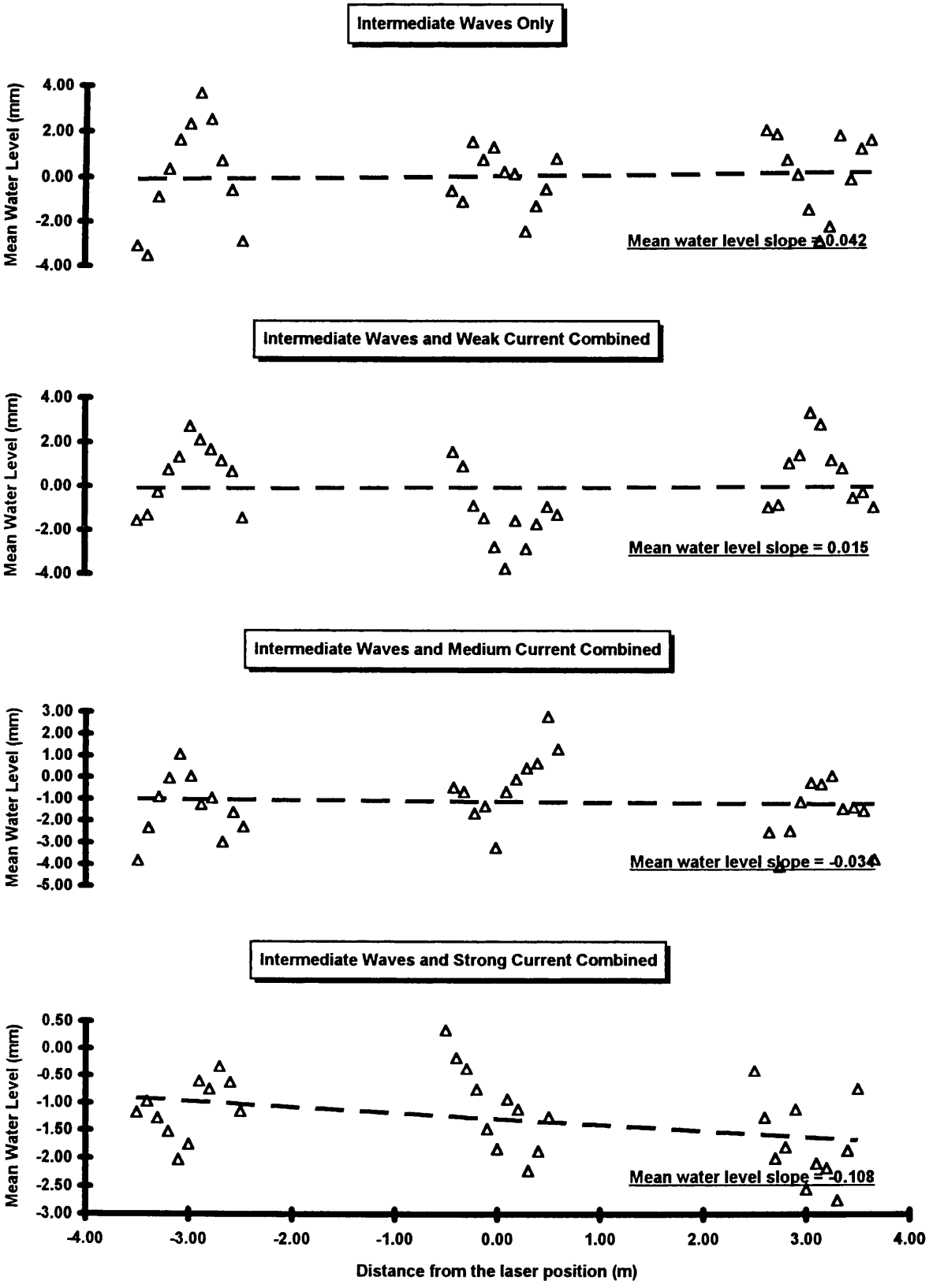

Figure 5.4 The slope of the mean water level along the channel for waves in still water and combined flows; T = 1.0s

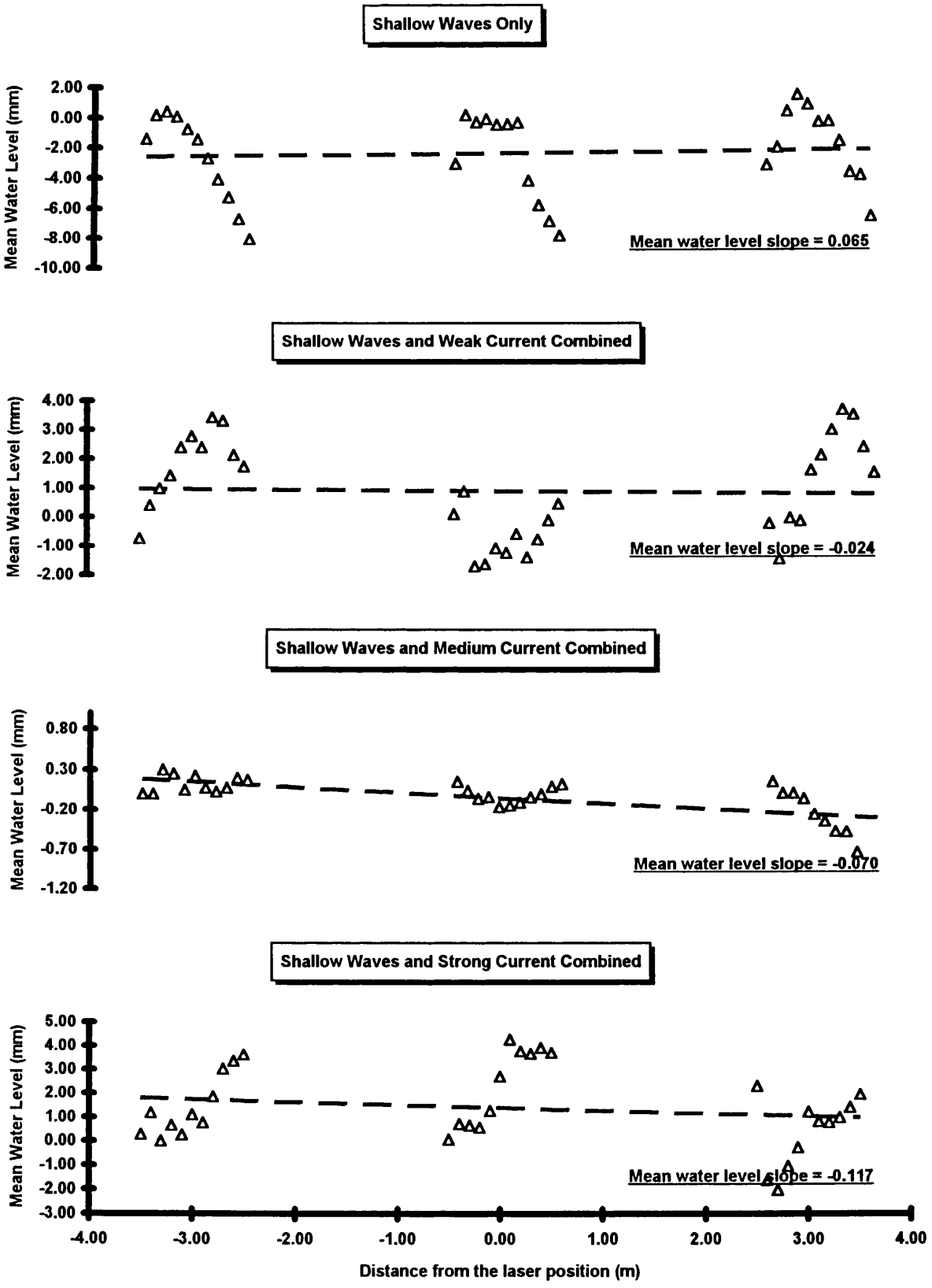

Figure 5.5 The slope of the mean water level along the channel for waves in still water and combined flows; T = 1.2s

	Steady Current mm/s	Mean Water Level Slope
0.7s waves	0	0.062
	50	0.042
	100	-0.085
	180	-0.173
1.0s waves	0	0.042
	50	0.015
	90	-0.034
	140	-0.103
1.2s waves	0	0.065
	50	-0.024
	90	-0.070
	140	-0.117

Table 5.3 Measured mean water level slope for the three waves in still and combined flows

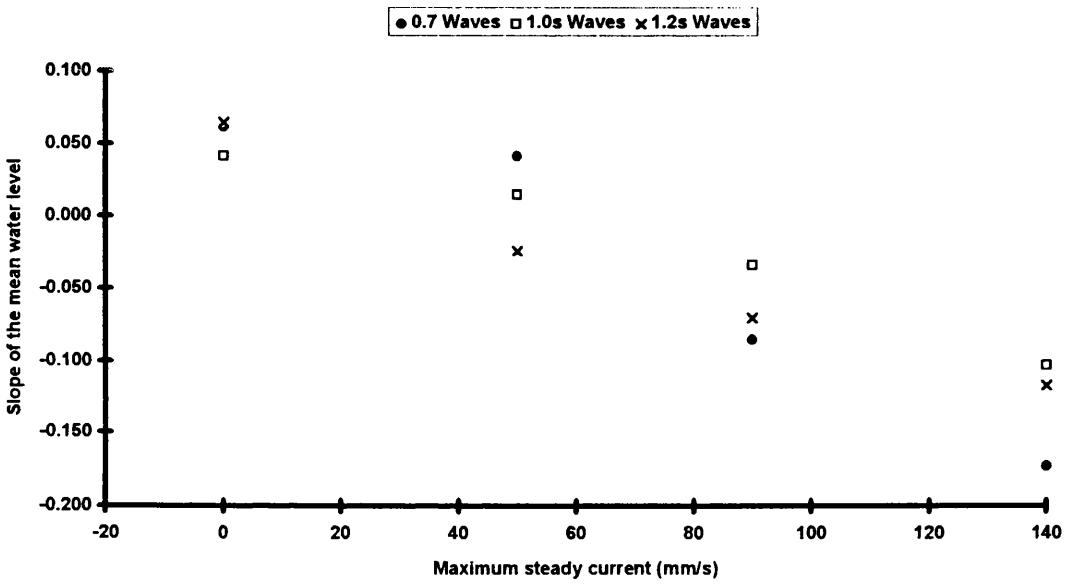

Figure 5.6 The trend in the slope of the MWL for the 0.7s, 1.0s, and 1.2s waves

5.3 Wave height Attenuation Measurements

Section 5.3.1 considers the effect of water surface contamination on wave height attenuation. Section 5.3.2 presents the results of the wave height measurements for the full width channel. Additional tests were performed for similar flow conditions in very narrow channels to minimise the effect of the bottom boundary. The results of these tests are presented in section 5.3.3.

5.3.1 Effect Of Surface Contamination On Wave Damping

Water surface contamination can markedly affect wave height attenuation. Observations during the course of the experiments showed that the water in the channel rapidly formed a surface film. This to some degree was attributed to the fact that the water used for the tests was from a recirculating laboratory supply. Van Dorn (1966) however, discovered that even initially clean water will quickly form a surface film. Sleath (1984) states that there does not seem to be any satisfactory way of estimating the effect of surface contamination in advance. Thus, to ensure continuity through the experiments, it was necessary to use a wetting agent to keep the water surface constantly clean.

A series of experiments was performed in the narrow channel to demonstrate the effect of surface contamination on wave height damping and the effectiveness of cleaning agents. Table 5.4. summarises the results of the water surface contamination experiments. It shows the wave height attenuation for each test and the percentage increase in damping with increasing water surface contamination. Test ADW20.35-1 was performed with fresh water, ADW20.35-2 done a day after, ADW20.35-3 was carried out on the 4th day,

TEST CODE	Period of Contamination Day	Attenuation Coefficient X 0.0001	Percentage Change %
A-DW20.35-1	1	2.31	0.0%
A-DW20.35-2	2	2.41	4.3%
A-DW220.35-3	4	2.68	16.0%
A-DW20.35-4	Detergent Applied	2.35	1.7%

Table 5.4 The effect of water surface contamination on wave damping

and finally ADW20.35-4 was performed after "cleaning" the water surface with a wetting agent.

5.3.2 Wave Height Attenuation in the Wide Channel

Wave height attenuation was measured in the 457 mm wide channel for all the flow conditions in the test programme. Measurements were taken by resistance probes at 100 mm intervals in three regions along the channel. These were at between -3.5m to -2.5m upstream from the laser position, -0.5m to 0.5m at the laser position, and between 2.5m and 3.5m downstream of the laser position. The data were recorded and an ensemble averaged value for 100 waves was computed for each measurement by the on line data analysis system. The results for each test were plotted on graphs of wave height against distance along the channel. Figure 5.7 shows an example of one such graph.

To compare wave damping in various flow conditions, it was necessary to choose a common mean for quantifying wave decay. Since it was shown that wave heights should decay exponentially along the channel in wave only laminar flows, researchers such as Biesel (1949), Hunt (1952) and Treloar and Brebner (1970) fitted their data with the exponential damping expression $H=H_0e^{-\alpha x}$. In the formula, "H" is the Wave height at a distance "x" from the inlet, and "H_0" is the initial Wave height. Thus, they were able to obtain a coefficient for Wave height attenuation to act as a measure of wave damping in various wave only regimes. The exponential decay theory has been derived for wave only conditions and a similar theory that is applicable to the combined wave and current flows

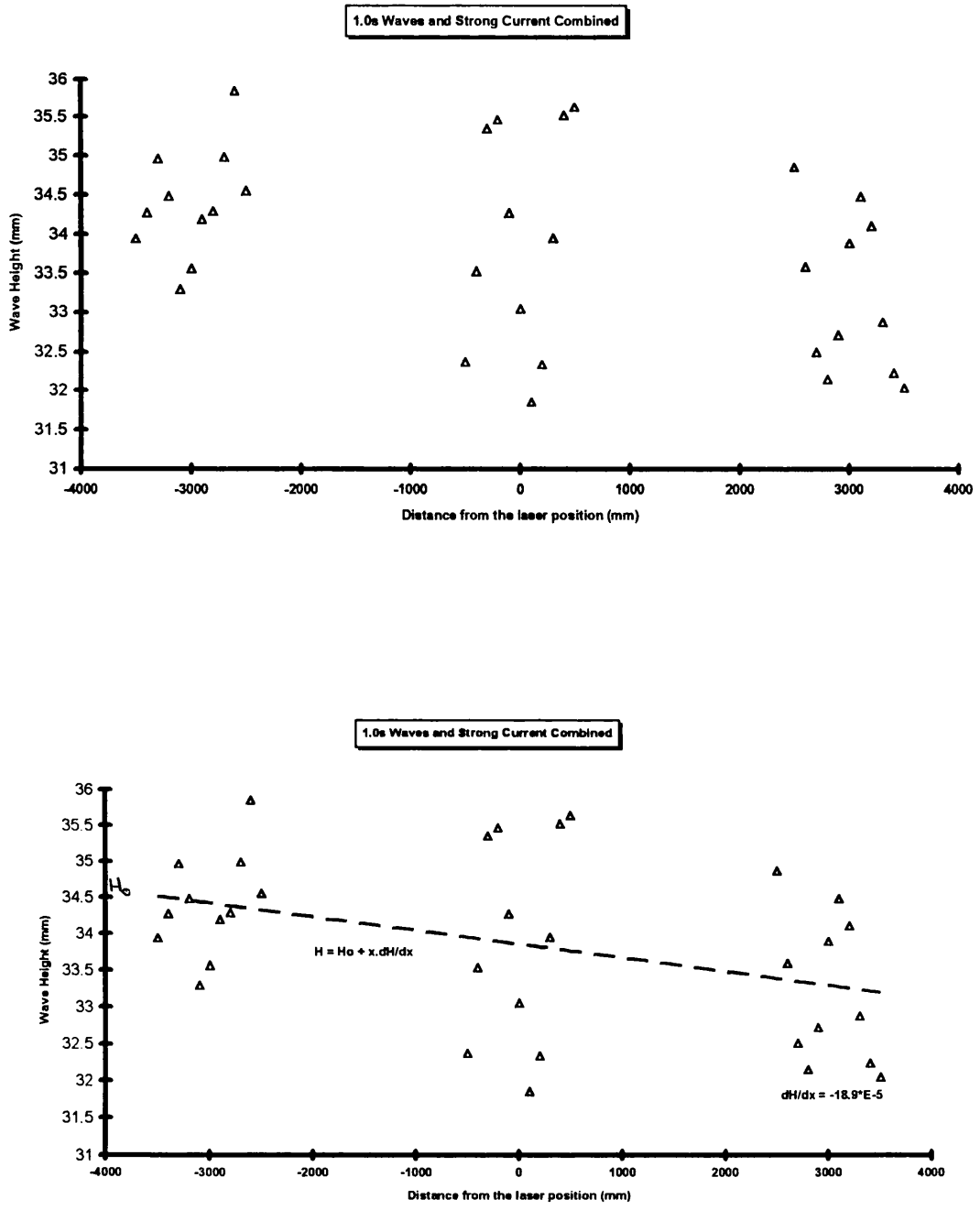

Figure 5.7 Atypical example of wave damping measurements, and the evaluation of initial wave height and the rate of wave attenuation along the wider channel; Test SIWSC.150, T=1.0s and Uc = 140mm/s

does not exist. Many past researchers who worked on wave height attenuation in combined flows, such as van Hoften and Karaki (1976), Brevik and Aas (1980), and Kemp and Simons (1982) overcame the problem by assuming that the exponential damping formula was still valid. For the purposes of this study however, it was decided that this approach is not appropriate since the flow was turbulent. Thus, the "wave attenuation equations", presented in Chapter two, evaluates wave height attenuation in terms of the dimensionless parameter, dH/dx. This could be obtained directly from the experimental data by fitting a straight decay line, $H=H_0+x.dH/dx$, through the measured wave heights. Both the initial wave height and the rate of wave height decay with distance along the channel could then be directly read from the prepared graphs of H against x. Figure 5.7 shows how these values are quantified. Kyriacou (1988) employed both the linear and the exponential curve fits for his data and found that the two approaches generally produced the same values for the initial wave height, the wave height at the laser position, and for dH/dx. Any discrepancies were not greater than 1%.

Figure 5.8 shows the wave height decay for the deep water waves alone and compares it with the attenuation for the same waves combined with 50mm/s, 90mm/s and 140mm/s steady current. It demonstrates a decrease in wave height attenuation with the superposition of stronger currents. This trend agrees with the conclusion of previous researchers who also found a reduction of wave damping in waves combined with a following current. Figures 5.9 and 5.10 present the same comparison for the intermediate waves and the near shallow water waves. Each measurement was repeated a number of times, and the illustrated data represent the averaged results achieved. Table 5.5. summarises the result of all the wave attenuation tests. It shows the wave height at the

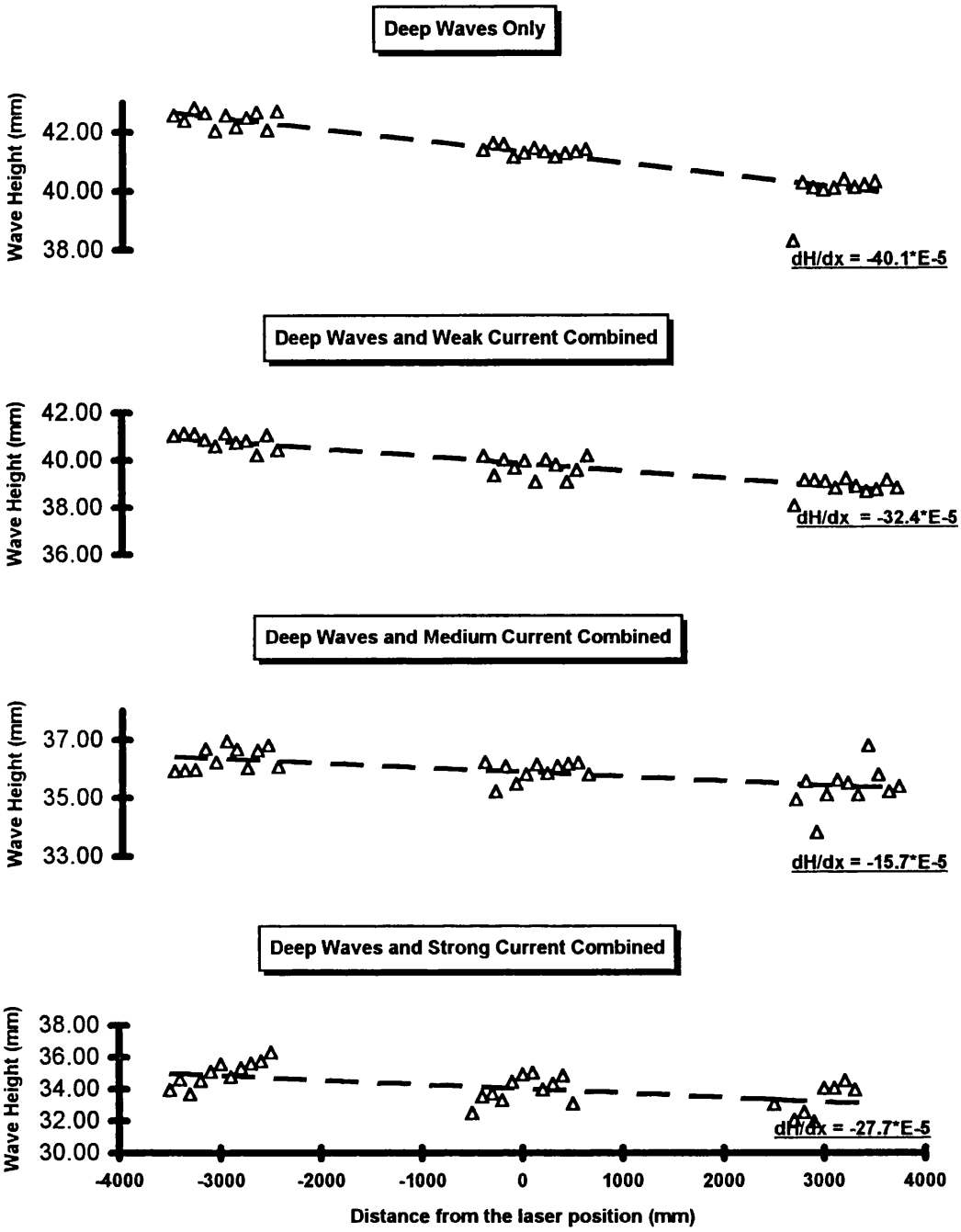

Figure 5.8 Comparison between wave height attenuation in still water and combined flows for the 0.7s waves

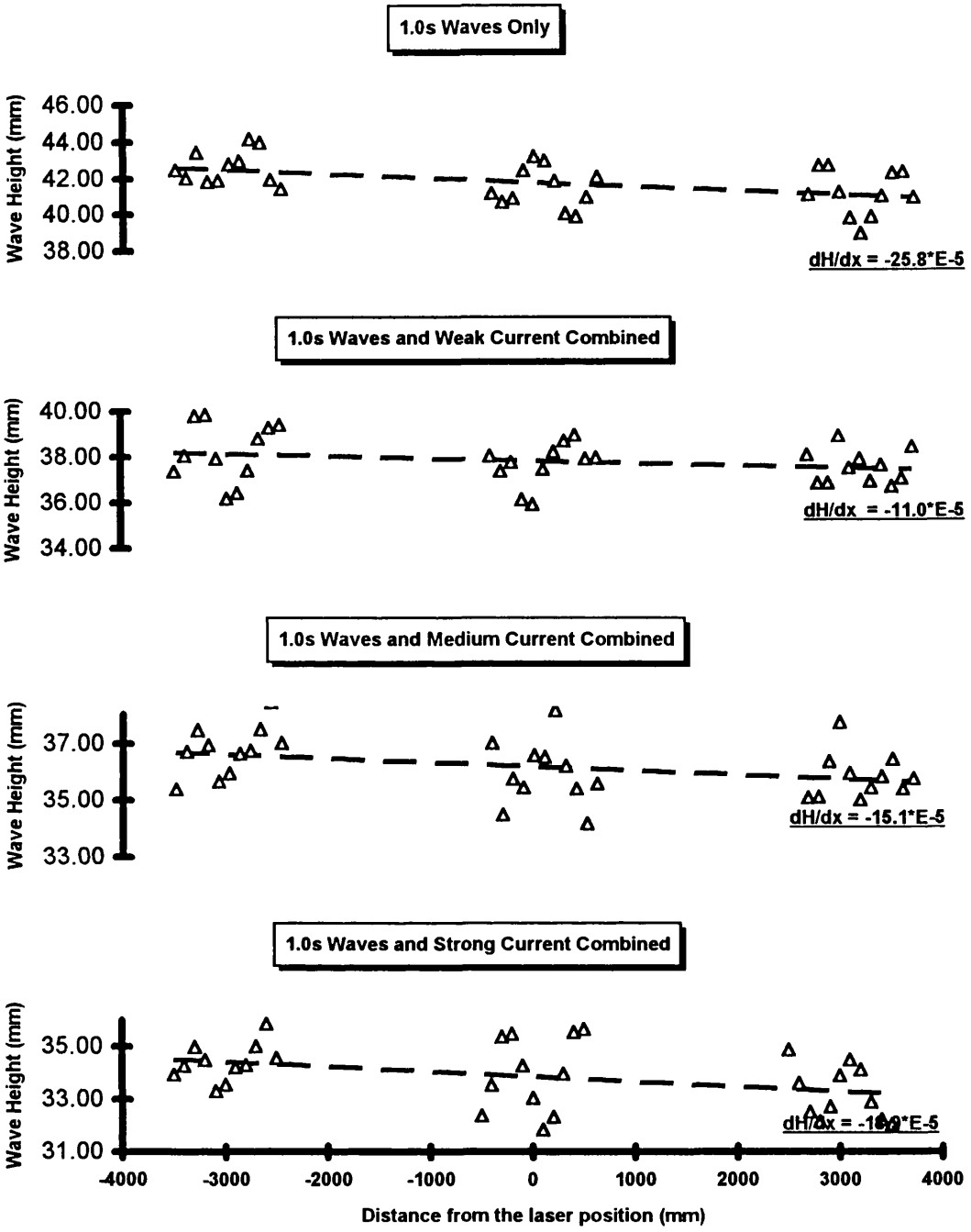

Figure 5.9 Comparison between wave height attenuation in still water and combined flows for the 1.0s waves

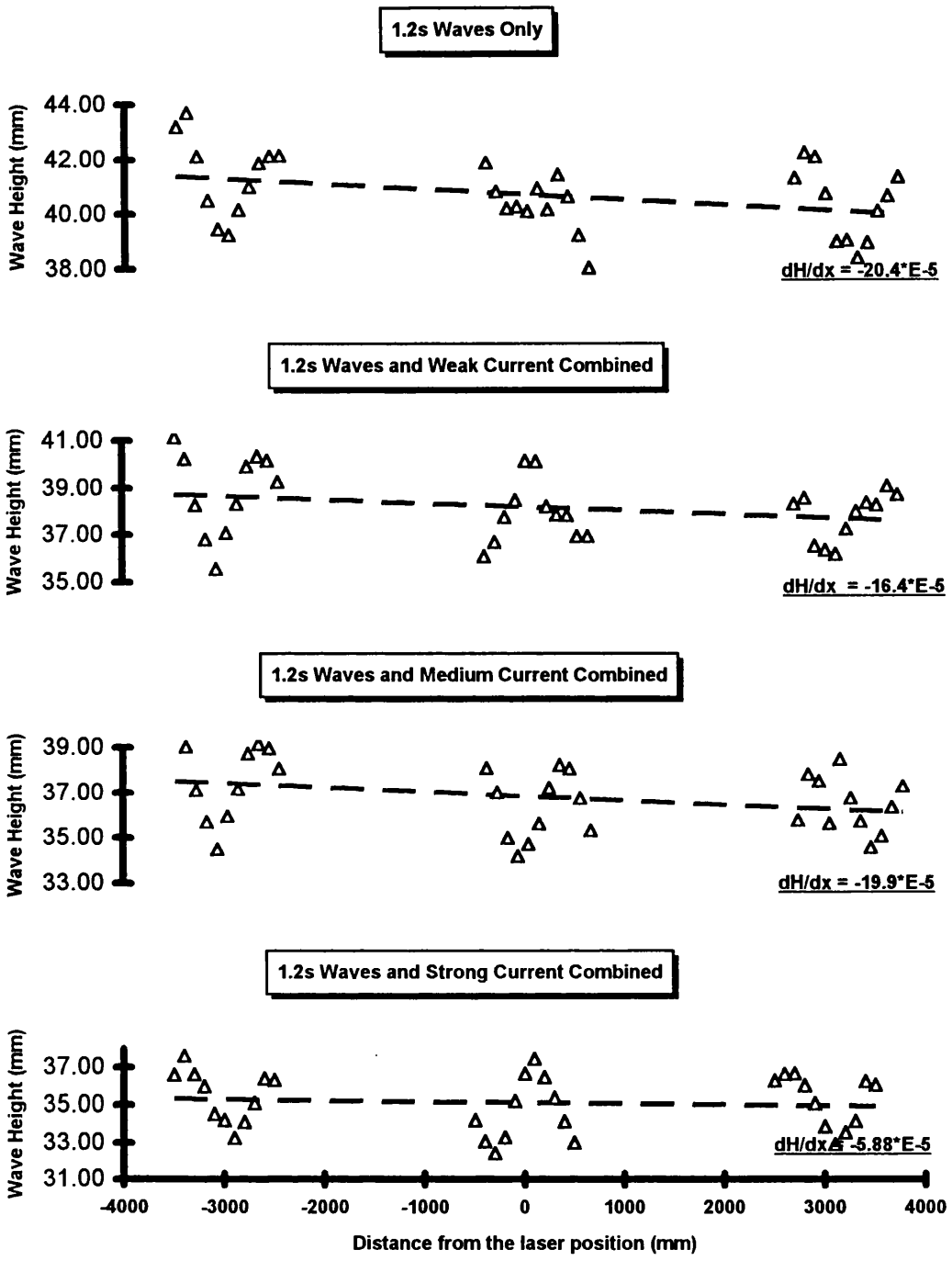

Figure 5.10 Comparison between wave height attenuation in still water and combined flows for the 1.2s waves

laser position, the initial wave height, the rate of decay of wave height with distance along the channel, the change in wave height per wave length, and the attenuation coefficient for each flow condition. The attenuation coefficient is obtained from the relationship $\alpha=-(1/H_0).dH/dx$.

It was shown in section 3.1 that the length of the waves increased with the addition of currents. This phenomenon had to be taken into account for comparison of the data from the wave alone and the combined flow tests. Thus, table 5.5. also presents the wave height loss per wave length, which is calculated as $dH/L = dH/dx \, . \, dx/L$

5.3.3 Wave height Attenuation In The Narrow Channels

As described in chapter four, wave height attenuation was measured in three narrow channels of 10 mm, 20 mm, and 30 mm width to investigate the effect of the sidewalls and changing aspect ratio on wave damping. For experiments in each channel, two different wave periods of 0.7s and 1.2s were used in combination with three values of steady current (0 mm/s, 50 mm/s, and 90 mm/s). Three initial wave heights of 20mm, 35mm, and 45mm were used for each combination of waves and currents. Wave heights were measured at intervals of 100 mm along the channels, starting from the inlet of the partitioned channel and ending approximately 2 metres upstream of the beach, thus minimising reflection effects. As the narrow width of the channels did not allow the use of resistance probes, the measurements were taken using a ruler positioned vertically on the channel wall.

TEST CODE		U mm/s	L mm	Ho mm	dH/dx *E - 5	dH/L *E - 3	α *E - 3
0.7s waves		0	740	40.0	-40.10	-2.97	10.03
		50	780	40.0	-32.40	-2.53	8.10
		90	820	40.0	-15.70	-1.29	3.93
		140	908	40.0	-27.70	-2.52	6.93
1.0s waves		0	1300	40.0	-25.80	-3.35	6.45
		50	1370	40.0	-11.00	-1.51	2.75
		90	1450	40.0	-15.10	-2.19	3.78
		140	1650	40.0	-18.90	-3.12	4.73
1.2s waves		0	1700	40.0	-20.40	-3.47	5.10
		50	1800	40.0	-16.40	-2.95	4.10
		90	1820	40.0	-19.90	-3.62	4.98
		140	2030	40.0	-5.88	-1.19	1.47

Table 5.5 Wave height attenuation parameters for various flow conditions in the wide channel; B = 457 mm.

A graphical presentation of wave height attenuation along the length of the channel was produced for each test. User written software (described in chapter 4) evaluated the theoretical (Hunt 1952) and empirical wave height attenuation coefficients, and the percentage difference between them. Figure 5.11 shows a typical example of graphs produced for all the tests performed. The lower exponential line is obtained from the experimental data presented in the figure, while the upper line is the Hunt prediction of wave height attenuation. In some cases, the experimental results had to be corrected analytically. Figure 5.12 demonstrates one such case, where the exaggerated data at 700mm along the channel and the collapse of the Wave height near the beach (after 4000mm downstream) resulted in a gross discrepancy between the theoretical and empirical wave height attenuation. Ignoring both the 700mm data and those after 4000mm lead to a much more acceptable discrepancy.

Comparisons between the empirically obtained attenuation coefficients and those calculated from the formula proposed by Hunt (1952) and Treloar and Brebner (1970) showed that Hunt gives a better estimate. Figure 5.13 demonstrates this comparison for one of the tests. Thus, Hunt's expression was used as the theoretical model for comparison with test results. Tables 5.6, 5.7, and 5.8 present the results of the tests in 10mm, 20mm and 30mm wide channels respectively. In addition to the attenuation coefficient and the rate of wave height attenuation along the channel, the tables show the test parameters for each experiment. Figure 5.14 demonstrates how the wave damping increases with the reduction in the aspect ratio.

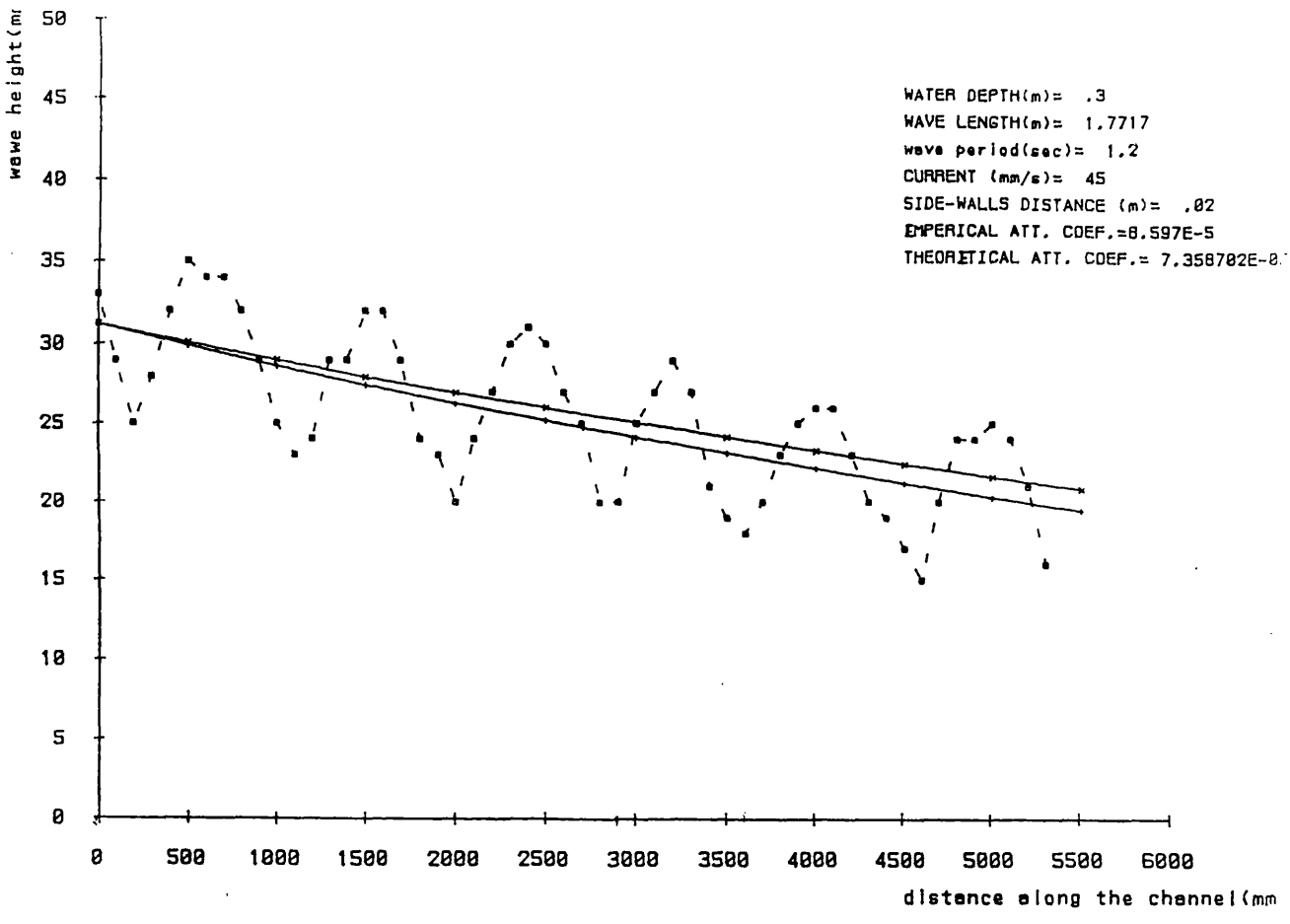

Figure 5.11 Example of wave height attenuation along the narrow channel; graph produced by an user-written software.

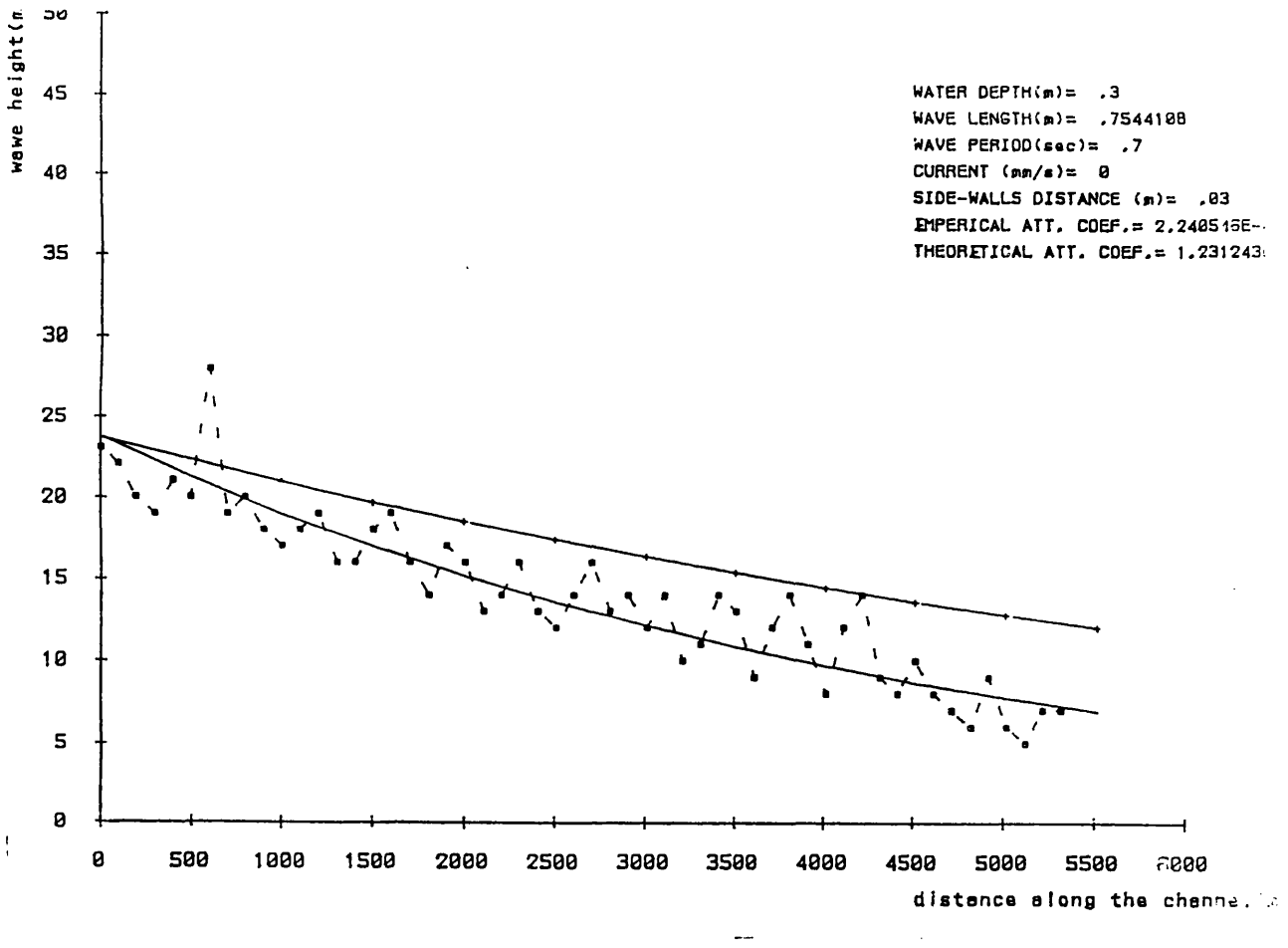

Figure 5.12 Example of a wave height attenuation profile along the narrow channel which required data manipulation.

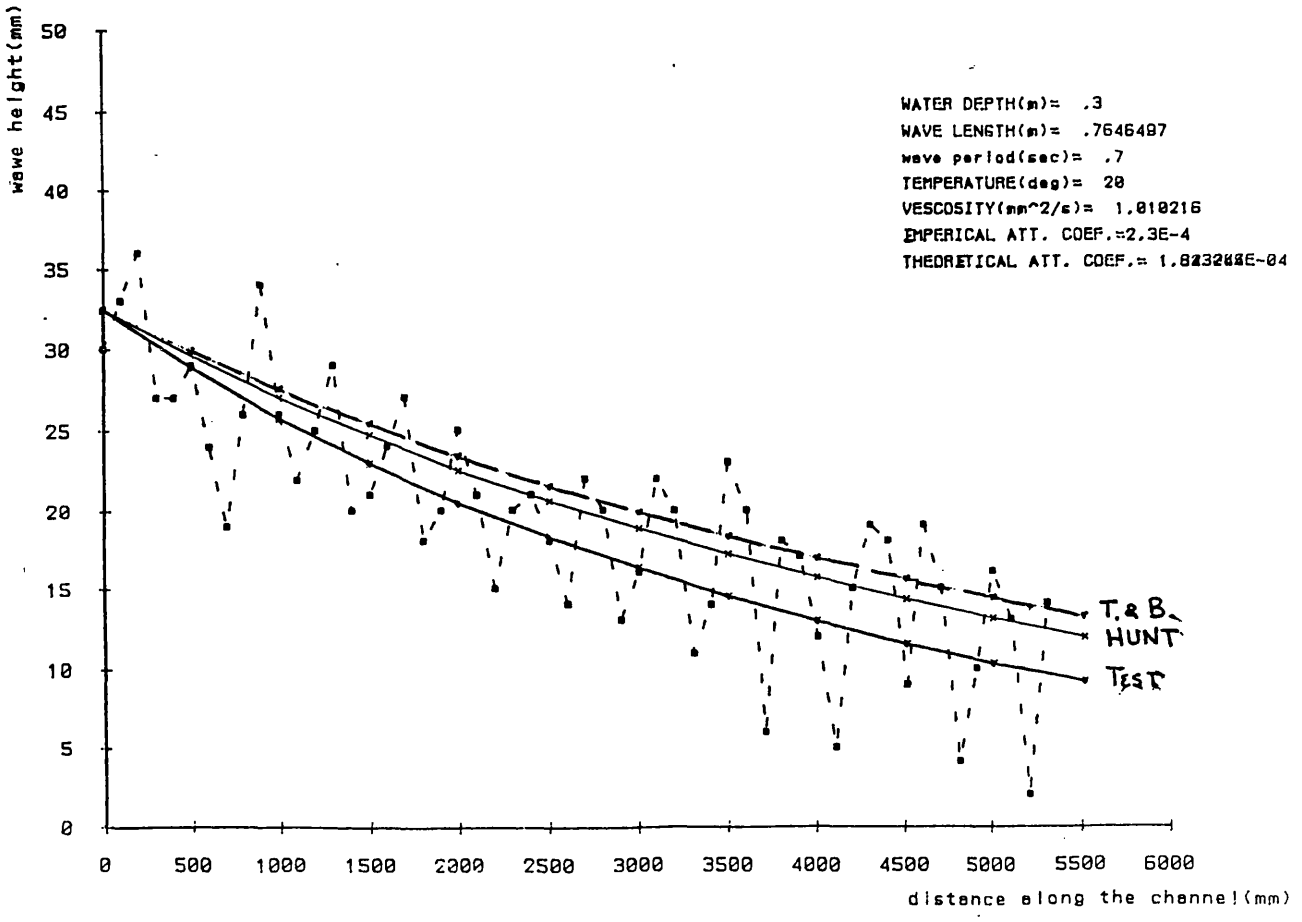

Figure 5.13 Comparison between the measured wave height damping and the predictions of Hunt (1952), and Treloar and Brebner (1973).

test Code	B mm	T 1/s	Uc mm/s	Ho mm	α *E-3
ADW10.20	10	0.7	0.00	18	430.00
ADW10.35	10	0.7	0.00	33	419.00
ADW10.45	10	0.7	0.00	50	430.00
ADWWC10.20	10	0.7	50	19	390.00
ADWWC10.35	10	0.7	50	34	400.00
ADWWC10.45	10	0.7	50	48	410.00
ADWMC10.20	10	0.7	90	20	373.00
ADWMC10.35	10	0.7	90	34	385.00
ADWMC10.45	10	0.7	90	47	390.00
ASW10.20	10	1.2	0.00	18	188.00
ASW10.35	10	1.2	0.00	32	189.00
ASW10.45	10	1.2	0.00	47	190.00
ASWWC10.20	10	1.2	50	17	180.00
ASWWC10.35	10	1.2	50	32	182.00
ASWWC10.45	10	1.2	50	47	185.00
ASWMC10.20	10	1.2	90	18	150.00
ASWMC10.35	10	1.2	90	31	156.00
ASWMC10.45	10	1.2	90	41	160.00

Table 5.6 Flow parameters for tests in 10 mm wide channel.

test Code	B mm	T 1/s	Uc mm/s	Ho mm	α *E-3
ADW20.20	20	0.7	0.00	20	230.00
ADW20.35	20	0.7	0.00	33	220.00
ADW20.45	20	0.7	0.00	48	222.00
ADWWC20.20	20	0.7	50	21	210.00
ADWWC20.35	20	0.7	50	37	201.00
ADWWC20.45	20	0.7	50	50	210.00
ADWMC20.20	20	0.7	90	22	187.00
ADWMC20.35	20	0.7	90	41	188.60
ADWMC20.45	20	0.7	90	48	181.00
AIWMC20.20	20	1.0	0.00	19	127.00
AIWMC20.35	20	1.0	0.00	33	125.00
AIWMC20.45	20	1.0	0.00	51	131.00
ASW20.20	20	1.2	0.00	18	94.00
ASW20.35	20	1.2	0.00	32	93.00
ASW20.45	20	1.2	0.00	48	95.00
ASWWC20.20	20	1.2	50	19	85.00
ASWWC20.35	20	1.2	50	32	86.00
ASWWC20.45	20	1.2	50	48	87.00
ASWMC20.20	20	1.2	90	18	78.50
ASWMC20.35	20	1.2	90	32	80.00
ASWMC20.45	20	1.2	90	52	74.00

Table 5.7 Flow parameters for tests in the 20 mm wide channel.

test Code	B mm	T 1/s	Uc mm/s	Ho mm	α *E-3
ADW30.20	30	0.7	0.00	23	172.00
ADW30.35	30	0.7	0.00	32	162.20
ADW30.45	30	0.7	0.00	51	165.00
ADWWC30.20	30	0.7	50	21	147.70
ADWWC30.35	30	0.7	50	32	160.00
ADWWC30.45	30	0.7	50	45	156.00
ADWMC30.20	30	0.7	90	20	130.00
ADWMC30.35	30	0.7	90	36	156.00
ADWMC30.45	30	0.7	90	51	131.00
ASW30.20	30	1.2	0.00	21	64.00
ASW30.35	30	1.2	0.00	35	62.00
ASW30.45	30	1.2	0.00	50	69.00
ASWWC30.20	30	1.2	50	19	62.00
ASWWC30.35	30	1.2	50	34	60.00
ASWWC30.45	30	1.2	50	48	66.00
ASWMC30.20	30	1.2	90	20	56.20
ASWMC30.35	30	1.2	90	34	62.00
ASWMC30.45	30	1.2	90	47	66.00

Table 5.8 Flow parameters for tests in the 30 mm wide channel.

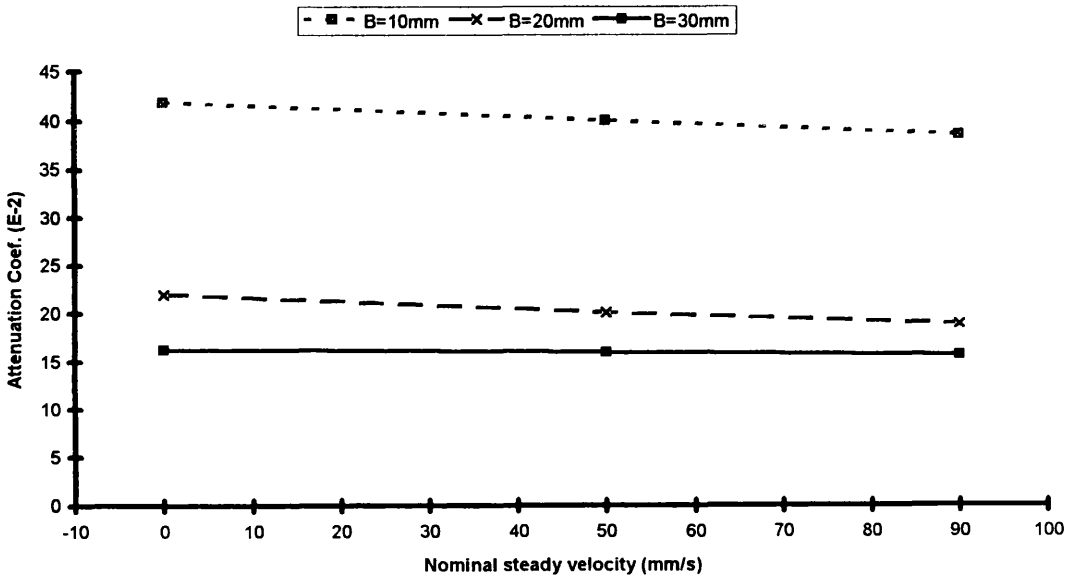

Figure 5.14 Comparison between wave damping in the three channels; T=0.7s

The rest of this chapter presents the results of the Laser Doppler Anemometry measurements, primarily aimed to investigate the flow behaviour near a vertical solid boundary. First, a brief section 5.4 reports the results of the velocity profile measurements from the bottom boundary. The aim of these tests was to establish an initial understanding of the effect of the sidewalls on the flow. Section 5.5 will then present the results of the tests on the vertical boundary for unidirectional, waves only and combined flows.

5.4. Velocity Profile Measurements From the Bottom Boundary

A set of identical velocity profile measurements away from the bed but at various distances from the sidewalls was made in order to assess the influence of the vertical boundary on the flow. In addition, these tests served as a checking measure for the new transverse L.D.A. measurements, described in the next section. Streamwise velocity profiles away from the bed were measured at 25 mm, 72 mm, 150 mm, 222 mm, 290 mm, and 330 mm distances from the sidewall. Only a unidirectional steady current with surface velocity of 90 mm/s was employed at this stage. As the width of the channel was 457 mm, tests carried out at distances of 290 mm and 330 mm from one sidewall were respectively 167 mm and 127 mm away from the other.

Figure 5.15 presents the velocity profiles measured at various intervals from the sidewalls. As expected there is a clear increase in mean velocity with distance from a vertical boundary. Since the velocity profiles at equal distances from the two sidewalls are almost identical, the figure also confirms the flow symmetry about the centre of the channel. In all cases however, there was a reduction in velocity in the upper half of the flow. This retardation when approaching the free surface was due to the three dimensional nature of the flow in a flume with such low aspect ratio.

Table 5.9 summarises the mean flow properties. In the case of each profile, the kinematic viscosity was calculated from the water temperature. The mean shear stress was computed from the velocity gradient in the viscous sublayer and, consequently, the bed shear velocity was calculated from the shear stress. As expected bed shear stress and shear velocity increase with distance from the wall boundary. The value of Von Karman's constant for each experiment was obtained from the slope of the logarithmic layer. These values were different from that found by Nikuradse and generally quoted as 0.4, but were in agreement with those obtained by Kyriacou (1988). It is interesting to note that both these tests and those performed by Kyriacou were conducted at Reynolds numbers in the range of 10^3 and 10^4, while Nikuradse's experiments were in general for higher Reynolds numbers of order 10^5 and above.

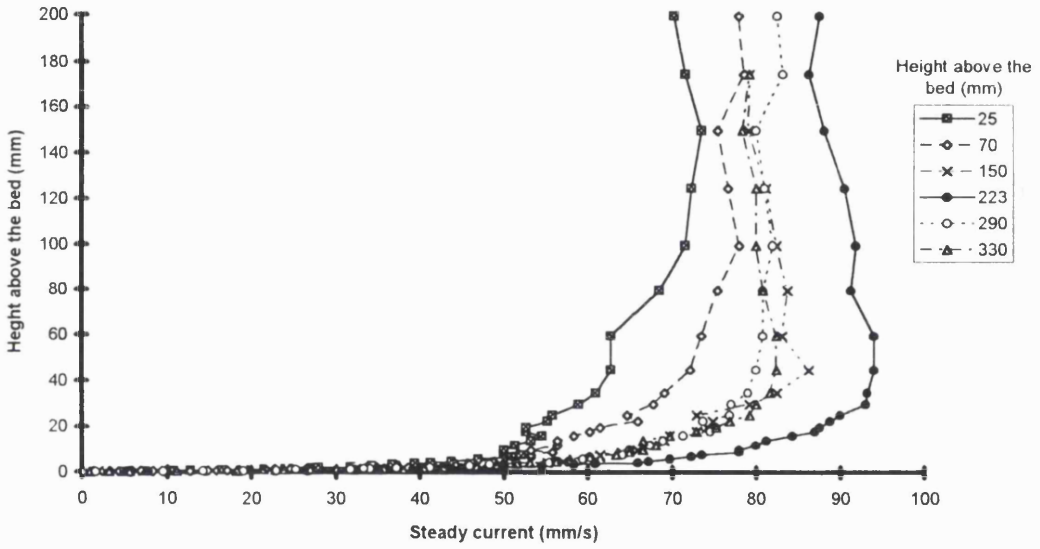

Figure 5.15 Mean bed velocity profile of the steady current measured at various distances from the sidewall; Tests BMC

TEST CODE	B-BMC 25	B-BMC 72	B-BMC 150	B-BMC 222	B-BMC 290	B-BMC 330
Velocity (mm/s)	90	90	90	90	90	90
Water Temperature (C)	16	16	15	18	18	18
Kinematic Viscosity (mm^2/s)	1.12	1.12	1.15	1.06	1.06	1.06
dU/dz (1/s)	9.7	13.9	19.7	27.4	23.8	21.8
Bed Shear Stress (mm/s)^2	10.86	15.57	22.66	29.04	25.23	23.11
Bed Shear Velocity (mm/s)	3.3	3.95	4.76	5.39	5.02	4.81
Von Karman's Constant	0.34	0.35	0.34	0.35	0.34	0.34
Reynolds Number	26786	26786	26087	18302	28302	28302

Table 5.9 Mean flow parameters of the steady current over the bed at different distances from the sidewall

5.5. Transverse Side-wall Measurements

The core section of the experimental investigation consisted of transverse velocity profile measurements away from the sidewall and at various distances from the bed. The tests covered a wide range of flow conditions, including current only, waves only and combined flows. As these are among the first comprehensive measurements of sidewall velocity profiles, the results are presented below in some detail .

5.5.1 Confirming System Reliability

Following Chapter 3, the horizontal L.D.A. system arrangement designed by Simons (1980) is referred to as System B , and the perpendicular arrangement developed during this project is referred to as System C. To test the reliability of the System C, velocity profiles away from the sidewall were measured for a selected set of flow conditions at various distances from the bed, using both L.D.A arrangements. Comparisons between the results obtained from the two arrangements as shown for the case of "medium current only" measurements at 75 mm from the bed in figures 5.16 proved the reliability of the System C, and its ability to obtain acceptable readings in the immediate vicinity of the channel wall. The 3mm/s discrepancy seen in the figure, occuring in the outer layer of the flow is attributed to a small change in flow rate between the tests carried out in separate days.

The L.D.A. arrangement C was unable to make accurate measurements at a distance of 10mm or less from the bed. Figure 5.17 shows the change in velocity profile with

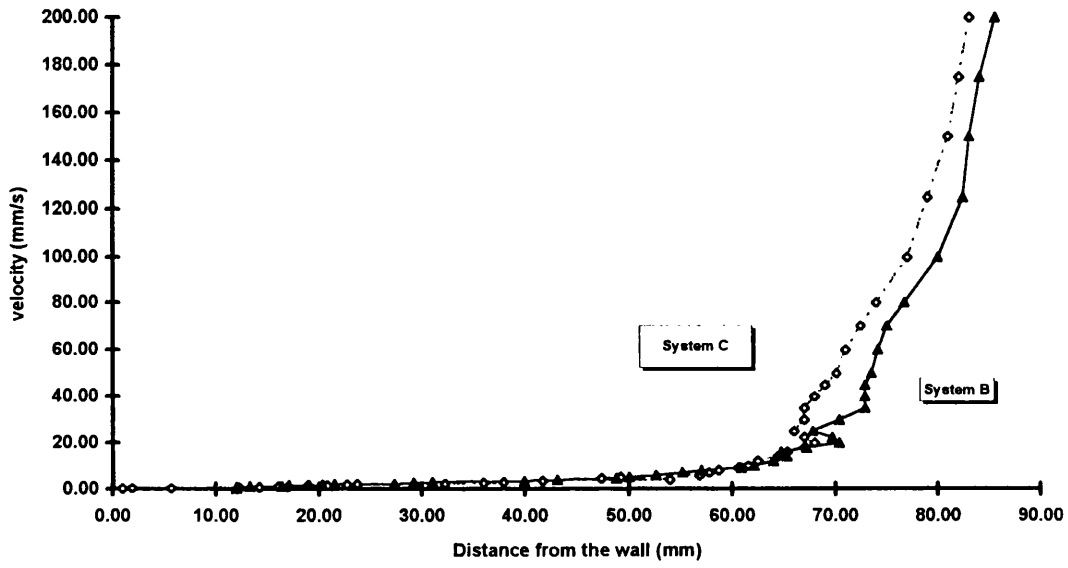

Figure 5.16 Comparison between velocity profile measurements obtained by the two L.D.A. system arrangements; Tests B-SMC.75 and C-SMC.75.

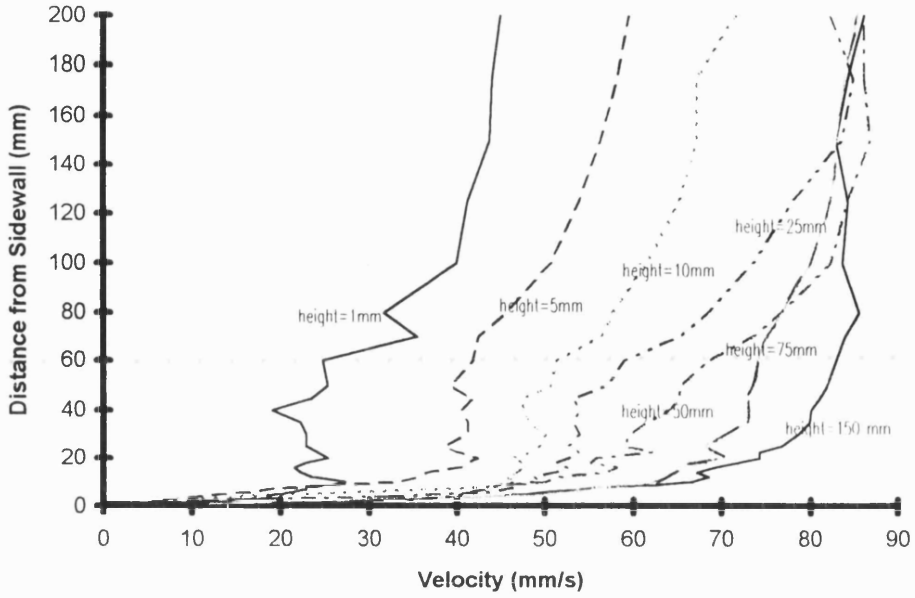

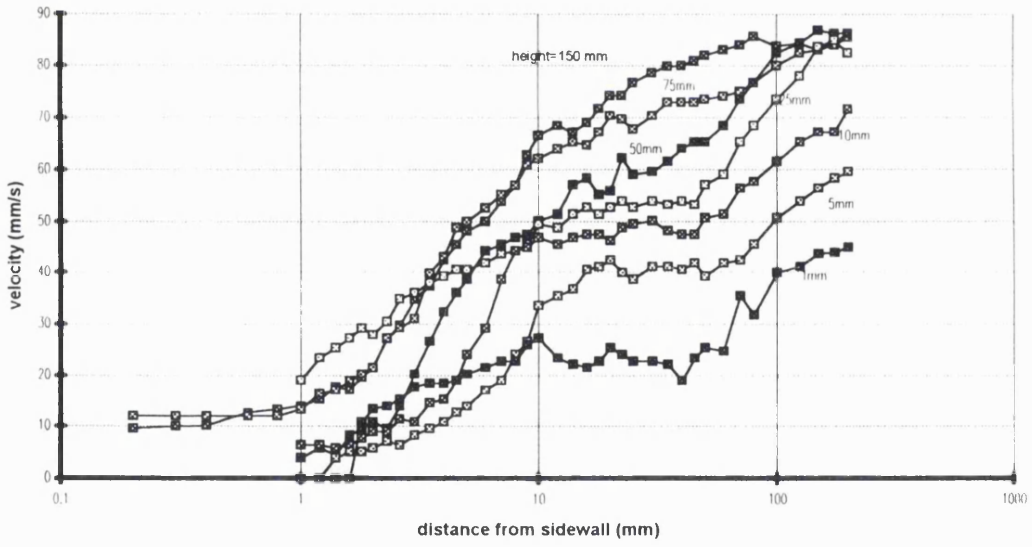

Figure 5.17 Mean transverse velocity profile measurements by system B through the depth of the flow. Also showing the logarithmic region; Tests B-SMC.

distance from the bed, including distances less than 10 mm. These measurements were taken with Simons' horizontal optical arrangement (System B) and demonstrate the distribution of velocity through the depth with distance from the channel wall.

Having confirmed the reliability of system C, the results of its measurements in the vicinity of the sidewall are presented below.

5.5.2 Current Only Regimes

Three different unidirectional steady current strengths were employed, with the surface velocities of 50 mm/s (weak), 90 mm/s (medium), and 140 mm/s (strong). The measurements were taken at three distances from the bed of 20 mm, 50 mm and 150 mm. In case of the medium current, a transverse profile at 75 mm from the bed was also measured. Figure 5.18 shows the mean horizontal velocity profiles for the medium current measured along the four different depth lines perpendicular to the sidewall and across the channel. Most of the measurements taken at 75 mm from the channel bed demonstrated that there is not any significant development between the transverse velocity profiles at 150 mm and 75 mm from bed. Thus, measurements at this particular height were not repeated for the weak and strong current tests. Figures 5.19 and 5.20 present the profiles of the weak current only and strong current only tests at various heights.

For each profile, the mean shear stress was obtained from the viscous sublayer. The kinematic viscosity was calculated from the water temperature measured during each test. The gradient of the data in the viscous sublayer was obtained by a Microsoft Excel

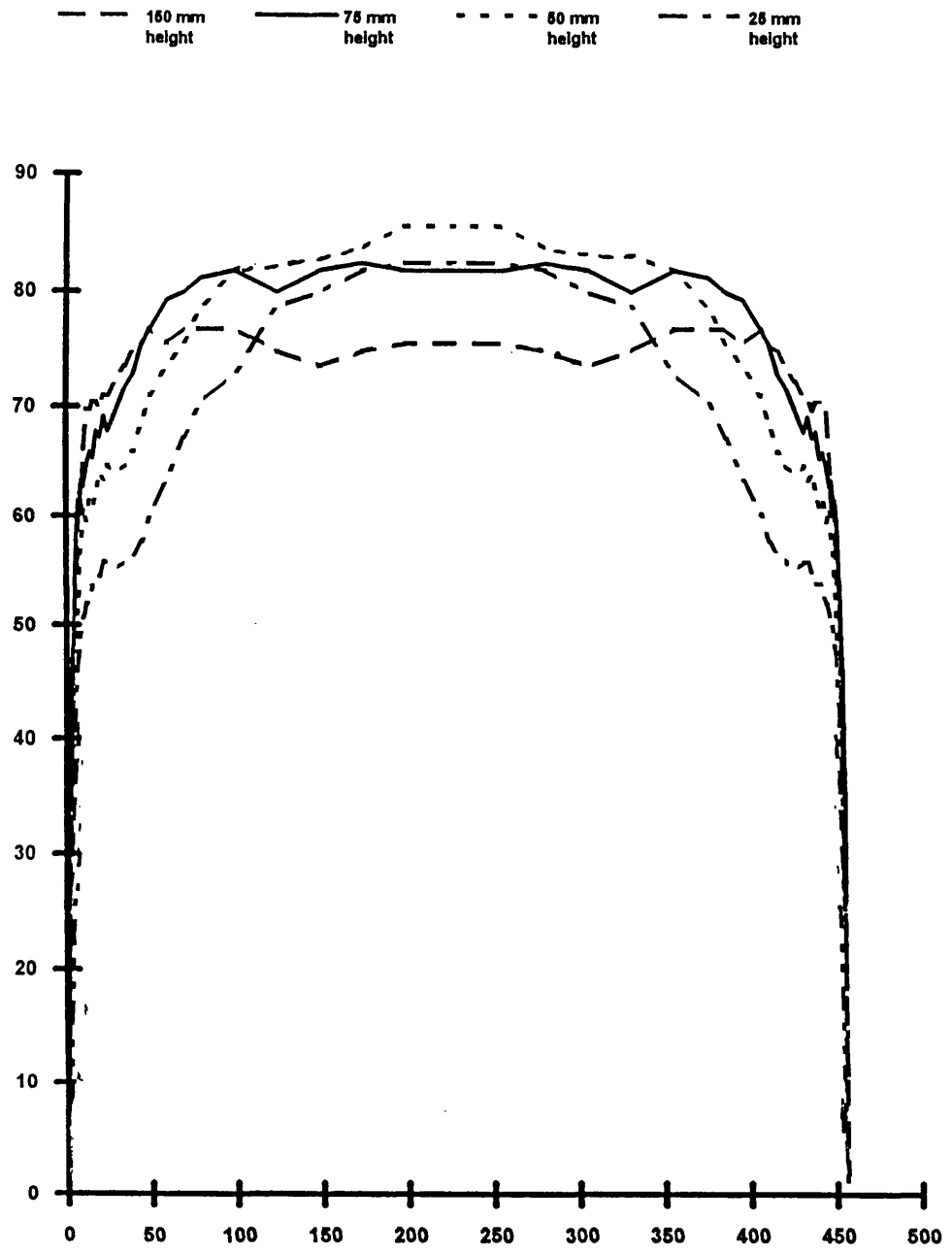

Figure 5.18 Mean velocity profiles of the medium current measured at various heights from the bed; Tests B-SMC

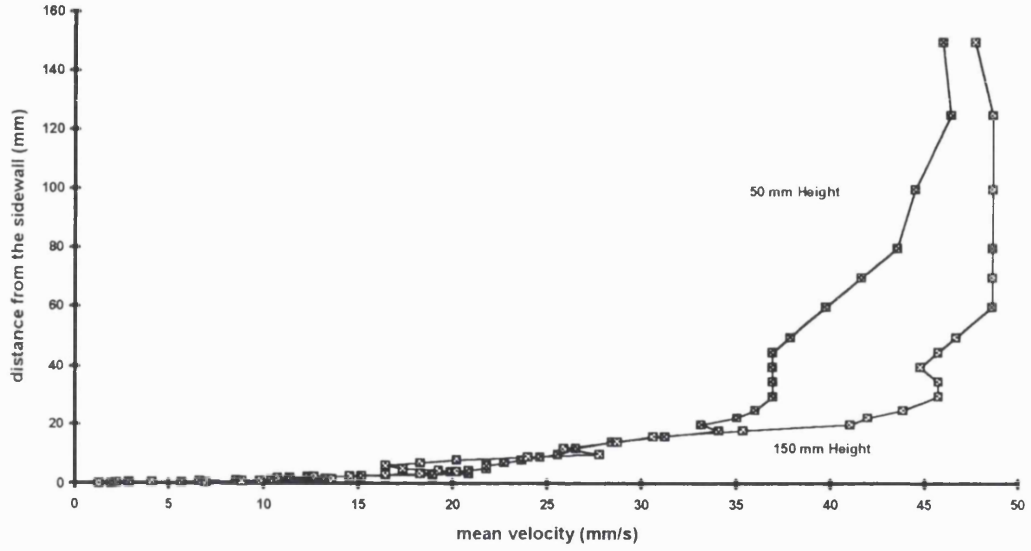

Figure 5.19 Mean velocity profiles of the weak current measured at heights of 50mm, and 150mm from the bed; Tests C-SWC.50 and C-SWC.150.

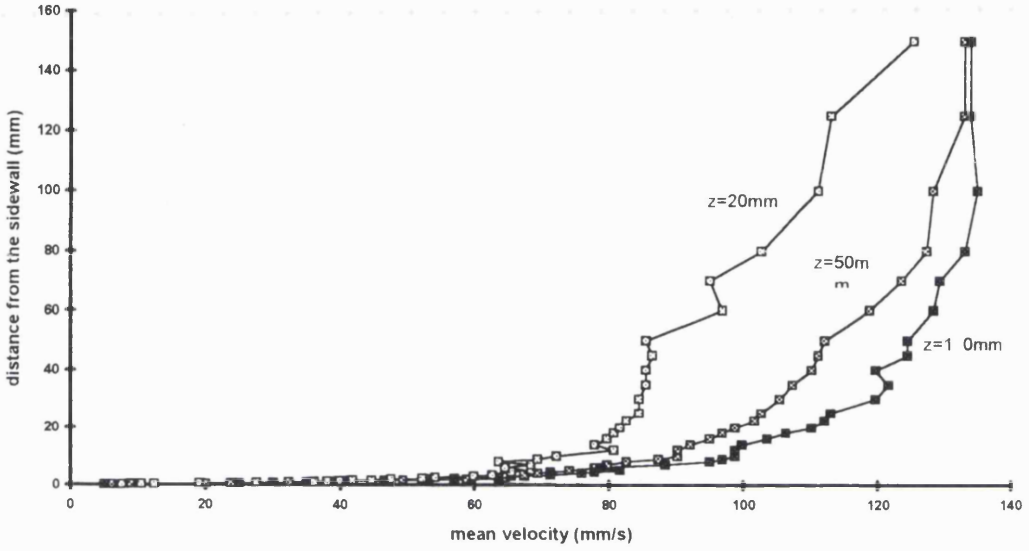

Figure 5.20 Mean velocity profile of the strong current measured at heights of 20mm, 50mm, and 150mm from the bed; C-SSC.20,50,150.

function. Figures 5.21 zooms into the region in the immediate vicinity of the channel wall for the strong current to provide an example of the calculation procedure.

The value of the mean shear velocity, U^*, is calculated and used to produce the non dimensionalised graphs of the logarithmic region of each velocity profile (Figures 5.22). For each profile, the local mean velocity was scaled on U^* and the Y coordinate were scaled on U^*/ν. The figures demonstrate the logarithmic nature of the mean velocity profiles within the current wall boundary layer, which proved to be similar in character to those within the bed boundary layer. The gradient of the logarithmic layer was found by fitting a best-fit line through the points in the region between its upper and lower limits. The upper limit of the logarithmic layer was defined using the criteria $z/h=0.15$ as a theoretical guide. To achieve a more precise definition of the upper limit for each profile, the experimental data were visually inspected following Stuart (1984) who concluded that the upper limit is characterised by an inflexion in the mean velocity profile when plotted on a semi-log scale. The inspection of experimental data showed that the expression $zU^*/\nu=30$ is a good guide for the lower limit. The value of the Von Karman's constant, κ, for each profile was obtained from the gradient of the log-layer. Similar to the bed boundary measurements in section 5.4, the values found for κ did not agree with the commonly quoted constant, 0.4. However, they were in agreement with values found by Grass (1967) for flows of similar Reynolds numbers. Calculations were avoided at the lowest height, which was deemed to close to the bed.

Table 5.10 summarises the mean flow properties of all the unidirectional current only tests. It gives the surface velocity, water temperature, kinematic viscosity, slope of velocity profile in the inner layer, wall shear stress, Reynolds number of the flow, and the

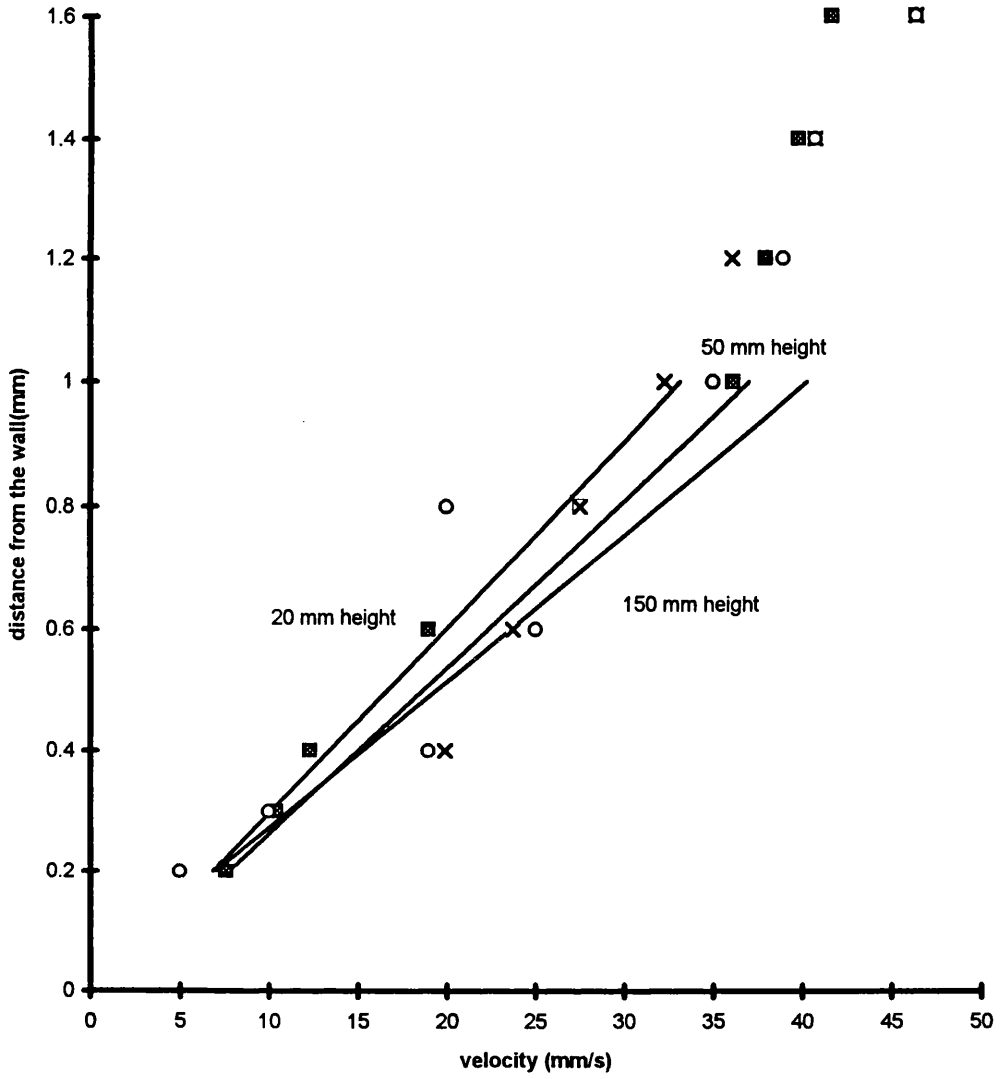

Test Name		C-SSC20	C-SSC50	C-SSC150
Height above the bed :	mm	20.00	50.00	150.00
Slope :	1/s	32.91	36.60	41.64
υ:	mm^2/s	1.01	1.01	1.01
τ/ρ :	(mm/s)^2	33.25	36.97	42.06
Shear Velocity	mm/s	5.77	6.08	6.49

Figure 5.21 Mean velocity profiles of the strong current in the vicinity of the sidewall. Tests C-SSC.20,50,150.

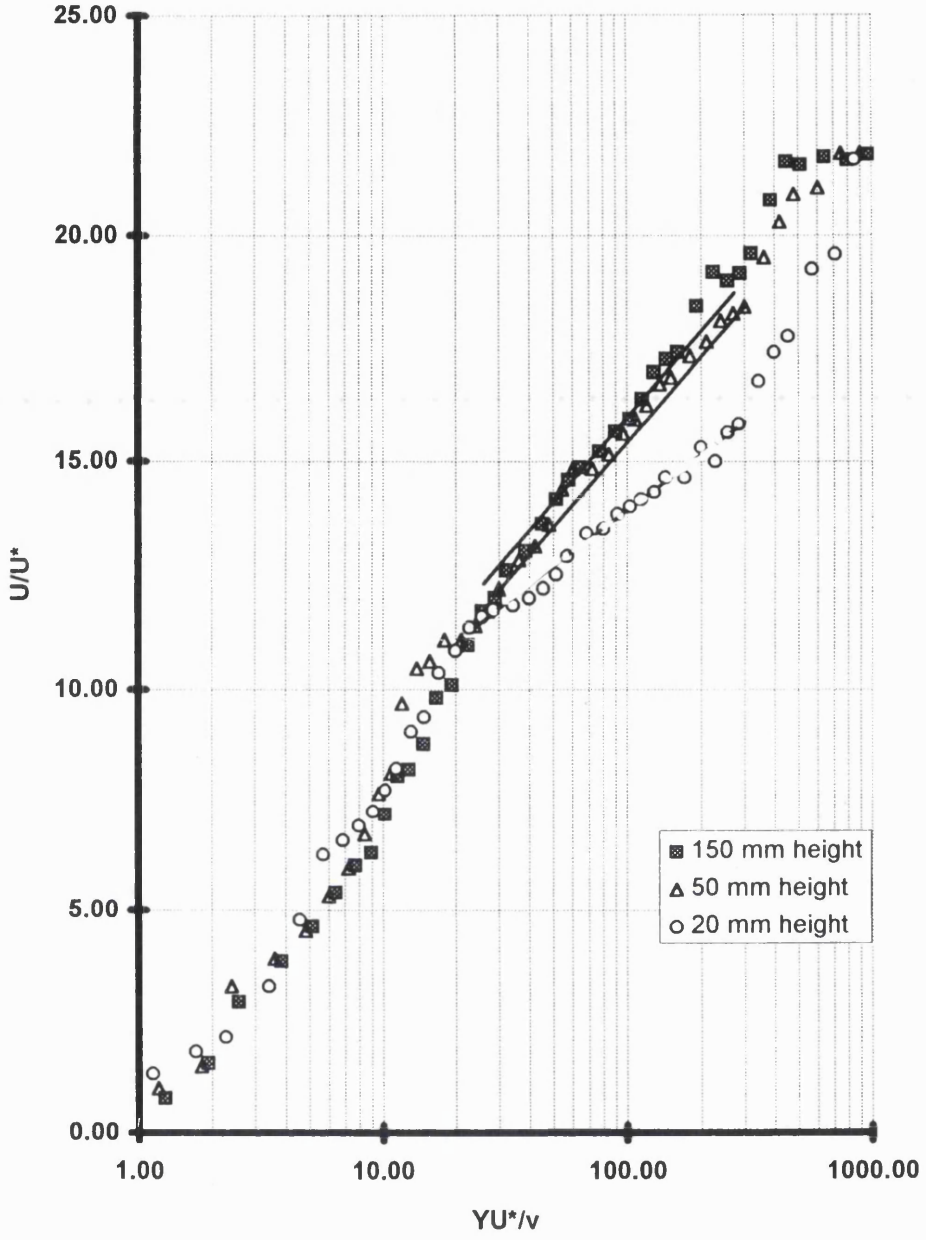

Height above the bed	(mm)	20	50	150
Von Karman's Constant			0.35	0.35

Figure5.22 Logarithmic overlap layer for unidirectional strong current at different heights from the bed; Tests C-SS.20,50&150.

Test Code	Uc mm/s	Temp. "C	υ mm^2/s	dU/dy 1/s	τ/ρ (mm/s)^2	U* mm/s	R 10^3	κ
C-SWC.50	45	20	1.01	8.33	8.41	2.90	14.85	0.37
C-SWC-150	49	20	1.01	13.14	13.28	3.64	14.85	0.37
C-SMC.25	80	19	1.06	5.81	6.16	2.48	28.30	
C-SMC.50	84	19	1.06	13.86	14.69	3.83	28.30	0.36
C-SMC.75	83	19	1.06	20.53	21.76	4.67	28.30	0.36
C-SMC.150	85	19	1.06	21.36	22.64	4.79	28.30	0.35
C-SSC.20	120	20	1.01	32.91	33.95	5.77	53.47	
C-SSC.50	133	20	1.01	36.60	36.97	6.08	53.47	0.35
C-SSC.150	135	20	1.01	41.64	42.06	6.49	53.47	0.35

Table 5.10 Mean flow parameters of the unidirectional steady current measured on perpendicular lines to the sidewall and at various heights from the bed.

Von Karman's constant for each experiment. It allows the reader to compare the effect of the change in steady current strength and distance from the bed on the various properties of the flow.

5.5.3 Waves Only Regime

Tests were carried out for three different wave periods ranging from near shallow to near deep flows. A wave period of 0.7 second was used for near deep water conditions, a wave period of 1.0 second for intermediate depth conditions, and 1.2 seconds for near shallow wave conditions. For the near shallow and the near deep waves, velocity profiles were measured at three different heights above the bed; 20 mm, 50 mm and 150 mm heights. For the intermediate wave conditions, tests were carried out at 25 mm, 50 mm, 75 mm, and 150 mm above the bed. Table 5.11 summarises the parameters of the waves alone tests. It describes the test code, wave period, wave length, wave height at the laser position, and height above the bed for each experiment.

At every measuring position, both the mean and the orbital horizontal velocities were evaluated by the L.D.A. system. The mean horizontal velocity of the waves or mass transport was obtained from the digital read out of the tracker, while the orbital velocities were computed by a Macintosh software as the final outcome of an on-line data analysis system. As described in detail in Chapter 4, this produced a record of the orbital velocities through the wave cycle by ensemble averaging a total of 200 waves.

Test Code	z mm	T s	L mm	H mm
C-SDW.20	20	0.70	740	40
C-SDW.50	50	0.70	740	40
C-SDW.150	150	0.70	740	40
C-SIW.25	25	1.00	1300	40
C-SIW.50	50	1.00	1300	40
C-SIW.75	75	1.00	1300	40
C-SIW.150	150	1.00	1300	40
C-SSW.20	20	1.20	1700	40
C-SSW.50	50	1.20	1700	40
C-SSW.150	150	1.20	1700	40

Table 5.11 The test parameters for the experiments on pure waves.

5.5.3.1 Mass Transport

Both Simons (1980) and Kyriacou (1988) measured mass transports of waves propagating in still water at the centre of their open channels. They discovered that at the centre of the flume, there was a net motion in the direction of wave propagation within 20 mm of the bed. They found that above that height the mean wave velocities became negative, with the magnitude of the velocity increasing with distance above the bed, as well as with the wave height. Their measurements implied a net fluid motion towards the paddle. Simons (1980) explained the net motion towards the paddle by a compensating forward motion at the sidewalls. It was part of the objective of this study to use the modified L.D.A. system to confirm this argument.

By carrying out transverse measurements at various heights, it became possible to construct an image of mass transport through a cross section of the channel. Figure 5.23 presents the values of mean velocities for a typical set of tests. It shows that while the mass transport remains in the direction of wave propagation within 20 mm of the bed and the sidewalls, it becomes negative at a certain distance from both boundaries. Using the results of the present tests and those carried out by Simons (1980) and Kyriacou (1988), figure 5.24 provides a guide on how the cross section of the channel might be divided between two positive and negative zones of mass transport.

0.7 second waves only

	Height Above The Bed		
	20 mm	50 mm	150 mm
Distance from wall mm	Mass Transport mm/s	Mass Transport mm/s	Mass Transport mm/s
0.2	1	0	7
0.3	3	2	7
0.4	7	4	8
0.6	8	6	8
0.8	14	8	8
1	13	8	7
1.2	9	7	7
1.4	8	9	6
1.6	10	8	6
1.8	12	8	6
2	9	7	6
2.3	7	8	6
2.6	6	7	6
3	9	5	7
3.5	7	6	6
4	6	3	4
4.5	6	4	2
5	5	3	1
6	4	6	3
7	4	5	4
8	5	6	3
9	5	7	2
10	6	7	1
12	5	7	0
14	5	5	-1
16	4	4	-1
18	6	2	-2
20	5	1	-3
22.5	4	1	-3
25	4	1	-2
30	2	3	-2
35	6	4	-1
40	3	3	-1
45	4	2	-2
50	3	4	-1
60	4	3	-1
70	2	3	-3
80	5	3	-2
100	1	4	-2
125	3	4	-2
150	1	3	-1

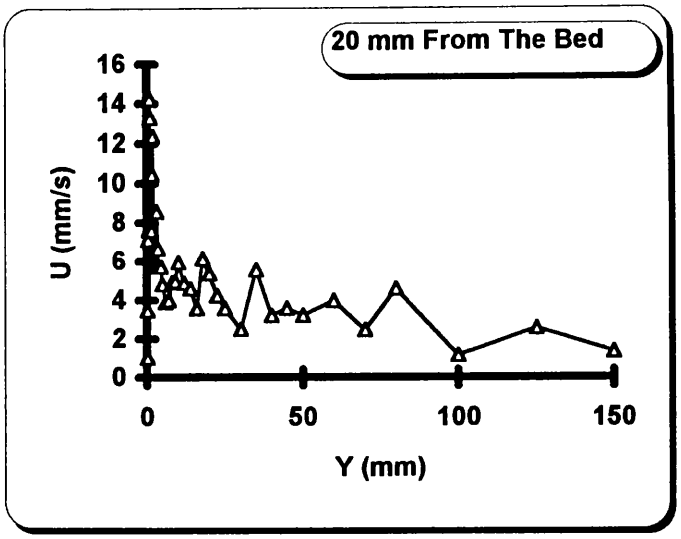

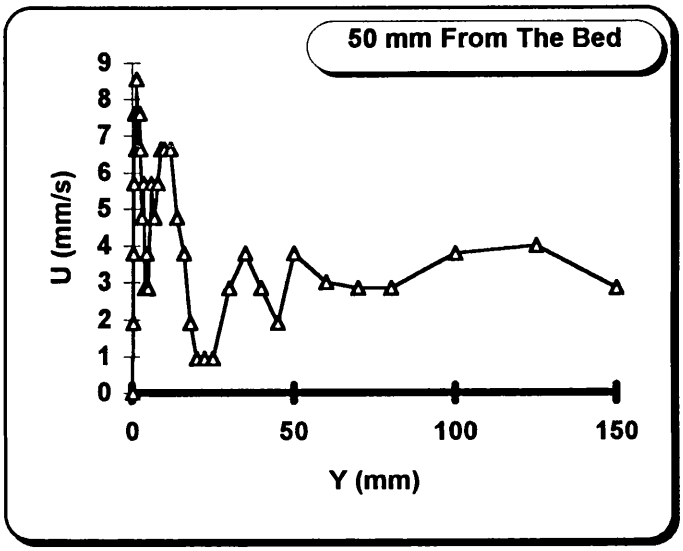

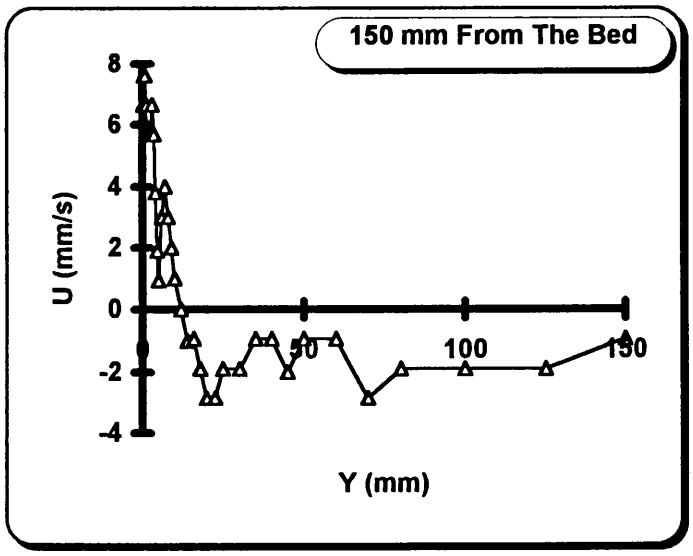

Figure 5.23 Mass transport profiles across the channel, at three different depths.

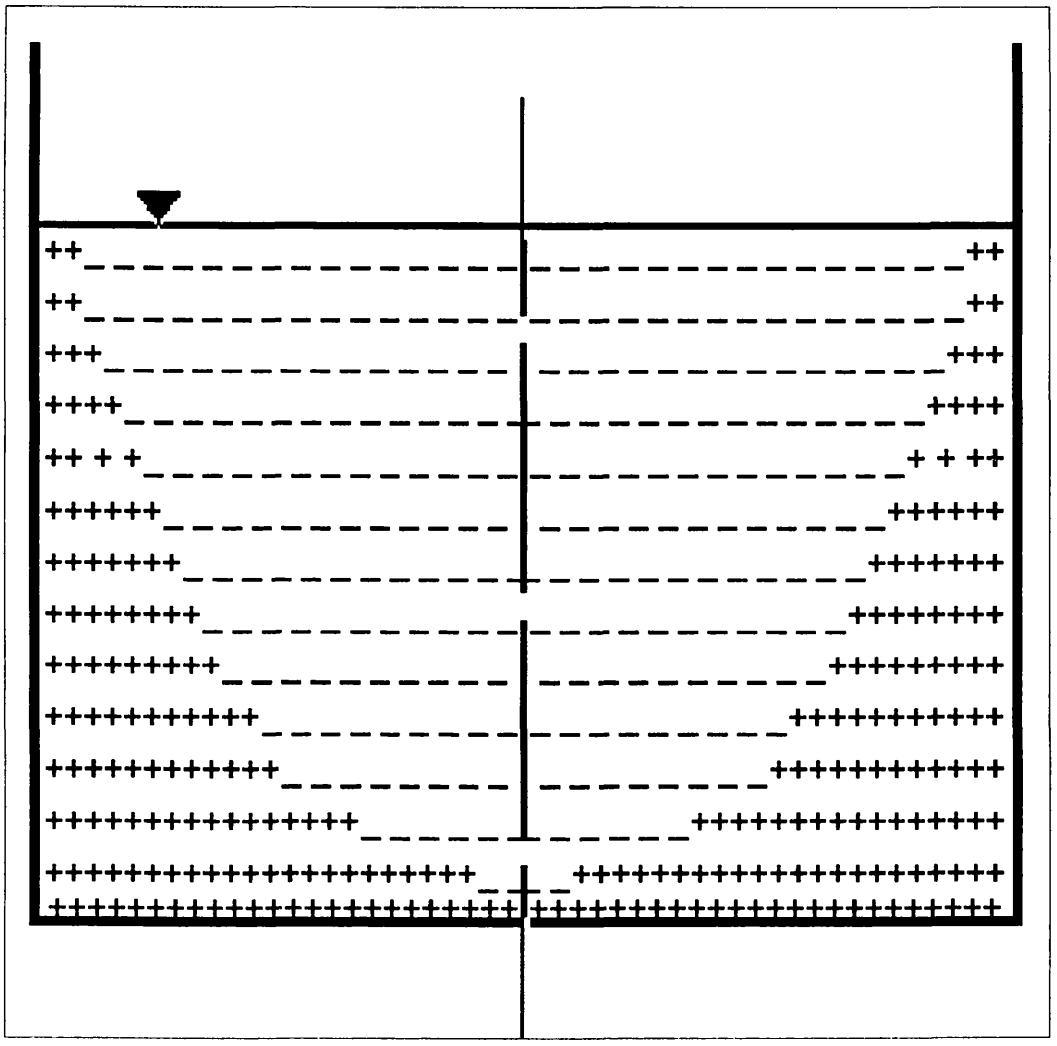

Figure 5.24 A cross sectional view of the channel depicting zones of positive and negative mass transport.

5.5.3.2 Periodic Velocities

At each measurement position, the orbital velocities were evaluated through the wave cycle and the value for each phase of the cycle was ensemble averaged to produce a representative waveform. Figure 5.25 shows one such waveform presenting the ensemble averaged periodic velocities throughout the cycle of a 1 second wave at a distance of 25mm from the bed and 0.6mm from the sidewall. It also shows the ability of the test apparatus to obtain results at such short distances from the sidewall.

The orbital velocity data obtained from each measurement position was used to construct transverse periodic velocity profiles within the 150 mm of the sidewall for all the performed tests. Table 5.12 presents the maximum, minimum, and average orbital velocities taken at the edge of the wave boundary layer. In addition it shows the average horizontal wave amplitude and the amplitude Reynolds number for each test. The amplitude Reynolds numbers indicated that the experiments were carried out in a laminar flow regime. Figure 5.26 demonstrates a profile of the maximum and minimum horizontal periodic velocities for the 1.2 seconds waves at a height of 150 mm from the bed. Zooming into the boundary zone within 5 mm of the sidewall, the lower figure shows the extent of the viscous wave boundary layer. It clearly demonstrates that the "overshoot" region described by Lamb (1932) for the bed boundary also exists in the case of a two dimensional sidewall boundary. Figure 5.27 compares the transverse periodic velocity distribution of the 1 second waves at various distances from the bed. This agrees with the work of previous researchers such as Kyriacou (1988) who showed a similar attenuation through the depth.

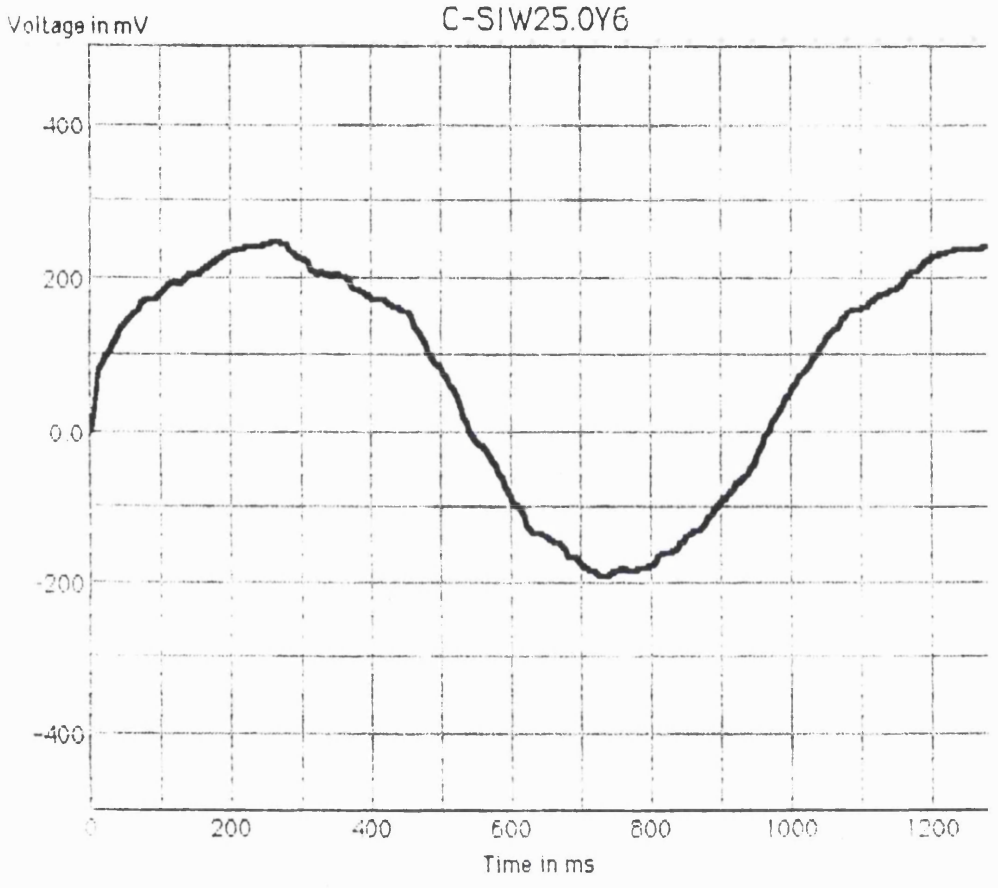

Figure 5.25 Ensemble averaged periodic velocity through the wave cycle for the 1.0s waves, measured at a distance of 25mm from the bed and 0.6mm from the sidewall.

Test Code	z mm	Umax mm/s	Umin mm/s	Uo mm/s	ω 1/s	Ao mm	R
C-SDW.20	20	28.00	-18.00	23.00	8.97	3	59
C-SDW.50	50	26.00	-22.00	24.00	8.97	3	64
C-SDW.150	150	53.00	-49.00	51.00	8.97	6	290
C-SIW.25	25	56.00	-47.00	51.50	6.28	8	422
C-SIW.50	50	61.00	-49.00	55.00	6.28	9	482
C-SIW.75	75	68.00	-57.00	62.50	6.28	10	622
C-SIW.150	150	71.00	-61.00	66.00	6.28	11	694
C-SSW.20	20	65.00	-55.00	60.00	5.23	11	688
C-SSW.50	50	71.00	-60.00	65.50	5.23	13	820
C-SSW.150	150	74.00	-66.00	70.00	5.23	13	936

Table 5.12 Maximum, minimum, and average orbital velocities taken at the edge of the wave boundary layer, together with the average horizontal wave amplitude and the amplitude Reynolds number for each pure waves test.

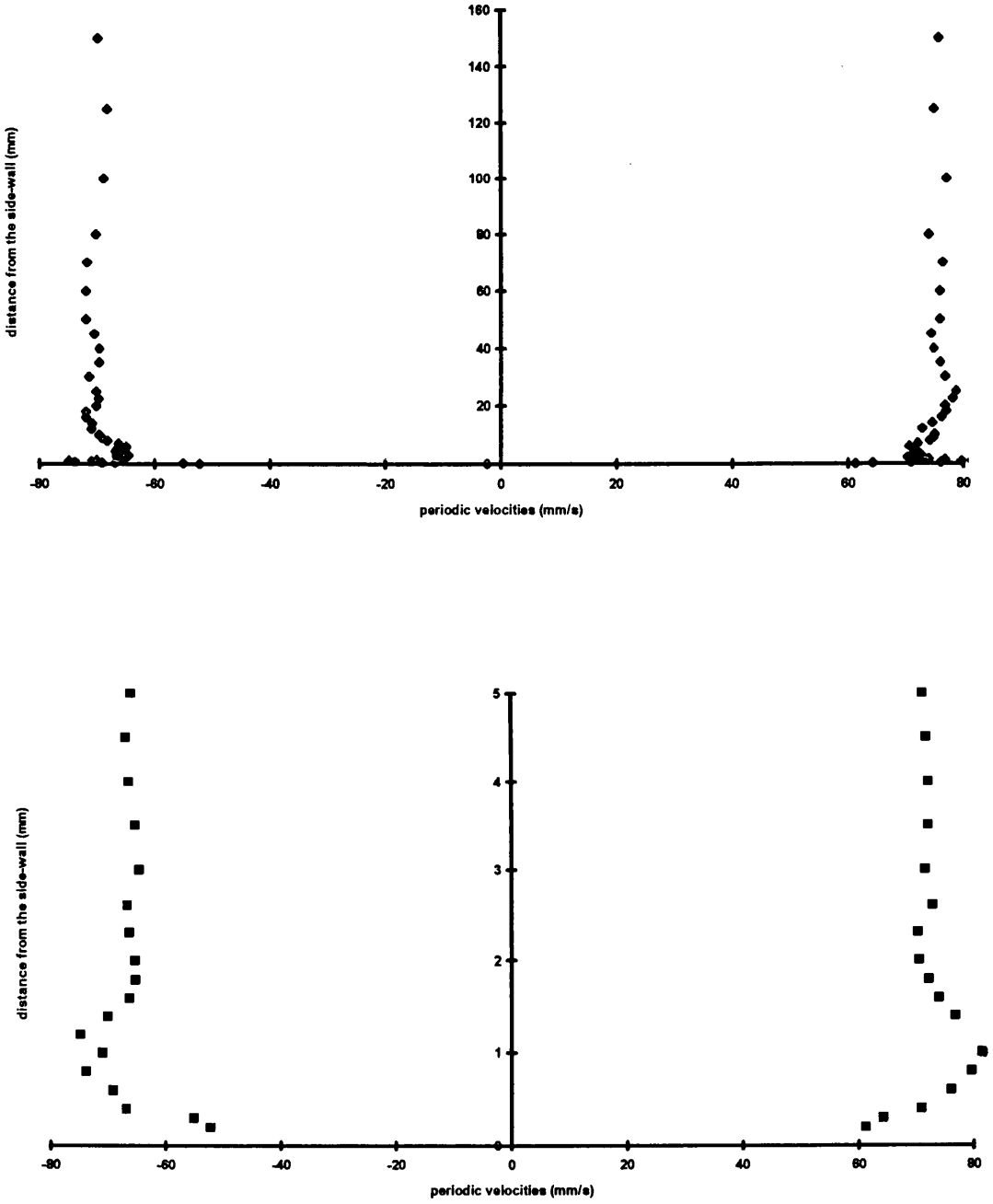

Figure 5.26 Maximum and minimum periodic velocities of the 1.2s waves, 150 mm from the bed; Test C-SSW.150.

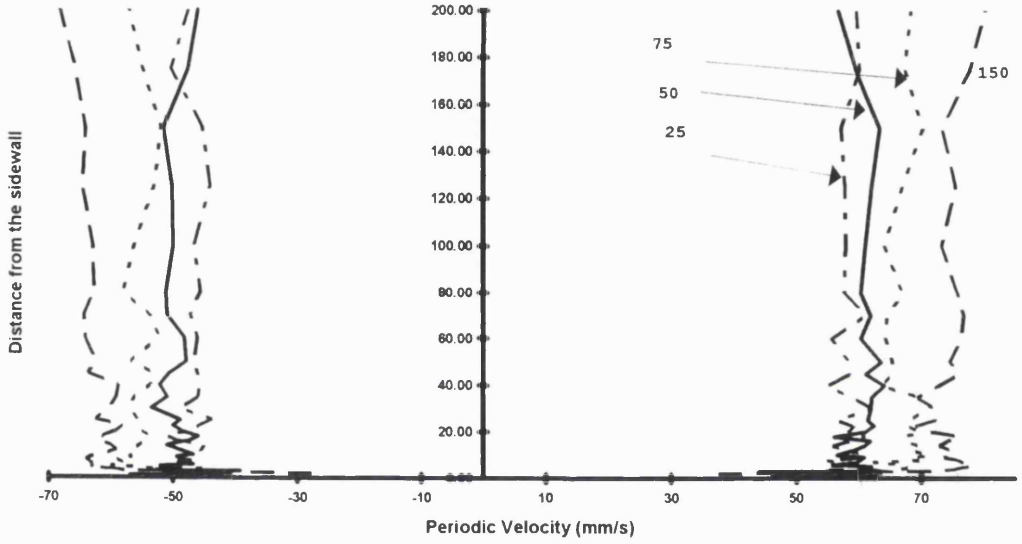

Figure 5.27 Periodic velocity distribution for the 1.0s waves, measured at four different heights above the bed. Tests C-SIW.25,50,75&150mm. T=1.0s.

Table 5.13 presents the value of the maximum shear stress at the sidewall for each test, calculated from the following commonly used laminar expression:

$$\tau_{0s} = \sqrt{2}\,\mu.\beta.\,u_{0s}$$

where

$$\beta = \sqrt{\{\omega_a / 2\,\nu\}}$$

5.5.4 Combined Waves and Current Flows

Experiments were carried out for three different waves, each combined with three different currents. As described in previous chapters, the wave periods were 0.7s, 1.0s and 1.2s and waves were generated using the same paddle stroke settings as those used in waves alone tests. The strength of the steady currents were chosen as 50mm/s for weak current, 90mm/s for the medium, and 140mm/s for the strong. For each wave and current setting, tests were performed at 20mm, 50mm, and 150mm distances from the bed. In the case of the intermediate waves combined with medium current, an additional set of tests was carried out at 75mm height above the bed. For each experiment, the mean and orbital velocities were measured and the total velocities were calculated by simple arithmetic addition. The results are presented below.

Test Code	Uo mm/s	ω 1/s	β	τ/ρ (mm/s)^2
C-SDW.20	23.00	8.97	2.12	68.89
C-SDW.50	24.00	8.97	2.12	71.89
C-SDW.150	51.00	8.97	2.12	152.76
C-SIW.25	51.50	6.28	1.77	129.06
C-SIW.50	55.00	6.28	1.77	137.83
C-SIW.75	62.50	6.28	1.77	156.62
C-SIW.150	66.00	6.28	1.77	165.40
C-SSW.20	60.00	5.23	1.62	137.26
C-SSW.50	65.50	5.23	1.62	149.84
C-SSW.150	70.00	5.23	1.62	160.14

Table 5.13 Maximum sidewall shear stress for the three waves at various heights through the depth of the flow.

5.5.4.1 Mean Velocities

Similar to the current only experiments, the mean velocity for the combined flows was measured using the L.D.A system. By measuring the horizontal mean velocity through half the width of the channel in lines perpendicular to the sidewall and at various heights from the bed, it was possible to construct a picture of the mean steady velocity at the laser position. Figure 5.28 shows the mean velocity profile through the cross section of the channel for the intermediate waves and medium current combined. The measurements were only taken up to 150 mm away from one sidewall. Thus, in order to construct an image for the entire cross section, it was necessary to assume that the flow was symmetrical about the mid axis of the cross section and that the mean velocity at the core of the flow (in the volume over 150 mm from both sidewalls) was constant. Within 20 mm of the bed it was not possible to take accurate readings with the L.D.A. system C. Therefore the conventional L.D.A. arrangement (System B) was employed to measure velocities at heights of 1m, 5mm, and 15 mm from the bed.

Figure 5.29 presents the mean velocity profile for the intermediate waves and strong current at heights of 150mm from the bed. It also shows the unidirectional strong current velocity profile at the same height for comparison. A reduction of the mean velocity in the combined flow over that of the current alone, particularly over 20 mm from the wall, is apparent from the diagram. This pattern was repeated for most the tests and is similar to the findings of other authors comparing the mean velocity profiles perpendicular to the bed of combined waves and current flows.

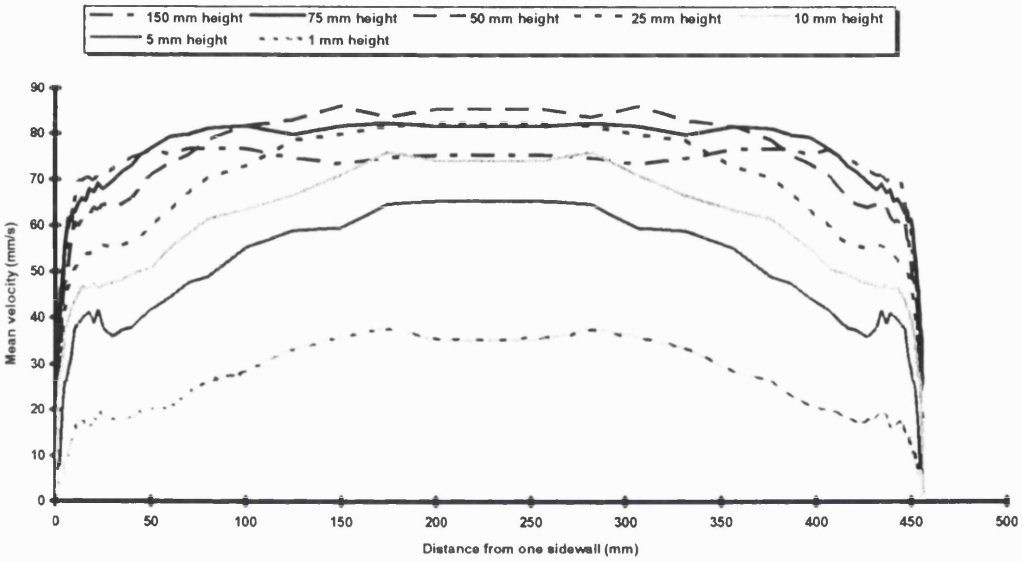

Figure 5.28 Mean velocity distribution through the cross section of the flow at laser position, for the combined 1.0s waves and medium current.

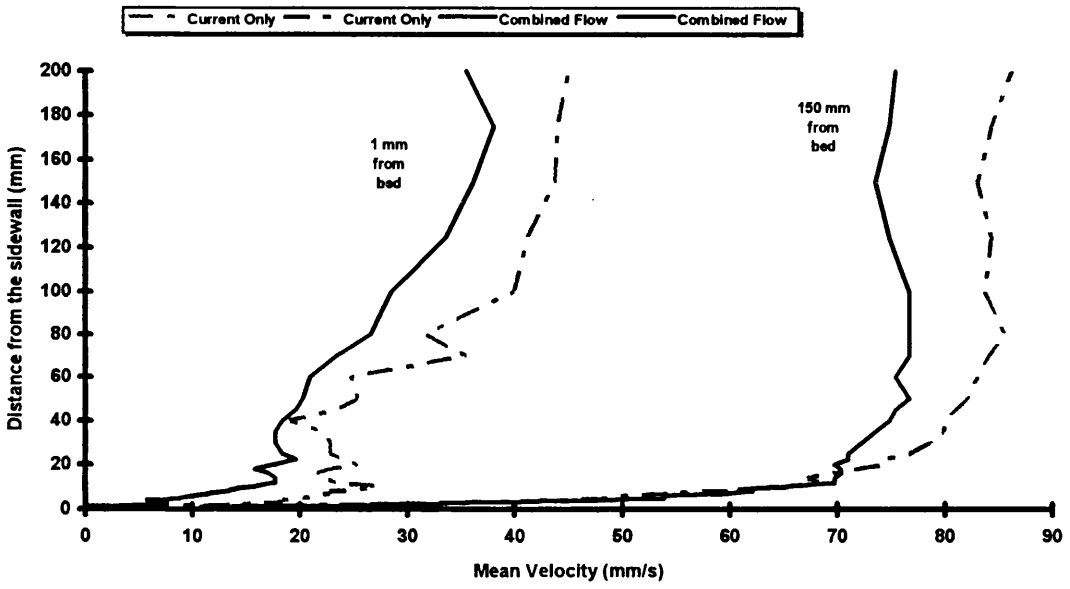

Figure 5.29 Comparison of mean velocity profiles between medium current only and combined 1.0s waves and medium current, at heights of 1mm and 150mm.

The mean wall shear stress was calculated by fitting a straight line through the data in the viscous sublayer. In accordance with the mean velocity behaviour described previously, the value of the mean shear stresses increased with height above the bed for approximately the bottom 30 mm. Above this height the mean wall shear stress became almost constant, with little variation demonstrated with increasing height of measurement. Figure 5.30 compares the mean velocity profiles of the combined deep waves and strong current flow at the heights of 20 mm, 50 mm, and 150 mm from the bed and in the immediate vicinity of the sidewall. This result was similar to the finding of corresponding tests in section 5.1 which discovered the same trend in bed shear stress with distance from the sidewall. The experiments also showed that the imposition of various waves on a current did not produce a marked difference in the values of wall shear stress at each height. For example, figure 5.31 illustrates the measured mean velocities within the viscous layer of the medium current at a height of 150 mm above the bed, for the cases of current only and with different period waves superimposed on it. The straight lines fitted through the profiles are almost parallel, with the difference in the resultant shear stresses not exceeding 10%. However, it should be noted that although in the case demonstrated here the addition of the waves produced a decrease in the mean wall shear stress, the trend was not universal. Thus, while the addition of waves to the current sometimes increased and sometimes decreased the mean shear stress, the period of the waves appear to have little effect.

The mean wall shear stresses obtained above were used to calculate the mean wall shear velocity for each test. Consequently, as for the current alone data, The computed shear velocities were used as a scaling factor to produce non dimensional graphs of U/u^* versus

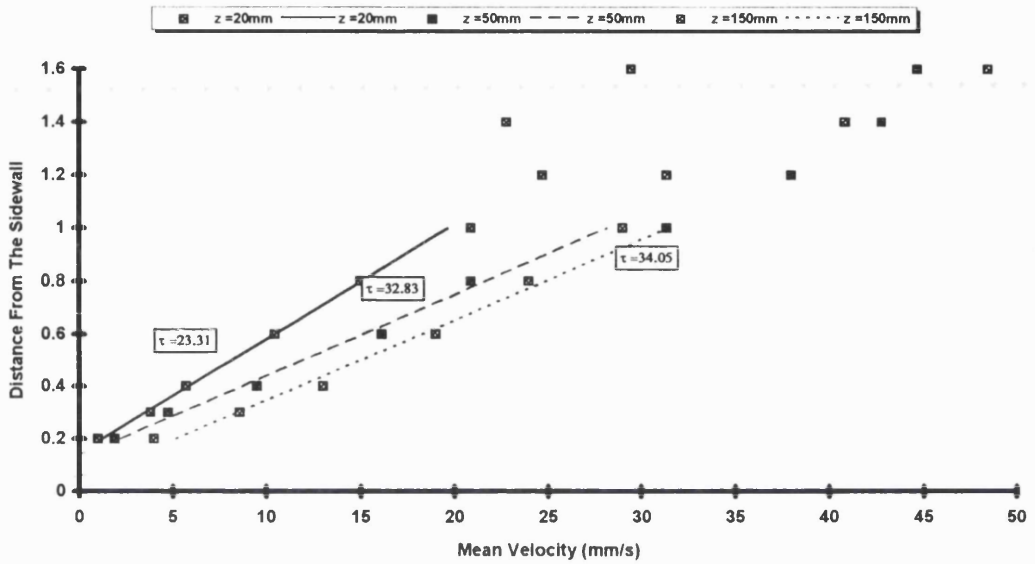

Figure 5.30 Comparison of mean velocity profiles in the immediate vicinity of the sidewall for the combined 0.7s waves and strong current, at heights of 20mm, 50mm and 150mm. Tests C-SDWSC.20,50&150.

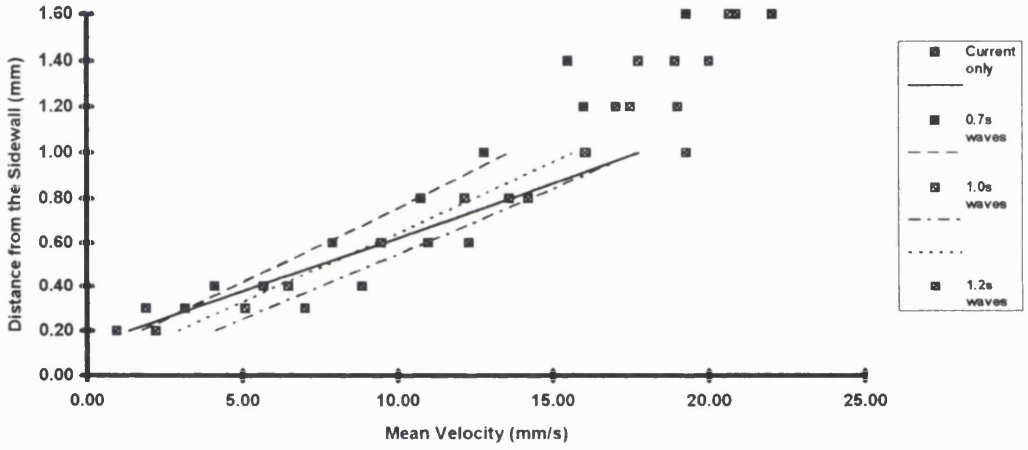

Figure 5.31 comparison of mean velocity profile in the immediate vicinity of the sidewall between the medium current only, and the combined medium current with 0.7s, 1.0s, and 1.2s waves.

zu^*/ν. These graphs, as in figure 5.32 demonstrated the existence of a logarithmic overlap layer for the mean velocities of combined wave-current flows. The slope of the log. layer was used to obtain the von Karman constant for each test.

Table 5.14 presents a summary of the measured mean parameters for the tests in combined waves and current. The mean shear stress increases steadily with height above the bed up to a height of between 40 to 60 mm, and then becomes almost constant. This follows closely the trend of the bed velocity profile in the channel. As expected, the mean shear stress also increases with the strength of the steady current, but is not affected considerably by the period of the waves.

5.5.4.2 Periodic Velocities

To extract the wave induced periodic velocities of the combined flow, a high pass filter (described in Chapter 3) was used to remove the mean velocity component from the total velocity. At each measuring position, the orbital velocities were recorded for between 200 to 500 waves and an ensemble averaged velocity through the wave cycle was produced. Figure 5.33 demonstrates one such waveform, measured in a combined intermediate waves and medium current flow at a height of 150 mm from the bed and only 0.3 mm from the sidewall. The maximum and minimum periodic velocities of each waveform at every measuring position were computed from the graph, and recorded separately. They were subsequently used to produce transverse profiles of the peak orbital velocities for each experiment.

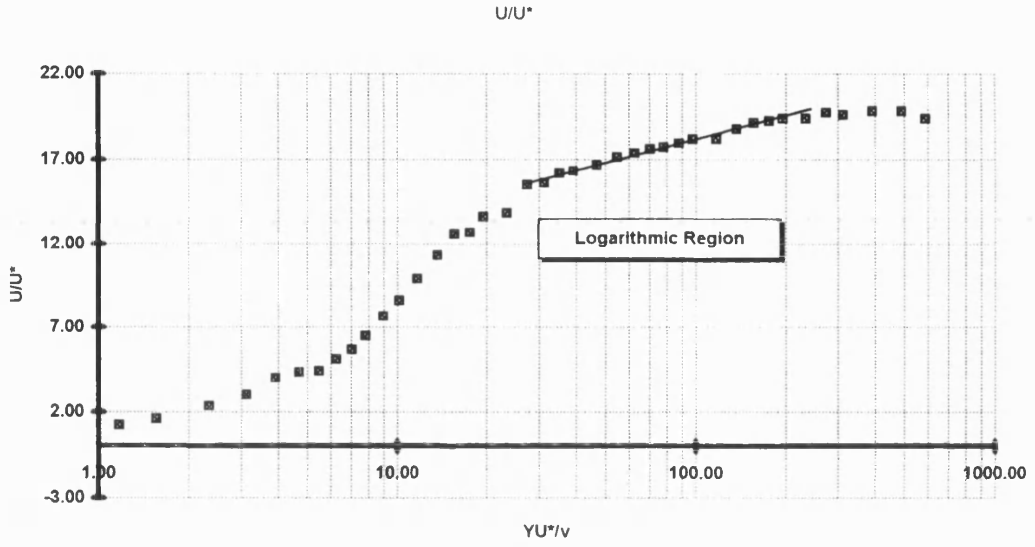

Figure 5.32 Logarithmic profile of the mean velocity in the combined flow.

test Code	z mm	H mm	U mm/s	L mm	τ (mm/s)^2	RE
C-SDWWC50	50	39	34	840	6.15	10,200
C-SDWWC150	150	40	54	840	11.97	16,200
C-SDWMC20	20	35	74	820	9.26	22,200
C--SDWMC.50	50	35	81	820	14.86	24,300
C-SDWMC.150	150	36	87	820	15.72	26,100
C-SDWSC20	20	30	122	908	23.31	36,600
C-SDWSC50	50	30	133	908	32.83	39,900
C-SDWSC150	150	30	129	908	34.05	38,700
C-SIWWC50	50	37	31	1370	4.08	9,300
C-SIWWC150	150	37	55	1370	10.20	16,500
C-SIWMC.50	50	36	82	1450	18.44	24,600
C-SIWMC.150	150	36	81	1450	16.46	24,300
C-SIWSC20	20	33	120	1654	23.91	36,000
C-SIWSC50	50	33	134	1654	32.70	40,200
C-SIWSC150	150	34	131	1654	29.24	39,300
C-SSWWC50	50	39	45	1800	12.04	13,500
C-SSWWC150	150	39	46	1800	11.46	13,800
C-SSWMC20	20	34	74	1830	16.37	22,200
C--SSWMC.50	50	34	84	1818	23.87	25,200
C-SSWMC.150	150	35	79	1830	18.02	23,700
C-SSWSC20	20	34	117	2030	28.98	35,100
C-SSWSC50	50	34	138	2030	39.37	41,400
C-SSWSC150	150	34	137	2030	39.91	41,100

Table 5.14 Mean flow parameter of the combined flows.

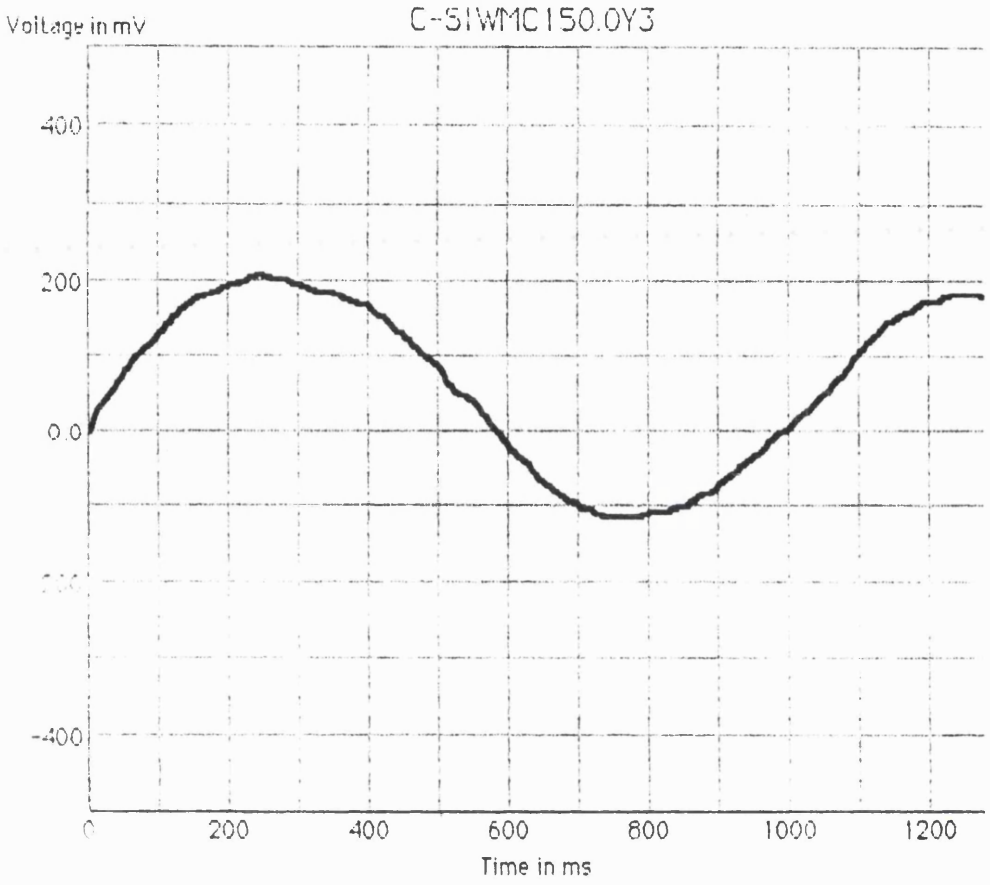

Figure 5.33 Ensemble averaged periodic velocity through a wave cycle measured at a height of 150mm from the bed and a distance of 0.3mm from the sidewall. Test C-SIWMC.150

Figure 5.34 for example, shows the maximum and minimum orbital velocity profiles measured at a height of 20 mm from the bed in the combined intermediate waves and strong current. the lower figure zooms into the 5 mm zone in the immediate vicinity of the sidewall to illustrate in details measurement near the boundary.

Table 5.15 summarises the results of the data described above for all the tests that were performed in combined flows. It presents the maximum, minimum and mean oscillatory velocities, as well as the wave amplitude. As can be seen from the table, in almost all cases the value of the minimum orbital velocity was smaller than the maximum velocity. This agrees with the assumption of this study that the waves were of a second order. The data also showed a clear increase in periodic velocities with height above bed. Figure 5.35 compares the measured orbital velocity profiles for the combined intermediate waves and strong current flows at heights of 20 mm, 50 mm, and 150 mm to demonstrate an example of this expected trend.

Kyriacou (1988) concluded from his measurements of the orbital velocities through the depth of flow in combined wave and current flows that the value of the wave period had an effect on the change in orbital velocity with the strength of the current. The data presented in table 5.15 shows that as expected the orbital velocities become larger with wave period and height above the bed. In general, the orbital velocities reduce with the strength of the current, although this trend was not universal.

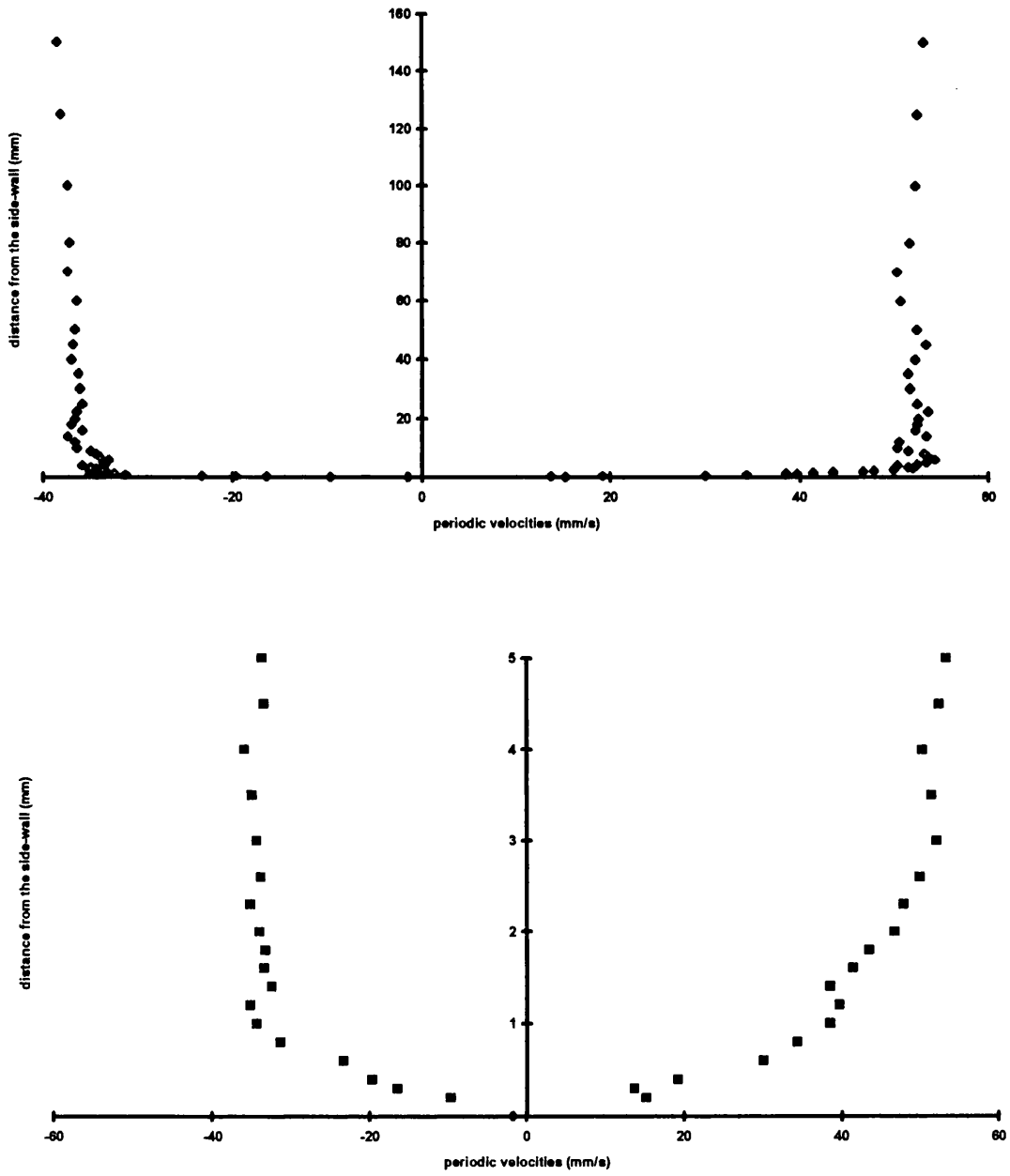

Figure 5.34 Maximum and minimum periodic velocities of the combined intermediate waves and strong current flow measured at a height of 20mm from the bed; Test C-SIWSC.20

test Code	U mm/s	L mm	Umax mm/s	Umin mm/s	Uo mm/s	w 1/s	Ao mm	RE
C-SDW.20	0	740	28.00	-18.00	23.00	8.97	3	59
C-SDW.50	0	740	26.00	-22.00	24.00	8.97	3	64
C-SDW.150	0	740	53.00	-49.00	51.00	8.97	6	290
C-DWWC.20	31	840	19	-11.00	15.00	8.74	2	9,300
C-SDWWC.50	34	840	22	-14	18.00	8.72	2	10,200
C-SDWWC.150	54	840	46	-36	41.00	8.57	5	16,200
C-SDWMC.20	74	820	20	-10	15.00	8.40	2	22,200
C--SDWMC.50	81	820	26	-11	18.50	8.35	2	24,300
C-SDWMC.150	87	820	41	-29	35.00	8.31	4	26,100
C-SDWSC.20	122	908	24	-10	17.00	8.13	2	36,600
C-SDWSC.50	133	908	35	-16	25.50	8.05	3	39,900
C-SDWSC.150	129	908	40	-24	32.00	8.08	4	38,700
C-SIW.25	0	1300	56.00	-47.00	51.50	6.28	8	422
C-SIW.50	0	1300	61.00	-49.00	55.00	6.28	9	482
C-SIW.75	0	1300	68.00	-57.00	62.50	6.28	10	622
C-SIW.150	0	1300	71	-61	66	6.28	10.51	693.63
C-SIWWC.50	31	1370	46	-39	42.50	6.14	7	9,300
C-SIWWC.150	55	1370	65	-50	57.50	6.03	10	16,500
C-SIWMC.50	82	1450	52	-40	46.00	5.92	8	24,600
C-SIWMC.150	81	1450	60	-46	53.00	5.93	9	24,300
C-SIWSC.20	120	1654	50	-34	42.00	5.82	7	36,000
C-SIWSC.50	134	1654	55	-39	47.00	5.77	8	40,200
C-SIWSC.150	131	1654	60	-40	50.00	5.78	9	39,300
C-SSW.20	0	1700	65.00	-55.00	60.00	5.23	11	688
C-SSW.50	0	1700	71.00	-60.00	65.50	5.23	13	820
C-SSW.150	0	1700	74.00	-66.00	70.00	5.23	13	936
C-SSWWC.50	45	1800	70	-53	61.50	5.08	12	13,500
C-SSWWC.150	46	1800	69	-55	62.00	5.07	12	13,800
C-SSWMC.20	74	1830	55	-45	50.00	4.98	10	22,200
C--SSWMC.50	84	1818	63	-49	56.00	4.94	11	25,200
C-SSWMC.150	79	1830	65	-44	54.50	4.96	11	23,700
C-SSWSC.20	117	2030	63	-40	51.50	4.87	11	35,100
C-SSWSC.50	138	2030	64	-44	54.00	4.81	11	41,400
C-SSWSC.150	137	2030	64	-42	53.00	4.81	11	41,100

Table 5.15 Near sidewall orbital motions for the tests in combined flows.

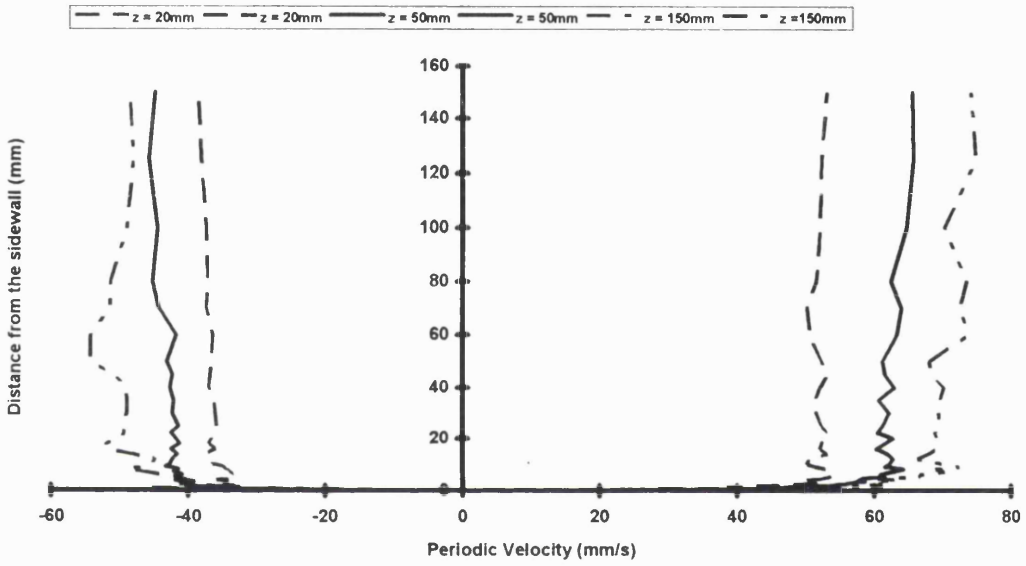

Figure 5.35 Comparison of maximum and minimum orbital profiles for the combined 1.0s waves and strong current, at heights of 20mm, 50mm and 150mm.

5.5.4.3 Total Velocities

It is possible to produce figures showing the total velocity profile of a combined flow by linear addition of the periodic velocities and the mean steady current velocity. Figure 5.36 shows the maximum and minimum total velocity profiles for the combined deep water waves and medium current at a height of 150 mm from the bed. As the graph illustrates, flow reversal takes place within the wave boundary layer. The lower figure zooms into the wall boundary to provide more detail of this reversal. Almost all the tests showed flow reversal in the immediate vicinity of the smooth sidewall. This agrees well with the findings of Kyriacou (1988) who also reported that flow reversal occurred near the smooth bed in his tests for all the three wave periods employed. Figure 5.37 compares the total velocities in the vicinity of the sidewall and at a height of 150 mm for deep, intermediate, and shallow water waves combined with medium current. It shows that the region of flow reversal extends further into the flow with increasing wave period, a trend also repeated in other experiments of this study. The tests also showed that for a given wave period (see figure 5.38), the size of the region of flow reversal in the vicinity of the sidewall reduces with the strength of the mean steady current. Figure 5.39 illustrates an extreme example of this where for the combined shallow water waves and weak current the flow experiences a reverse velocity during some phases of the cycle throughout the measured width of the channel.

The method employed for calculating the maximum and minimum shear stresses was an extension of the scheme used to calculate the mean shear stress from the viscous sublayer both in the current only and the combined tests. The peak sidewall shear stresses for each

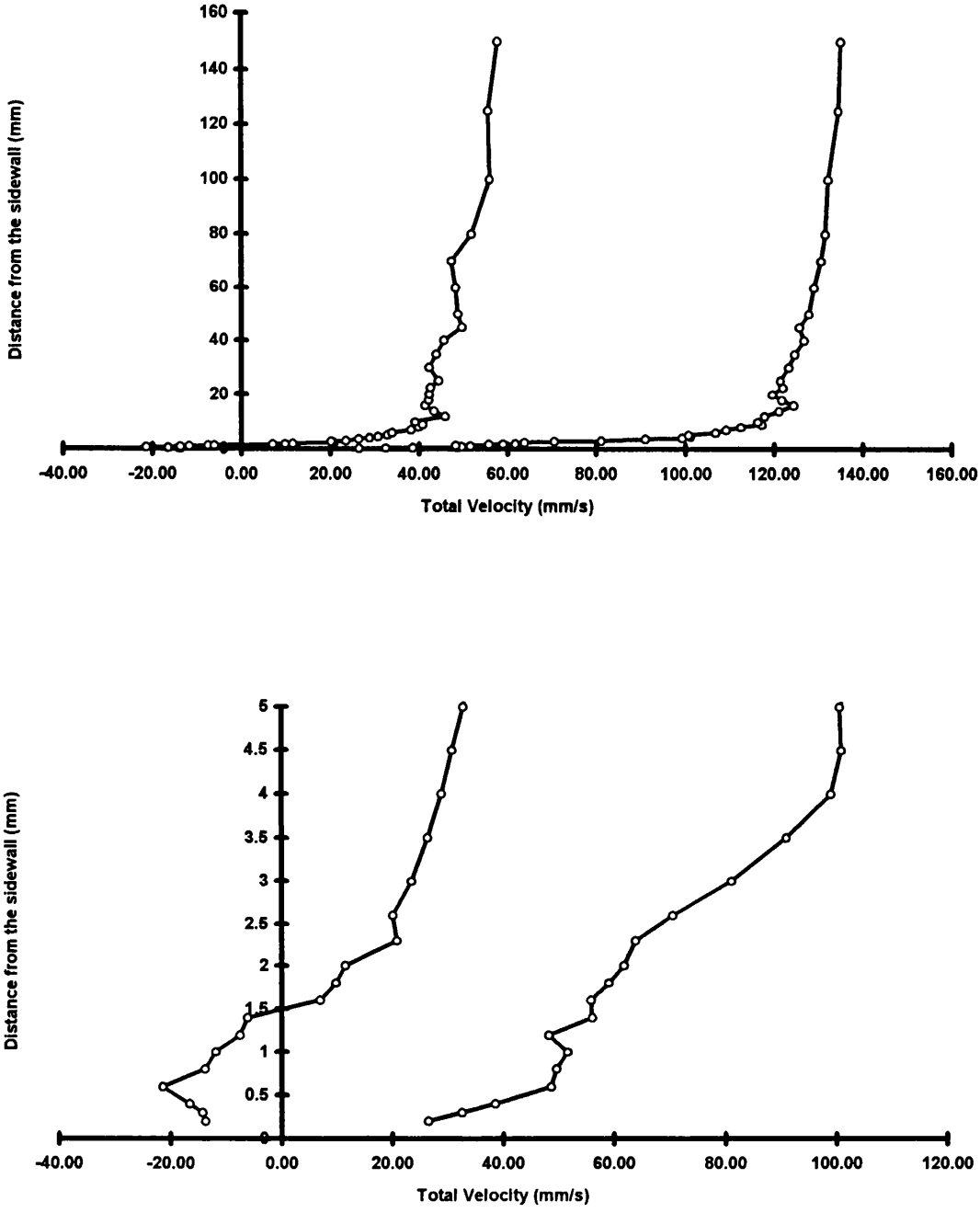

Figure 5.36 Maximum and minimum total velocity profiles for the combined 0.7s waves and medium current. Test C-SDWMC.150.

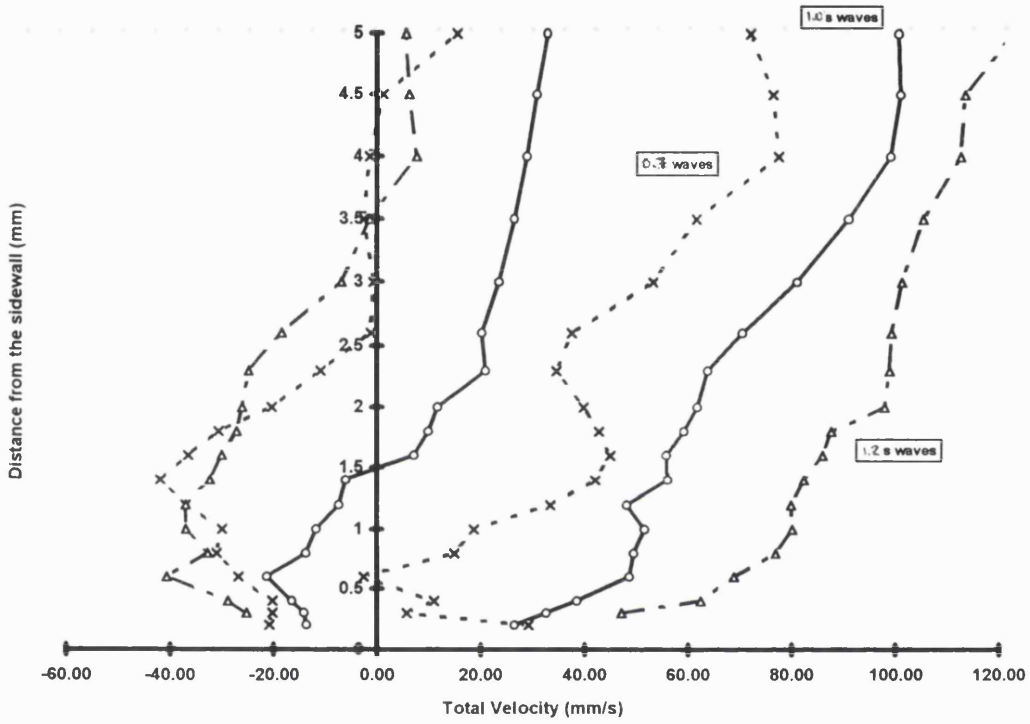

Figure 5.37 Comparison of maximum and minimum velocity profiles in the immediate vicinity of the sidewall between the flows combining the medium current with the 0.7s, 1.0s, and 1.2s waves

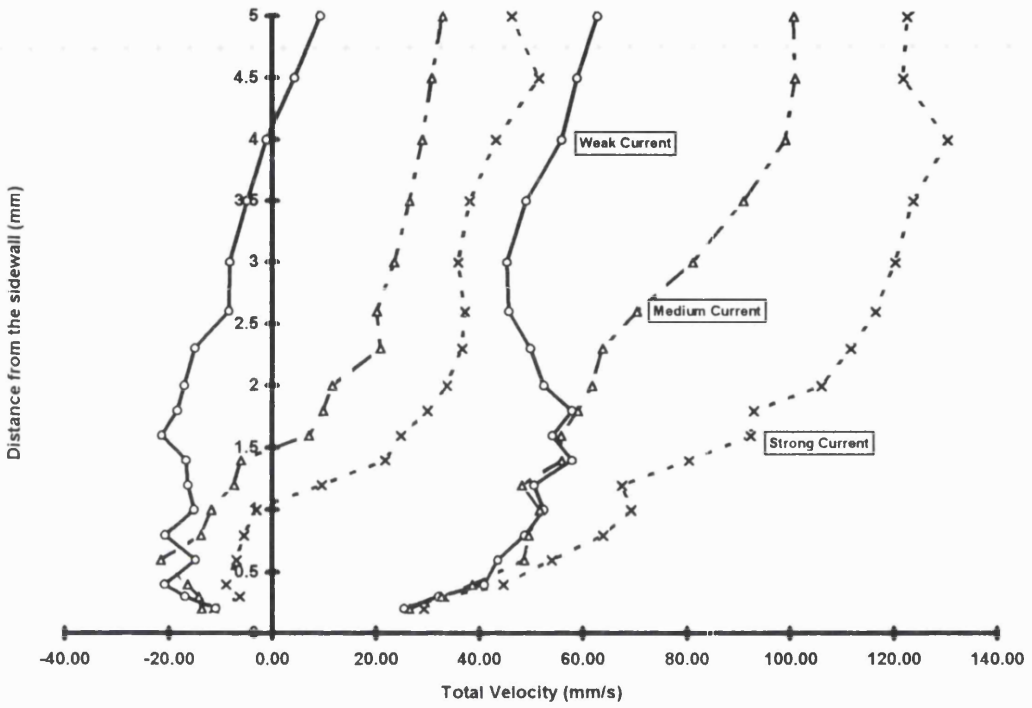

Figure 5.38 Comparison of total velocity profiles in the vicinity of the sidewall for the 0.7s waves to show the reduction in the height of the region of flow reversal with the increasing strength of the current.

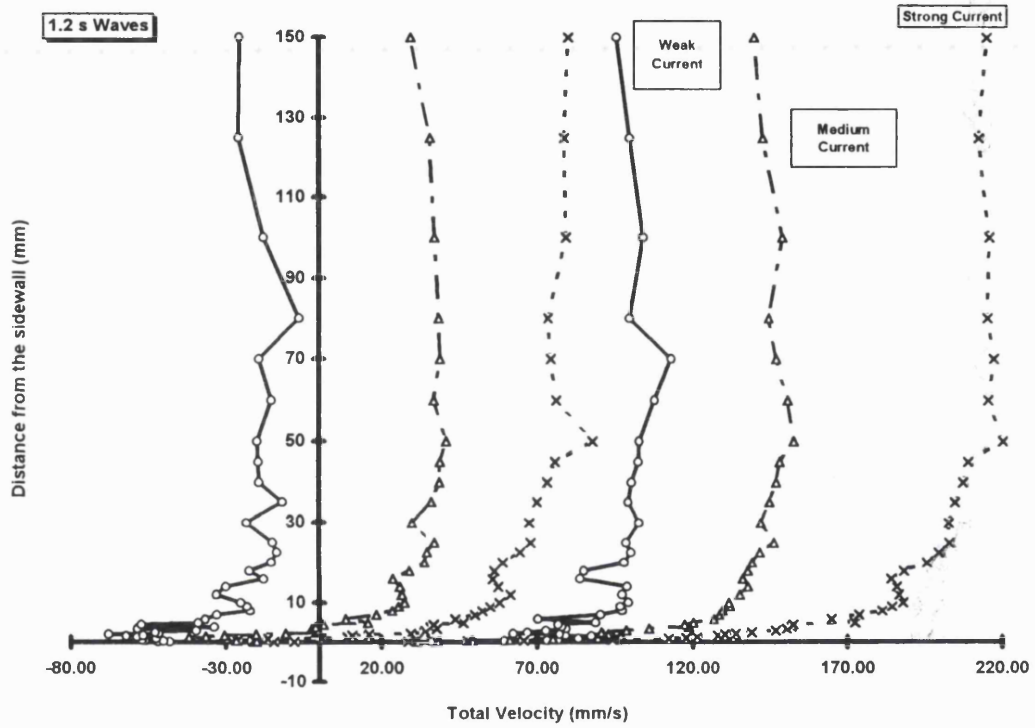

Figure 5.39 Comparison of total velocity profiles in the vicinity of the sidewall for the 1.2s waves with increasing current strength.

experiment were computed by fitting a straight line through the maximum and minimum total velocities. The value of the shear stress was consequently calculated from the slope of the straight line. The kinematic viscosity of the flow for each experiment was worked out from the water temperature measured during the tests. Figure 5.40 shows examples of the maximum and minimum shear stress for the case of the combined flows. The length of the inner layer reduced in combined flow conditions to between 0.6mm to 0.8mm, while in unidirectional current flows the length of the inner layer was typically 0.8mm to 1.0mm.

Table 5.16 summarises the results of the maximum wall shear stress calculations. It also presents the maximum wall shear velocity, the mean shear stress, the friction factor for the combined flow, and the waves and current interaction factors "m" and "σ". All the calculations were performed using the formulae described in Chapter 2.

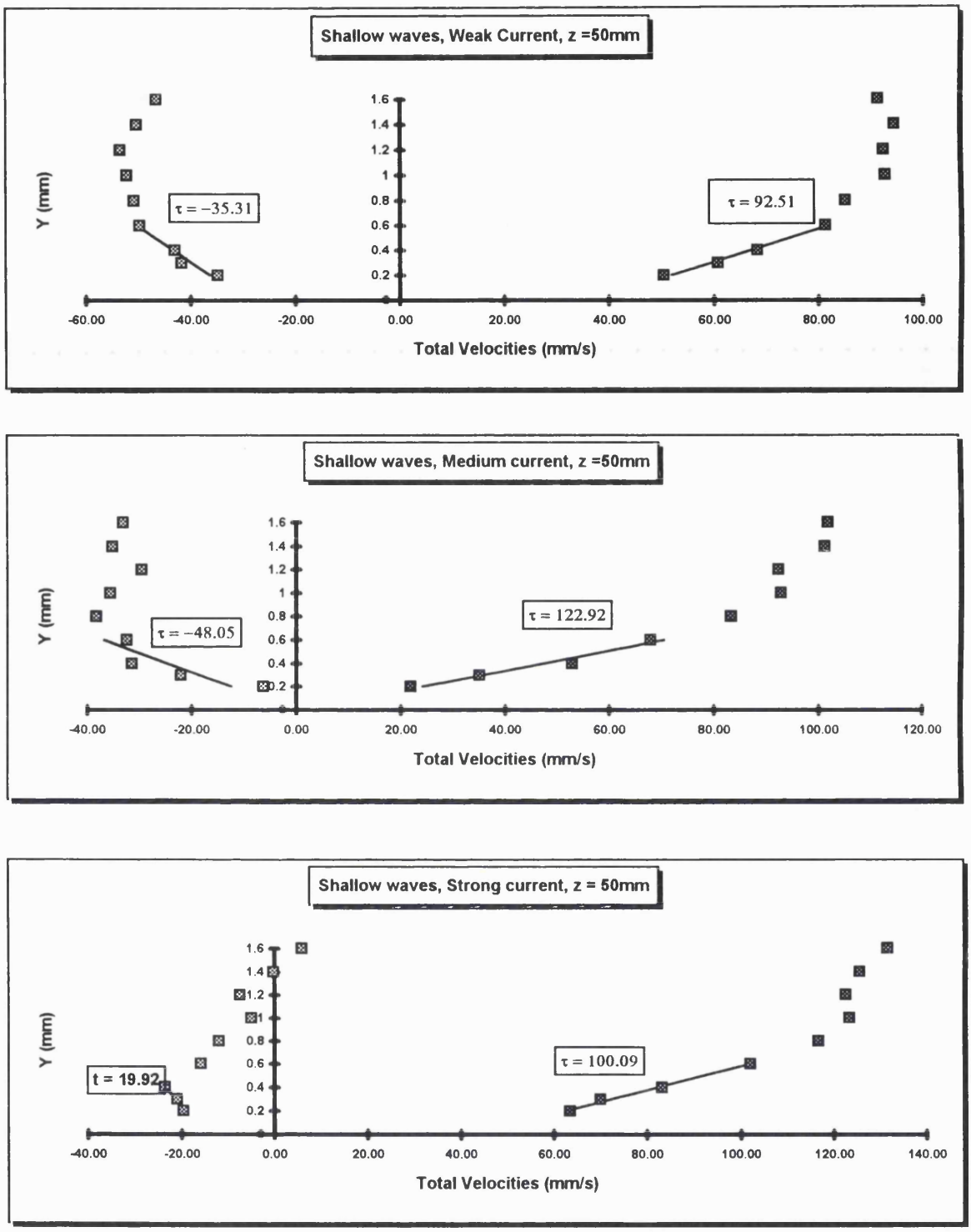

Figure 5.40 Examples of the maximum and minimum shear stress obtained from the inner layer of the total velocity profiles.

TEST CODE	τ mean (mm/s)^2	u^* mean (mm/s)	τ max (mm/s)^2	τ min. (mm/s)^2	u^* max (mm/s)	u^* min. (mm/s)	σ	m	f mean	f max
C-DWWC.20	4.58	2.14	15.58	5.69	3.95	-2.39	0.29	1.29	0.0095	0.1070
C-SDWWC.50	6.15	2.48	24.23	18.99	4.92	-4.36	0.25	1.25	0.0106	0.1193
C-SDWWC.150	11.97	3.46	78.42	49.05	8.86	-7.00	0.15	1.26	0.0082	0.1409
C-SDWMC.20	9.26	3.04	22.84	2.39	4.78	1.55	0.41	1.41	0.0034	0.1445
C--SDWMC.50	14.86	3.85	65.84	26.17	8.11	-5.12	0.23	1.23	0.0045	0.3139
C-SDWMC.150	15.72	3.96	58.66	21.49	7.66	-4.64	0.27	1.27	0.0042	0.1423
C-SDWSC.20	23.31	4.83	21.78	15.65	4.67	3.96	1.07	2.07	0.0031	0.0728
C-SDWSC.50	32.83	5.73	60.89	20.05	7.80	4.48	0.54	1.54	0.0037	0.1217
C-SDWSC.150	34.05	5.84	67.17	8.02	8.20	2.83	0.51	1.51	0.0041	0.0871
C-SIWWC.50	4.08	2.02	53.88	23.18	7.34	-4.81	0.08	1.08	0.0085	0.0555
C-SIWWC.150	10.20	3.19	88.94	6.59	9.43	-2.57	0.11	1.11	0.0067	0.0483
C-SIWMC.50	18.44	4.29	69.28	18.40	8.32	-4.29	0.27	1.27	0.0055	0.0517
C-SIWMC.150	16.46	4.06	78.86	45.29	8.88	-6.73	0.21	1.21	0.0050	0.0465
C-SIWSC.20	23.91	4.89	66.28	9.86	8.14	-3.14	0.36	1.36	0.0033	0.0552
C-SIWSC.50	32.70	5.72	89.61	8.09	9.47	-2.84	0.36	1.36	0.0036	2.0516
C-SIWSC.150	29.24	5.41	55.07	10.17	7.42	-3.19	0.53	1.53	0.0034	0.0288
C-SSWWC.50	12.04	3.47	76.37	35.31	8.74	-5.94	0.16	1.16	0.0119	0.0349
C-SSWWC.150	22.43	4.74	92.51	14.80	9.62	-3.85	0.24	1.24	0.0212	0.0387
C-SSWMC.20	16.37	4.05	64.53	13.85	8.03	-3.72	0.25	1.25	0.0060	0.0412
C--SSWMC.50	23.87	4.89	122.92	48.05	11.09	-6.93	0.19	1.19	0.0068	0.0656
C-SSWMC.150	18.02	4.24	47.60	20.25	6.90	-4.50	0.38	1.38	0.0058	0.0232
					0.00	0.00				
C-SSWSC.20	28.98	5.38	94.17	14.10	9.70	-3.75	0.31	1.31	0.0042	0.0543
C-SSWSC.50	39.37	6.27	100.09	19.92	10.00	-4.46	0.39	1.39	0.0041	0.0493
C-SSWSC.150	39.91	6.32	96.99	22.92	9.85	-4.79	0.41	1.41	0.0043	0.0489

Table 5.16 Measured parameters of the combined flow.

CHAPTER 6

DISCUSSION AND CONCLUSIONS

The Hydrodynamics of Flow near a Sidewall

The theoretical derivations to describe wave height attenuation presented in chapter 2 of this thesis assume that the flow near a sidewall behaves in a similar manner to that over a horizontal bed. In order to confirm the validity of this assumption, detailed measurements of the steady and periodic velocity profiles in "current only", "waves only" and "combined flows" were carried out near a channel sidewall. Before examining the effectiveness of the proposed theories, this section briefly discusses the results of these measurements and uses them to reassess for a vertical boundary some of the well established conclusions for flow over a horizontal bed.

6.1 Unidirectional Current

For the unidirectional current only flows, the calculated Reynolds numbers (defined as Ud/υ) ranged from 14,850 for the weak current to 53,470 for the strong current, indicating the existence of turbulent regimes for all the "current only" flows. As expected for a glass boundary, the "roughness Reynolds numbers" (U^*k_s/υ) remained well below 5, thus confirming a hydraulically smooth boundary.

The first series of the L.D.A. tests, which measured the velocity profiles on straight lines perpendicular to the bed at different distances from the channel wall (Figure 6.1), showed the degree of influence of the sidewall boundaries in the flow. It should be noted

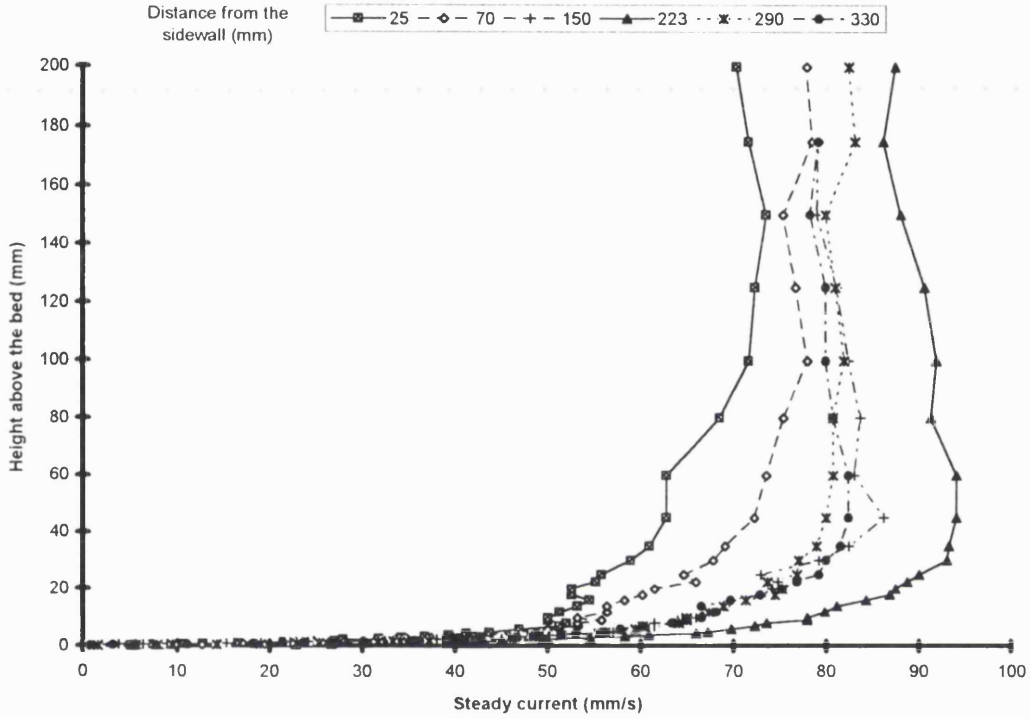

Figure 6.1 Velocity profiles of the medium strength, unidirectional current at various distances from the sidewall

that while the values shown for 223mm are at the centre of the channel, the 290mm and 330mm values are 167mm and 127mm from the other sidewall respectively. The measurements demonstrated that the velocity profiles peaked significantly below the water surface, especially toward the core of the flow. This is because flow distribution in flumes with an aspect ratio of less than 10 is inherently three dimensional. Authors such as Knight (1979) also found that, in their open channel experiments, the point of maximum velocity was suppressed to well below the water surface, and have published valuable research on the subject.

The L.D.A. test that measured the transverse velocity profiles in the sidewall boundary layer demonstrated the three distinctive regions associated with the inner layer, the overlap layer and the outer flow, similar to the case of unidirectional flow over the channel bed. In the immediate vicinity of the sidewall, the solid boundary restricts the turbulent eddies to such a degree that viscous stresses dominate the motion. This inner layer in which the mean velocity increased linearly with distance from the wall, was evident in all the tests performed. The thickness of the region (δs) varied between 0.8mm to 1.0mm. This gave a value of between 4.3-6.5 to the non-dimensional parameter, $\delta^+=u^*\delta s/\upsilon$. These are much lower than the value of 11.6 for the bed viscous sublayer quoted by Sleath (1984), but agreed more with the value of δ^+=5-6.7, suggested by Hinze (1975).

The shear stress at the sidewall was calculated from the linear velocity slope of the inner layer. As shown in Figure 6.2a for the case of the medium strength current, the values of

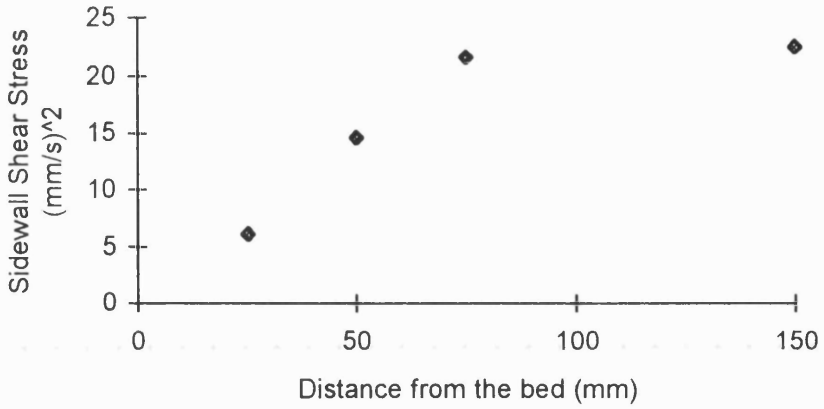

Figure 6.2a The change in sidewall shear stress with distance from the bed for unidirectional, medium strength current

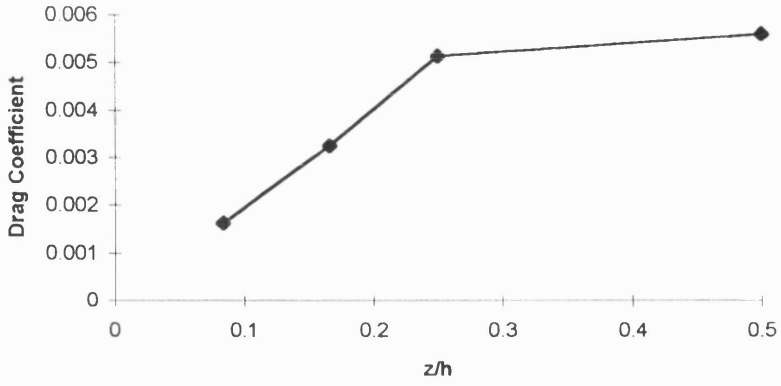

Figure 6.2b Change in coefficient drag with increasing height above the bed

mean wall shear stress generally increased with height above the bed, in a similar way to bed shear stress increasing with distance from the sidewall. Figure 6.2b shows the corresponding values of sidewall drag coefficients ($C_d=\tau/\rho U^2$) at various heights above the bed. The increase in C_d is because, while the mean velocity in the centre of the channel stayed more or less the same above 25mm from the bed (see Figure 6.1), the slope of the velocity increase in the sidewall sublayer increased with height above the bed (for an example see Figure 5.21).

The data obtained in the overlap layer of the flow near the wall boundary for various tests showed good agreement with the logarithmic expression of Prandtl-Von Karman. Figure 6.3 employs the data from the medium current tests carried out with the horizontal LDA system B (reported in Chapter 5) to show how mean velocity profiles (best fit lines) became steeper, and thus the wall shear stress became larger with distance from the bed. The same trend was confirmed by weak and strong current tests.

Von Karman's constant, κ is found to be different from the universally quoted 0.4. The value of κ in the present tests was between 0.35 to 0.37. Other authors found even a smaller range; 0.33 (Laufer, 1951), 0.30 (Laursen, 1963), and 0.344 (Grass, 1967). The reason for these discrepancies can be attributed to the three dimensionality of the flow and low Reynolds numbers.

The start of the outer flow region, where the velocity profile deviated from the straight line logarithmic distribution, was dependent on the strength of the steady current and the

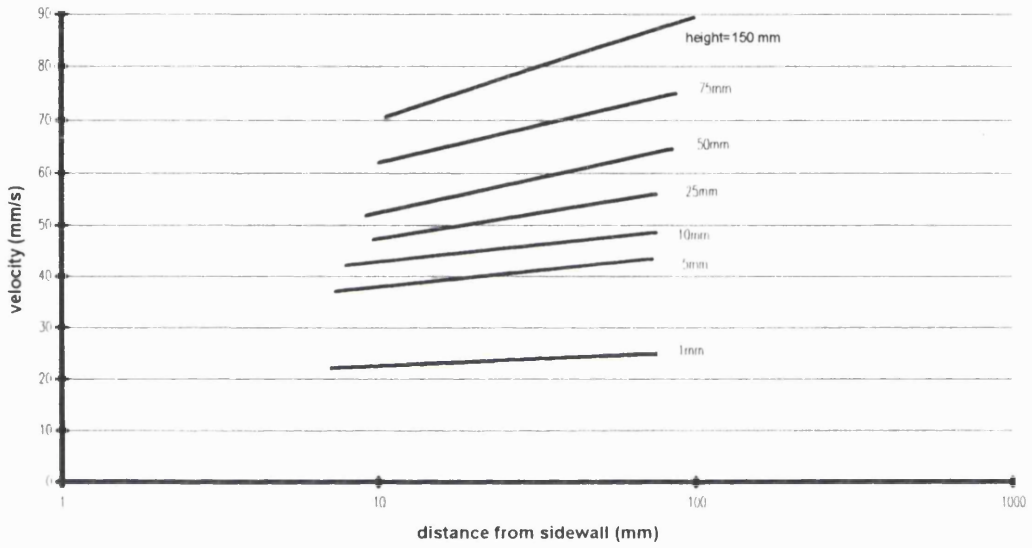

Figure 6.3 Change in the steepness of velocity profiles in the log. layer with height above the bed; medium strength, unidirectional current tests.

measuring height. The stronger the steady current, the higher the bottom limit of the outer flow region became. The value of zu^*/υ for this limit developed from 90 for the weak current profile measured at 50mm above the bed to 350 for the strong current profile measured at 150mm from the bed.

Although expected from the Navier Stokes equation, these tests confirmed that the unidirectional flow near the vertical boundary behaves very much like steady current over the horizontal bed. Thus, the assumption made in Chapter 2 about the behaviour of the unidirectional steady current near a sidewall is shown to be valid.

6.2. Waves in Still Water

Measuring the mass transport velocity profile from the bed at the centre of the UCL channel, Kemp and Simons (1982) discovered that there was a net fluid motion in the direction opposite to wave propagation at the centre of the channel. They found that while in the bottom 20mm of their measuring line the mass transport was in the direction of wave propagation, the mean velocities became increasingly negative above that height. They argued that the net motion towards the paddle at the centre of the channel must be compensated for by a net forward motion elsewhere in the cross section. In the course of the present tests, the mass transport was measured in transverse lines to the sidewall at heights of 20mm, 50mm and 150mm from the bed for deep, intermediate, and shallow water waves. The results reported in Chapter 5, made it possible to establish the pattern of mass transport distribution in the flow cross section. In general, the motion is in the

direction of wave propagation near the solid boundaries, and becomes negative towards the core of the flow. The positive velocity is largest within the immediate vicinity of the boundaries, while the negative velocities increase with distance from the walls as the result of the larger orbital motions away from the boundaries.

The periodic velocity profiles shown in Chapter 5 clearly demonstrated the "overshoot" region within the viscous dominated layer of the flow. This phenomenon was described by Lamb (1932) for the one dimensional wave motion at a solid boundary. However, these experiments showed that the "overshoot" region also exists in the case of a two dimensional sidewall boundary.

6.3. Combined Waves and Current Flows

At the sidewall, the addition of the current reduced the wave induced orbital velocities in the same manner as that already established for the bed boundary. This attenuation increased further with the strength of the current. While the current induced turbulence made the data less "smooth", the "overshoot" region continued to exist with the addition of the currents. It did, however, become less prominent and somewhat "blunted" with stronger currents.

The transverse mean velocity profile also changed as the result of the addition of waves. In comparison with the current only profiles, there was an increase near the sidewall, while a considerable velocity reduction took place towards the core of the flow. Figure 6.4

illustrates how a transverse current profile in the combined flow is altered when a wave induced mass transport is superimposed. The same phenomenon was reported by others such as Simons, Grass and Kyriacou (1988) who carried out velocity profile measurements from the bed. Using the transverse data collected in this project and those presented by the above researchers for the centre of the channel, it is possible to map this redistribution of the flow. The outcome is similar to the zones of positive and negative mass transport reported in Chapter 5 from measurements of waves in still water. This suggests the steady current velocity near the boundaries increases due to a positive wave induced mass transport, while away from the boundaries, mass transport increasingly opposes the following current. The measurements carried out showed that while the trend supports the suggestion, a simple arithmetic addition would not explain the whole phenomenon observed.

The combined flow results showed that the three dimensional nature of the flow continued to exist after the superposition of the waves. As discussed in section 6.1 for the unidirectional flows with small aspect ratios, the point of maximum velocity in the channel was suppressed to well below the water surface. Although this trend agrees with the findings of other researchers such as Simonet al (1988) mentioned above, in the present study the phenomenon was more exaggerated. This was due to the fact that the flow aspect ratio during these tests was over 30% smaller than in their experiments. In addition, their measurements were made at the centre of the channel, and cannot be directly compared with the present cross sectional measurement.

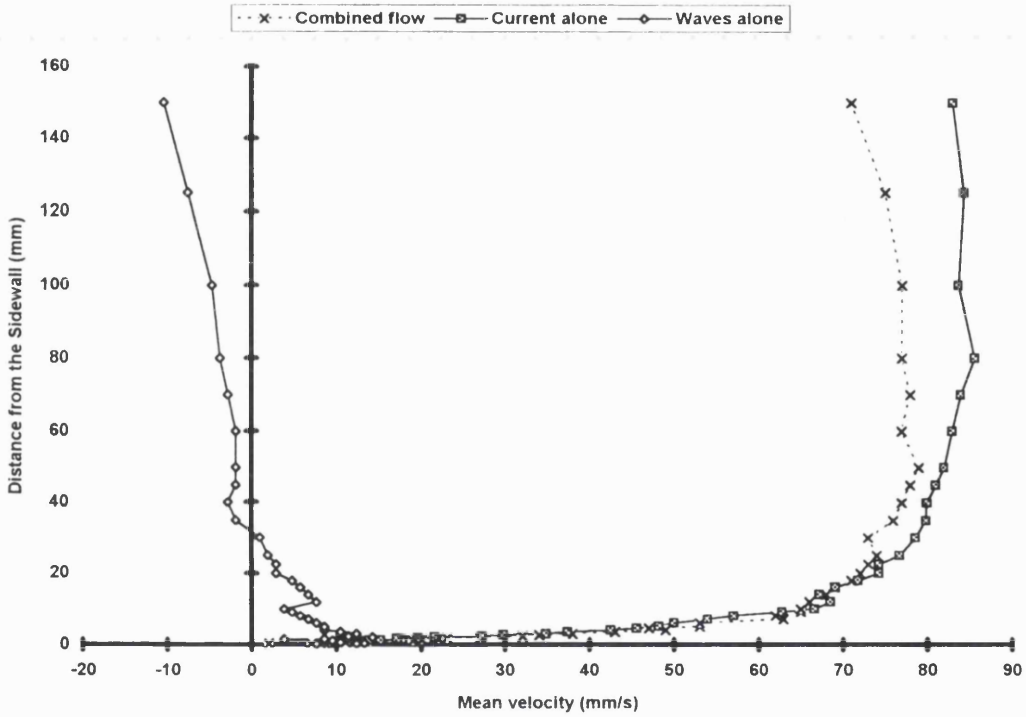

Figure 6.4 The velocity profiles of the steady components of the combined flow; 150mm above the bed

The three distinctive layers of flow continued to exist in the combined waves and current next to the vertical boundary. The mean velocity in the viscous sublayer grew in comparison with current only for all test conditions resulting in an increase in the sidewall shear stress. The thickness of the inner layer reduced after the superposition of the waves in comparison to the pure current value, especially when longer period waves were added. A logarithmic layer continued to exist after waves were superimposed on the current. It was found that the slope of the logarithmic region did not alter for various wave periods. Thus, within the present range of wave conditions, wave period does not have a significant effect on the wall shear stress. In the outer regions of the flow, mean velocity reduced significantly from the current alone values.

In general it is clear that employing the theories developed for the flow over a horizontal boundary, with necessary modifications to predict the flow behaviour near a sidewall, is justified. The most important amendment to the flat bed models addresses the fact that, while the wave movement over a bed is one dimensional, near a vertical boundary wave movement remains two-dimensional. The models developed in Chapter 2 take account of this difference. The following section will examine the ability of these models to predict the wave height attenuation of a combined flow in a test flume.

This section discusses the results of the wave height attenuation measurements presented in Chapter 5, and compares them with those predicted by the two models developed in Chapter 2. It assesses the validity of the "modified Hunt formula" derived for laminar flows, and the "wave attenuation equation" for turbulent flows. Finally, it projects its findings to conclude how a change in various properties of the flow will affect wave damping.

6.4 The Modified Hunt Formula

As described earlier, Hunt (1952) provided a simple estimate of wave height attenuation in a closed laboratory channel. Hunt's formula was amended in Chapter 2, employing a moving frame of reference to account for the current, to provide a first approximation of wave attenuation in combined flows. Table 6.1 compares wave height attenuation predicted by the "modified Hunt formula" with those measured in the three partitioned narrow channels. Wave height attenuation coefficients increase dramatically with the reduction of the channel breadth (Figure 6.5). In the derivation of Hunt's theory in Chapter 2, it was shown that the attenuation coefficient, in its most basic form, is the ratio between the energy dissipated at the boundaries and the rate of change of wave energy transmitted in the body of the flow. Reducing the aspect ratio of the flow reduces the total amount of energy flux in the fluid while the same energy is still dissipated at the boundaries. This change in the ratio of the energy dissipation to energy flux leads to the change in wave height attenuation coefficient.

test Code	B mm	T 1/s	Uc mm/s	α Measured *E -3	α Predicted *E -3	Discrepency %
ADW.10	10	0.7	0	420	370	12%
ADWWC.10	10	0.7	50	400	337	16%
ADWMC.10	10	0.7	100	382	319	16%
ASW.10	10	1.2	0	189	147	22%
ASWWC.10	10	1.2	50	182	140	23%
ASWMC.10	10	1.2	100	156	135	13%
ADW.20	20	0.7	0	223	185	17%
ADWWC.20	20	0.7	50	207	172	17%
ADWMC.20	20	0.7	100	186	157	16%
AIW.20	20	1	0	127	97	24%
ASW.20	20	1.2	0	94	74	21%
ASWWC.20	20	1.2	50	86	71	17%
ASWMC.20	20	1.2	100	78	68	13%
ADW.30	30	0.7	0	165	124	25%
ADWWC.30	30	0.7	50	154	114	26%
ADWMC.30	30	0.7	100	140	106	24%
ASW.30	30	1.2	0	64	50	22%
ASWWC.30	30	1.2	50	63	48	24%
ASWMC.30	30	1.2	100	61	46	25%

Table 6.1 A comparison between the measured wave height attenuations and those predicted by "the modified Hunt formula".

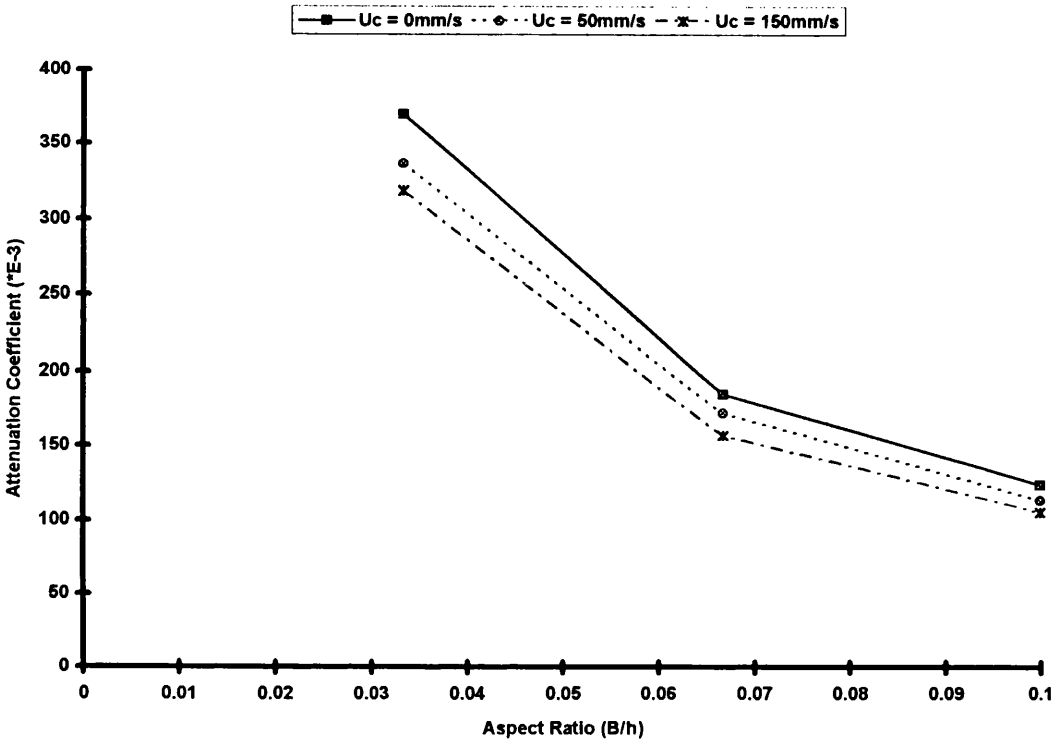

Figure 6.5 The effect of changing aspect ratio and current strength on wave height attenuation; 1.0 second waves.

It is also clear from Table 6.1 that the attenuation coefficient decreases with increasing wave period. In this respect the predictions of the modified Hunt theory are in line with the Hunt's original formula. However, the difference between the two versions comes to light when investigating combined waves and current flows. The modified theory predicts the reduction in wave height attenuation coefficient with growing current domination of the flow. In general, the reduction in wave damping with increasing current strength was larger for the deep water waves. Both the trend and the magnitude of the reduction agree with the series of measurements carried out at UCL during the last 15 years. Noting the attenuation coefficient is an expression of the ratio of the wave energy dissipated at the boundaries to the rate of wave energy transmitted in the body of the fluid, wave damping decreases with the addition of a current, as the following current increases the absolute group velocity of the waves and consequently the rate of energy transmission. Since an opposing current has the opposite effect and reduces the energy flux of the flow, this also explains why Kemp and Simons (1983) found that in their tests, when waves were propagating against the current, an increase in the wave damping was observed.

When compared to the measured attenuation coefficients, the "modified Hunt formula" underestimated wave damping in all the narrow channel tests. The discrepancy ranged between 13% and 25%. The discrepancy between theory and measured data does not seem to depend on the aspect ratio or wave period. But the most interesting finding is that the theory appears to correctly predict the amount of reduction in wave height attenuation due to the addition of current.

Table 6.2 compares the wave damping measured in the wider channel for both the waves alone and the combined flows with those predicted by the "modified Hunt formula". Here the rate of wave height attenuation along the channel is also presented and compared with the dH/dx measured during the tests. This is possible because, as demonstrated in the Figures 5.11 to 5.13 of Chapter 5, dH/dx is very small and can be considered linear.

As anticipated, the predictions from the modified Hunt theory showed a reduction in wave height attenuation with increasing $U_c/(U_c+u_0)$. The drop in the attenuation coefficient with current strength became smaller with decreasing h/gT^2 (increasing wave period). One possible explanation for this phenomenon is that shallow water waves have a larger rate of wave energy transmission. The addition to the waves energy flux by the following current is a smaller proportion of the overall energy flux of the longer waves, and thus has a smaller effect on wave damping. Therefore, when superimposing a current, the longer the period of waves, the smaller the effect on wave damping.

As expected, Table 6.2 also shows a reduction in wave height attenuation coefficient with decreasing h/gT^2. Attenuation coefficient reduces with increasing energy flux of the flow. shallower water waves have larger energy flux. Thus, the attenuation coefficient of waves with longer periods is smaller.

For the wider channel, the modified Hunt theory does not consistently underestimate the wave damping in the manner demonstrated for the narrow channel. In the present tests, the scale of waveheight attenuation is in the order of 0.1mm to 0.3mm per metre length;

test Code	h/(gT^2)	Uc/(Uc+u)	dH/dx Measured	α Measured	α Predicted	Discrepency
	1/s	mm/s	* E -5	*E -3	*E -3	%
SDW.150	0.062	0.00	-40	10.03	8.50	15%
SDWWC.150	0.062	0.57	-32	8.10	7.93	2%
SDWMC.150	0.062	0.62	-16	3.93	7.65	-95%
SDWSC150	0.062	0.80	-28	6.93	7.31	-6%
SIW.150	0.031	0.00	-26	6.45	5.32	18%
SIWWC.150	0.031	0.49	-11	2.75	5.11	-86%
SIWMC.150	0.031	0.60	-15	3.78	5.00	-32%
SIWSC.150	0.031	0.72	-19	4.73	4.86	-3%
SSW.150	0.021	0.00	-20	5.10	4.35	15%
SSWWC.150	0.021	0.43	-16	4.10	4.30	-5%
SSWMC.150	0.021	0.59	-20	4.98	4.23	15%
SSWSC.150	0.021	0.72	-6	1.47	2.86	-95%

Table 6.2 Comparison between the predictions of wave attenuation using the modified Hunt theory and the measured values in the wide channel; B=457 mm, h= 300 mm

i.e. a maximum of 2.5mm along the 8m measuring length. Thus, a very small error in measurement could have a significant effect on the discrepancy between the theoretical and empirical values. For instance, in the case of the SSWSC test, a 95% discrepancy represents an error of less than 1mm along the 8m span. The comparison between the predictions of the "modified Hunt formula" and the data obtained from the narrow partitioned channels, where the scale of wave damping was significantly more, should be considered a better guide to both the accuracy of the theory and its shortcomings.

Table 6.3 uses the data presented by Kyriacou (1988) to further assess the validity of the modified Hunt theory. Kyriacou performed experiments both in the smooth bed UCL channel and the rough bed flume at Hydraulics Research Station Ltd (HRS). Here, comparison is carried out with his "category three" wave heights which are on average between 40mm and 35mm and thus, closest to the values used during the present project. Values of h/gT^2 and $U_c/(U_c+u_0)$ are also comparable. It should be noted that the modified Hunt theory overpredicted the attenuation almost as many times as it underestimated it. Kyriacou (1988) too warned against an unconditional acceptance of his results, as the scale of measurements was such that it was not possible to avoid significant margins of error. He also performed a series of preliminary tests in narrow, partitioned channels. This time, he found that the original Hunt theory was consistent in underestimating the wave height attenuation in waves only tests. Once again it was only during these experiments that the magnitude of wave damping was large enough to make a reasonably accurate measurement for assessing the reliability of the theory.

Kyriacou (1988)'s Test Code	h/gT^2	Uc/(Uc+u)	Ho	dH/dx Measured	α Measured	α Predicted	Discrepency
			mm	* E -5	*E -3	*E -3	%
SDWA3	0.042	0.00	35.7	-45.3	12.69	9.28	27%
SDWC3	0.042	0.71	36.0	-16.2	4.50	8.07	-79%
SIWA3	0.020	0.00	40.0	-29.9	7.48	6.70	10%
SIWC3	0.020	0.65	35.2	-18.9	5.37	6.13	-14%
SSWA3	0.014	0.00	38.0	-15.0	3.95	5.93	-50%
SSWC3	0.014	0.67	34.9	-12.7	3.64	5.47	-50%
RDW3	0.062	0.00	26.5	-24.3	9.17	6.40	30%
RDWCW3	0.062	0.84	24.1	-18.6	7.72	5.95	23%
RDWCM3	0.062	0.92	17.6	-2.5	3.90	5.40	-38%
RDWCS3	0.062	0.94	16.0	-5.9	3.69	5.12	-39%
RIW3	0.031	0.00	46.5	-38.7	8.32	4.27	49%
RIWCW3	0.031	0.56	43.3	-30.0	6.93	4.06	41%
RIWCM3	0.031	0.79	33.4	-18.3	5.48	3.84	30%
RIWCS3	0.031	0.85	30.7	-19.1	6.22	3.69	41%

Table 6.3 Comparison between the predictions of wave attenuation using the modified Hunt theory and Kyriacou's (1988) category 3 data.

Both the original and the modified Hunt formula underestimate the amount of wave damping. The results, therefore, suggest that there are other factors contributing to wave damping that are not accounted for by Hunt's theory. Below, the more significant damping mechanisms and theoretical considerations that are not included in the Hunt expression are discussed and their relative importance and quantitative contribution to wave attenuation are assessed.

Theoretically, Hunt's solution was derived from the first order small amplitude wave theory. Thus, by definition, it has the same limitations. Many of the assumptions of first order wave theory such as the waves being sinusoidal or the flow being irrotational are clearly not correct in the case of the present experiments. Although it was argued previously that this does not create a fundamental flaw in the application of the Hunt solution to the employed waves, it should still be noted that the theory can only provide a first approximation.

In addition, while Hunt's theory considers the energy dissipated at the solid boundaries, it ignores any energy dissipation in the body of the fluid. The internal viscous dissipation term is $4\upsilon k^2 E$, which is an order of $k(\omega/2\upsilon)^{1/2}$ higher than that given by Hunt. Including the effect of the internal dissipation in the present tests leads to an increase of only about 2% in the total attenuation coefficient for the shorter period waves, and an even smaller increase of 1% for the remaining tests. Thus, when compared with the overall magnitude of uncertainties involved, it is justified to exclude the internal viscous dissipation for tests in laboratory flumes. The situation is however different, when an engineer is attempting to predict wave height attenuation in the offshore environment, when there is no energy

dissipation at the sidewalls, and the depth of water can be very large.

The effect of the free surface of the fluid on wave damping was first highlighted in a paper written by van Dorn (1966). It was also demonstrated in a series of tests during the present study that surface contamination can markedly change wave attenuation. During these tests, a thin film quickly formed on the water surface for waves only tests. The effect of the surface contamination was to increase wave attenuation. This accounts for some of the discrepancy between the Hunt predictions and the measured attenuation. But the magnitude of its effect, which as reported in Chapter 5 was no larger than 5% of the overall attenuation (for the worst possible case), was not large enough to account for the amount that Hunt's theory underestimates attenuation.

In addition, it should be noted that the derivation of the Hunt formula does not make any allowance for roughness on the solid boundaries. It is clear that far more energy is dissipated at a rough boundary than a smooth one, but Hunt's formula makes no distinction between the two.

Hunt's theory can also be used to determine what the contribution of each boundary is to wave attenuation. Table 6.4 presents the attenuation coefficient due to both the bed and the two sidewall boundaries in the three partitioned narrow channels. The narrower the channel, the less significant the role of the bed boundary becomes in wave damping. In the narrowest of the channels over 99% of damping was caused by the sidewall boundaries.

test Code	Bed α *E -3	Bed contribution %	Sidewall α *E -3	Sidewall contribution %
ADW.10	0.40	0.11%	369.50	99.89%
ADWWC.10	0.50	0.15%	337.60	99.85%
ADWMC.10	0.60	0.19%	318.77	99.81%
ASW.10	1.20	0.82%	145.30	99.18%
ASWWC.10	1.25	0.89%	138.90	99.11%
ASWMC.10	1.25	0.92%	134.00	99.08%
ADW.20	0.40	0.22%	184.70	99.78%
ADWWC.20	0.50	0.29%	171.50	99.71%
ADWMC.20	0.60	0.38%	156.80	99.62%
AIW.20	1.13	1.17%	95.80	98.83%
ASW.20	1.20	1.63%	72.60	98.37%
ASWWC.20	1.25	1.76%	69.80	98.24%
ASWMC.20	1.25	1.84%	66.80	98.16%
ADW.30	0.40	0.32%	123.20	99.68%
ADWWC.30	0.50	0.44%	113.40	99.56%
ADWMC.30	0.60	0.57%	105.50	99.43%
ASW.30	1.20	2.42%	48.40	97.58%
ASWWC.30	1.25	2.62%	46.50	97.38%
ASWMC.30	1.25	2.73%	44.50	97.27%

Table 6.4 The contribution of the bed and siewalls to wave attenuation in the three partitioned channels, as predicted by the "modified Hunt formula"; B=10, 20, and 30 mm, h = 300 mm.

The purpose of these narrow channel tests was to eliminate the effect of the bed boundary, which according to these results was achieved. The value of the attenuation coefficient due to the sidewall boundaries dropped sharply with the addition of each 10mm to the width of the channel. Table 6.5 compares the contribution of each boundary to the attenuation in the wider channel tests. Here, the sidewalls were still responsible for most of the attenuation.

In general, as h/gT^2 increases, becoming nearer to deep water waves, the relative significance of the sidewall for the wave attenuation grows. A closer study of the attenuation coefficients caused by the bed and sidewall boundaries reveals that while the overall attenuation coefficient falls with decreasing h/gT^2, according to the "modified Hunt formula", this is solely caused by the reduction of the attenuation due to the sidewalls. The bed attenuation in fact increases with longer waves (Figure 6.6).

Both tables 6.4 and 6.5 show that the "modified Hunt formula" predicts the bed attenuation coefficient, α_b, to increase with the growing influence of the steady current. Figure 6.7 demonstrates how α_b and α_s react differently to the addition of current. T he reduction in α_s with growing current strength is smaller in percentage terms than the increase in α_b. But the absolute values of the sidewall contribution during these tests were so large that they ensured a similar trend in the overall attenuation coefficients.

test Code	Bed α *E -3	Bed contribution %	Sidewall α *E -3	Sidewall contribution %
SDW.150	0.42	4.94%	8.08	95.06%
SDWWC.150	0.53	6.68%	7.40	93.32%
SDWMC.150	0.59	7.72%	7.05	92.28%
SDWSC150	0.67	9.17%	6.63	90.83%
SIW.150	1.13	21.24%	4.19	78.76%
SIWWC.150	1.16	22.75%	3.94	77.25%
SIWMC.150	1.18	23.60%	3.82	76.40%
SIWSC.150	1.21	24.90%	3.65	75.10%
SSW.150	1.24	28.12%	3.17	71.88%
SSWWC.150	1.25	29.07%	3.05	70.93%
SSWMC.150	1.25	29.55%	2.98	70.45%
SSWSC.150	1.26	30.58%	2.86	69.42%

Table 6.5 The contribution of the bed and sidewalls to wave attenuation in the wider channel, as predicted by the "modified Hunt formula"; B= 457mm, h = 300 mm.

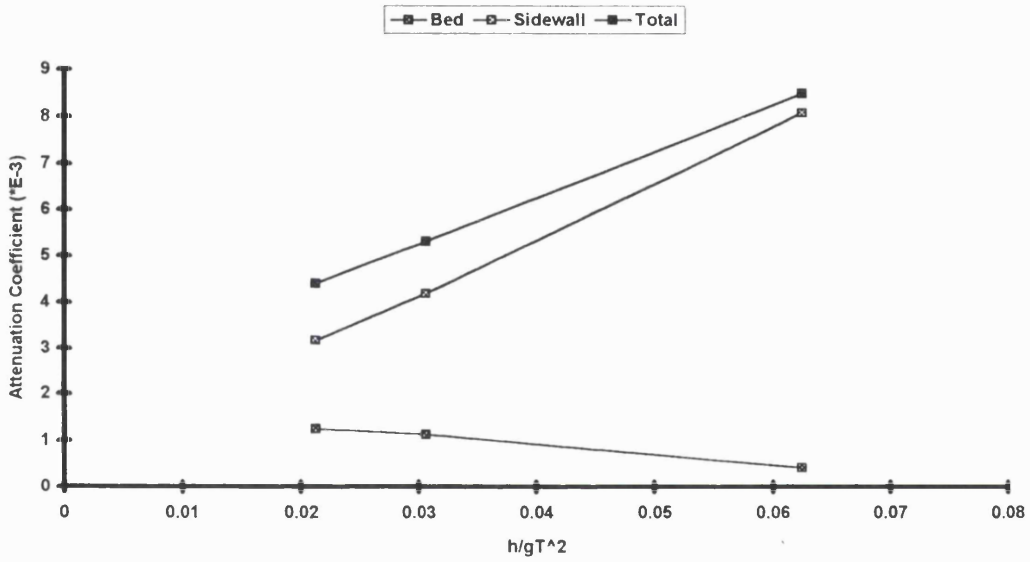

Figure 6.6 Variation of bed and sidewall attenuation coefficient with wave period, predicted by the "modified Hunt formula". B=457mm, U_c = 0 mm/s.

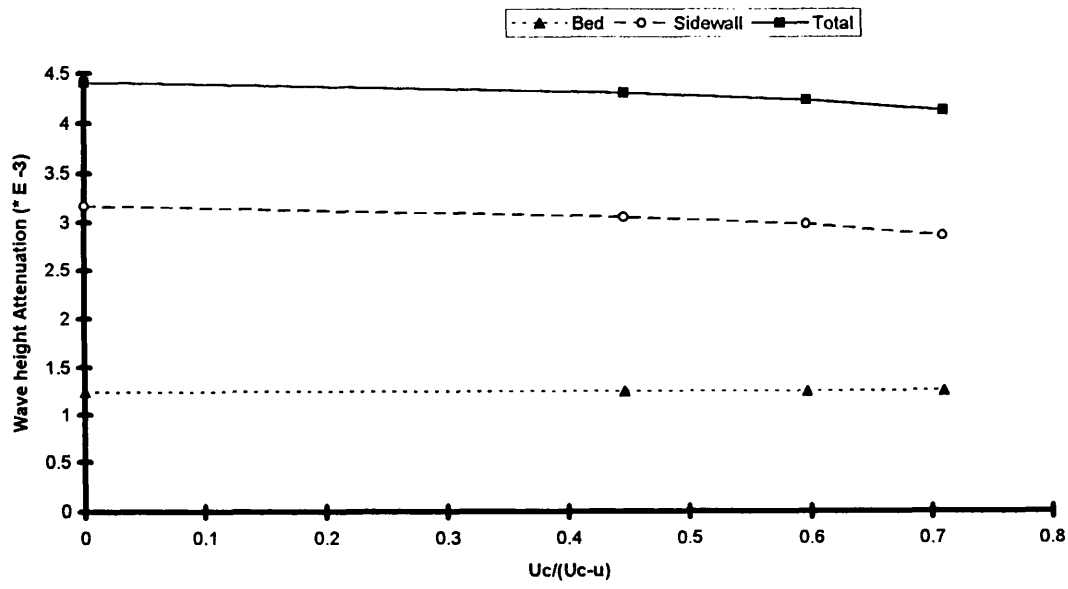

Figure 6.7 Variation of bed and sidewall attenuation coefficient with steady current velocity, as predicted by the modified Hunt formula, B=457mm, T = 1.2s.

Table 6.6 presents the amount of wave energy dissipated at the bed and sidewalls as well as the wave energy transmitted in the flow for all the tests in the main (457mm wide) channel. Both the energy dissipation at the boundaries and the wave energy flux increase as the flow becomes more current dominated (Figure 6.8). The wave energy dissipated at the bed increases at a higher rate with the current strength than that at the sidewall. The total attenuation coefficient reduces with h/gT^2 (larger orbital velocities), because the wave energy dissipated at the sidewall increases at a slower rate than the wave energy flux. On the other hand, the energy dissipated at the bed grows at a faster rate with wave period than does the wave energy flux. This explains why the attenuation coefficient due to the bed boundary grows with shallow water waves (larger orbital velocities). As h/gT^2 falls, the rate of reduction of total attenuation coefficient with shallower water waves decreases. This is partly because in deep water waves, the bed attenuation coefficient plays a less important role in the overall wave damping mechanism.

In a similar manner, it is possible to explain why the total attenuation coefficient falls with $U_c/(U_c+u_o)$ while the bed attenuation coefficient increases. According to the "modified Hunt formula", the wave energy dissipated at the sidewall, which constitutes the greater part of the total energy dissipation of the waves, increases at a slower rate with growing current domination than the wave energy flux. At the same time however, the energy dissipated at the bed grew at a larger rate with $U_c/(U_c+u)$ than the energy flux. The reduction of attenuation coefficient with the current strength falls with shallower water waves because the gap closes between the wave energy dissipated and transmitted.

test Code	Energy Dissipated At the Bed g/s^3 *E -3	Energy Dissipated At the Sidewall g/s^3 *E -3	Energy Flux g/s^3 * E -3
SDW.150	0.15	2.92	362.00
SDWWC.150	0.22	2.99	400.00
SDWMC.150	0.26	3.00	430.00
SDWSC150	0.31	3.10	460.00
SIW.150	0.95	3.50	833.00
SIWWC.150	1.06	3.57	904.00
SIWMC.150	1.11	3.58	940.00
SIWSC.150	1.20	3.66	999.00
SSW.150	1.49	3.82	1200.00
SSWWC.150	1.59	3.88	1270.00
SSWMC.150	1.66	3.93	1310.00
SSWSC.150	1.77	4.01	1400.00

Table 6.6 Energy flux through the flow, and energy dissipation at the bed and sidewall, as predicted by the "modified Hunt formula"; B=457mm, z =150mm.

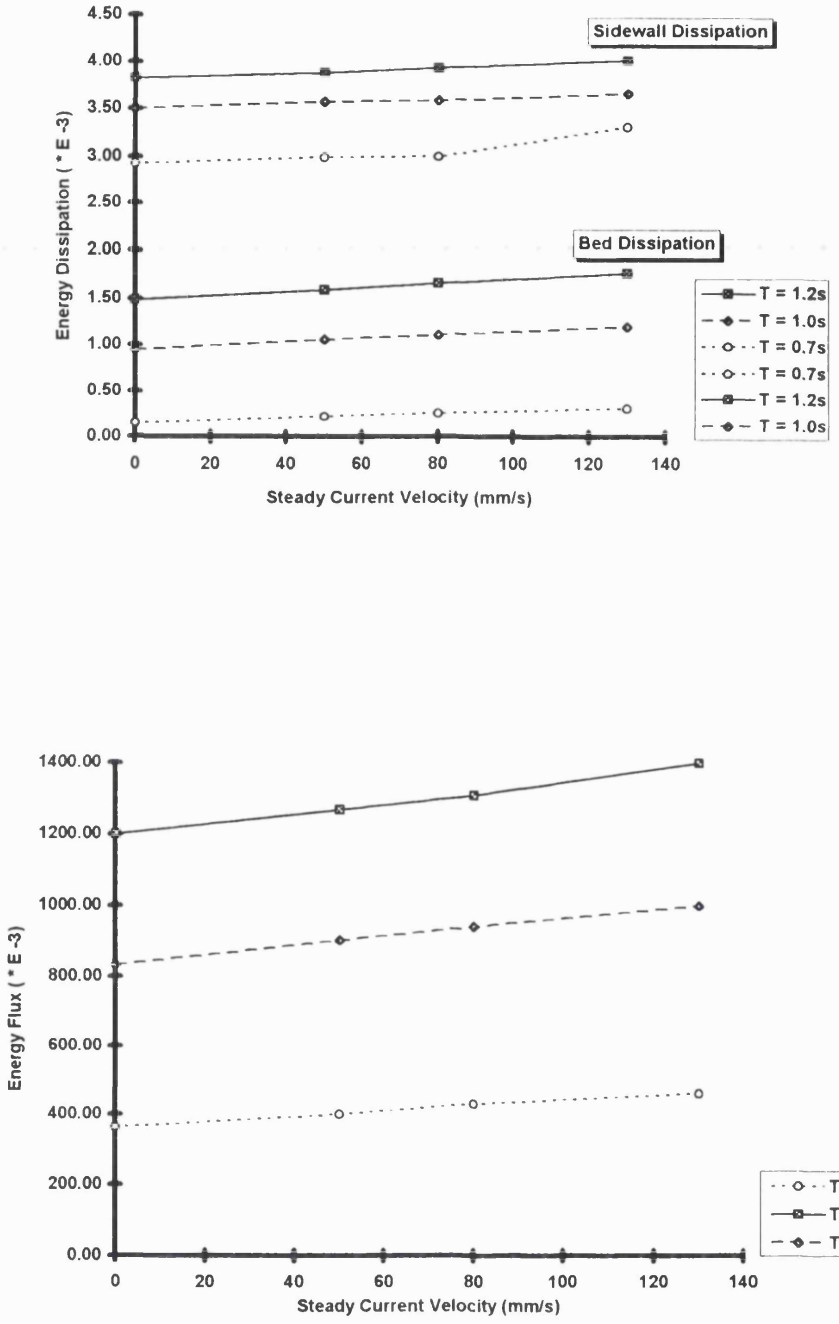

Figure 6.8 Variation in the wave energy flux and wave energy dissipation at the boundaries with current strength and wave period. B=457mm.

The above study shows that in spite of its simplicity, the modified Hunt formula provides a useful method for obtaining a first approximation of wave attenuation in combined flows with smooth boundaries. The theory also helps to explain how a variation in wave and current properties affects the damping mechanism. At the end of this chapter, this finding is employed in an attempt to provide a guide to the trends and magnitude of wave attenuation through a wide range of flow conditions.

6.5 The Wave Attenuation Equation

Although Hunt's theory provided an approximation of wave damping, it was derived for laminar waves and is not strictly applicable to combined flows, which are usually turbulent. When there is a superimposed mean current added, the calculation becomes considerably more complicated. For turbulent flows, in place of the attenuation coefficient, the rate of wave height attenuation along the channel has to be obtained. This can still be defined as the ratio of the energy dissipated at the boundaries to the rate of energy transmitted along the flume. Here however, the energy dissipated within the turbulent inner layer at the boundaries can no longer be calculated analytically and the use of friction factors becomes necessary. A more appropriate approach, "the wave attenuation equation", was derived in Chapter 2. A computer model, the "wave attenuation software" (WAS), was developed to evaluate the equation and to provide a detailed analysis of various components of the combined flow. A discussion of the computer model's outputs follows.

An advantage of "WAS" is the very small number of flow properties it requires as input.

These are limited to the wave period, wave height, water depth and the maximum current strength as well as the dimensions of the flume and a description of its solid boundaries. Its output includes such basic terms as depth averaged steady current strength, periodic velocities, wavelength, steady and oscillatory shear velocities, wave and current Reynolds numbers, absolute and relative wave numbers and frequencies, absolute and relative wave and group velocity, wave energy, radiation stress, and apparent bed and sidewall roughness. The model also computes the shear velocities, friction factors and shear stresses for waves alone and pure currents as well as those relating to wave and current components of a combined flow. In doing so, it provides a detailed breakdown of energy dissipation through the whole wave cycle, showing how each component behaves during various phases of the oscillation. All the calculations are performed separately for the bed and sidewalls. Finally, "WAS" evaluates the "wave attenuation equation", determining the relative contribution of each boundary to wave damping (see Appendix A for a copy of the software and a step by step description of its calculations).

In this case, Brink-Kjaer and Jonsson's (1976) theory is employed to predict the orbital velocities. It should be noted that an advantage of the model is that it is written in a modular manner which makes the substitution of any of its elements possible. At the bed, the output of the "wave attenuation software" showed a number of identifiable trends. The wave friction coefficient in a combined flow, f_{bcw}, increased with current domination and deeper water waves. The current friction factor in the combined flow fell with the strength of the steady current, and increased with shallower water waves. The amplitude shear stress also increased with shallower water waves, while the mean shear stress was dependent mainly on $U_c/(U_c+u_o)$. The energy dissipation for each component of the flow

was calculated at one degree intervals and then integrated through the wave cycle (see Chapter 2) to provide the total energy loss per wave period. It was assumed that the instantaneous velocity in the vicinity of a boundary obeyed a logarithmic velocity distribution so as to enable the instantaneous value of shear stress and consequently energy dissipation to be calculated. The energy loss by the current in a combined flow clearly grew with the current domination of the flow, and became the significant factor in the dissipation of the total flow energy as $U_c/(U_c+u_o)>0.7$. The term that affects waveheight attenuation directly, though, is the energy dissipated by the waves in a combined flow. According to the model, wave energy dissipation at the bed increased in general with both shallower water waves and current domination of the flow.

The mechanism of the dissipation of energy on the sidewall is similar to the bed boundary. The difference here is that the wave motion on the vertical sidewall is two dimensional. Energy dissipation is not a directional entity, and the total energy loss due to the cyclic motion of the fluid particles next to the sidewall should be determined. To facilitate the calculation, it was assumed that energy dissipation can be resolved in the horizontal and vertical directions, and then added together at the end to produce the total energy loss. Figure 6.9 demonstrates various horizontal components of the energy dissipation on the sidewall at the height of 150 mm from the bed, through the 360 degrees of a wave cycle, for the case of $U_c/(U_c+u_o)=0.4$ and the shallow water waves, SSWMC. The pattern predicted by the computer model for the change in various components of shear stress and energy dissipation at the sidewall with $U_c/(U_c+u_{s0})$ and h/gT^2 resembled what was described above for the bed boundary. However, the wave energy dissipation at the sidewall fell with growing current strength.

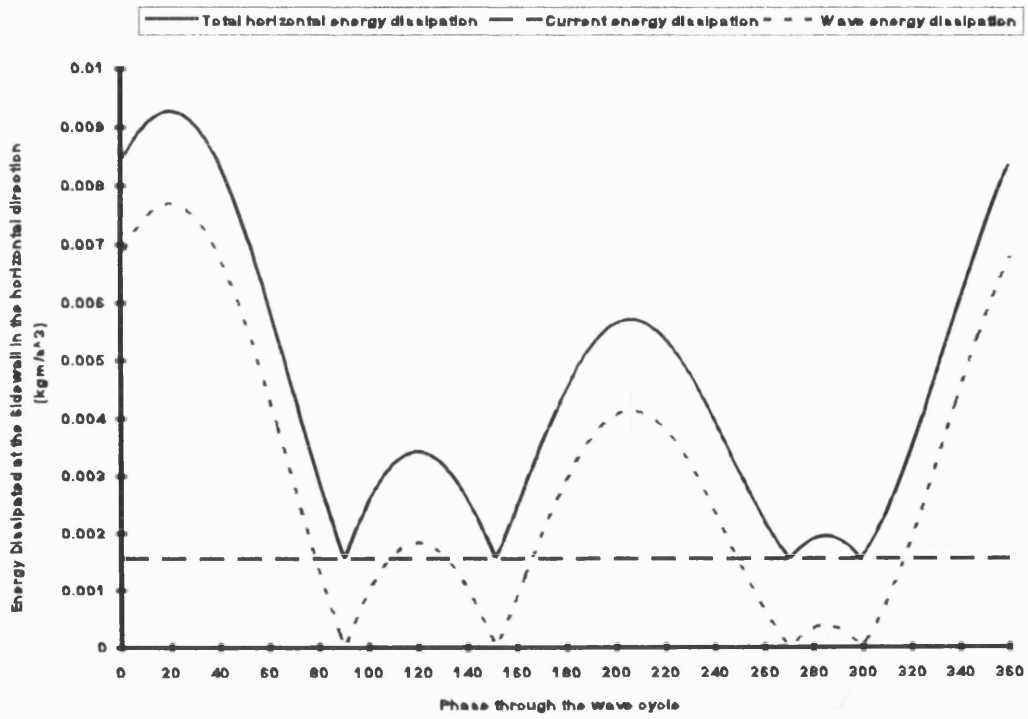

Figure 6.9 Variation in horizontal energy dissipation through a wave cycle according to the computer model's calculations.

In the vertical direction, the value of the steady current is assumed to be zero, making the flow of a waves alone nature. Thus, the wave energy dissipation in the vertical direction is calculated using a pure waves friction factor (see Chapter 2). Due to the geometry of the wave oscillation at the sidewall, for the shallow water waves considered, the vertical component of the orbital velocity is very much smaller than the horizontal component, leading to a smaller energy loss. For the near deep water waves tests, where the particle motions are more circular, the amounts of energy loss in the vertical and horizontal directions are closer. In addition to the wave period, this is also dependent on the height of the segment under consideration from the bed. The nearer to the surface one gets, the more circular the orbital motion of the waves is, and thus, the closer the amount of energy loss in the vertical and horizontal directions.

The various terms necessary to evaluate the rate of change of energy flux through the body of the fluid are calculated by the model for each experiment and presented in Table 6.7. All the terms were computed from first order linear theory. As expected, it shows that the wave celerity as well as both the absolute and the relative group wave velocities increase with current strength and wave period. Meanwhile the internal wave energy remains unaffected by h/gT^2. As a function that is very much dependent on the wave height, the wave energy falls as the waves stretch with current strength. The radiation stress term or wave thrust reduces with h/gT^2 and $U_c/(U_c+u_0)$.

It is now possible to present all the terms necessary to evaluate the wave attenuation equation. These are listed for all the wide channel tests in Table 6.8. For the present test conditions, the first two terms are clearly dominant in the numerator of the equation.

		Cr	Cgr	Cga	Sxx	E
TEST CODE		m/s	m/s	m/s	kg/s^2	kg/s^3
SDW		1.06	0.58	0.58	1.11	1.96
SDWWC		1.11	0.64	0.68	1.10	1.86
SDWMC		1.17	0.67	0.75	0.91	1.50
SDWSC		1.30	0.72	0.84	0.69	1.10
SIW		1.30	0.94	0.93	1.68	1.96
SIWWC		1.37	0.96	1.04	1.56	1.77
SIWMC		1.45	1.04	1.10	1.43	1.58
SIWSC		1.65	1.10	1.21	1.24	1.33
SSW		1.42	1.13	1.13	1.99	1.96
SSWWC		1.50	1.18	1.22	1.93	1.86
SISWMC		1.53	1.21	1.29	1.57	1.50
SSWSC		1.69	1.28	1.40	1.52	1.41

Table 6.7 Wave parameters calculated from linear theory and used in assessing the energy flux in the flow.

	The Wave Attenuation Equation							
	The Numerator Terms				The Denominator Terms			
TEST CODE	1st term	2nd term	3rd term	4th term	1/4 pgH	1st term	2nd term	3rd term
	*E-3	*E-3	*E-6	*E-6	*E-3	*E-3	*E-3	*E-3
SDW	0.14	2.99	0.00	0.00	24.53	579.00	0.00	0.00
SDWWC	0.16	2.65	0.06	0.35	23.91	675.00	0.82	0.27
SDWMC	0.18	2.35	0.45	8.23	21.46	735.00	1.04	0.65
SDWSC	0.21	2.11	2.22	42.82	18.39	859.00	5.92	2.45
SIW	0.76	2.83	0.00	0.00	24.53	939.00	0.00	0.00
SIWWC	0.77	2.64	0.73	2.22	23.30	1036.00	0.65	0.34
SIWMC	0.79	2.50	2.31	14.05	22.07	1126.00	2.08	1.24
SIWSC	0.82	2.38	5.49	47.59	20.23	1213.00	4.26	2.73
SSW	1.16	2.86	0.00	0.00	24.53	1134.00	0.00	0.00
SSWWC	1.15	2.75	0.46	0.57	23.91	1202.00	0.38	0.25
SISWMC	1.16	2.60	3.27	14.86	21.46	1288.00	1.54	1.10
SSWSC	1.18	2.54	7.45	49.66	20.85	1409.00	4.65	3.80

First term of the numerator ; $-B.\Gamma_{wb}$

second term of the numerator ; $-2h.\Gamma_{ws}$

third term of the numerator ; $\frac{U_c^2}{gh}.B(-\Gamma_b+\frac{1}{2}U_c\tau_b)$

fourth term of the numerator ; $\frac{U_c^2}{gh}.2h(-\Gamma_s+\frac{1}{2}U_c\tau_s)$

First term of the denominator ; C_{ga}

second term of the denominator ; $-\frac{1}{2}\frac{U_c^2}{C_r}$

third term of the denominator ; $\frac{U_c^2}{gh}.(C_{ga}+\frac{1}{2}U_cG+\frac{1}{2}\frac{U_c^2}{C_r})$

Table 6.8 Terms of the "wave attenuation equation" calculated for the wide channel tests. All units in kgm/s^3.

The two remaining terms become more significant as the current strength grows. The absolute group velocity term (1/4 $\rho g H.C_{ga}$) dominates the denominator of the "wave attenuation equation". Thus, as shown in Chapter 2, one can simplify the "wave attenuation equation" by reducing it to the ratio of wave energy dissipated at the bed and the two sidewalls over the absolute group velocity term.

Table 6.9 presents the rates of wave height attenuation along the channel as predicted by the full equation. It also shows the predicted wave attenuation after employing Christofferssen and Jonsson's (1985) energy dissipation approximation (equations 2.81 and 2.82). The proposed approximations clearly work better for current dominated flows. Figure 6.10 compares wave dampings predicted by the above two methods and shows how wave attenuation due to each boundary reactsto changing h/gT^2 and $U_c/(U_c+u_0)$. For combined flows with steady following current, the model successfully predicts the reduction in the total wave damping as $U_c/(U_c+u_0)$ grows. It should be noted, the results here do not agree with the predictions of the "modified Hunt formula" that the wave attenuation caused by the bed increases with the addition of current. While according to the model, this was the case for the deeper water waves, the bed attenuation actually dropped with steady current strength for both the intermediate and shallow waves.

Figure 6.11.a compares the predictions of the model with wave attenuation values measured in the wider channel during this study.

		dH/dx	C&J Eq.	(dH/dx)b	(dH/dx)s
TEST CODE		*E - 5	*E - 5	*E - 5	*E - 5
SDW		-33.39	-41.22	-1.51	-31.87
SDWWC		-27.35	-34.00	-1.56	-25.79
SDWMC		-23.00	-28.35	-1.62	-21.38
SDWSC		-19.30	-23.30	-1.73	-17.57
SIW		-17.04	-21.78	-3.63	-13.41
SIWWC		-15.10	-18.90	-3.41	-11.69
SIWMC		-13.67	-16.80	-3.36	-10.31
SIWSC		-12.26	-14.35	-3.15	-9.11
SSW		-13.17	-16.34	-3.79	-9.38
SSWWC		-12.03	-14.66	-3.56	-8.47
S $WMC		-11.12	-12.50	-3.35	-7.77
SSWSC		-10.21	-11.35	-3.23	-6.97

Table 6.9 Comparison between wave height attenuation predicted by the full "wave attenuation equation" and the reduced formula. The contribution of each boundary to wave damping is also shown.

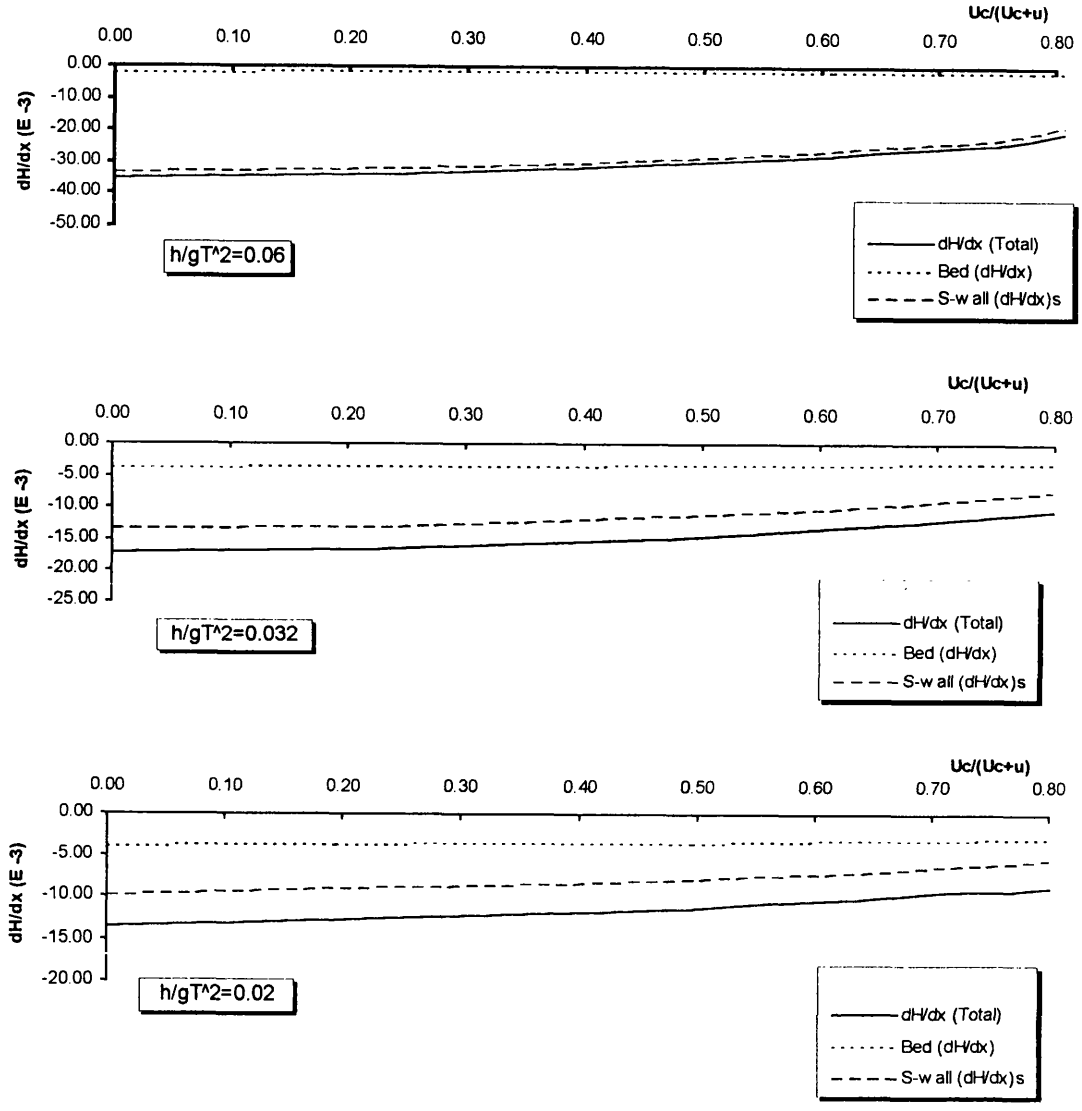

Figure 6.10 Variation in wave damping with $U_c/(U_c+u)$ and h/gT^2; as predicted by the "wave attenuation equation".

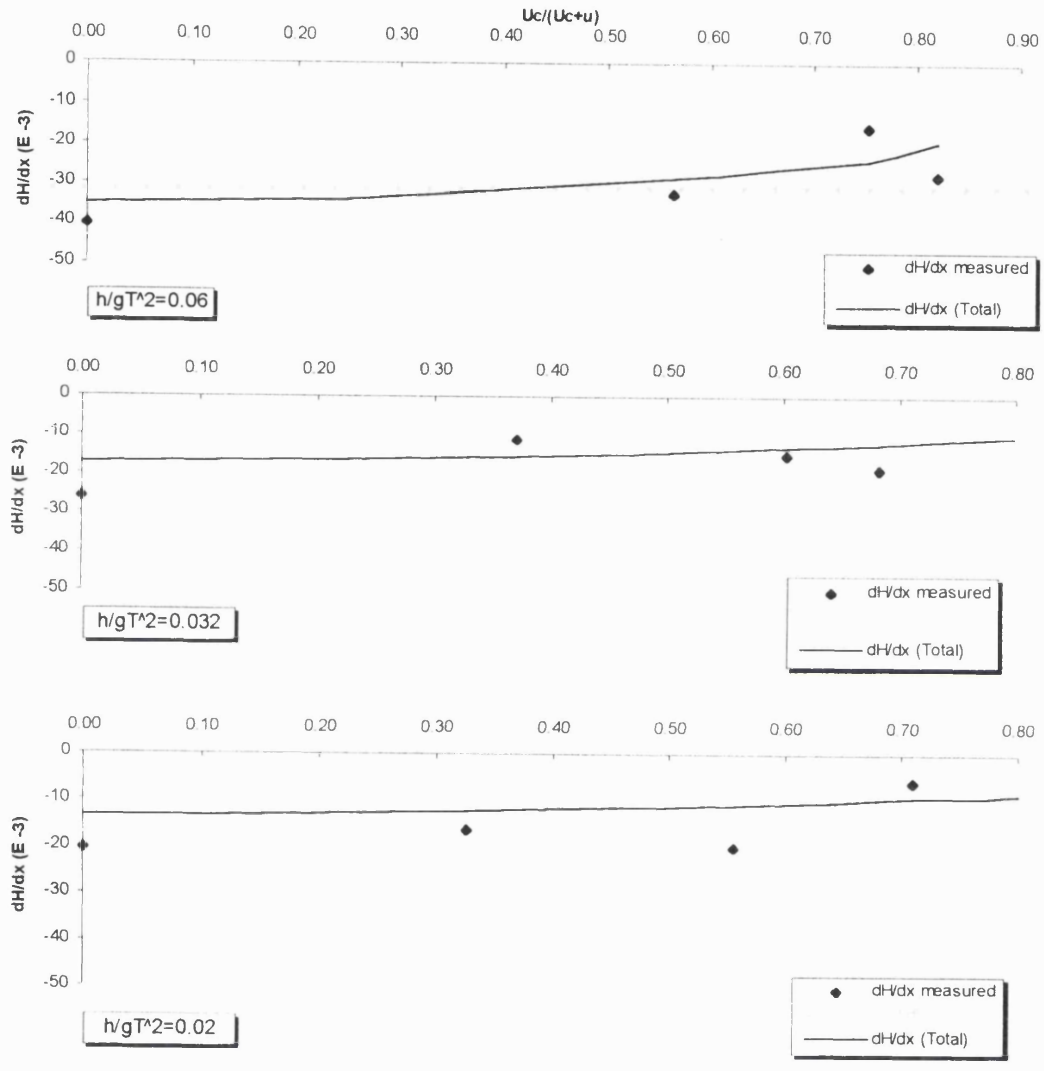

Figure 6.11.a Comparison between the measured wave attenuation and those predicted by the "wave attenuation equation".

Considering the degree of accuracy of the experiments, the comparison shows a good agreement between the theoretical and the empirical values. Figure 6.11b makes a similar comparison between the predictions of the "wave attenuation equation" and the data presented by Simons, Grass and Kyriacou (1988). Their measurements included combined flows over both smooth and rough beds. Here again, the model is successful in predicting both the trend and the magnitude of wave height attenuation. Kemp and Simons (1983) measured wave damping in combined flows with an adverse steady current. They found that wave damping increased considerably after the addition of an opposing current. Figure 6.11c compares their data with the predictions of the model, and shows the ability of the "wave attenuation equation" to account for damping of waves that are propagating against the direction of steady current.

The agreement between the output of the model and the empirical values is in fact very good when one considers the difficulties discussed earlier in measuring the actual wave height attenuation during the experiments. In their study of various existing models for the predictions of shear stress in combined flows, Soulsby *et al* (1993) found that a large variation (up to a factor of 4 for mean values and up to 30% for maximum values) exists between the models. The calculation of the wave energy dissipation (from shear stress) in turbulent flows is numerically one of the most significant terms in the "wave attenuation equation" and any uncertainty in its evaluation would have a direct effect on the prediction of wave damping. In spite of all the above uncertainties, the good agreement between the outputs of "WAS" and the available data demonstrates the ability of the derived theory to successfully account for wave height attenuation in combined flows. The "wave attenuation equation" is equally successful in predicting wave damping in wave dominated

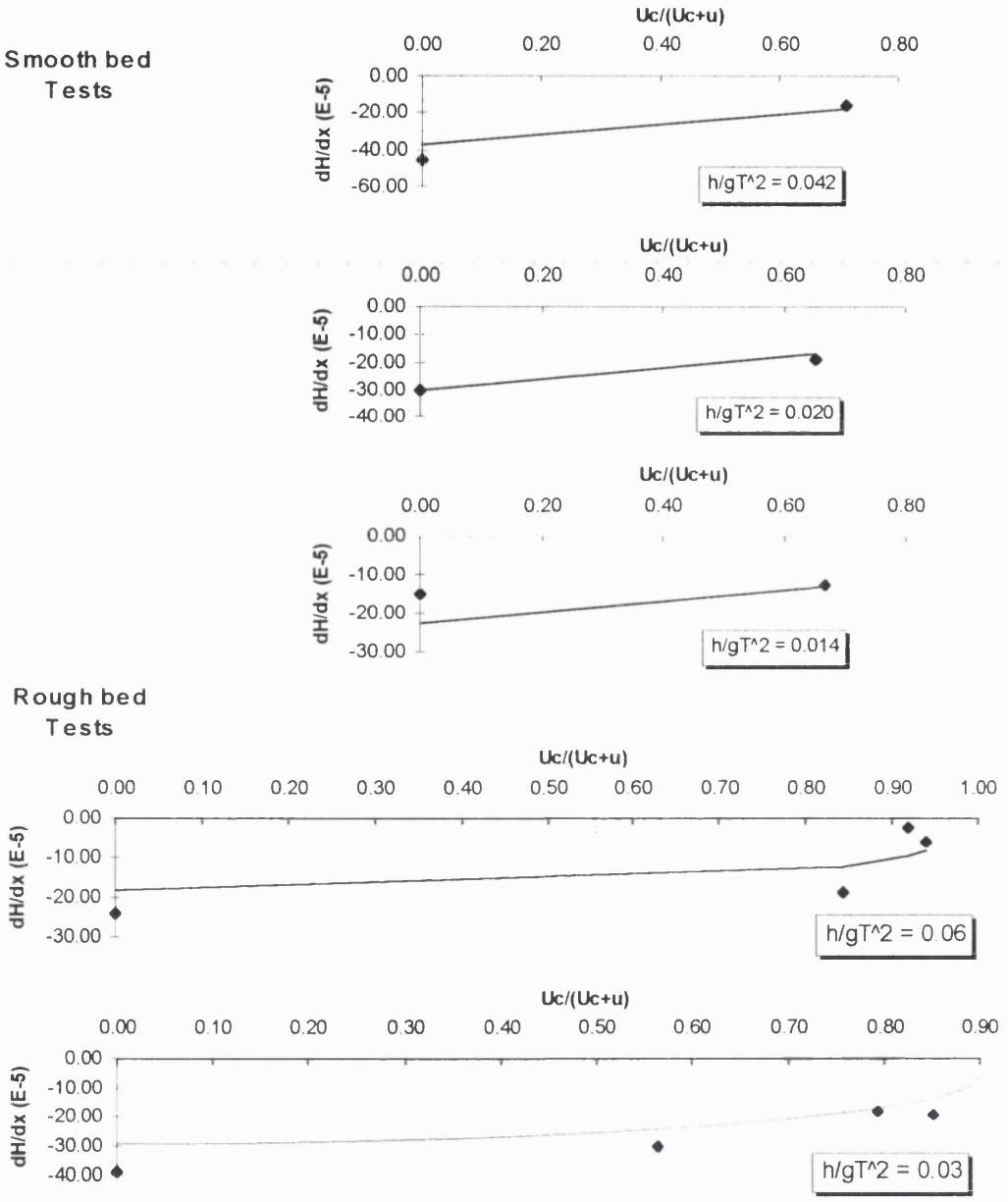

Figure 6.11.b Comparison between the wave attenuations measured by Simons, Grass and Kyriacou (1988) and those predicted by the "wave attenuation equation".

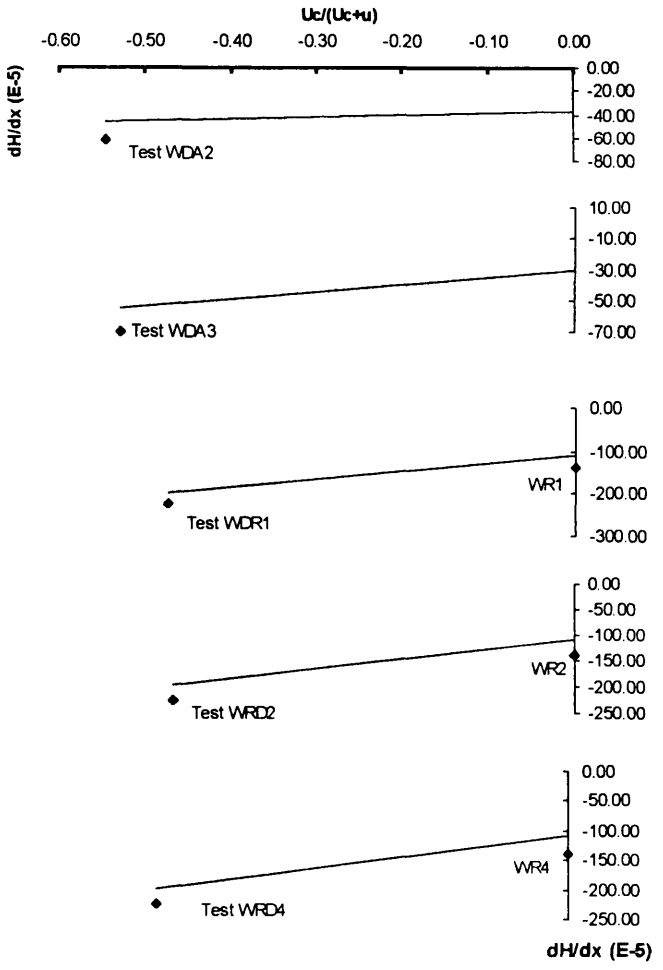

Figure 6.11.c Comparison between the wave attenuations measured by Kemp and Simons (1983), and those predicted by the "wave attenuation equation". $h/gT^2=0.02$

and current dominated flows, after the addition of following and opposing currents, and in accounting for the effect of smooth and rough boundaries .

6.6 Some Theoretical Projections

The above two sections of this chapter demonstrated the strengths of the two models derived in Chapter 2 in predicting the wave attenuation. Below, the "modified Hunt formula" and the "wave attenuation equation" are employed to predict the wave damping mechanism through a wide range of flow conditions. Computer programmes calculated wave height attenuations for slowly changing aspect ratios, h/gT^2, H/h, and $U_c/(U_c+u_0)$. In each case, the flow environment was changed marginally to obtain a new wave height attenuation. By repeating the calculations hundreds of times, a comprehensive projection of wave damping in various flow conditions was obtained.

Figure 6.12 provides a general guide to the behaviour of wave damping mechanism with changing aspect ratio. Calculations were performed for aspect ratios ranging from 0.1 to 1000, while the wave period (T= 1s), initial waveheight (H= 40mm) and steady current velocity (Uc=0 mm/s) were kept constant. This showed that wave damping increases greatly for very small aspect ratios, leading to infinity as B/D approaches zero. This is due to the significant growth of the sidewall contribution to wave attenuation. As the aspect ratio increases, the sidewall contribution quickly falls, and wave height attenuation becomes practically constant. For the flow conditions considered, the bed contribution became more significant at B/D=5, and was entirely dominant (80%) from B/D>30.

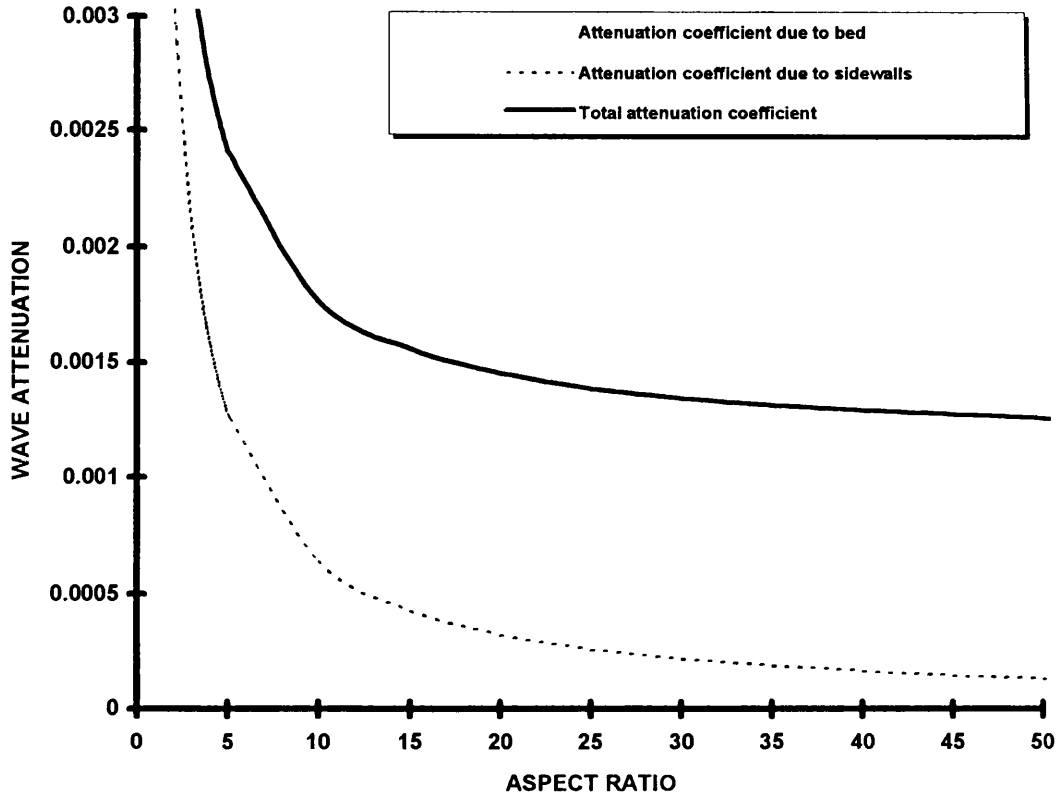

Figure 6.12 Variation in wave attenuation with aspect ratio; T=1.0s; H=40mm, Uc=0mm/s. Modified Hunt Frmula.

Figure 6.13 demonstrates the effect of increasing wave height on energy transmitted through the body of the fluid and the energy dissipated at the boundaries. In both figures, the energy values are non-dimensionalised by dividing the energy at each point by a reference value. The reference value is the energy flux and the energy dissipated at H/D=0.1 . For these calculations, the wave period was 1.0s, the aspect ratio was 3.3, the water level height was 300mm, and the steady current velocity was 0 mm/s. As can be seen from the figures, according to Hunt's solution, energy flux and dissipation increase at almost the same rate with growing H/D. Thus, the wave height attenuation remains unaffected by increasing H/D.

Figure 6.14 shows the result of the calculations performed to examine the effect of changing h/gT^2. Here the aspect ratio was kept constant at 3.3, wave height was 40mm, the water depth was 300 mm, and the steady current velocity was 0 mm/s. In general, wave height attenuation increases with h/gT^2. It is interesting to note how the sidewall contribution grows faster than the bed contribution with increasing h/gT^2, making the bed attenuation coefficient dominant for shallow water waves. Thus, the relative contribution of each of the boundaries to wave damping is not only dependent on the aspect ratio of the channel, but also depends on the value of the wave period.

Figure 6.15 demonstrates the effect of increasing steady current strength on the wave damping mechanism. The wave period was kept constant at 1.20s, the channel aspect ratio was 1.5, the waveheight was 40mm, and the water depth was 300mm, while the steady current strength grew from a wave only flow to a current dominated flow. The figure covers both currents in the direction of wave propagation and those in the opposite

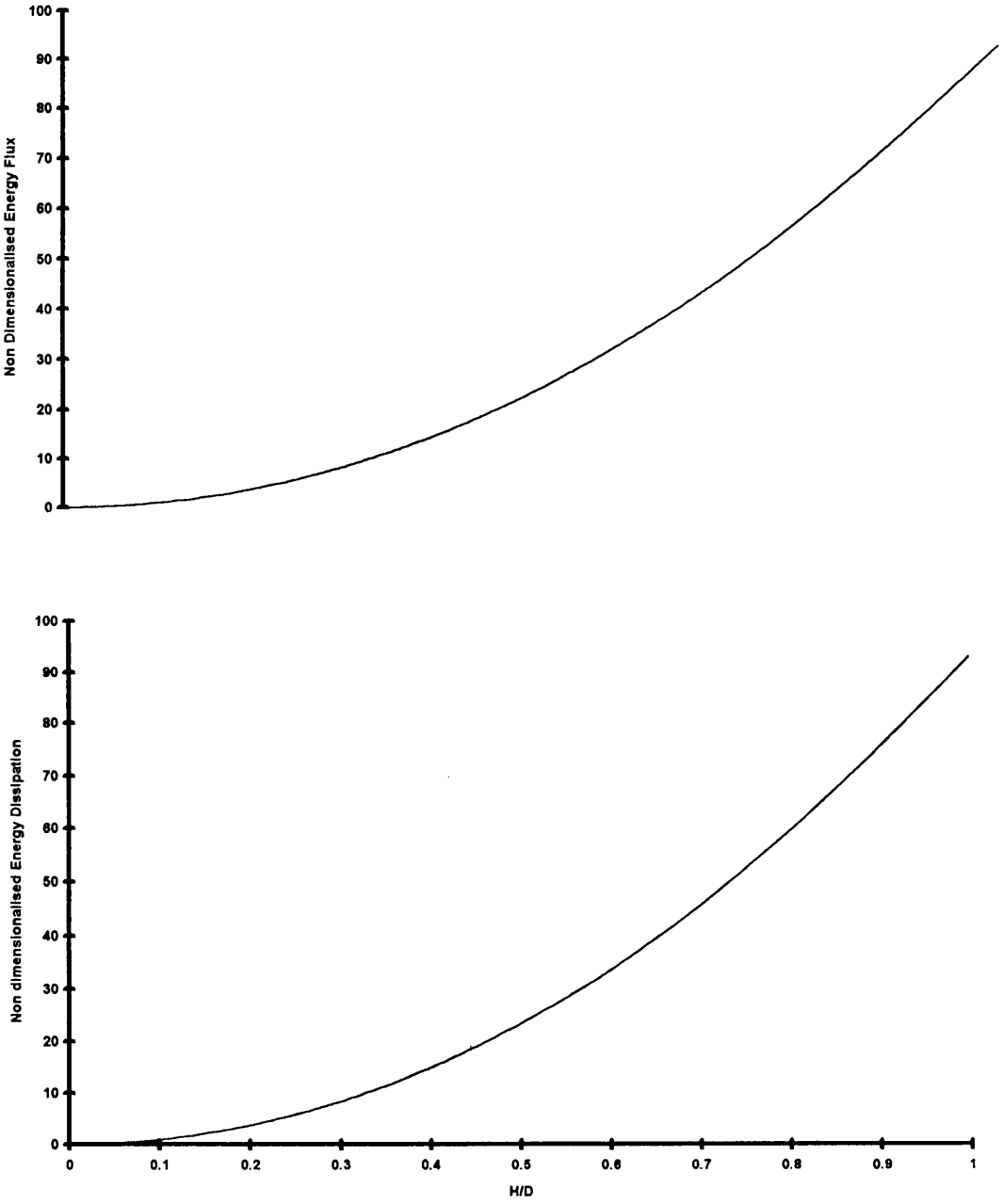

Figure 6.13 Variation in energy flux and energy dissipations at the boundaries with waveheight."Modified Hunt formula".

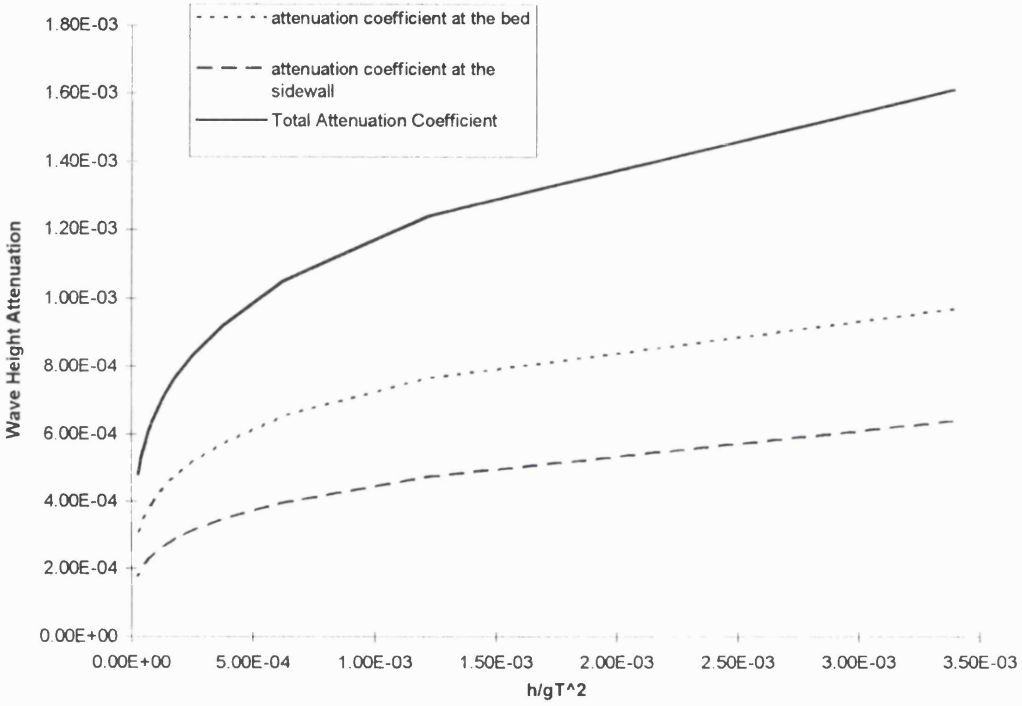

Figure 6.14 Variation in wave attenuation with wave period; B/D=3.3, H=40mm, Uc=0mm/s. Modified Hunt formula

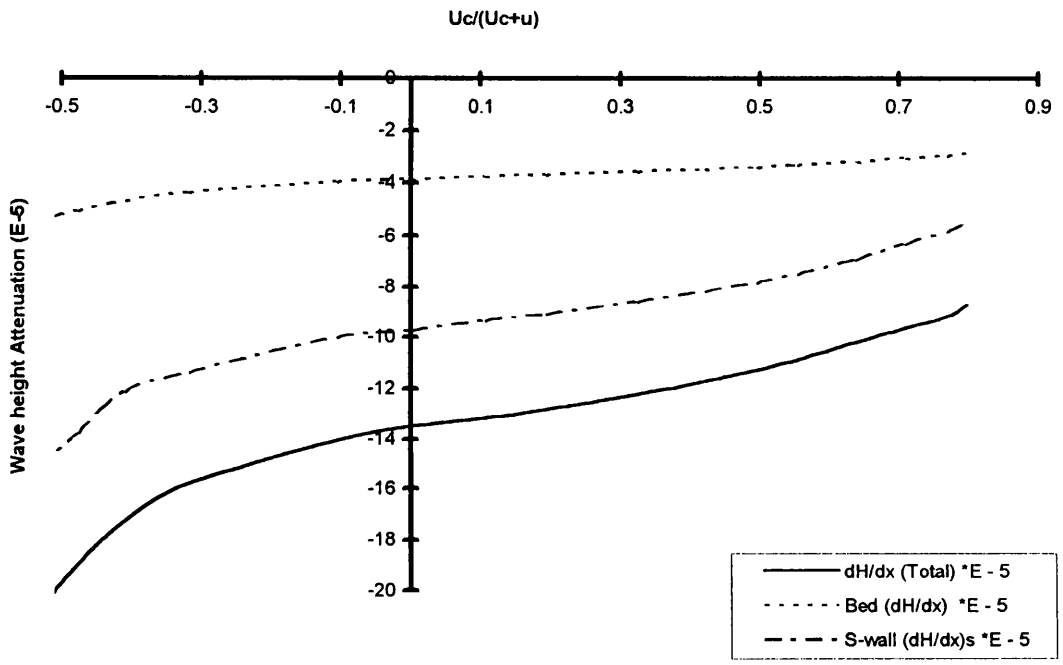

Figure 6.15 Variation in wave attenuation with steady current. B/D=3.3, H=40mm, T=1.0s. The vertical dotted line separates the current dominated flow.

direction. Uc/(Uc+u)=0 indicates a wave only flow and Uc/(Uc+u)=1 indicates a current only flow. As expected, wave damping reduced with increasing following current strength. However, the trend changed as the direction of the steady current was reversed. Attenuation coefficient increased sharply with the strength of opposing current. This was the result of opposing currents increasing wave energy loss at the boundaries while significantly reducing the wave energy flux though the flow.

Conclusions

The aim of this study was to investigate the effect of sidewall boundaries on wave height attenuation in a laboratory flume. Detailed L.D.A. measurements of the steady and orbital transverse velocity profiles provided new documented information on the flow behaviour near the vertical boundary. This enabled the development of two theoretical approaches to account for the influence of the sidewalls on wave height attenuation. Both the "modified Hunt formula" and the "wave attenuation equation" evaluate the contribution of the horizontal and vertical boundaries to wave damping. The theories proved successful in predicting wave height attenuation in a wide range of flow conditions, be they wave or current dominated, with following or opposing currents, and rough or smooth boundaries. While the "modified Hunt formula" has been derived for laminar flows and the "wave attenuation equation" for turbulent flows, the former can be used to provide an approximation for wave damping in turbulent regimes, especially over smooth boundaries. Employing these theories, researchers can carry out experiments on interacting waves and currents in laboratory flumes, and project their results to much wider circumstances by accounting for the effect of the sidewalls. The following is a summary of some other conclusions drawn from this study:

1. The steady flow near a vertical boundary behaves in the same manner as it does near a horizontal boundary. The vertical boundary layer of a unidirectional flow near a sidewall demonstrates the three distinctive regions associated with the inner layer, the overlap layer and the outer flow.

2. The "overshoot" regions described by Lamb (1932) for one-dimensional oscillatory wave motion near the bed, also clearly exist in the case of the two-dimensional vertical boundary.

3. For waves in still water, there is a positive velocity in the direction of wave propagation near the solid boundaries, which becomes negative towards the centre of the flume. The positive velocity is largest within the immediate vicinity of the boundaries, while the negative velocities increase with distance from the boundaries as the result of the larger orbital motions. The above is based on Eulerian velocity measurements at the laser positions.

4. In combined waves and current flows, increasing current strength reduces the orbital velocities near the vertical boundary. Meanwhile, the "overshoot" region near the vertical boundary continues to exist with the addition of currents, although it becomes less prominent with current strength.

5. The propagation of waves onto the current results in a redistribution of the mean flow across the channel. The transverse mean velocity profiles undergo a significant change in comparison with the current only profiles. The mean velocity increases near the sidewall, while there is a velocity reduction towards the core of the flow in the flume.

6. A comparison with zones of positive and negative mass transport in a cross section of the flume suggests that the steady current velocity near the boundaries is increased due to a positive wave induced mass transport, while away from the boundaries the same wave induced mass transport opposes the following current.

7. The value of h/gT^2 of the waves in a combined flow does not have any significant effect on the sidewall mean shear stress. The sidewall shear stress increases rapidly with height above the bed for $z/h<0.15$ and then stays almost uniform through the depth of measurement.

8. In combined flows, flow reversal takes place in the near wall region in a similar manner to that observed over the bed. The region of flow reversal extends further into the flow with shallower water waves. Similarly, the more wave dominated the flow is, the longer the reversal region becomes.

9. From the above it is clear that the flow near a vertical boundary behaves in a similar way to that over a horizontal bed. Thus, employing the theories developed for the flow over a horizontal boundary, with necessary modifications to predict the flow behaviour near a sidewall is justified. The most important amendment to be made is concerned with the fact that while the wave movement over a bed is one-dimensional, near a vertical boundary wave flow remains two-dimensional.

10. The "modified Hunt formula" successfully predicts the effect of changing aspect ratio, h/gT^2, and $U_c/(U_c+u_0)$ on wave height attenuation. However, it should only be employed for flows over smooth boundaries.

11. Both the original and modified versions of Hunt's theory tend to underestimate measured wave attenuation by an average of 15%. Considering the overall uncertainties involved in a complex fluid problem, this indicates that contributions to wave attenuation from the factors ignored by the theory are relatively small.

12. The "wave attenuation equation" also successfuly predicts wave damping. Its advantage over the simpler "modified Hunt theory" is that it is derived for turbulent flows and can account for the effect of rough boundaries. It is possible to simplify the "wave attenuation equation" by reducing it to the ratio of wave energy dissipated at the bed and the two sidewalls to the absolute group velocity term, for the present test range.

13. The predictions of the wave attenuation equation show a reduction in wave attenuation with the following current strength, but a larger increase when waves are propagating against the steady current.

14. The wave energy dissipation increases with shallower water waves, while the mean energy loss at the boundary is only marginally affected by h/gT^2, and is dependent mainly on the current strength. The maximum energy dissipation grows considerably with both current domination of the flow and shallower water waves.

The following conclusions are based on the predictions of the two developed models. They provide a useful guide to wave damping over a wide range of flow properties that were not possible to test within the limitation of the available apparatus:

15. A general guide to the behaviour of wave damping mechanism with changing aspect ratio is as follows: wave damping increases sharply for very small aspect ratios, becoming infinite as B/h approaches its lowest limit. This is due to the growth of the sidewall contribution to wave attenuation. As the aspect ratio increases, the significance of sidewall quickly falls, and wave height attenuation becomes practically constant as the sidewall contribution becomes negligible.

16. For a typical range of laboratory experiments with smooth boundaries, where h/gT^2 is in the order of 10^{-2}, the aspect ratio should be at least 5 in order to ensure that sidewalls are not the main source of energy dissipation. Alternatively, the bed boundary should have a larger roughness value in comparison with the sidewall boundary.

17. Both the rate of energy transmitted through the body of the fluid and the energy dissipated at the boundaries increase at the same rate with the growing ratio of wave height to water depth (H/h).

18. The rate of the reduction in wave damping with growing wave period is very high for deep water waves. For shallower water waves the reduction in wave damping becomes more moderate.

19. The relative contribution of each of the boundaries to wave damping is not only dependent on the aspect ratio of the channel, but also on h/gT^2. In general, the lower the aspect ratio and h/gT^2, the higher is the significance of sidewalls in wave damping.

APPENDIX A

WAVE HEIGHT ATTENUATION SOFTWARE

```
10 '
20 '
30 '
40 '  ================================================================
50 '     ========WAVE ATTENUATIONSOFTWARE================
60 '  ================================================================
70 '
80 '
90    'THE "WAVE ATTENUATION EQUATION" IS PROGRAMMED TO
      PREDICT THE RATE OF WAVE HEIGHT DAMPING OF COMBINED
      TURBULENT FLOWS IN OPEN CHANNELS;
100 '
110 '
120 ' This programme takes as its input the basic charecteristics of the flow, and
      computes a comprehensive set of flow properties both in the body of the fluid
      and at the bed and sidewall boundaries.
130 '
140'  These include among other properties: The steady current averaged through
      the depth of the flow; Wavelength; The friction factors due to
150 ' The waves, current, and combined flow; Mean and amplitude shear velocity
      Mean and maximum shear stress, and the contibution of the waves and
160 ' current to the stress; Relative and group wave velocity; Wave energy;
170 ' Radiation Stress; And the energy dissipated by the wave and current
      component of the flow at each boundary.
180 '  In addition, the programme computes the rate of waveheight damping,
190 ' and determines the contribution of the bed and sidewall boundary
      seperately.
200 '
210 '
220 '

230 '================== NOMENCLATURE ====================
240 '
250 ' AB0       MAXIMUM WAVE AMPLITUDE NEAR THE BED
260 ' AS0       MAXIMUM WAVE AMPLITUDE NEAR THE SIDEWALL
270 ' AS0V      MAXIMUM VERTICAL WAVE AMPLITUDE AT THE
               SIDEWALL
280 ' B         WIDTH OF THE CHANNEL
290 ' CR        RELATIVE WAVE VELOCITY
300 ' CGR       THE RELATIVE GROUP VELOCITY OF THE WAVES
310 ' CGA       THE ABSOLUTE GROUP VELOCITY OF THE WAVES
320 ' D         MEAN WATER DEPTH
330 ' DWB       WAVE BOUNDARY LAYER AT THE BED
340 ' DWS       WAVE BOUNDARY LAYER AT THE SIDEWALL
350 ' E         THE WAVE ENERGY
360 ' EBC       THE ENERGY LOSS AT THE BED DUE TO THE
               STEADY CURRENT
370 ' EBW       THE ENERGY LOSS AT THE BED DUE TO THE
               WAVES
```

```
380 ' EBWC     MEAN ENERGY DISSIPATION AT THE BED BY THE
               COMBINED FLOW
390 ' EBWCC    MEAN ENERGY DISSIPATION AT THE BED IN THE
               COMBINED FLOW BY THE CURRENT
400 ' EBWCW    MEAN ENERGY DISSIPATION AT THE BED IN THE
               COMBINED FLOW BY THE WAVES
410 ' EP       EXP(1)
420 ' ESC      THE ENERGY LOSS AT THE SIDEWALL DUE TO
               THE STEADY CURRENT
430 ' ESW      THE ENERGY LOSS AT THE SIDEWALL DUE TO
               THE WAVES
440 ' ESWC     MEAN ENERGY DISSIPATION AT THE SIDEWALL
               BY THE COMBINED FLOW
450 ' ESWCX    THE ENERGY LOSS AT THE SIDEWALL IN THE
               HORIZONTAL DIRECTION
460 ' ESWCXC   THE ENERGY LOSS AT THE SIDEWALL IN THE
               HORIZONTAL DIRECTION OF
               THE COMBONED FLOW DUE TO THE CURRENT
470 ' ESWCXW   THE ENERGY LOSS AT THE SIDEWALL IN THE
               HORIZONTAL DIRECTION OF
               THE COMBONED FLOW DUE TO THE WAVES
480 ' ESWCZ    THE ENERGY LOSS AT THE SIDEWALL IN THE
               VERTICAL DIRECTION
490 ' FBC0     FRICTION COEFFICIENT FOR CURRENT WITHOUT
               WAVES
500 ' FBC      FRICTION FACTOR AT THE BED FOR THE
               CURRENT IN A COMBINED FLOW
510 ' FBW      FRICTION FACTOR FOR PURE WAVES
520 ' FBWC     FRICTION FACTOR AT THE BED FOR COMBINED
               FLOW
530 ' FSC      FRICTION FACTOR AT THE SIDEWALL FOR THE
               CURRENT IN A
               COMBINED FLOW
540 ' FSW      FRICTION FACTOR FOR PURE WAVES AT THE
               SIDEWALL
550 ' FSWC     FRICTION FACTOR AT THE SIDEWALL FOR
               COMBINED FLOW
560 ' FSWV     VERTICAL FRICTION FACTOR FOR PURE WAVES
               AT THE SIDEWALL
570 ' G        (2KD+SINH (2KD)) / SINH (2KD)
580 ' GR       EARTH GRAVITATIONAL FORCE
590 ' H        WAVE HEIGHT
600 ' KB       Nikuradse's equivalent sand roughness
              parameter FOR THE BED
610 ' KS       Nikuradse's equivalent sand roughness
              parameter FOR THE SIDEWALL
620 ' L        WAVELENGTH
630 ' RF       SCHLICHTING MEASURE OF TURBULENCE
640 ' RO       (KG/M^3) DENSITY OF WATER
650 ' RWB      The wave Reynold's number at the bed
660 ' RWB      The wave Reynold's number at the sidewall
670 ' SXX      THE RADIATION STRESS TERM IN THE
```

```
                HORIZONTAL DIRECTION
680 ' T           WAVE PERIOD
690 ' TBWC        MEAN SHEAR STRESS OF THE COMBINED FLOW AT
                THE BED
700 ' TOBC        THE MEAN SHEAR STRESS FOR COMBINED FLOW
710 ' TOBC0       SHEAR STRESS AT THE BED ASSOCIATED WITH
                CURRENT ONLY FLOWS
720 ' TOBW        THE MAXIMUM BED SHEAR STRESS OF THE WAVES
                IN THE COMBINED FLOW
730 ' TOBWC       THE MAXIMUM BED SHEAR STRESS OF THE
                COMBINED FLOW
740 ' TOBW0       The maximum wave only shear stress
750 ' TOSC        THE MEAN SHEAR STRESS FOR COMBINED FLOW
                AT THE SIDEWALL
760 ' TOSC0       THE MEAN SHEAR STRESS FOR CURRENT ONLY
                FLOW AT THE SIDEWALL
770 ' TOSW        THE MAXIMUM SIDEWALL SHEAR STRESS OF THE
                WAVES IN THE
                COMBINED FLOW
780 ' TOSWC       THE MAXIMUM SIDEWALL SHEAR STRESS OF THE
                COMBINED FLOW
790 ' TOSW0       The maximum wave only shear stress at the
                sidewall
800 ' TOSW0V      THE MAXIMUM WAVE SHEAR STRESS AT THE
                SIDEWALL DUE TO
                THE VERTICAL OSCILATION
810 ' TSWC        MEAN SHEAR STRESS OF THE COMBINED FLOW AT
                THE SIDEWALL
820 ' TSWCX       THE SHEAR STRESS IN THE HORIZONTAL
                DIRECTION AT THE SIDEWALL
830 ' TSWCZ       THE SHEAR STRESS IN THE VERTIVAL
                DIRECTION AT THE SIDEWALL
840 ' UBC0        CURRENT SHEAR VELOCITY ASSOCIATED WITH
                CURRENT ONLY FLOWS
850 ' UBT         TOTAL HORIZONTAL FLOW VELOCITY
860 ' UBW         AMPLITUDE OF THE ORBITAL VELOCITY NEAR
                THE BED
870 ' UBWC        THE BED SHEAR VELOCIY IN COMBINED FLOW
880 ' UC          MAXIMUM STEADY CURRENT VELOCITY
890 ' UST         TOTAL HORIZONTAL FLOW VELOCITY AT THE
                SIDEWALL
900 ' USW         AMPLITUDE OF THE ORBITAL VELOCITY NEAR
                THE SIDEWALL
910 ' USW         AMPLITUDE OF THE ORBITAL VELOCITY NEAR
                THE SIDEWALL
920 ' USWC        THE SIDEWALL SHEAR VELOCIY IN COMBINED
                FLOW
930 ' V           KINEMATIC VISCOSITY OF WATER
940 ' VF          4/(RO*GR*H)
950 ' VSWCF       THE CORRECTION FACTOR FOR THE VERTICAL
                COMPONENT OF THE ORBITAL
                VELOCITY AT THE SIDEWALLS
```

```
960 ' VSW       THE MAXIMUM VERTICAL WAVE VELOCITY NEAR
              THE SIDEWALL
970 ' WA        ABSOLUTE WAVE FREQUENCY
980 ' WR        RELATIVE WAVE FREQUENCY
990 ' XR        THE ANGLE BETWEEN THE DIRECTION OF THE
              WAVES AND STEADY CURRENT
1000 ' ZB0      ROUGHNESS LENGTH PARAMETER AT THE BED
1010 ' ZB0A      APPARENT BED ROUGHNESS AT THE BED
1020 ' ZS0       ROUGHNESS LENGTH PARAMETER AT THE
              SIDEWALL
1030 ' ZS0A      APPARENT BED ROUGHNESS AT THE SIDEWALL
1040 '
1050 '

1070 '

1080 '==================== PROGRAMME ================
1090 '
1100 DIM
     UBT(360),EBWC(360),EBWCC(360),EBWCW(360),MEBWC(360),
     MEBWCC(360),MEBWCW(360)
1110 DIM
     TBWC(360),TBWCC(360),TBWCW(360),MTBWC(360),MTBWCC(36
     0),MTBWCW(360)
1120 DIM UST(360)
1130 DIM
     ESWCX(360),ESWCXC(360),ESWCXW(360),TSWCX(360),TSWCXW
     (360),TSWCXC(360)
1140 '
1150 '
1160 WRITE"WELCOME TO WAVE ATTENUATION SOFTWARE"
1170 '
1180 RO=1000          '(KG/M^3)
1190 PI=3.14159
1200 GR=9.810001
1210 EP=EXP(1)
1220 KP=.4

     ==============INPUT OF FLOW PROPERTIES==============
1230 '
1240 INPUT"TEST NAME";FIL3$
1250 PRINT"TEST NAME ";FIL3$
1260 'Creating two output files for bed and sidewall
     dissipation
1270 'B$=FIL3$+CHR$(66)
1280 'PRINT B$
1290 'S$=FIL3$+CHR$(87)
1300 'PRINT S$
1310 'OPEN B$ FOR OUTPUT AS #1
1320 'OPEN S$ FOR OUTPUT AS #2
1330 '
1340 'INPUT "CHANNEL BREADTH (mm)";BM
```

```
1350 BM=457
1360 B=BM/1000
1370 '
1380 DM=300
1390 'INPUT  "WATER DEPTH (mm)";DM
1400 D=DM/1000
1410 '
1420 'T=1
1430 INPUT"WAVE PERIOD (S)";T
1440 '
1450 'HMW=40
1460 INPUT "WAVE HEIGHT (mm)";HMW
1470 HW=HMW/1000
1480 INPUT "MAXIMUM STEADY CURRENT VELOCITY (MM/S)";UCM
1490 UC=UCM/1000
1500 '
1510 WC=20
1520 'INPUT "WATER TEMPERATURE";WC
1530 KB=.0001
1540 KS=.0001
1550 '
1560 XD=0
1570 XR=XD*PI/180
1580 '

1590 '===CALCULATING KINEMATIC VISCOSITY OF THE WATER===
1600 '
1610
     V=(1.78*(1+(.03368*(WC))+(.000221*(WC)^2))^-1)*.0000
     01
1620 WRITE"KINEMATIC VISCOSITY OF THE WATER, V =";V
1630 '
1640 IF UC=0 THEN GOTO 1910
1650 '


1660 '=========CALCULATING FBC0 AND UBC0===============
1670 'IF UC<0 THEN FBC0=.002
1680 'IF UC<0 THEN UCBAR=UC
1690 'IF UC<0 THEN GOTO 750
1700 FBC02=.005
1710 UC0BAR=ABS(UC/2)
1720 FBC01=FBC02
1730 UBC0=SQR((1/2)*FBC01)*UC0BAR
1740 ZB0=((KB/30)*(1-EXP(-KB*UBC0/(27*V))))+(V/(9*UBC0))
1750 ' FROM EQUATION B9 OF M&S  (1990)
1760 UC0BAR=ABS(UC)*(1-(1/LOG(D/ZB0)))
1770 UBC0=UC0BAR*KP/(LOG(D/(EP*ZB0)))
1780 FBC0=2*((UBC0/UC0BAR)^2)
1790 WHILE ABS(1-(FBC0/FBC01))>.005
1800 FBC02=(.2*FBC0)+(.8*FBC01)
1810 GOTO 1720
```

```
1820 WEND
1830 UCBAR=UC0BAR
1840 IF UC<0 THEN UCBAR=-UCBAR
1850 WRITE"UBC0 = ";UBC0
1860 WRITE"FBC0 = ";FBC0
1870 TOBC0=RO*UBC0^2
1880 WRITE"TOBC0 = ";TOBC0
1890 '


1900 '======calculating the wavelength (LW) BEFORE THE
     ADDITION OF CURRENT
1910 '
1920 WA=2*PI/T
1930 LO=(9.8*T^2)/(2*PI)
1940 LW=LO
1950 WHILE ABS(L1-LW)>.005*LW
1960 L1=LW
1970 Z=(2*PI*D)/L1
1980 TANHZ=(EXP(Z)-EXP(-Z))/(EXP(Z)+EXP(-Z))
1990 LW=((2*PI*GR)/WA^2)*TANHZ
2000 KW=2*PI/LW
2010 CW=LW/T
2020 WEND
2030 WRITE"LW (m)= ";LW
2040 '


2050 '====wavelength and relative frequency
                  after the addition of current====
2060 WA=2*PI/T
2070 LO=(9.8*T^2)/(2*PI)
2080 WR=WA
2090 L=LO
2100 WHILE ABS(L1-L)>.005*L
2110 L1=L
2120 Z=(2*PI*D)/L1
2130 TANHZ=(EXP(Z)-EXP(-Z))/(EXP(Z)+EXP(-Z))
2140 L=((2*PI*GR)/WR^2)*TANHZ
2150 K=2*PI/L
2160 WR=WA-(K*UCBAR)
2170 WEND
2180 WRITE"WAVELENGTH (m)= ";L
2190 '
```

```
2200 '========CALCULATING THE WAVE HEIGHT AFTER THE
     ADDITION OF CURRENT======
2210 '
2220 ' FOLLOWING A FORMULA PRESENTED BY LONGUET-HIGGINS
     AND STEWART (1964)
2230 '
2240 K2D=2*K*D
2250 SINHK2D=(EXP(K2D)-EXP(-K2D))/2
2260 KWD=2*KW*D
2270 SINHKWD=(EXP(KWD)-EXP(-KWD))/2
2280 HN1=1-((K*UCBAR)/(KW*CW))
2290 HN2=1+(KWD/SINHKWD)
2300 HD1=(KW/K)-(UCBAR/CW)
2310 HD2=(2*UCBAR)/CW
2320 HD3=1+(K2D/SINHK2D)
2330 H=HW*SQR((HN1*HN2)/((HD1*HD3)+HD2))
2340 PRINT"H (mm)";H
2350 PRINT"SINHK2D";SINHK2D
2360 '
2370 '


2380 '==================CALCULATING UBW==============
390 '
2400 '  UBW IS THE MAXIMUM PERIODIC VELOCITY OF THE WAVE
     JUST ABOVE THE WAVE
2410 ' BOUNDARY LAYER, CALCULATED USING BRINK-KJAER AND
     JONSSON
2420 'ZB IS THE HEIGHT CHOSEN TO BE JUST ABOVE THE WAVE
     BOUNDARY LAYER.
2430 '
2440 ZB=.002
2450 W0=(.5*UC)/(D-ZB)
2460 KD=K*D
2470 SINHKD=(EXP(KD)-EXP(-KD))/2
2480 COSHKD=(EXP(KD)+EXP(-KD))/2
2490 KZB=K*ZB
2500 COSHKZB=(EXP(KZB)+EXP(-KZB))/2
2510 SINHKZB=(EXP(KZB)-EXP(-KZB))/2
2520 PRINT "K =";K
2530 CA=L/T
2540 PRINT "CA =";CA
2550 CR=CA-UC
2560 PRINT "CR =";CR
2570 D1=CR/SINHKD
2580 PRINT "D1 =";D1
2590
     D2=((3*K*CR)/(8*(SINHKD)^4))+(W0*(COSHKD/(8*((SINHKD
     )^3)))*(((3*GR)-(2*W0*CR))/(GR-(W0*CR))))
2600 PRINT "D2 =";D2
2610 KZB2=K*ZB*2
2620 COSHKZB2=(EXP(KZB2)+EXP(-KZB2))/2
```

```
2630 PRINT "COSHKZB=";COSHKZB
2640 SINHKZB2=(EXP(KZB2)-EXP(-KZB2))/2
2650
     'UBWT=UC+(W0*(ZB-D))-((((2*GR)-(WA*CR))/(4*D*CR))*(H
     /2)^2)+(D1*K*(H/2)*COSHKZB)+(2*D2*K*(H/2)^2*COSHKZB2
     )
2660 UBW=(D1*K*(H/2)*COSHKZB)+(2*D2*K*(H/2)^2*COSHKZB2)
2670 PRINT "TB1";(D1*K*(H/2)*COSHKZB)
2680 PRINT "TB2=";(2*D2*K*(H/2)^2*COSHKZB2)
2690 PRINT "UBW =";UBW
2700 '
2710 AB0=UBW/WR
2720 PRINT "AB0=";AB0
2730 '


2740 '=======Calculating the initial FBW based on the
     wave only formula========
2750 'From M&S EQ.16
2760 '
2770 RWB=((UBW)^2)/(WA*V)      'where RWB is the wave
     Reynold's number
2780 WRITE" RWB = ";RWB
2790 'as a firrst approximation FBW is calculated for a
     laminar smooth flow
2800 FBW=1/SQR(RWB)
2810 WRITE"FBW = ";FBW
2820 '
2830 IF UC=0 THEN GOTO 3930
2840 '


2850 '====CALCULATING WETHER THE BOUNDARY IS
     HYDRAULICALY ROUGH OR SMOOTH =====
2860 '
2870 RF=KB*ABS(UBC0)/V
2880 WRITE"KB*UBC0/V =";RF
2890 IF RF<5 GOTO 2910
2900 IF RF>5 GOTO 3420
2910 '



2920 '=======CALCULATIONS FOR SMOOTH BED BOUNDARY ======

2930 WRITE"THE BOUNDARY IS SMOOTH"
2940 '
```

```
2950 '========CALCULATING THE BED FRICTION FACTOR ======
2960 '
2970 FBWC2=FBW
2980 FBC2=FBC0
2990 FBC1=FBC2
3000 FBWC1=FBWC2
3010 '
3020 'FROM EQ.A5  OF M&S 90
3030 OMB=(FBC1/FBWC1)*((UCBAR/UBW)^2)
3040 '
3050 'FROM EQ. A7
3060 MB=(1+(2*OMB*COS(XR))+(OMB^2))^(1/2)
3070 UBWC=(((1/2)*FBWC1*MB)^(1/2))*UBW
3080 'WHERE UBW=THE BED SHEAR VELOCIY IN COMBINED FLOW
     FROM EQUATION A8 OF M&S
3090 C=.3 'CONSTANT GIVEN BY EQ.17 OF M&S
3100 DWB=C*(UBWC/WA)
3110 'DWB=WAVE BOUNDARY LAYER AT THE BED FROM EQ.B5 OF
     M&S
3120 'FROM EQUATION 3 OF M&S, :
3130 ZB0=((KB/30)*(1-EXP(-KB*UBWC/(27*V))))+(V/(9*UBWC))
3140 'WHERE ZB0=ROUGHNESS LENGTH PARAMETER, AND UBC=BED
     SHEAR VELOCITY
3150 ZB0A=ZB0*((DWB/ZB0)^(1-(SQR(OMB/MB))))
3160 'ZB0A IS DEFINED BY EQUATION B6 OF M&S
3170 UCBAR=UC*(1-(1/LOG(D/ZB0A)))
3180 'FBCA=THE CURRENT ONLY FRICTION FACTOR FROM EQ. B10
     OF M&S
3190 RHSB8=SQR(2/FBC0)-((1/KP)*(LOG(ZB0A/ZB0)))
3200 FBC=2/((RHSB8)^2)
3210 '
3220 ' Substituting into the equation 14 of the M&S 90
3230 BB=1.28       'CONSTANT GIVEN BY EQ.17 OF M&S
3240 RHS14=((LOG(4.5*C*RWB*MB*FBWC1))^2)+(BB^2)
3250 FBWC=(((KP)^2)*(2*MB))/RHS14
3260 IF ABS(FBWC1-FBWC)>ABS(FBC1-FBC) THEN GOTO 3280
3270 IF ABS(FBWC1-FBWC)<ABS(FBC1-FBC) THEN GOTO 3300
3280 WHILE ABS(FBWC-FBWC1)>.01*FBWC
3290 GOTO 3320
3300 WHILE ABS(FBC-FBC1)>.01*FBC
3310 GOTO 3320
3320 FBWC2=(.8*FBWC1)+(.2*FBWC)
3330 'FBC2=(.8*FBC1)+(.2*FBC)
3340 FBC2=FBC
3350 GOTO 2990
3360 WEND
3370 WEND
3380 GOTO 3830
3390 '
```

```
3400 ======CALCULATIONS FOR ROUGH BED BOUNDARY =========
3410 '
3420 WRITE"THE BOUNDARY IS ROUGH"
3430 FBWC2=FBW
3440 FBC2=FBC0
3450 FBC1=FBC2
3460 FBWC1=FBWC2
3470 'FROM EQ.A5
3480 OMB=(FBC1/FBWC1)*((UCBAR/UBW)^2)
3490 'FROM EQ. A7
3500 MB=SQR(1+(2*OMB*COS(XR))+(OMB^2))
3510 UBWC=SQR((1/2)*FBWC1*MB)*UBW
3520 C=.3 'CONSTANT GIVEN BY EQ.17 OF M&S
3530 DWB=C*(UBWC/WA)
3540 'DWB=WAVE BOUNDARY LAYER AT THE BED FROM EQ.B5 OF
     M&S
3550 'WHERE UBWC=THE BED SHEAR VELOCIY IN COMBINED FLOW
     FROM EQUATION A8 OF M&S
3560 ZB0=((KB/30)*(1-EXP(-KB*UBWC/(27*V))))+(V/(9*UBWC))
3570 ZB0A=ZB0*((DWB/ZB0)^(1-(SQR(OMB/MB))))
3580 'ZB0A IS DEFINED BY EQUATION B6 OF M&S
3590 UCBAR=UC*(1-(1/LOG(D/ZB0A)))
3600 '
3610 'FBC0=THE CURRENT ONLY FRICTION FACTOR FROM EQ. B10
     OF M&S
3620 RHSB8=SQR(2/FBC0)-((1/KP)*(LOG(ZB0A/ZB0)))
3630 FBC=2/((RHSB8)^2)
3640 'FBC, THE CURRENT SHEAR STRESS IN THE COMBINED
     FLOW, IS CALCULATED FROM THE EQ. B8
3650 ' Substituting into the equation 13 of the M&S 90
3660 BB=1.28       'CONSTANT GIVEN BY EQ.17 OF M&S
3670
     RHS13=(LOG(30*C*(UBW/(WA*KB))*SQR(MB*FBWC1/2))^2)+(B
     B^2)
3680 FBWC=((KP)^2)*(2*MB)/RHS13
3690 IF ABS(FBWC-FBWC1)>ABS(FBC-FBC1) THEN GOTO 3710
3700 IF ABS(FBWC1-FBWC)<ABS(FBC1-FBC) THEN GOTO 3730
3710 WHILE ABS(FBWC-FBWC1)>.01*FBWC
3720 GOTO 3750
3730 WHILE ABS(FBC-FBC1)>.01*FBC
3740 GOTO 3750
3750 FBWC2=(.8*FBWC1)+(.2*FBWC)
3760 'FBC2=(.8*FBC1)+(.2*FBC)
3770 FBC2=FBC
3780 GOTO 3450
3790 WEND
3800 WEND
3810 GOTO 3830
3820 '
```

```
3830 '=======CALCULATING THE MEAN SHEAR STRESS FOR
     COMBINED FLOW, TOBC=========
3840 TOBC=(1/2)*FBC*RO*(UCBAR^2)
3850 '


3860 '===========CALCULATING THE MAXIMUM BED SHEAR
     STRESS ASSOCIATED WITH THE
     OSCILLATORY WAVE MOTION IN THE COMBINED FLOW, TOBW,
     FROM EQ. A3====
3870 TOBW=(1/2)*RO*FBWC*((UBW)^2)
3880 '


3890 '=======CALCULATING THE MAXIMUM BED SHEAR STRESS
     FROM EQUATION A6==========
3900 '
3910 TOBWC=(1/2)*RO*FBWC*MB*(UBW^2)
3920 '

3930 '===EVALUATING THE ENERGY LOSS AT THE BED DUE TO
     THE STEADY CURRENT ALONE==
3940 '
3950 EBC=.5*RO*FBC0*(UCBAR)^3
3960 WRITE"EBC=";EBC
3970 '
3980 IF UC=0 THEN FBWC=FBW
3990 IF UC=0 THEN MB=1




4000 '====EVALUATING THE ENERGY LOSS AT THE BED DUE TO
     THE WAVES============
4010 '
4020 'FOLLOWING CHRISTOFFERSEN AND JONSON(1985) EQUATION
     3.12 for waves alone
4030 'THE FOLLOWING EQUATION ALLOWS AN APPROXIMATION FOR
     THE PHASE SHIFT
4040 EBW=(2/(3*PI))*RO*FBW*(UBW^3)
4050 WRITE"EBW=";EBW
4060 'IF UC=0 THEN EBWCW=EBW
4070 'IF UC=0 THEN GOTO 3310
4080 '


4090 '=======EVALUATING THE ENERGY LOSS AT THE BED IN
     THE COMBINED FLOW=======
4100 '
4110 FOR PBD=1 TO 360
4120 PBH=((2*PI)/360)*PBD
4130 TBH=PBH-(PI/4)
```

```
4140 UBT(PBD)=UCBAR+(UBW*COS(PBH))
4150 TBWCW(PBD)=(1/2)*RO*FBWC*(UBW)^2*COS(TBH)
4160 TBWCC(PBD)=(1/2)*RO*FBC*(UCBAR)^2
4170 TBWC(PBD)=TBWCC(PBD)+TBWCW(PBD)
4180 EBWCC(PBD)=ABS(.5*RO*FBC*(UCBAR)^3)
4190
     EBWCW(PBD)=ABS(.5*RO*FBWC*((UBW)^2*COS(TBH))*(UBW*CO
     S(PBH)))
4200 EBWC(PBD)=ABS(EBWCC(PBD)+EBWCW(PBD))
4210 TTBWC=TTBWC+TBWC(PBD)
4220 TTBWCC=TTBWCC+TBWCC(PBD)
4230 TTBWCW=TTBWCW+TBWCW(PBD)
4240 TEBWC=TEBWC+EBWC(PBD)
4250 TEBWCC=TEBWCC+EBWCC(PBD)
4260 TEBWCW=TEBWCW+EBWCW(PBD)
4270 MTBWC(PBD)=TTBWC/PBD
4280 MTBWCC(PBD)=TTBWCC/PBD
4290 MTBWCW(PBD)=TTBWCW/PBD
4300 MEBWC(PBD)=TEBWC/PBD
4310 MEBWCC(PBD)=TEBWCC/PBD
4320 MEBWCW(PBD)=TEBWCW/PBD
4330 'PRINT #1
     ,PBD,UBT(PBD),TBWC(PBD),EBWC(PBD),EBWCC(PBD),EBWCW(P
     BD)
4340 NEXT PBD
4350 TBWCW=.5*RO*FBWC*UBW^2
4360 TBWCC=MTBWCC(360)
4370 TBWC=TBWCW+TBWCC
4380 EBWC=MEBWC(360)
4390 EBWCC=MEBWCC(360)
4400 EBWCW=MEBWCW(360)
4410 'EBWCW=EBWC-EBWCC
4420 '
4430 '
4440 '==============SIDEWALL CALCULATIONS ==============
4450 '

4460 '=============CALCULATING USW & AS0 ==============
4470 STZ=.02
4480 FOR ZI=.02 TO (D-STZ) STEP STZ
4490 ZS=ZI
4500 PRINT "ZS = ";ZS
4510 KZS=K*ZS
4520 COSHKZS=(EXP(KZS)+EXP(-KZS))/2
4530 SINHKZS=(EXP(KZS)-EXP(-KZS))/2
4540 KZS2=K*ZS*2
4550 COSHKZS2=(EXP(KZS2)+EXP(-KZS2))/2
4560 SINHKZS2=(EXP(KZS2)-EXP(-KZS2))/2
4570
     'USWT=US+(WA*ZS)-((((2*GR)-(WA*CR))/(4*D*CR))*(H/2)^
     2)+(D1*K*(H/2)*COSHKZS)+(2*D2*K*(H/2)^2*COSHKZS2)
4580 USW=(D1*K*(H/2)*COSHKZS)+(2*D2*K*(H/2)^2*COSHKZS2)
```

```
4590 AS0=USW/WR
4600 WRITE"MAXIMUM WAVE AMPLITUDE AT THE BOUNDARY, AS0 =
     ";AS0
4610 WRITE"MAXIMUM ORBITAL VELOCITY OUTSIDE THE
     BOUNDARY, USW = ";USW
4620 '


4630 '======Calculating the initial FSW based on the
     wave only formula========
4640 '
4650 'From M&S EQ.16
4660 RWS=((USW)^2)/(WA*V)      'where RWB is the wave
     Reynold's number
4670 'FSW is computed, as a first approximation, for
     smooth laminar flow
4680 FSW=1/SQR(RWS)
4690 WRITE"FSW = ";FSW
4700 '
4710 IF UC=0 THEN GOTO 5540
4720 '


4730 '==========CALCULATING FSC0 AND USC0 ============
4740 '
4750 IF UC<0 THEN FSC0=.002
4760 IF UC<0 THEN UCBAR=UC
4770 IF UC<0 THEN GOTO 4950
4780 'CALCULATE FSC0 AND USC0 BY ITERATION BASED ON THE
     CURRENT ONLY FORMULAE OF      M&S (1990), EQUATIONS
     3, A10, AND B10
4790 '
4800 FSC02=.005
4810 UCBAR=UC/2
4820 FSC01=FSC02
4830 USC0=SQR((1/2)*FSC01)*UCBAR
4840 ZS0=((KS/30)*(1-EXP(-KS*USC0/(27*V))))+(V/(9*USC0))
4850 UCBAR=UC*(1-(1/LOG((B/2)/ZS0)))
4860 USC0=UCBAR*KP/(LOG((B/2)/(EP*ZS0)))
4870 FSC0=2*((USC0/UCBAR)^2)
4880 WHILE ABS(1-(FSC0/FSC01))>.005
4890 FSC02=(.2*FSC0)+(.8*FSC01)
4900 GOTO 4820
4910 WEND
4920 WRITE"USC0 = ";USC0
4930 WRITE"FSC0 = ";FSC0
4940 '

4950 WRITE"THE SIDEWALL BOUNDARY IS SMOOTH"
```

```
4960 '=================CALCULATING FSWC ===============
4970 '
4980 'ITERATION SCHEME TO CALCULATE THE FRICTION FACTOR
     AT THE SIDEWALL FOR SMOOTH TURBULANT COMBINED FLOW
     (MYRHAUG AND SLAATTELID - 1990)
4990 '
5000 'The initial values for FSWC and FSC are taken as
     wave only friction factor ,FSW, and current only
     friction factor, FSC0
5010 '
5020 FSWC2=FSW
5030 FSC2=FSC0
5040 FSC1=FSC2
5050 FSWC1=FSWC2
5060 '
5070 'FROM EQ.A5
5080 OMS=(FSC1/FSWC1)*((UCBAR/USW)^2)
5090 '
5100 'FROM EQ. A7
5110 MS=(1+(2*OMS*COS(XR))+(OMS^2))^(1/2)
5120 '
5130 USWC=(((1/2)*FSWC1*MS)^(1/2))*USW
5140 'WHERE USWC=THE SIDEWALL SHEAR VELOCIY IN COMBINED
     FLOW FROM EQUATION A8 OF M&S
5150 DWS=C*(USWC/WA)
5160 'DWS=WAVE BOUNDARY LAYER AT THE SIDEWALL FROM EQ.B5
     OF M&S
5170 '
5180 'FROM EQUATION 3 OF M&S, :
5190 ZS0=((KS/30)*(1-EXP(-KS*USWC/(27*V))))+(V/(9*USWC))
5200 'WHERE ZS0=ROUGHNESS LENGTH PARAMETER,
5210 '
5220 ZS0A=ZS0*((DWS/ZS0)^(1-(SQR(OMS/MS))))
5230 'ZS0A IS DEFINED BY EQUATION B6 OF M&S
5240 UCBAR=UC*(1-(1/LOG((B/2)/ZS0A)))
5250 'FSCA=THE CURRENT ONLY FRICTION FACTOR FROM EQ. B10
     OF M&S
5260 RHSB8S=SQR(2/FSC0)-((1/KP)*(LOG(ZS0A/ZS0)))
5270 FSC=2/((RHSB8S)^2)
5280 ' Substituting into the equation 14 of the M&S 90
5290 RHS14S=((LOG(4.5*C*RWS*MS*FSWC1))^2)+(BB^2)
5300 FSWC=(((KP)^2)*(2*MS))/RHS14S
5310 IF ABS(FSWC1-FSWC)>ABS(FSC1-FSC) THEN GOTO 5330
5320 IF ABS(FSWC1-FSWC)<ABS(FSC1-FSC) THEN GOTO 5350
5330 WHILE ABS(FSWC-FSWC1)>.01*FSWC
5340 GOTO 5370
5350 WHILE ABS(FSC-FSC1)>.01*FSC
5360 GOTO 5370
5370 FSWC2=(.8*FSWC1)+(.2*FSWC)
5380 'FSC2=(.8*FSC1)+(.2*FSC)
5390 FSC2=FSC
5400 GOTO 5040
```

```
5410 WEND
5420 WEND


5430 '======CALCULATING THE MEAN SHEAR STRESS FOR
     COMBINED FLOW, TOSC==========
5440 '
5450 USC=(SQR((1/2)*FSC))*UCBAR
5460 TOSC=(USC^2)*RO
5470 '


5480 ' =======CALCULATING THE MAXIMUM SIDEWALL SHEAR
     STRESS ASSOCIATED WITH THE OSCILLATORY WAVE MOTION
     IN THE COMBINED FLOW, TOSW, FROM EQ. A3======
5490 '
5500 TOSW=(1/2)*RO*FSWC*((USW)^2)


5510 '=======CALCULATING THE MAXIMUM SIDEWALL SHEAR
     STRESS FROM EQUATION A6=====
5520 TOSWC=(1/2)*RO*FSWC*MS*(USW^2)
5530 '


5540 '====SIDEWALL CALCULATIONS FOR THE VERTICAL
     COMPONENT OF THE VELOCITY====
5550 '
5560 VSW=(WR*H*SINHKZS)/(2*SINHKD)
5570 WRITE" THE MAXIMUM VERTICAL WAVE VELOCITY NEAR THE
     SIDEWALL = ";VSW
5580 '
5590 'CALCULATING THE MAXIMUM VERTICAL WAVE AMPLITUDE AT
     THE SIDEWALL, AS0V
5600 AS0V=VSW/WR
5610 WRITE"MAXIMUM VERTICAL WAVE AMPLITUDE AT THE
     SIDEWALL, AS0V= ";AS0V
5620 '
5630 'From M&S EQ.16
5640 RWSV=((VSW)^2)/(WA*V)      'where RWSV is the waves
     Reynolds' number
5650 WRITE" RWSV= ";RWSV
5660 FSWV=1/SQR(RWSV)
5670 WRITE"FSWV= ";FSWV


5680  'calculating the maximum VERTICAL wave only shear
     stress AT THE SIDEWALL
5690 TOSW0V= .5*RO*FSWV*(VSW^2)
5700 WRITE"TOSW0V=";TOSW0V
5710 '
5720 'IN THE CASE OF UNIDIRECTIONAL FLOW, WITH NO MEAN
```

```
    VERTICAL VELOCITY, THE MEAN VERTICAL FRICTION FACTOR
    AND SHEAR STRESS ARE ZERO, AND THE MAXIMUM FRICTION
    FACTOR AND SHEAR STRESS OF THE FLOW ARE THE SAME AS
    THOSE CALCULATE
5730 '
5740 '
5750 'EVALUATING THE ENERGY LOSS AT THE SIDEWALL DUE TO
    THE STEADY CURRENT ALONE
5760 '
5770 ESCL=.5*RO*FSC0*(UCBAR)^3
5780 WRITE"ESCL=";ESCL
5790 ESC=ESC+(ESCL*STZ)
5800 '


5810 '=====EVALUATING THE ENERGY LOSS OF THE COMBINED
    FLOW AT THE SIDEWALL=====
5820 IF UC=0 THEN FSWC=FSW
5830 IF UC=0 THEN MS=1
5840 '


5850 '====EVALUATING THE HORIZ0NTAL ENERGY LOSS AT THE
    SIDEWALL DUE TO THE WAVES ALONE=====
5860 '
5870 'FOLLOWING CHRISTOFFERSEN AND JONSON(1985) EQUATION
    3.12
5880 'THE FOLLOWING EQUATION ALLOWS AN APPROXIMATION FOR
    THE PHASE SHIFT
5890 ESWXL=(2/(3*PI))*RO*FSW*(USW^3)
5900 ESWX=ESWX+(ESWXL*STZ)
5910 WRITE"ESWXL=";ESWXL
5920 WRITE"ESWX=";ESWX
5930 'IF UC=0 THEN ESWCXW=ESWX
5940 'IF UC=0 THEN GOTO 5080
5950 '


5960 '=========EVALUATING THE ENERGY LOSS IN THE
    HORIZONTAL DIRECTION==========
5970 '
5980 TTSWCX=0
5990 TTSWCXC=0
6000 TTSWCXW=0
6010 TESWCX=0
6020 TESWCXC=0
6030 TESWCXW=0
6040 FOR PSD=1 TO 360
6050 PSH=((2*PI)/360)*PSD
6060 TSH=PSH-(PI/4)
6070 UST(PSD)=UCBAR+(USW*COS(PSH))
6080 TSWCXC(PSD)=(1/2)*RO*FSC*(UCBAR^2)
```

```
6120
     ESWCXW(PSD)=ABS(.5*RO*FSWC*(USW)^2*COS(TSH)*(USW*COS
     (PSH)))
6130 ESWCX(PSD)=ABS(ESWCXW(PSD)+ESWCXC(PSD))
6140 TTSWCX=TTSWCX+TSWCX(PSD)
6150 TTSWCXC=TTSWCXC+TSWCXC(PSD)
6160 TTSWCXW=TTSWCXW+TSWCXW(PSD)
6170 TESWCX=TESWCX+ESWCX(PSD)
6180 TESWCXC=TESWCXC+ESWCXC(PSD)
6190 TESWCXW=TESWCXW+ESWCXW(PSD)
6200 'PRINT #2
     ,PSD,UST(PSD),TSWCX(PSD),ESWCX(PSD),ESWCXC(PSD),ESWC
     XW(PSD)
6210 NEXT PSD
6220 TSWCXWL=.5*RO*FSWC*USW^2
6230 TSWCXCL=TTSWCXC/PSD
6240 TSWCXL=TSWCXWL+TSWCXCL
6250 ESWCXL=TESWCX/PSD
6260 ESWCXCL=TESWCXC/PSD
6270 ESWCXWL=TESWCXW/PSD
6280 TSWCX=TSWCX+(TSWCXL*STZ)
6290 TSWCXC=TSWCXC+(TSWCXCL*STZ)
6300 TSWCXW=TSWCXW+(TSWCXWL*STZ)
6310 ESWCX=ESWCX+(ESWCXL*STZ)
6320 ESWCXC=ESWCXC+(ESWCXCL*STZ)
6330 ESWCXW=ESWCXW+(ESWCXWL*STZ)
6340 '


6370 '==========EVALUATING THE ENERGY LOSS IN THE
     VERTICAL DIRECTION==========

6380 'FOLLOWING CHRISTOFFERSEN AND JONSON(1985) EQUATION
     3.12
6390 'THE FOLLOWING EQUATION ALLOWS AN APPROXIMATION FOR
     THE PHASE SHIFT
6400 ESWCZL=(4/(3*PI))*RO*FSWV*(VSW/(SQR(2)))^3
6410 ESWCZ=ESWCZ+(ESWCZL*STZ)
6420 WRITE"ESWCZ=";ESWCZ
6430 '
6440 NEXT ZI

6450 '====THE ENERGY LOSS OF THE COMBINED FLOW AT THE
     SIDEWALL , ESWC=====
6460 ESWC=ESWCX+ESWCZ
6470 WRITE"ESWC=";ESWC
6480 '
```

```
6490 '==THE WAVE ENERGY LOSS OF THE COMBINED FLOW AT THE
                                    SIDEWALL , ESWCW==
6500 ESWCW=ESWCXW+ESWCZ
6510 WRITE"ESWCW=";ESWCW
6530 '


6540 '=====EVALUATING THE SHEAR STRESS IN THE VERTIVAL
    DIRECTION, TSWCZ========
6550 'TSWCZ=(1/2)*RO*(FSWV*(VSW)^2)
6560 'WRITE"TSWCZ=";TSWCZ
6570 '


6580 '=====THE SHEAR STRESS 0F THE COMBINED FLOW AT THE
    SIDE WALL, TSWC========
6590 'TSWC=TSWCX+TSWCZ
6600 'WRITE"TSWC=";TSWC
6610 '
6620 '
6630 'CLOSE #1
6640 'CLOSE #2
6650 '
6660 '


6670 '===============EVALUATING THE RELATIVE WAVE
    VELOCITY, CR==============
6680 CR=L/T
6690 PRINT "CR =";CR
6700 '
6710 '


6720 '=========EVALUATING THE RELATIVE GROUP VELOCITY OF
                                    THE WAVES, CGR========
6730 '
6740 K2D=2*K*D
6750 SINHK2D=(EXP(K2D)-EXP(-K2D))/2
6760 PRINT "K2D";K2D
6770 PRINT "SINHK2D";SINHK2D
6780 CGR=(CR/2)*(1+(K2D/SINHK2D))
6790 WRITE"THE RELATIVE GROUP VELOCITY OF THE WAVES, CGR
    =";CGR
6800 '


6810 '========EVALUATING THE ABSOLUTE GROUP VELOCITY OF
    THE WAVES, CGA========
6820 CGA=CGR+UCBAR
6830 WRITE"THE ABSOLUTE GROUP VELOCITY OF THE WAVES, CGA
    =";CGA
```

```
6840 '


6850 '===========EVALUATING THE WAVE ENERGY, E =========
6860 E=(1/8)*RO*GR*(H)^2
6870 WRITE"E=";E
6880 '


6890 '===EVALUATING THE RADIATION STRESS TERM, SXX ====
6900 SXX=E*((K2D/SINHK2D)+(1/2))
6910 WRITE"SXX=";SXX
6920 '


6930 '========EVALUATING THE FACTOR G, G ===============
6940 G=(K2D+SINHK2D)/SINHK2D
6950 PRINT "G=";G
6960 '
6970 '


6980
    '=================================================
6990 '==========EVALUATING THE FINAL FORMULA ===========
7000 '

7010 '===========Eevaluating the variable factor
                        (4/rho g H) ,VF==============
7020 VF=1/((1/4)*(RO*GR*H))
7030 PRINT "the variable factor (4/rho g H)=";VF
7040 '


7050 '=============EVALUATING THE FIRST TERM OF THE
    NUMERATOR, N1==============
7060 N1=-B*(EBWCW)
7070 PRINT " THE FIRST TERM OF THE NUMERATOR, N1=";N1
7080 '
7090 'OR ALTRNATIVELY TAKING THE AVERAGED VALUE
7100 VN1=-B*(EBW)
7110 PRINT " VN1=";VN1
7120 '

7130 '=============EVALUATING THE SECOND TERM OF THE
    NUMERATOR, N2=============
7140 N2=2*(-ESWCW)
7150 PRINT " THE SECOND TERM OF THE NUMERATOR, N2=";N2
7160 '
7170 'OR ALTRNATIVELY TAKING THE AVERAGED VALUE
7180 VN2=-(2*(ESWX+ESWCZ))
7190 PRINT " VN2=";VN2
```

```
7200 '


7210 '=============EVALUATING THE THIRD TERM OF THE
     NUMERATOR, N3==============
7220
     N3=(1/(GR*D))*(UCBAR^2)*B*(-EBWC+((1/2)*TBWC*UCBAR))
7230 PRINT " THE THIRD TERM OF THE NUMERATOR, N3=";N3
7240 '


7250 '=============EVALUATING THE FOURTH TERM OF THE
     NUMERATOR, N4==============
7260
     N4=(1/(GR*D))*(UCBAR^2)*(2*D)*(-ESWC+((1/2)*TSWCX*UC
     BAR))
7270 PRINT " THE FOURTH TERM OF THE NUMERATOR, N4=";N4
7280 '


7290 '===========EVALUATING THE FIRST TERM OF THE
     DENOMINATOR, D1===============
7300 D1=CGA
7310 PRINT " THE FIRST TERM OF THE DENOMINATOR, D1=";D1
7320 '


7330 '===========EVALUATING THE SECOND TERM OF THE
     DENOMINATOR, D2=============
7340 D2=(1/2)*((UCBAR^2)/CR)
7350 PRINT " THE SECOND TERM OF THE DENOMINATOR, D2=";D2
7360 '


7370 '============EVALUATING THE THIRD TERM OF THE
     DENOMINATOR, D3=============
7380
     D3=((UCBAR^2)/(GR*D))*(CGA+((1/2)*UCBAR*G)+((1/2)*(U
     CBAR^2)/CR))
7390 PRINT " THE THIRD TERM OF THE DENOMINATOR, D3=";D3
7400 '
7410 '


7420 '======== EVALUATING THE TOTAL RATE OF WAVEHEIGHT
     DAMPING WITH X;DHDX======
7430 DHDX=VF*(N1+N2+N3+N4)/((B*PI/WR)*(D1-D2+D3))
7440 PRINT "DHDX =";DHDX
7450 '
7460 '
7470 'OR ALTRENATIVELY FOR THE AVERAGED VALUES
7480 VDHDX=VF*(VN1+VN2+N3+N4)/((B*PI/WR)*(D1-D2+D3))
```

```
7490 PRINT "VDHDX =";VDHDX
7500 '


7510 ' ===EVALUATING THE TOTAL SIMPLIFIED ATTENUATION,
     DHDXS=================
7520 DHDXS=VF*(N1+N2)/(B*PI*D1/WR)
7530 PRINT "DHDXS=";DHDXS
7540 '


7550 '=EVALUATING THE SIMPLIFIED ATTENUATION COEFFICIENT
                              DUE TO THE BED, DHDXSB=
7560 DHDXSB=VF*N1/(B*PI*D1/WR)
7570 PRINT "DHDXSB =";DHDXSB
7580 '


7590 '=EVALUATING THE SIMPLIFIED ATTENUATION COEFFICIENT
                              DUE TO THE WALL,DHDXSS=
7600 DHDXSS=VF*N2/(B*PI*D1/WR)
7610 PRINT "DHDXSS =";DHDXSS
7620 '


7630 '=EVALUATING THE ATTENUATION COEFFICIENT ,ALPHA====
7640 ALPHA=DHDX/.04
7650 PRINT "ALPHA =";ALPHA
7660 'END
7670 '
7680 '==============PRINTING OUT THE RESULTS===========
7690 '
7700 '
7710 LPRINT
     "WAS.BAS*********************************************
     ******";FIL3$

7720 LPRINT "====**********TEST INPUTS*********====

30 'LPRINT
     "================================================="
7740 LPRINT USING"CHANNEL BREADTH (M)= ##.###";B
7750 LPRINT "WAVE PERIOD (S)";T,
7760 LPRINT "HW (M)";HW
7770 LPRINT "WAVE HEIGHT (M)";H
7780 'LPRINT USING" UBWE (M/S)= ##.###";UBWE,
7790 'LPRINT USING"         USWE (M/S)= ##.###";USWE
7800 LPRINT USING "MAXIMUM STEADY CURRENT VELOCITY
     (M/S)= #.###";UC
7810 LPRINT "WATER TEMPERATURE (C)";WC,
7820 LPRINT USING "KINEMATIC VISCOSITY, V = #.##^^^^";V
7830 LPRINT USING" Kb= ##.####";KB,
```

```
7840 LPRINT USING"        Ks= ##.####";KS
7850 LPRINT USING"LW= #.###";LW,
7860 LPRINT USING"              WAVELENGTH= #.###";L
7870 LPRINT
7880 LPRINT "=================BED CALCULATIONS========
7890 LPRINT USING"UC0BAR = #.###";UC0BAR,
7900 LPRINT USING"               UBC0 = #.####";UBC0
7910 LPRINT USING"FBC0 = #.##^^^^";FBC0,
7920 LPRINT USING"               TOBC0 = #.##^^^^";TOBC0
7930 LPRINT USING"AB0 = #.####";AB0,
7940 LPRINT USING" RWB = ####.##";RWB,
7950 LPRINT USING"UBW = ##.###";UBW
7960 LPRINT USING"FBW = #.##^^^^";FBW,
7970 'LPRINT USING"           TOBW0 =#.##^^^^";TOBW0
7980 LPRINT "KB*UBC0/V =";RF
7990 LPRINT USING"UCBAR = #.###";UCBAR,
8000 LPRINT "BED SHEAR VELOCITY OF THE COMBINED FLOW,
    UBWC=";UBWC
8010 LPRINT "BED ROUGHNESS PARAMETER, ZB0=";ZB0
8020 LPRINT "APPARENT BED R., ZB0A=";ZB0A
8030 LPRINT "MB=";MB,
8040 LPRINT "FBC=";FBC,
8050 LPRINT "FBWC=";FBWC
8060 LPRINT "TOBW = ";TOBW,
8070 LPRINT "TOBC = ";TOBC,
8080 LPRINT "TOBWC = ";TOBWC
8090 LPRINT
8100 LPRINT "=========SIDEWALL CALCULATIONS==========
8110 LPRINT "AS0 = ";AS0,
8120 LPRINT " RWS = ";RWS,
8130 LPRINT USING"USW = ##.###";USW
8140 LPRINT "FSW = ";FSW,
8150 'LPRINT "TOSW0 =";TOSW0
8160 LPRINT "USC0 = ";USC0,
8170 LPRINT "FSC0 = ";FSC0
8180 LPRINT "USWC=";USWC,
8190 LPRINT "ZS0=";ZS0,
8200 LPRINT "ZS0A=";ZS0A
8210 LPRINT "MS=";MS,
8220 LPRINT "FSC=";FSC,
8230 LPRINT "FSWC=";FSWC
8240 LPRINT "TOSW = ";TOSW,
8250 LPRINT "TOSC = ";TOSC,
8260 LPRINT "TOSWC = ";TOSWC
8270 LPRINT
8280 LPRINT "=======SIDEWALL CALCULATIONS FOR THE
    VERTICAL COMPONENT ==============="
8290 LPRINT "MAXIMUM VERTICAL WAVE AMPLITUDE AT THE
    SIDEWALL, AS0V= ";AS0V
8300 LPRINT " THE MAXIMUM VERTICAL WAVE VELOCITY NEAR
    THE SIDEWALL = ";VSW
8310 LPRINT " RWSV= ";RWSV
```

```
8320 LPRINT "FSWV= ";FSWV
8330 LPRINT "TOSW0V=";TOSW0V
8340 LPRINT "    "
8350 LPRINT "====EVALUATING THE WAVE ENERGY EQUATION====
8360 LPRINT "TBWC=";TBWC,
8370 LPRINT "TBWCW=";TBWCW,
8380 LPRINT "TBWCC=";TBWCC,
8390 LPRINT "EBC=";EBC,
8400 LPRINT "EBW=";EBW
8410 LPRINT "EBWCC=";EBWCC,
8420 LPRINT "EBWCW=";EBWCW,
8430 LPRINT "EBWC=";EBWC
8440 LPRINT "ESC=";ESC,
8450 LPRINT "ESWX=";ESWX
8460 LPRINT "ESWCXC=";ESWCXC,
8470 LPRINT "ESWCXW=";ESWCXW,
8480 LPRINT "ESWCX=";ESWCX
8490 LPRINT "ESWCZ=";ESWCZ,
8500 LPRINT "ESWC=";ESWC
8510 LPRINT "TSWCX=";TSWCX,
8520 LPRINT "TSWCXW=";TSWCXW,
8530 LPRINT "TSWCXC=";TSWCXC
8540 'LPRINT "TSWCZ=";TSWCZ,
8550 'LPRINT "TSWC=";TSWC
8560 'LPRINT "VEBWCW=";VEBWCW,
8570 'LPRINT "VESWCXW=";VESWCXW
8580 LPRINT "CR =";CR,
8590 LPRINT "CGR =";CGR,
8600 LPRINT "CGA =";CGA
8610 LPRINT "WR =";WR,
8620 LPRINT "WAVE ENERGY, E=";E
8630 LPRINT "SXX=";SXX,
8640 LPRINT "G=";G
8650 LPRINT " THE VARIABLE FACTOR,VF=";VF
8660 LPRINT " THE FIRST TERM OF THE NUMERATOR, N1=";N1,
8670 LPRINT " VN1=";VN1
8680 LPRINT " THE SECOND TERM OF THE NUMERATOR, N2=";N2,
8690 LPRINT " VN2=";VN2
8700 LPRINT " THE THIRD TERM OF THE NUMERATOR, N3=";N3
8710 LPRINT " THE FOURTH TERM OF THE NUMERATOR, N4=";N4
8720 LPRINT " THE FIRST TERM OF THE DENOMINATOR, D1=";D1
8730 LPRINT " THE SECOND TERM OF THE DENOMINATOR,D2=";D2
8740 LPRINT " THE THIRD TERM OF THE DENOMINATOR, D3=";D3
8750 LPRINT "DHDX =";DHDX,
8760 LPRINT "VDHDX =";VDHDX
8770 LPRINT "ALPHA=";ALPHA
8780 LPRINT "DHDXS=";DHDXS,
8790 LPRINT "DHDXSB =";DHDXSB,
8800 LPRINT "DHDXSS =";DHDXSS
8810 '
8840 CLOSE
8850 END
```

APPENDIX B

SIDEWALL L.D.A. MEASUREMENTS SUMMARY SHEETS

TEST NO. : C-SDW20

Distance from the bed(mm):	20	Water Depth (mm):	300
Surface current before waves (mm/s):	0	Wave height (mm):	40
Head difference (inch):	0	Wave length(mm):	740
Temperature (C) :	19	Wave period (s):	0.7

Distance from wall mm	Mean velocity mm/s	Periodic Velocities max mm/s	min mm/s
0.2	1		
0.3	3		
0.4	7	22	-15
0.6	8	25	-21
0.8	14	26	-26
1	13	30	-19
1.2	9	25	-17
1.4	8	28	-21
1.6	10	31	-18
1.8	12	29	-15
2	9	28	-17
2.3	7	27	-16
2.6	6	21	-18
3	9	24	-15
3.5	7	25	-14
4	6	27	-15
4.5	6	30	-19
5	5	26	-21
6	4	23	-20
7	4	20	-17
8	5	30	-17
9	5	29	-17
10	6	28	-16
12	5	28	-21
14	5	27	-19
16	4	29	-16
18	6	26	-15
20	5	25	-17
22.5	4	27	-15
25	4	28	-16
30	2	25	-13
35	6	24	-16
40	3	23	-17
45	4	22	-13
50	3	21	-15
60	4	22	-15
70	2	25	-13
80	5	21	-16
100	1	20	-14
125	3	18	-14
150	1	20	-15

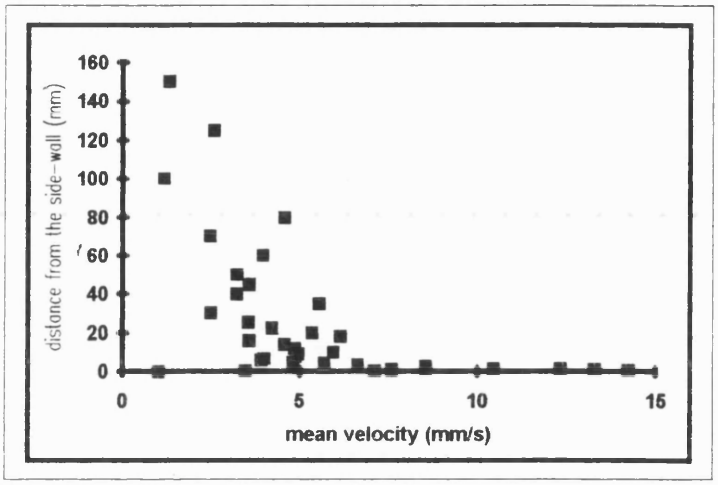

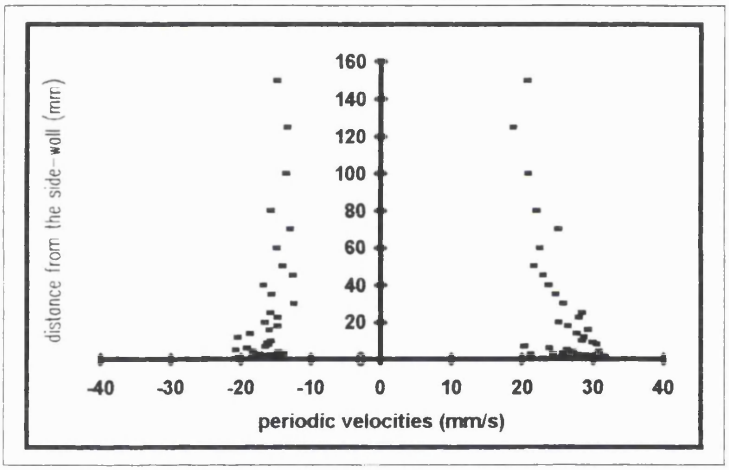

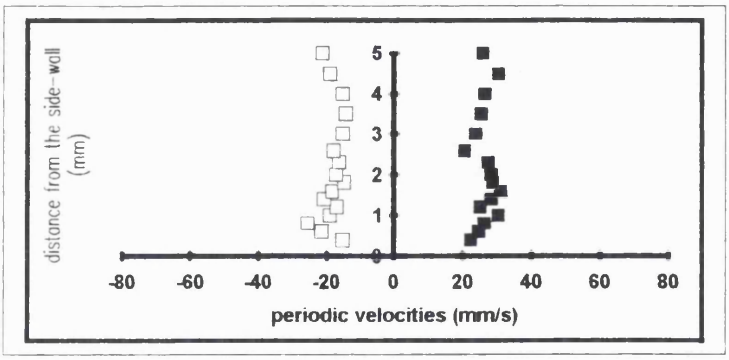

TEST NO. : C-SDW50

Distance from the bed(mm):	50	Water Depth (mm):	300
Surface current before waves (mm/s):	0	Wave height (mm):	40
Head difference (inch):	0	Wave length(mm):	740
Temperature (C) :	20	Wave period (s):	0.7

Distance from wall	Mean velocity	Periodic Velocities max	min
mm	mm/s	mm/s	mm/s
0.2	0	20	-15
0.3	2	23	-19
0.4	4	27	-17
0.6	6	29	-20
0.8	8	28	-19
1	8	29	-20
1.2	7	29	-20
1.4	9	27	-23
1.6	8	28	-23
1.8	8	27	-21
2	7	27	-21
2.3	8	28	-19
2.6	7	28	-23
3	5	28	-25
3.5	6	27	-24
4	3	27	-23
4.5	4	27	-22
5	3	28	-19
6	6	27	-17
7	5	26	-17
8	6	24	-17
9	7	25	-19
10	7	25	-21
12	7	24	-21
14	5	26	-22
16	4	27	-21
18	2	28	-21
20	1	27	-22
22.5	1	27	-24
25	1	28	-23
30	3	30	-24
35	4	29	-24
40	3	26	-24
45	2	28	-23
50	4	27	-22
60	3	29	-23
70	3	28	-24
80	3	27	-24
100	4	25	-23
125	5	25	-23
150	3	26	-23

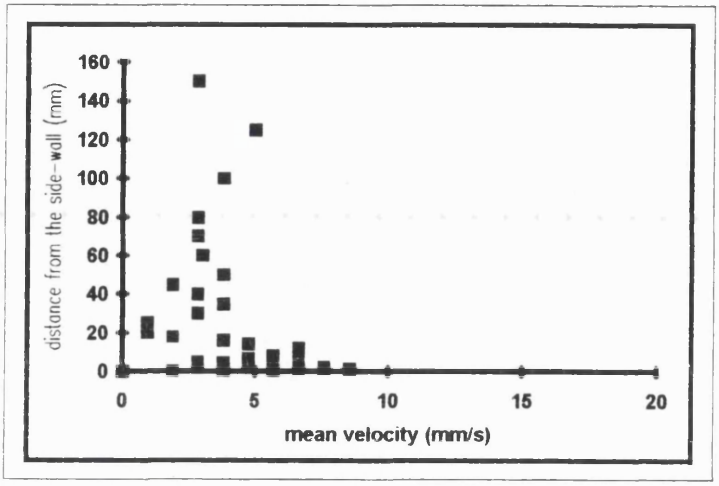

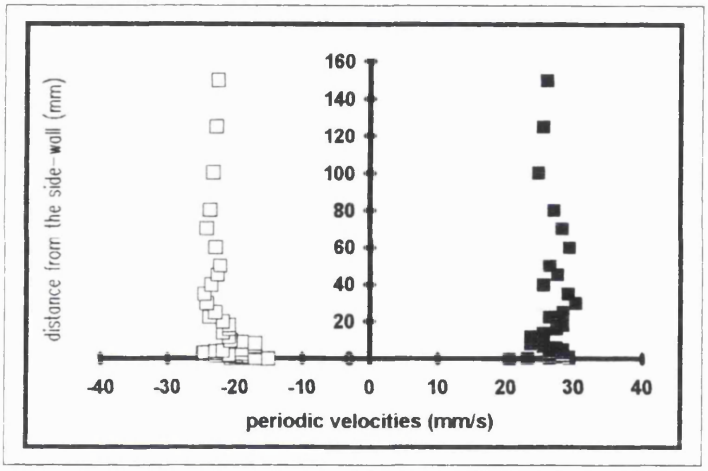

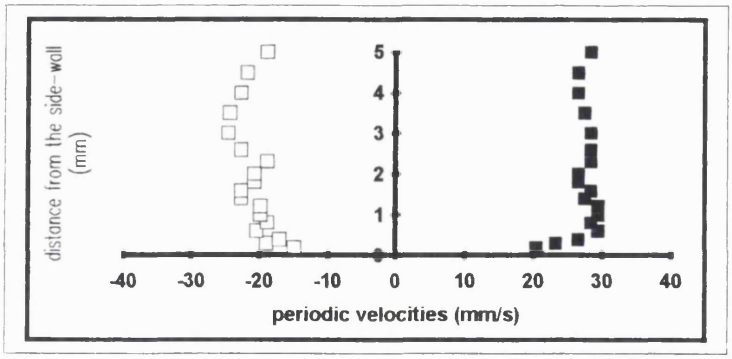

TEST NO. : C-SDW150

Distance from the bed(mm):	150	Water Depth (mm):	300
Surface current before waves (mm/s):	0	Wave height (mm):	40
Head difference (inch):	0	Wave length(mm):	720
Temperature (C) :	21	Wave period (s):	0.7

Distance from wall	Mean velocity	Periodic Velocities max	min
mm	mm/s	mm/s	mm/s
0.2	7	41	-28
0.3	7	48	-41
0.4	8	55	-47
0.6	8	60	-48
0.8	8	63	-52
1	7	62	-49
1.2	7	58	-52
1.4	6	58	-51
1.6	6	49	-53
1.8	6	55	-53
2	6	50	-51
2.3	6	47	-50
2.6	6	49	-49
3	7	53	-49
3.5	6	53	-49
4	4	52	-48
4.5	2	52	-48
5	1	53	-48
6	3	55	-46
7	4	55	-47
8	3	56	-48
9	2	55	-45
10	1	55	-44
12	0	51	-51
14	-1	47	-45
16	-1	47	-37
18	-2	44	-32
20	-3	43	-32
22.5	-3	44	-28
25	-2	44	-27
30	-2	48	-33
35	-1	46	-29
40	-1	45	-27
45	-2	46	-27
50	-1	48	-28
60	-1	46	-28
70	-3	45	-30
80	-2	43	-32
100	-2	38	-26
125	-2	45	-31
150	-1	42	-30

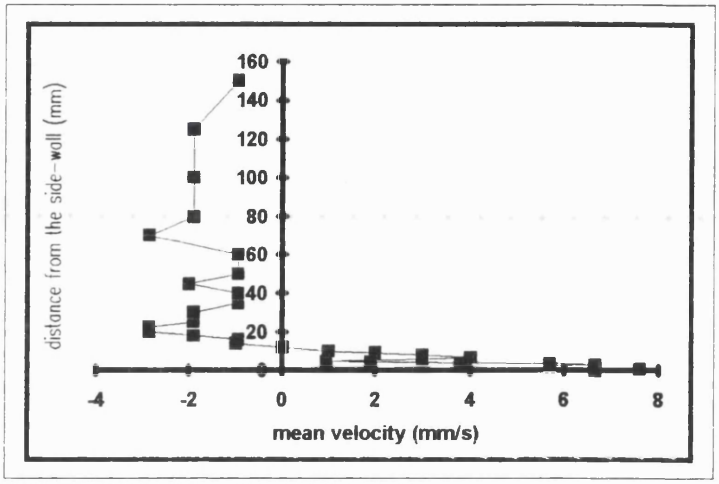

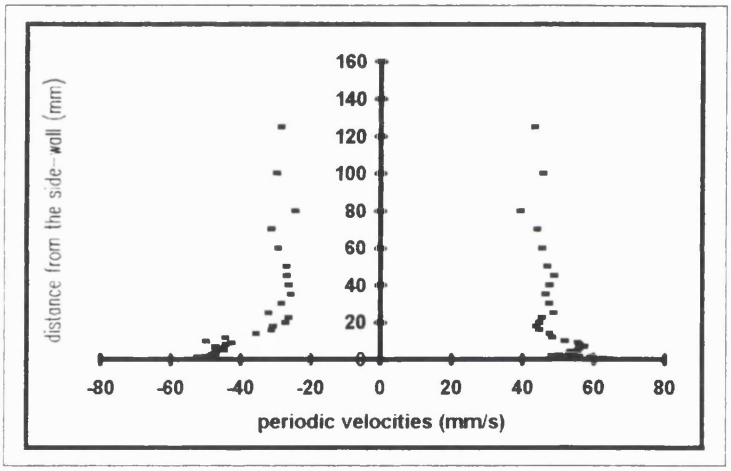

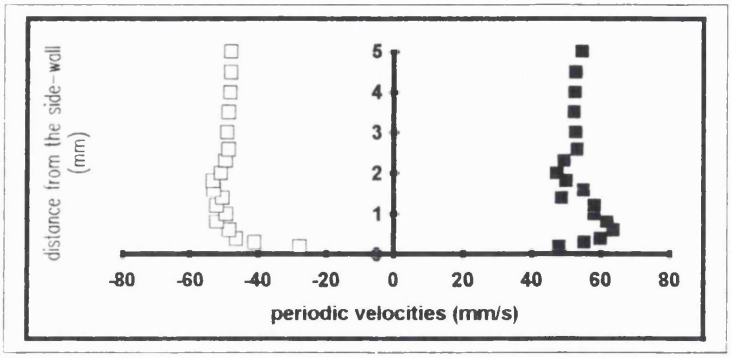

TEST NO. : C-SDWWC50

Distance from the bed(mm):	50	Water Depth (mm):	300
Surface current before waves (mm/s):		Wave height (mm):	39
Head difference (inch):	2.5	Wave length(mm):	
Temperature (C) :	20	Wave period (s):	0.7

Distance from wall mm	Mean velocity mm/s	Periodic Velocities max mm/s	min mm/s
0.2	1	15	-7
0.3	1	18	-12
0.4	2	22	-15
0.6	3	22	-18
0.8	4	24	-23
1	5	26	-17
1.2	7	23	-16
1.4	8	27	-18
1.6	7	25	-20
1.8	8	27	-19
2	7	24	-17
2.3	8	22	-17
2.6	9	21	-13
3	9	20	-11
3.5	12	19	-14
4	15	20	-15
4.5	16	20	-13
5	19	20	-11
6	17	19	-7
7	19	18	-15
8	22	22	-11
9	25	22	-14
10	27	22	-16
12	28	20	-11
14	28	19	-11
16	29	19	-9
18	30	20	-12
20	31	18	-11
22.5	30	19	-12
25	31	19	-13
30	33	19	-13
35	34	21	-11
40	34	21	-12
45	33	20	-12
50	34	18	-12
60	33	21	-12
70	34	20	-12
80	34	20	-11
100	33	19	-12
125	32	18	-13
150	32	21	-12

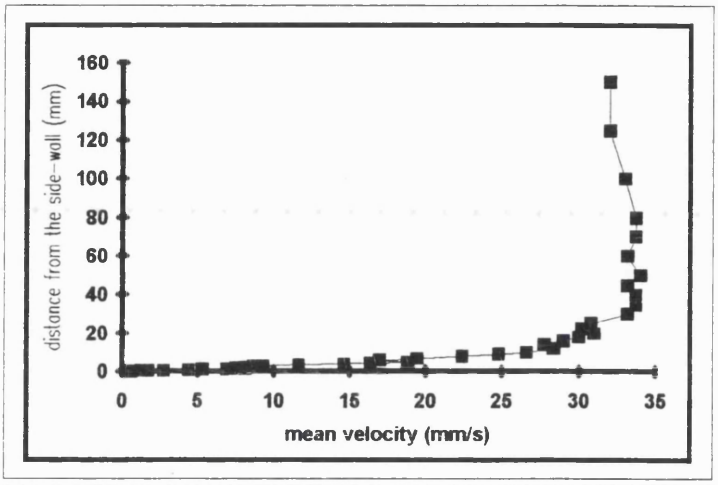

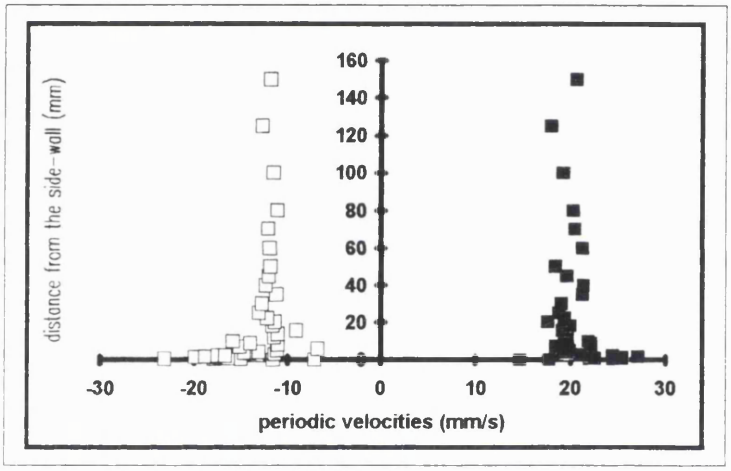

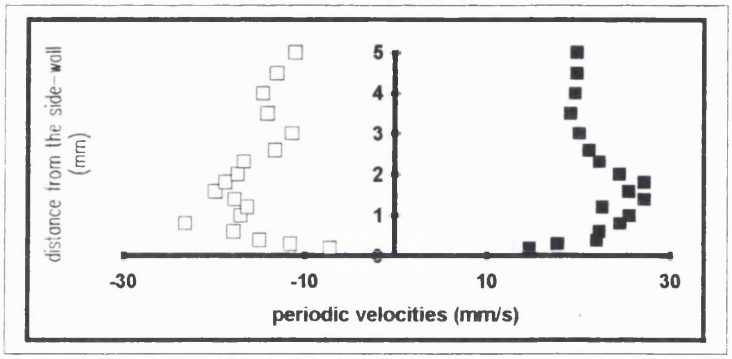

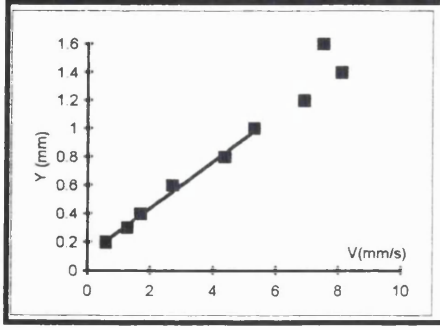

Slope of the inner layer :	6.09
kinematic viscosity	1.01
Wall shear stress over density:	6.15

TEST NO. : C-SDWWC150

Distance from the bed(mm):	150	Water Depth (mm):	300
Surface current before waves (mm/s):		Wave height (mm):	40
Head difference (inch):	2.5	Wave length(mm):	840
Temperature (C) :	20	Wave period (s):	0.7

Distance from wall	Mean velocity	Periodic Velocities max	Periodic Velocities min
mm	mm/s	mm/s	mm/s
0.2	1	24	-12
0.3	2	30	-19
0.4	4	37	-25
0.6	7	37	-21
0.8	8	41	-29
1	10	43	-25
1.2	11	40	-27
1.4	13	45	-30
1.6	12	42	-33
1.8	13	45	-31
2	12	41	-29
2.3	13	37	-28
2.6	14	32	-22
3	15	31	-23
3.5	19	31	-24
4	23	33	-24
4.5	26	33	-22
5	30	33	-21
6	27	31	-23
7	31	31	-23
8	36	35	-20
9	39	35	-23
10	42	34	-23
12	45	33	-19
14	44	32	-18
16	44	29	-17
18	43	30	-18
20	46	29	-19
22.5	48	31	-20
25	49	31	-22
30	53	32	-21
35	54	35	-20
40	54	35	-21
45	53	33	-20
50	52	33	-20
60	53	36	-18
70	54	34	-15
80	54	34	-19
100	53	32	-19
125	54	30	-21
150	53	32	-20

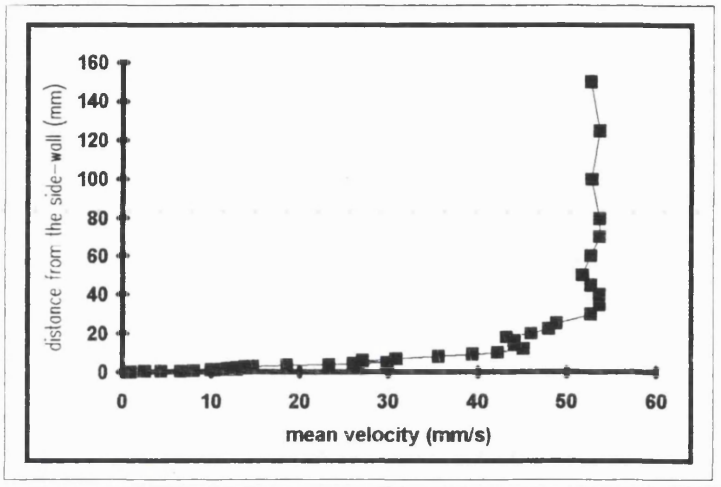

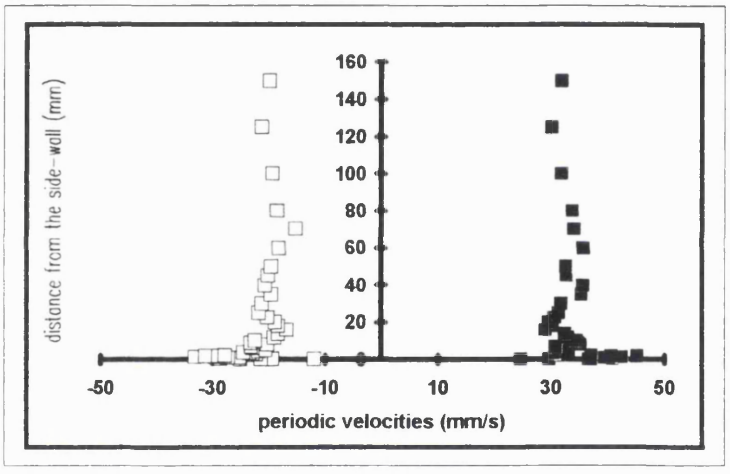

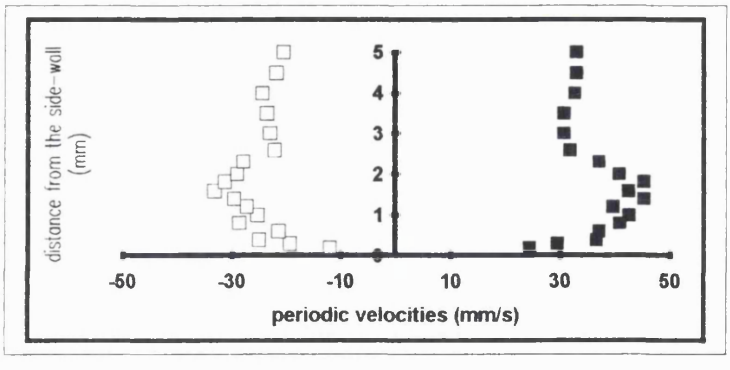

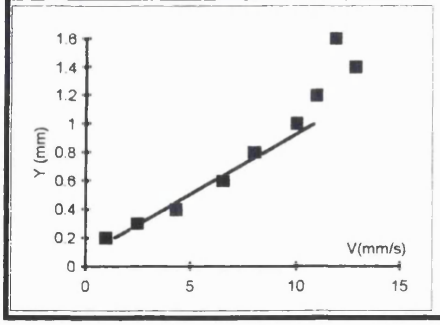

Slope of the inner layer :	11.84
kinematic viscosity	1.01
Wall shear stress over density:	11.97

TEST NO. : C-SDWMC20

Distance from the bed(mm):	20	Water Depth (mm):	300
Surface current before waves (mm/s):		Wave height (mm):	35
Head difference (inch):	8.5	Wave length(mm):	820
Temperature (C) :	20	Wave period (s):	0.7

Distance from wall mm	Mean velocity mm/s	Periodic Velocities max mm/s	min mm/s
0.2	1	11	-6
0.3	2	13	-7
0.4	2	15	-6
0.6	4	17	-8
0.8	7	20	-11
1	10	21	-10
1.2	12	17	-7
1.4	16	19	-10
1.6	20	18	-8
1.8	24	20	-8
2	27	22	-9
2.3	27	26	-11
2.6	25	25	-11
3	31	29	-13
3.5	31	29	-12
4	30	30	-11
4.5	28	30	-10
5	27	29	-12
6	37	33	-16
7	41	33	-15
8	36	33	-17
9	43	30	-14
10	47	34	-14
12	49	33	-15
14	50	34	-15
16	50	35	-17
18	50	34	-15
20	51	33	-14
22.5	52	34	-15
25	52	33	-17
30	51	35	-19
35	52	35	-17
40	53	35	-16
45	54	35	-17
50	55	36	-17
60	58	35	-18
70	62	34	-18
80	66	33	-18
100	69	37	-18
125	74	36	-18
150	69	36	-22

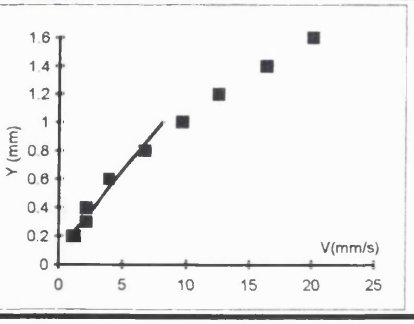

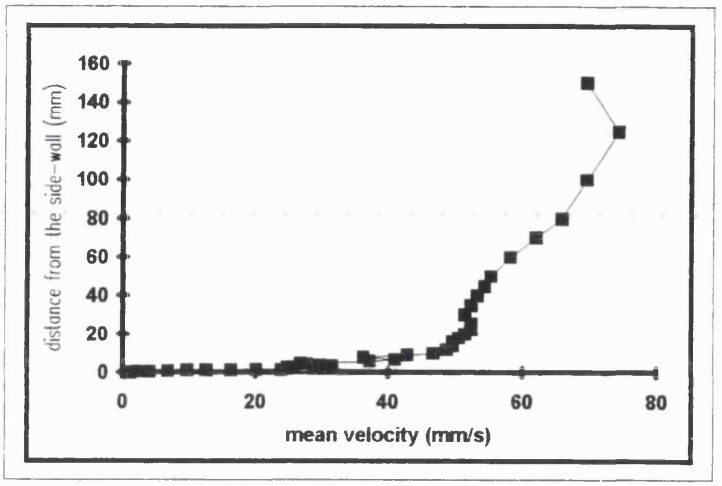

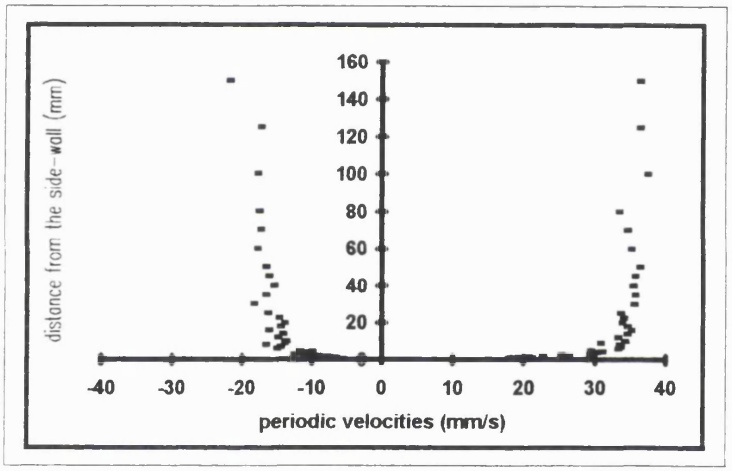

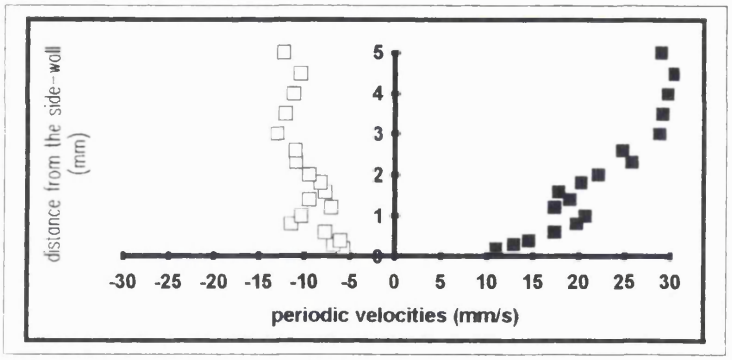

Slope of the inner layer :	9.17
kinematic viscosity	1.01
Wall shear stress over density:	9.26

TEST NO. : C-SDWMC50

Distance from the bed(mm):	50	Water Depth (mm):	300
Surface current before waves (mm/s):		Wave height (mm):	35
Head difference (inch):	804	Wave length(mm):	820
Temperature (C) :	18	Wave period (s):	0.7

Distance from wall mm	Mean velocity mm/s	Periodic Velocities max mm/s	min mm/s
0.2	1	8	-1
0.3	3	16	-6
0.4	4	23	-13
0.6	6	28	-16
0.8	10	29	-18
1	13	28	-15
1.2	16	27	-16
1.4	19	26	-14
1.6	23	26	-12
1.8	24	26	-11
2	28	27	-11
2.3	32	28	-10
2.6	35	29	-11
3	37	30	-12
3.5	39	30	-11
4	39	31	-11
4.5	42	31	-13
5	44	32	-12
6	45	33	-14
7	47	32	-13
8	49	34	-14
9	50	34	-16
10	53	31	-13
12	54	33	-16
14	53	32	-16
16	54	30	-16
18	56	31	-15
20	58	34	-15
22.5	59	32	-12
25	60	31	-10
30	64	28	-13
35	66	28	-12
40	67	27	-11
45	65	28	-12
50	65	30	-11
60	67	32	-13
70	70	32	-13
80	73	34	-11
100	75	34	-10
125	79	35	-12
150	81	32	-13

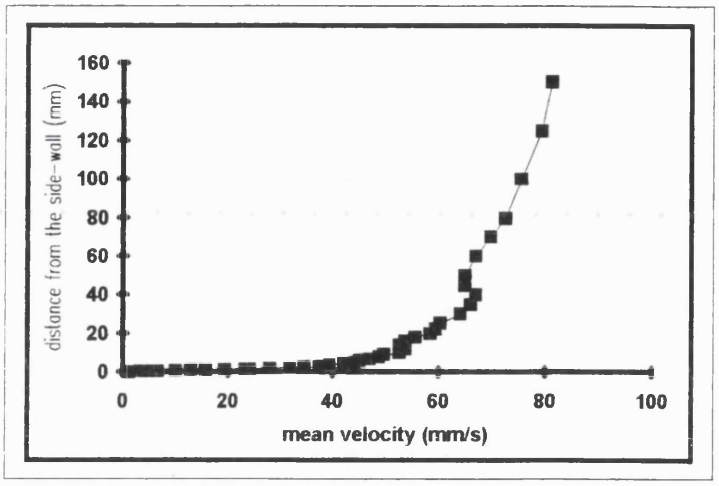

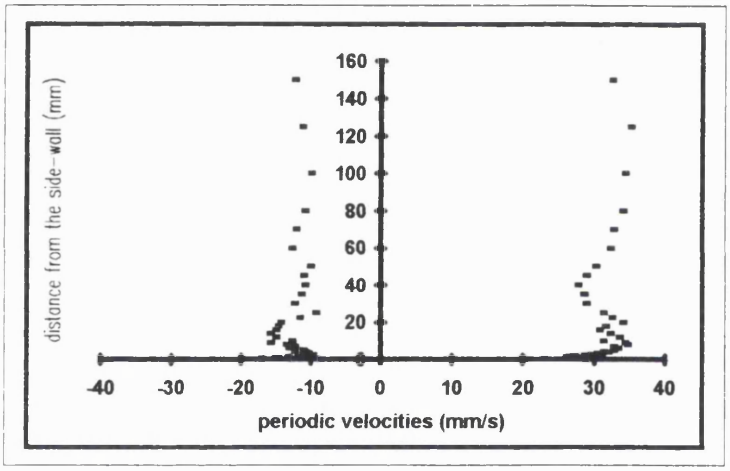

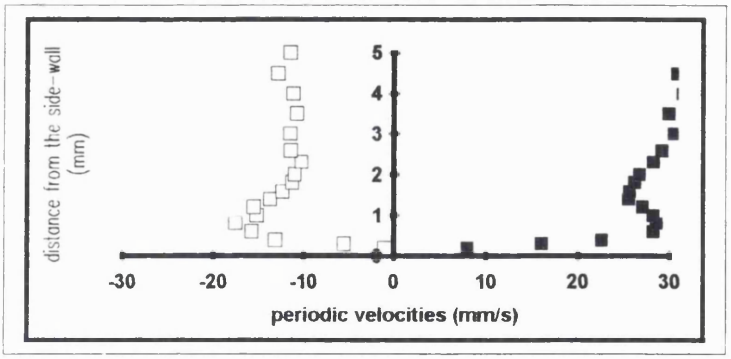

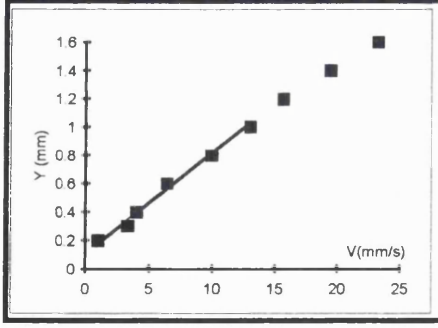

Slope of the inner layer :	14.01
kinematic viscosity	1.06
Wall shear stress over density:	14.86

TEST NO. : C-SDWMC150

Distance from the bed(mm):	150	Water Depth (mm):	300
Surface current before waves (mm/s):		Wave height (mm):	36
Head difference (inch):	8.4	Wave length(mm):	820
Temperature (C) :	18	Wave period (s):	0.7

Distance from wall mm	Mean velocity mm/s	Periodic Velocities max mm/s	min mm/s
0.2	2	24	-16
0.3	3	29	-17
0.4	4	34	-21
0.6	8	41	-29
0.8	11	39	-25
1	13	39	-25
1.2	16	32	-23
1.4	15	41	-22
1.6	19	37	-12
1.8	23	36	-13
2	26	36	-14
2.3	31	33	-10
2.6	35	35	-15
3	42	39	-19
3.5	49	42	-22
4	53	46	-25
4.5	56	45	-26
5	57	43	-24
6	59	48	-25
7	63	46	-25
8	65	48	-25
9	67	50	-26
10	68	48	-29
12	70	48	-24
14	72	49	-28
16	72	52	-31
18	72	49	-30
20	72	48	-29
22.5	72	49	-30
25	73	48	-29
30	74	49	-32
35	76	48	-32
40	78	48	-33
45	78	48	-28
50	78	50	-29
60	80	49	-32
70	82	49	-35
80	82	49	-30
100	84	48	-28
125	86	49	-30
150	87	48	-29

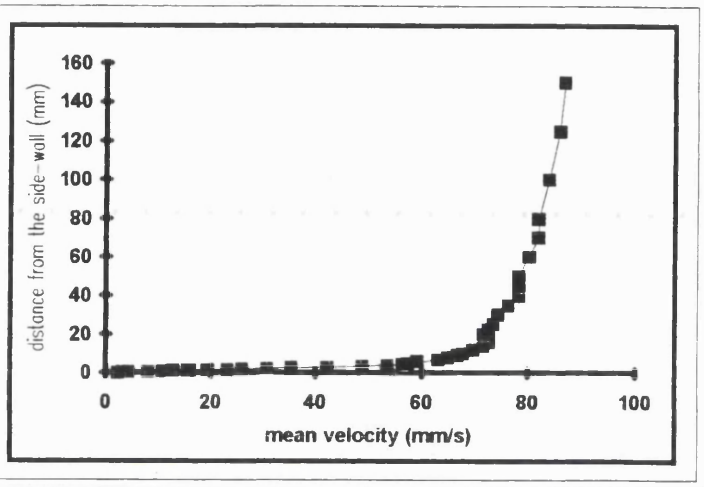

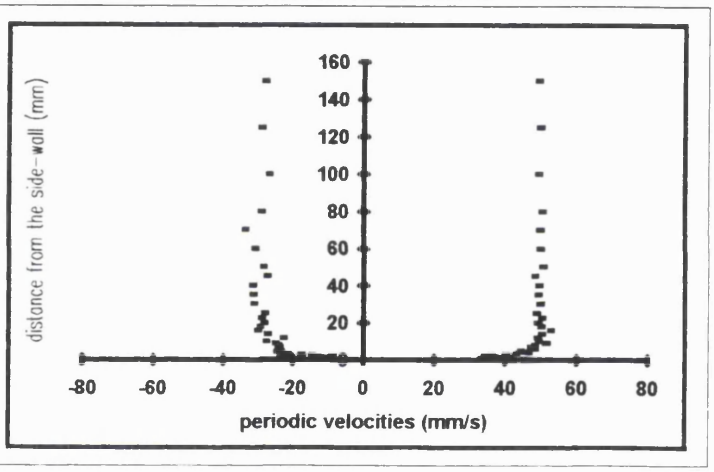

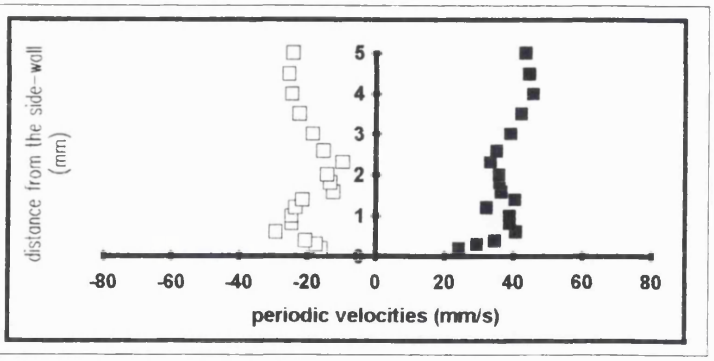

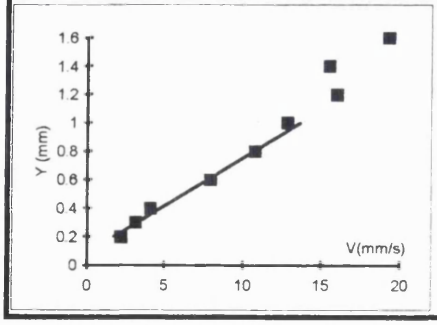

Slope of the inner layer :	14.82
kinematic viscosity	1.06
Wall shear stress over density:	15.72

TEST NO. : C-SDWSC20

Distance from the bed(mm):	20	Water Depth (mm):	300
Surface current before waves (mm/s):		Wave height (mm):	30
Head difference (inch):	25	Wave length(mm):	
Temperature (C) :	20	Wave period (s):	0.7

Distance from wall mm	Mean velocity mm/s	Periodic Velocities max mm/s	min mm/s
0.2	1	19	0
0.3	4	18	-1
0.4	6	15	-2
0.6	10	14	-3
0.8	15	19	-8
1	21	24	-9
1.2	25	22	-5
1.4	23	19	-5
1.6	29	17	-4
1.8	34	17	-6
2	39	24	-8
2.3	45	28	-6
2.6	48	31	-11
3	53	29	-20
3.5	61	33	-18
4	62	35	-17
4.5	60	36	-17
5	60	35	-16
6	59	35	-17
7	62	36	-16
8	63	38	-13
9	65	35	-16
10	67	32	-17
12	69	35	-18
14	71	37	-17
16	68	36	-17
18	74	36	-19
20	78	33	-21
22.5	81	37	-20
25	83	38	-19
30	83	36	-18
35	84	36	-16
40	84	35	-17
45	85	36	-17
50	86	35	-19
60	89	35	-18
70	97	34	-21
80	104	35	-22
100	113	36	-21
125	122	35	-20
150	121	35	-20

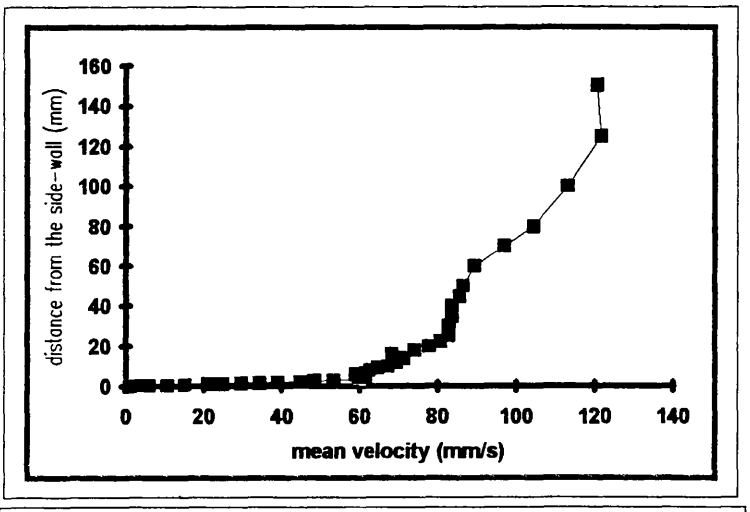

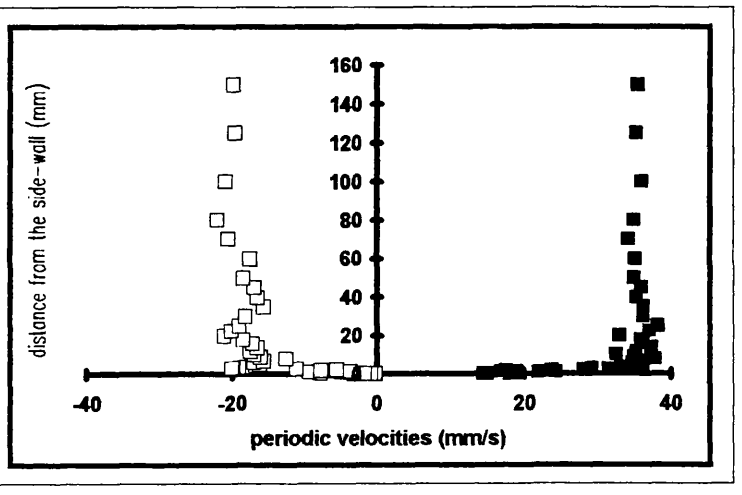

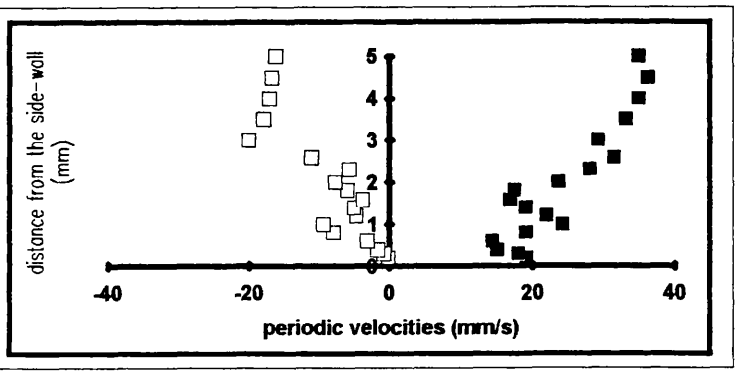

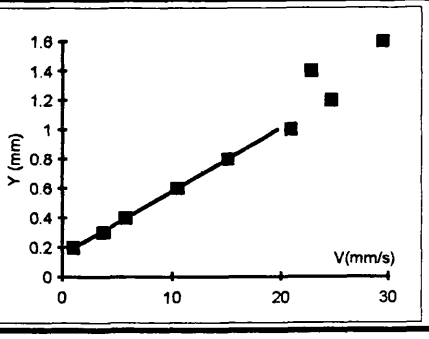

Slope of the inner layer :	23.07
kinematic viscosity	1.01
Wall shear stress over density:	23.31

TEST NO. : C-SDWSC50

Distance from the bed(mm):	50	Water Depth (mm):	300
Surface current before waves (mm/s):		Wave height (mm):	30
Head difference (inch):	25	Wave length(mm):	920
Temperature (C) :	20	Wave period (s):	0.7

Distance from wall mm	Mean velocity mm/s	Periodic Velocities max mm/s	min mm/s
0.2	2	16	-6
0.3	5	20	-4
0.4	9	20	-6
0.6	16	26	-10
0.8	21	30	-12
1	31	34	-13
1.2	38	35	-14
1.4	43	35	-15
1.6	45	36	-16
1.8	48	37	-19
2	51	37	-19
2.3	55	38	-21
2.6	58	38	-21
3	66	41	-21
3.5	69	36	-22
4	71	32	-22
4.5	72	33	-22
5	75	35	-24
6	79	38	-23
7	83	41	-25
8	77	43	-22
9	80	42	-23
10	83	41	-24
12	84	42	-27
14	87	41	-25
16	89	39	-25
18	90	38	-23
20	90	39	-21
22.5	89	38	-21
25	93	38	-23
30	95	38	-25
35	98	40	-24
40	99	41	-23
45	102	37	-20
50	106	41	-25
60	114	40	-25
70	119	39	-24
80	125	40	-26
100	128	41	-22
125	130	40	-23
150	133	40	-22

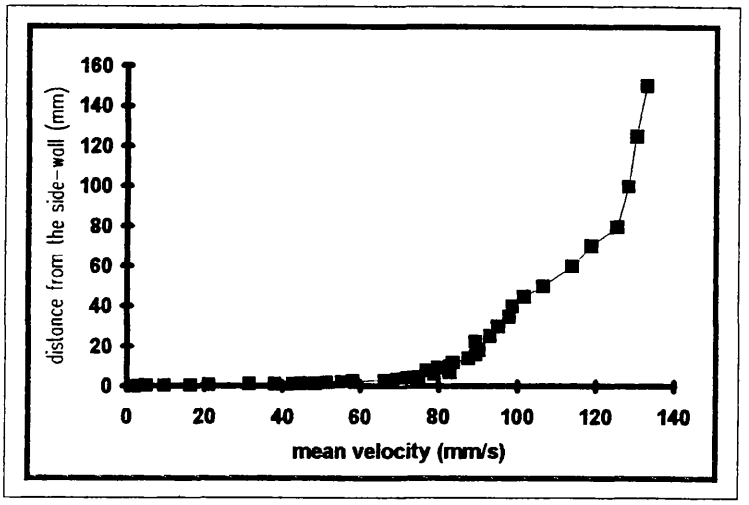

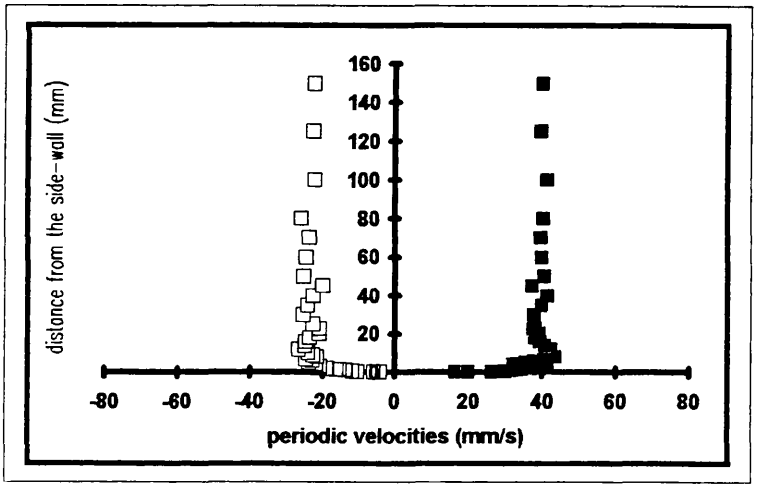

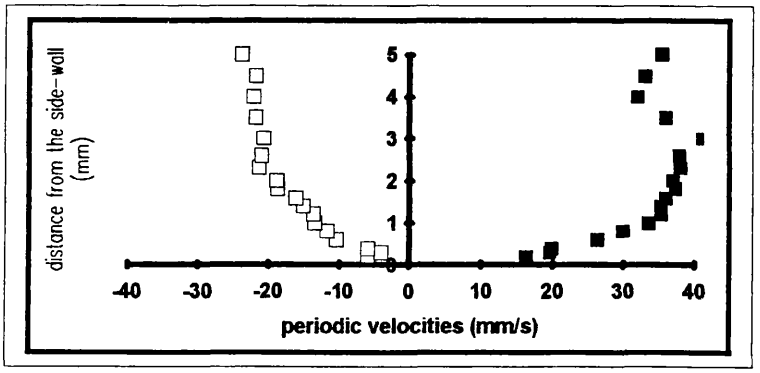

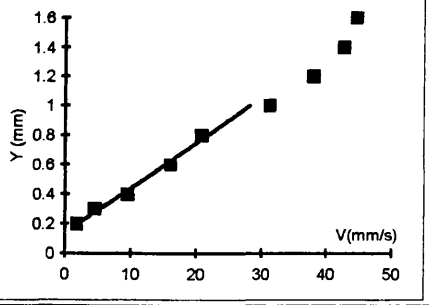

Slope of the inner layer :	32.50
kinematic viscosity	1.01
Wall shear stress over density:	32.83

TEST NO. : C-SDWSC150

Distance from the bed(mm):	150	Water Depth (mm):	300
Surface current before waves (mm/s):		Wave height (mm):	30
Head difference (inch):	25	Wave length(mm):	908
Temperature (C) :	19	Wave period (s):	0.7

Distance from wall mm	Mean velocity mm/s	Periodic Velocities max mm/s	min mm/s
0.2	4	25	-15
0.3	9	25	-15
0.4	13	32	-22
0.6	19	35	-26
0.8	24	40	-30
1	29	40	-32
1.2	31	36	-22
1.4	41	40	-19
1.6	48	44	-24
1.8	55	38	-25
2	61	45	-27
2.3	66	46	-29
2.6	68	48	-31
3	69	51	-34
3.5	72	52	-34
4	78	52	-35
4.5	78	44	-26
5	76	47	-30
6	91	60	-38
7	92	58	-39
8	94	55	-34
9	96	57	-37
10	98	57	-39
12	94	54	-34
14	95	54	-36
16	101	52	-33
18	107	55	-38
20	108	56	-38
22.5	112	57	-37
25	116	55	-38
30	118	53	-40
35	121	57	-40
40	123	59	-40
45	123	58	-40
50	125	57	-40
60	123	53	-32
70	125	55	-37
80	125	56	-34
100	128	58	-43
125	129	53	-35
150	129	55	-37

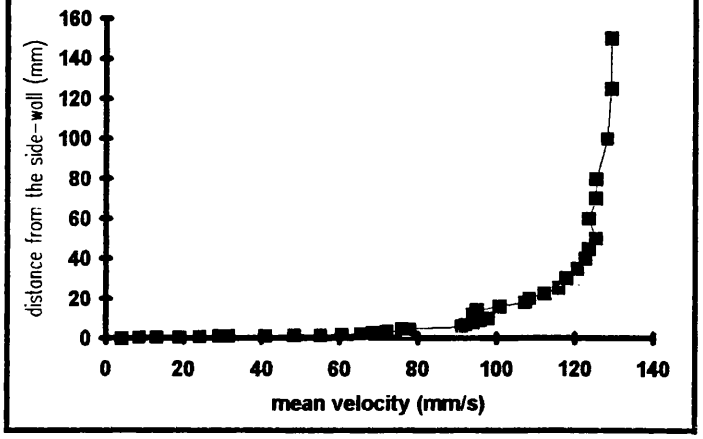

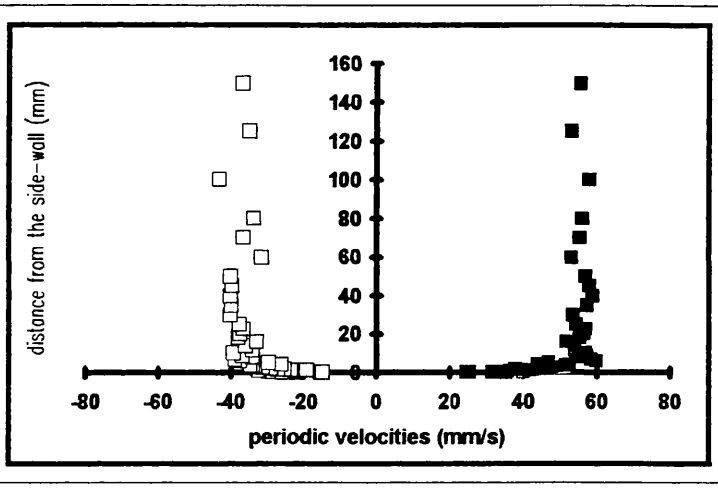

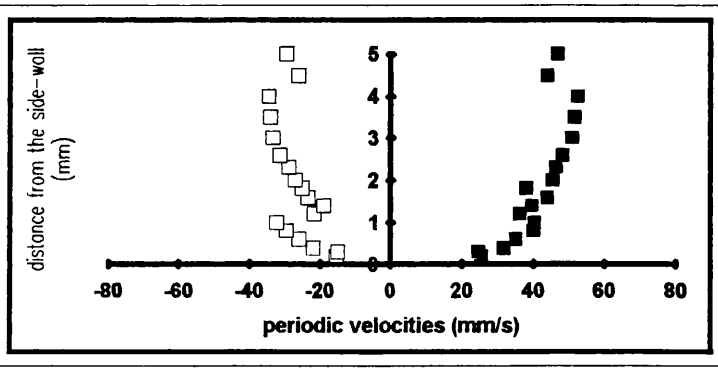

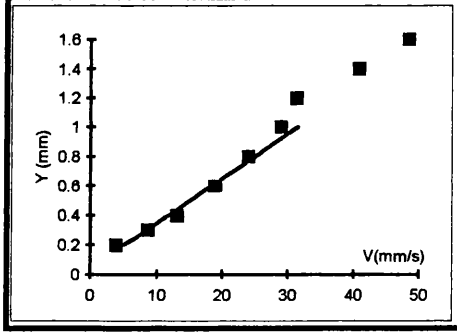

Slope of the inner layer :	32.90
kinematic viscosity	1.04
Wall shear stress over density:	34.05

TEST NO. : C-SIW20

Distance from the bed(mm):	20	Water Depth (mm):	300
Surface current before waves (mm/s):	0	Wave height (mm):	40
Head difference (mm):	0	Wave length(mm):	1300
Temperature (C) :	20	Wave period (s):	1

Distance from wall	Mean velocity	Periodic Velocities max	min
mm	mm/s	mm/s	mm/s
0.2	6	41	-9
0.3	6	46	-29
0.4	7	41	-28
0.6	9	45	-39
0.8	12	50	-49
1	10	56	-35
1.2	9	46	-31
1.4	9	52	-38
1.6	10	57	-34
1.8	12	53	-27
2	10	52	-32
2.3	8	48	-29
2.6	7	37	-32
3	9	42	-27
3.5	7	45	-26
4	6	47	-27
4.5	6	54	-34
5	5	46	-38
6	6	41	-35
7	6	35	-30
8	7	53	-30
9	7	52	-30
10	8	49	-29
12	8	50	-37
14	6	48	-34
16	4	51	-29
18	7	48	-27
20	9	45	-31
22.5	7	51	-28
25	5	51	-29
30	4	46	-23
35	6	44	-29
40	4	43	-31
45	6	41	-24
50	6	39	-26
60	5	40	-28
70	5	45	-24
80	5	40	-29
100	3	37	-26
125	4	33	-25
150	5	37	-28

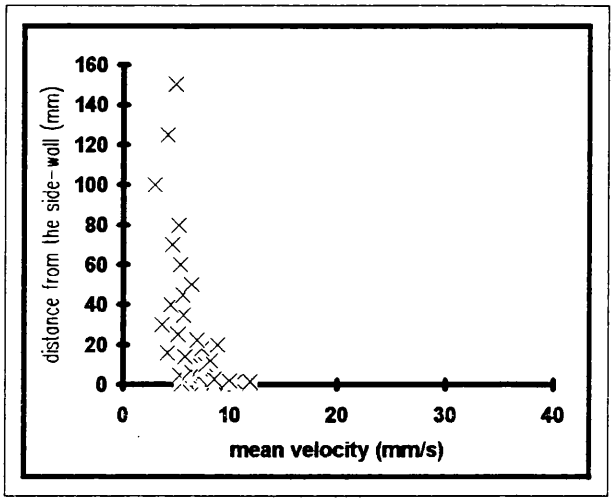

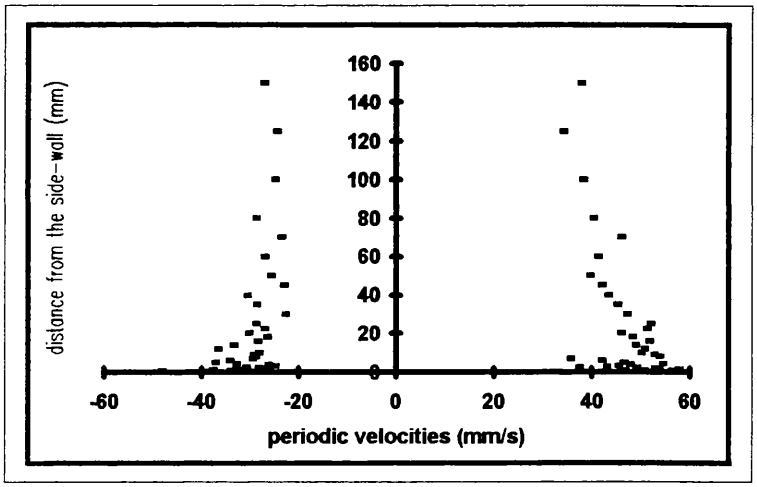

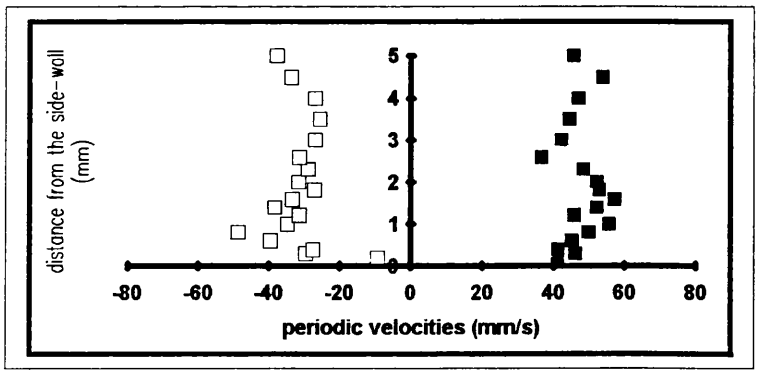

TEST NO. : C-SIW150

Distance from the bed(mm):	150	Water Depth (mm):	300
Surface current before waves (mm/s):	0	Wave height (mm):	40
Head difference (inch):	0	Wave length(mm):	1300
Temperature (C) :	21	Wave period (s):	1.0

Distance from wall	Mean velocity	Periodic Velocities max	Periodic Velocities min
mm	mm/s	mm/s	mm/s
0.2	7	42	-33
0.3	10	58	-38
0.4	10	75	-44
0.6	9	78	-56
0.8	8	83	-52
1	8	80	-66
1.2	8	83	-72
1.4	5	81	-71
1.6	7	79	-73
1.8	9	76	-69
2	10	78	-69
2.3	9	74	-65
2.6	8	70	-64
3	9	69	-66
3.5	8	66	-60
4	6	67	-57
4.5	5	66	-59
5	5	63	-57
6	5	63	-58
7	5	74	-56
8	4	74	-52
9	3	76	-57
10	2	78	-51
12	4	72	-53
14	3	68	-51
16	2	69	-48
18	1	76	-49
20	0	78	-53
22.5	0	78	-55
25	0	80	-62
30	0	78	-57
35	-1	74	-56
40	-2	82	-60
45	-2	79	-58
50	-1	83	-55
60	-1	78	-57
70	-3	81	-62
80	-3	79	-65
100	-3	78	-58
125	-5	77	-62
150	-6	76	-58

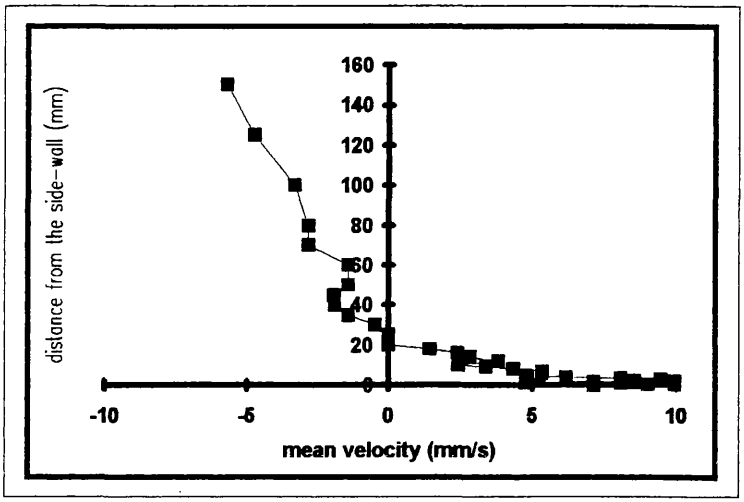

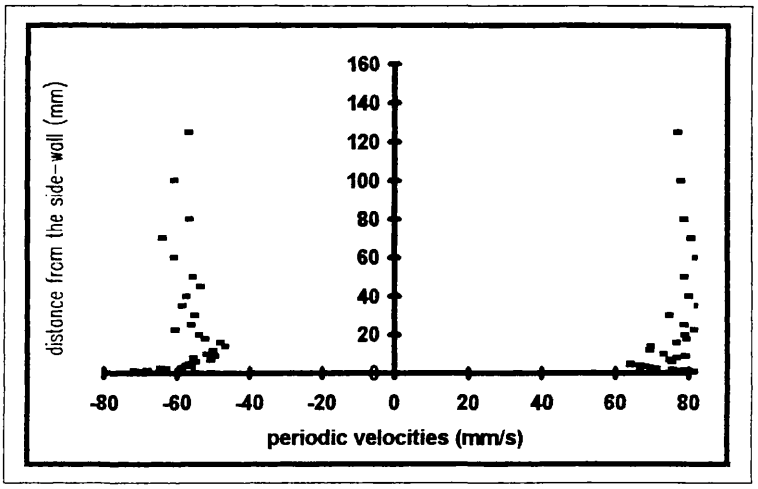

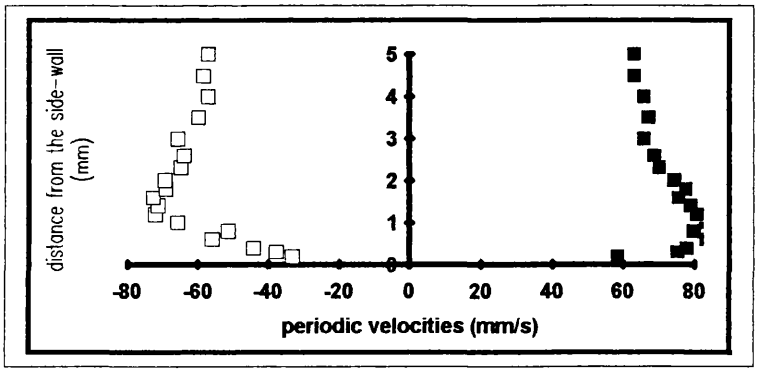

TEST NO. : C-SIWWC50

Distance from the bed(mm):	50	Water Depth (mm):	300
Surface current before waves (mm/s):		Wave height (mm):	37
Head difference (inch):	2.5	Wave length(mm):	
Temperature (C) :	20	Wave period (s):	1.0

Distance from wall	Mean velocity	Periodic Velocities max	Periodic Velocities min
mm	mm/s	mm/s	mm/s
0.2	1	34	-31
0.3	2	38	-41
0.4	2	44	-42
0.6	3	54	-44
0.8	4	58	-43
1	4	57	-47
1.2	5	59	-45
1.4	5	49	-41
1.6	5	51	-42
1.8	6	46	-39
2	5	43	-38
2.3	6	46	-38
2.6	9	48	-40
3	10	47	-41
3.5	10	43	-42
4	12	45	-40
4.5	12	44	-38
5	13	43	-41
6	12	40	-38
7	13	44	-36
8	14	43	-33
9	13	45	-35
10	15	43	-33
12	17	44	-31
14	19	45	-30
16	20	44	-27
18	21	43	-26
20	22	44	-24
22.5	24	47	-27
25	26	41	-25
30	26	42	-29
35	27	43	-26
40	26	41	-30
45	27	43	-27
50	27	45	-35
60	27	43	-29
70	27	42	-26
80	28	42	-29
100	30	43	-34
125	33	42	-27
150	31	45	-29

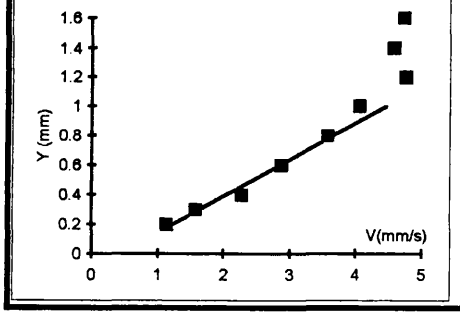

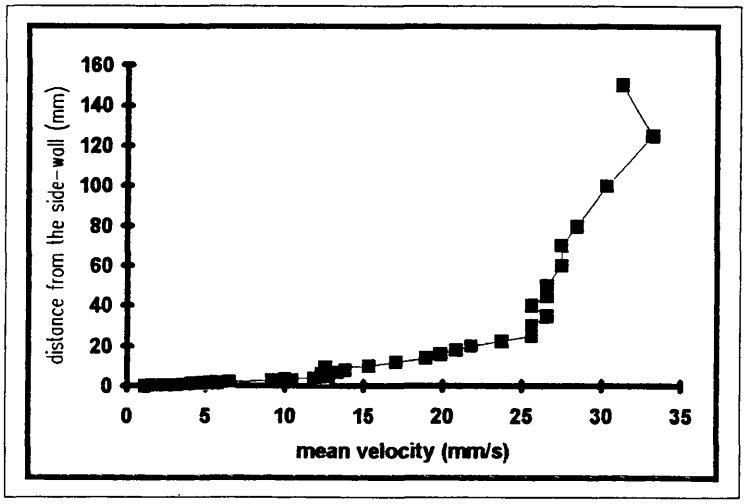

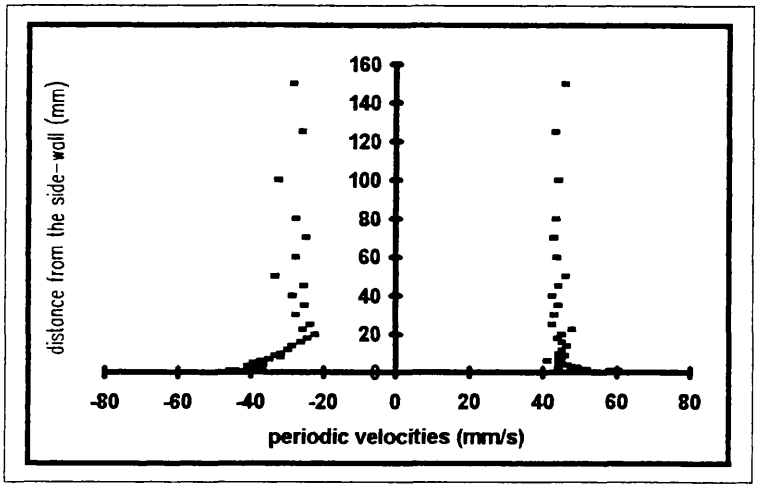

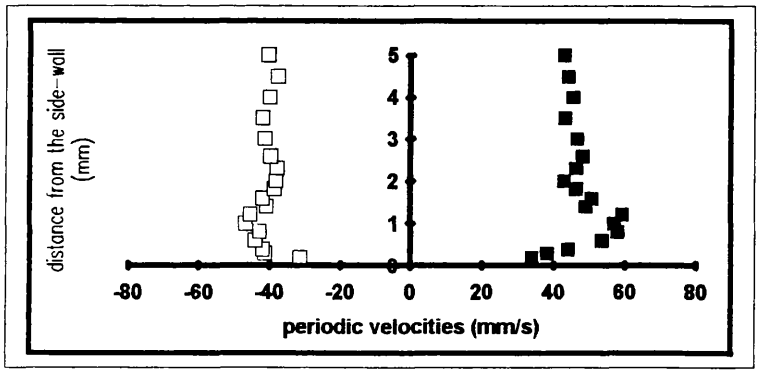

Slope of the inner layer :	4.04
kinematic viscosity	1.01
Wall shear stress over density:	4.08

TEST NO. : C-SIWWC150

Distance from the bed(mm):	150	Water Depth (mm):	300
Surface current before waves (mm/s):		Wave height (mm):	37
Head difference (inch):	2.5	Wave length(mm):	1370
Temperature (C) :	20	Wave period (s):	1.0

Distance from wall mm	Mean velocity mm/s	Periodic Velocities max mm/s	min mm/s
0.2	1	39	-31
0.3	2	54	-35
0.4	2	69	-41
0.6	4	72	-52
0.8	7	74	-46
1	8	74	-61
1.2	8	74	-67
1.4	10	78	-66
1.6	9	73	-67
1.8	10	70	-64
2	12	72	-64
2.3	14	71	-62
2.6	18	64	-65
3	22	62	-53
3.5	20	63	-48
4	25	60	-49
4.5	26	63	-51
5	28	68	-55
6	28	70	-54
7	34	71	-54
8	37	71	-50
9	37	72	-54
10	41	75	-49
12	40	69	-51
14	40	65	-49
16	41	66	-46
18	42	70	-47
20	45	72	-50
22.5	47	72	-52
25	49	74	-58
30	51	72	-54
35	52	68	-53
40	51	75	-56
45	52	73	-55
50	53	77	-51
60	54	72	-54
70	55	75	-58
80	56	73	-61
100	55	72	-54
125	51	78	-58
150	51	75	-55

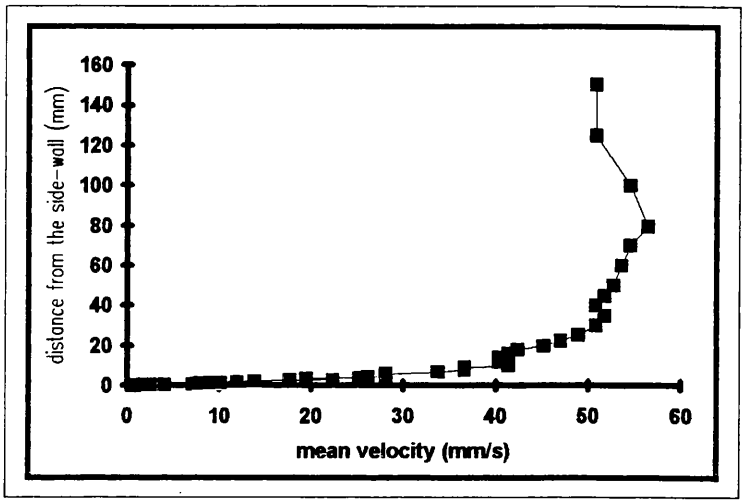

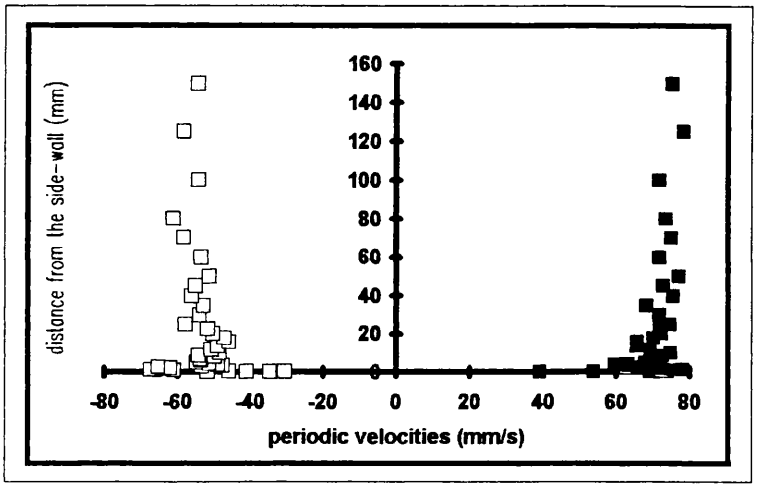

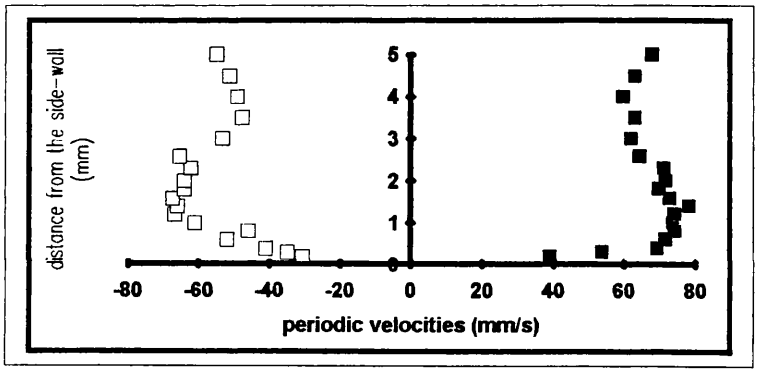

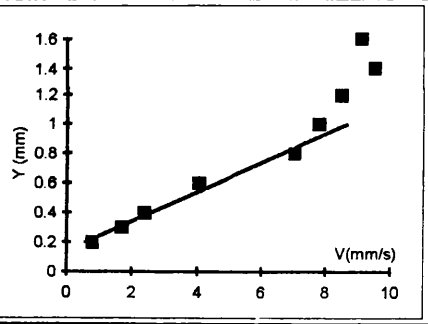

Slope of the inner layer :	10.10
kinematic viscosity	1.01
Wall shear stress over density:	10.20

TEST NO. : C-SIWWC50

Distance from the bed(mm):	50	Water Depth (mm):	300
Surface current before waves (mm/s):		Wave height (mm):	37
Head difference (inch):	2.5	Wave length(mm):	1450
Temperature (C) :	20	Wave period (s):	1.0

Distance from wall mm	Mean velocity mm/s	Periodic Velocities max mm/s	min mm/s
0.2	2	25	-21
0.3	4	33	-30
0.4	6	40	-33
0.6	9	46	-36
0.8	13	53	-39
1	17	52	-43
1.2	20	53	-42
1.4	23	48	-39
1.6	25	50	-40
1.8	28	48	-39
2	31	48	-39
2.3	35	51	-39
2.6	37	52	-40
3	38	52	-41
3.5	42	51	-42
4	42	52	-41
4.5	47	51	-40
5	50	52	-41
6	51	50	-40
7	54	53	-39
8	55	54	-37
9	56	53	-39
10	58	53	-38
12	59	53	-37
14	58	54	-36
16	58	52	-35
18	59	52	-33
20	60	53	-33
22.5	63	54	-35
25	65	51	-33
30	67	52	-36
35	69	52	-34
40	70	52	-36
45	71	52	-34
50	72	53	-39
60	74	53	-35
70	75	53	-35
80	79	52	-37
100	81	54	-39
125	82	54	-36
150	82	55	-37

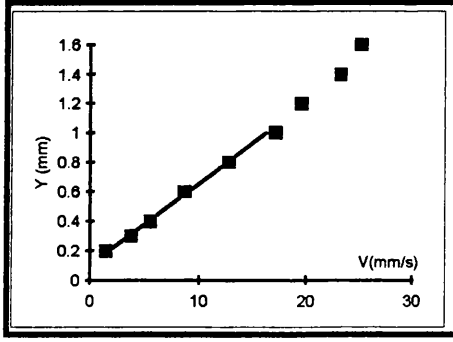

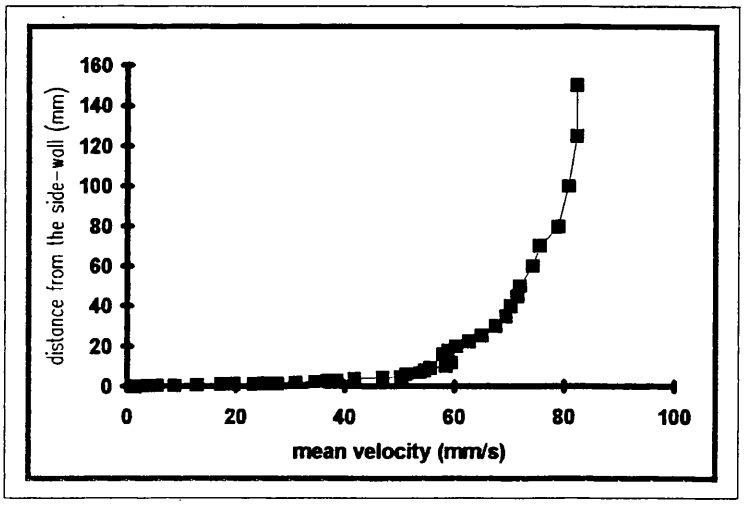

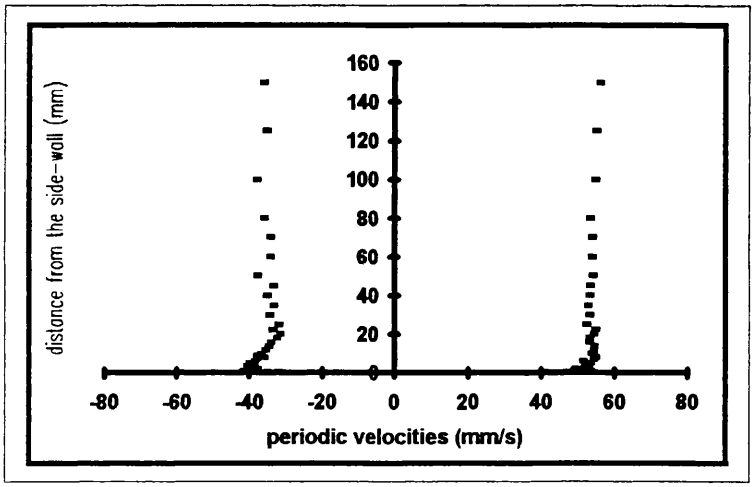

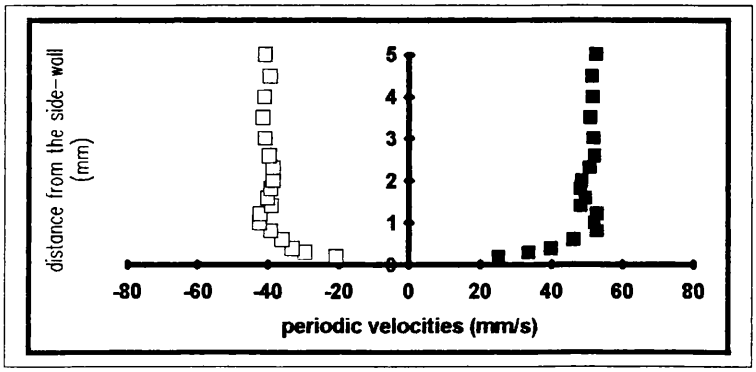

Slope of the inner layer :	18.26
kinematic viscosity	1.01
Wall shear stress over density:	18.44

TEST NO. : C-SIWMC150

Distance from the bed(mm):	150	Water Depth (mm):	300
Surface current before waves (mm/s):		Wave height (mm):	36
Head difference (inch):	8.6	Wave length(mm):	1450
Temperature (C) :	19	Wave period (s):	1.0

Distance from wall mm	Mean velocity mm/s	Periodic Velocities max mm/s	min mm/s
0.2	2	37	-26
0.3	5	42	-30
0.4	6	56	-35
0.6	9	59	-50
0.8	12	65	-45
1	16	64	-53
1.2	18	62	-55
1.4	18	65	-50
1.6	21	65	-51
1.8	23	65	-50
2	26	72	-53
2.3	31	68	-56
2.6	35	34	-53
3	40	61	-47
3.5	46	59	-47
4	51	62	-44
4.5	52	62	-46
5	55	67	-50
6	56	63	-49
7	63	71	-50
8	63	70	-49
9	66	72	-50
10	66	73	-47
12	68	65	-48
14	70	67	-49
16	71	67	-44
18	72	70	-50
20	72	71	-50
22.5	73	70	-51
25	74	72	-54
30	74	71	-51
35	76	66	-46
40	78	73	-53
45	78	71	-53
50	79	72	-53
60	79	73	-54
70	80	74	-55
80	80	73	-56
100	81	71	-52
125	81	77	-53
150	79	71	-51

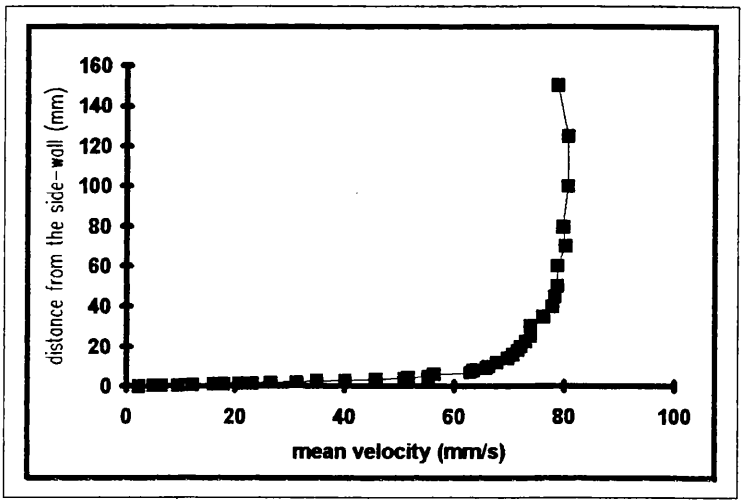

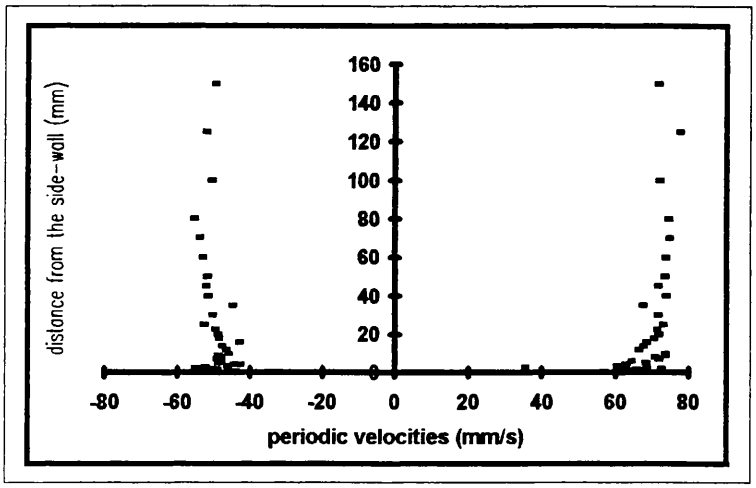

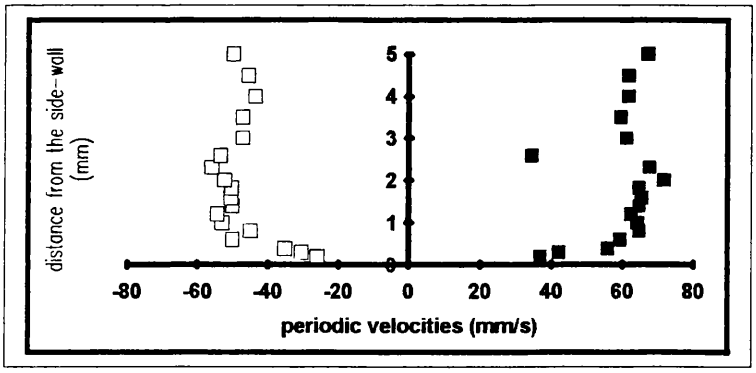

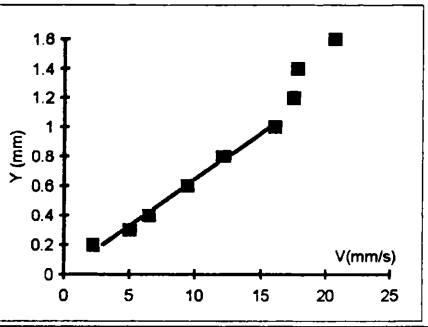

Slope of the inner layer :	15.90
kinematic viscosity	1.04
Wall shear stress over density:	16.46

TEST NO. : C-SIWSC20

Distance from the bed(mm):	20	Water Depth (mm):	300
Surface current before waves (mm/s):		Wave height (mm):	33
Head difference (inch):	25	Wave length(mm):	1654
Temperature (C) :	19	Wave period (s):	1.0

Distance from wall mm	Mean velocity mm/s	Periodic Velocities max mm/s	min mm/s
0.2	1	15	-10
0.3	4	14	-17
0.4	7	19	-20
0.6	10	30	-23
0.8	15	34	-31
1	22	39	-34
1.2	25	40	-35
1.4	28	39	-32
1.6	31	41	-33
1.8	35	43	-33
2	41	47	-34
2.3	44	48	-35
2.6	50	50	-34
3	54	52	-34
3.5	60	51	-35
4	62	50	-36
4.5	61	52	-33
5	63	53	-34
6	63	54	-33
7	64	54	-34
8	65	53	-34
9	66	51	-35
10	67	50	-36
12	70	50	-37
14	70	53	-37
16	72	52	-36
18	75	52	-37
20	80	53	-37
22.5	82	54	-36
25	80	52	-36
30	83	52	-36
35	84	51	-36
40	86	52	-37
45	88	53	-37
50	89	52	-37
60	95	51	-36
70	103	50	-37
80	109	52	-37
100	117	52	-37
125	120	52	-38
150	119	53	-39

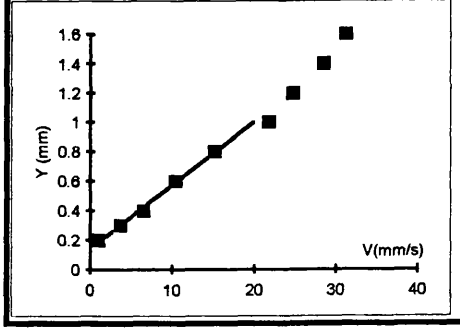

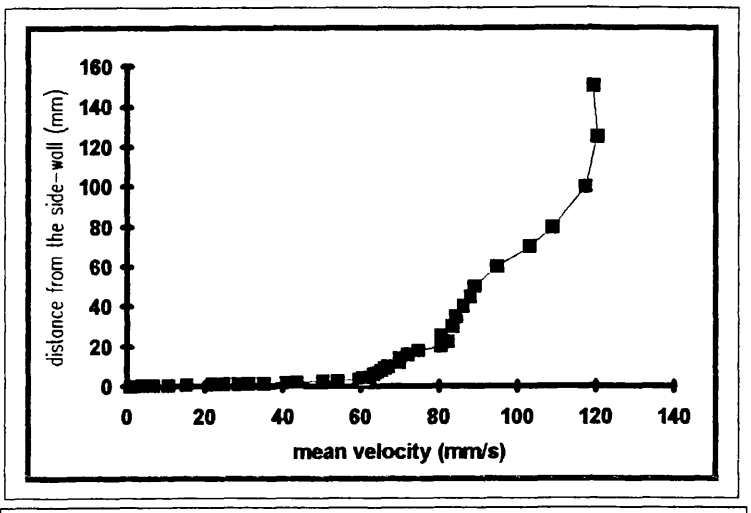

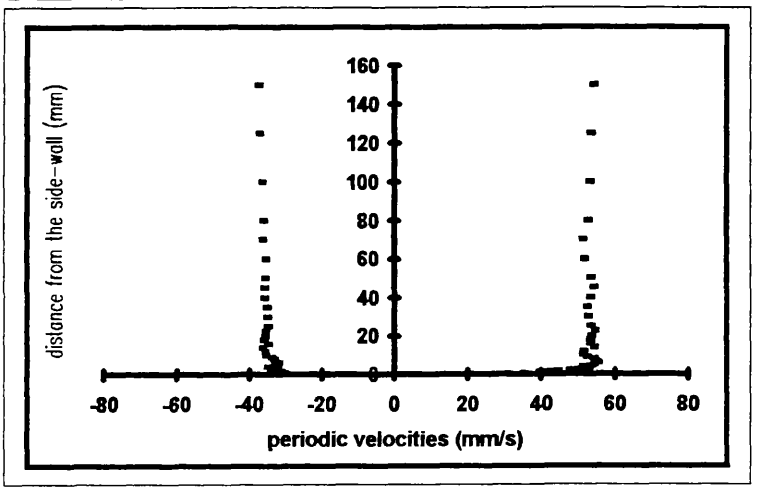

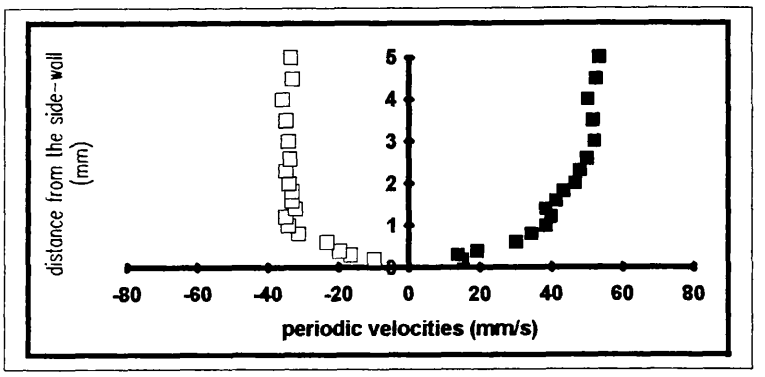

Slope of the inner layer :	23.10
kinematic viscosity	1.04
Wall shear stress over density:	23.91

TEST NO. : C-SIWSC50

Distance from the bed(mm):	50	Water Depth (mm):	300
Surface current before waves (mm/s):	- - -	Wave height (mm):	33
Head difference (inch):	25	Wave length(mm):	1654
Temperature (C) :	19	Wave period (s):	1.0

Distance from wall	Mean velocity	Periodic Velocities max	Periodic Velocities min
mm	mm/s	mm/s	mm/s
0.2	3	16	-10
0.3	6	29	-18
0.4	11	35	-24
0.6	16	39	-28
0.8	22	48	-36
1	30	47	-38
1.2	38	46	-39
1.4	41	47	-37
1.6	44	48	-38
1.8	49	50	-40
2	52	54	-39
2.3	55	55	-39
2.6	59	56	-40
3	66	57	-40
3.5	70	59	-41
4	72	58	-42
4.5	75	58	-42
5	76	62	-41
6	78	61	-41
7	79	63	-42
8	80	64	-41
9	80	62	-43
10	84	62	-43
12	87	63	-42
14	88	62	-42
16	89	60	-43
18	91	62	-41
20	90	63	-42
22.5	91	61	-43
25	94	61	-41
30	97	62	-42
35	98	61	-42
40	100	63	-43
45	108	62	-42
50	112	61	-43
60	116	63	-42
70	119	64	-44
80	124	62	-45
100	126	65	-44
125	132	66	-46
150	134	65	-45

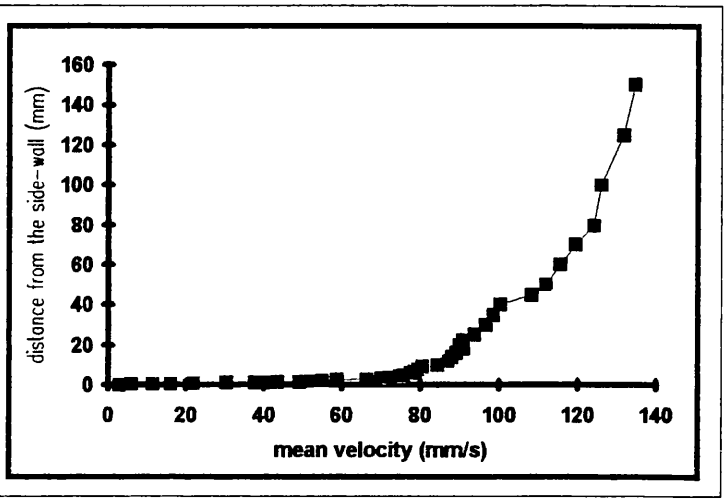

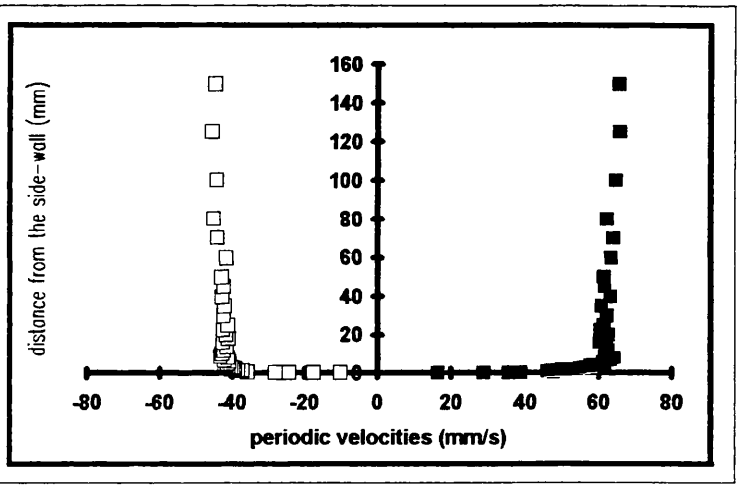

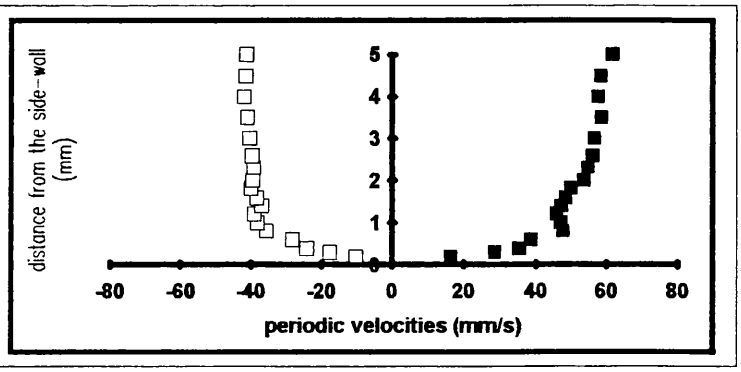

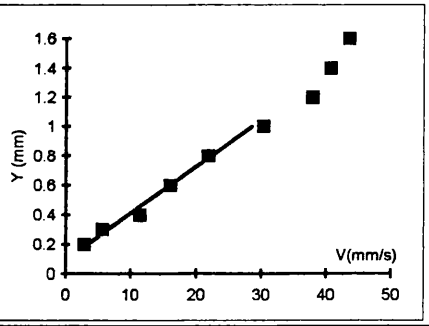

Slope of the inner layer :	31.59
kinematic viscosity	1.04
Wall shear stress over density:	32.70

TEST NO. : C-SIWSC150

Distance from the bed(mm):	150	Water Depth (mm):	300
Surface current before waves (mm/s):		Wave height (mm):	34
Head difference (inch):	25	Wave length(mm):	1654
Temperature (C) :	19	Wave period (s):	1.0

Distance from wall mm	Mean velocity mm/s	Periodic Velocities max mm/s	min mm/s
0.2	5	35	-21
0.3	7	40	-26
0.4	9	42	-30
0.6	14	47	-39
0.8	22	55	-44
1	28	54	-45
1.2	37	51	-42
1.4	40	51	-34
1.6	47	58	-34
1.8	50	59	-37
2	55	61	-41
2.3	66	59	-40
2.6	68	61	-42
3	66	60	-41
3.5	73	60	-39
4	74	64	-42
4.5	77	61	-40
5	79	67	-40
6	92	67	-44
7	94	70	-47
8	96	69	-49
9	97	72	-46
10	98	70	-45
12	101	66	-45
14	102	68	-49
16	101	69	-52
18	104	69	-52
20	110	69	-50
22.5	115	69	-49
25	117	70	-50
30	120	69	-49
35	118	70	-49
40	123	70	-49
45	124	68	-51
50	126	68	-54
60	128	74	-54
70	131	72	-51
80	131	73	-51
100	129	70	-49
125	129	75	-48
150	129	74	-49

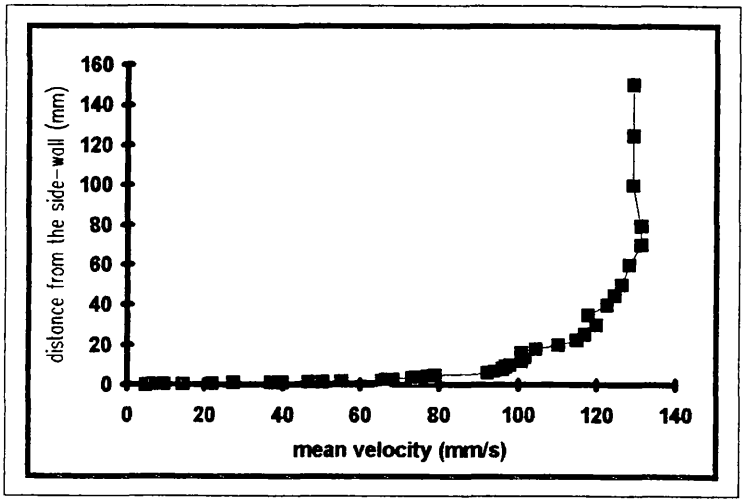

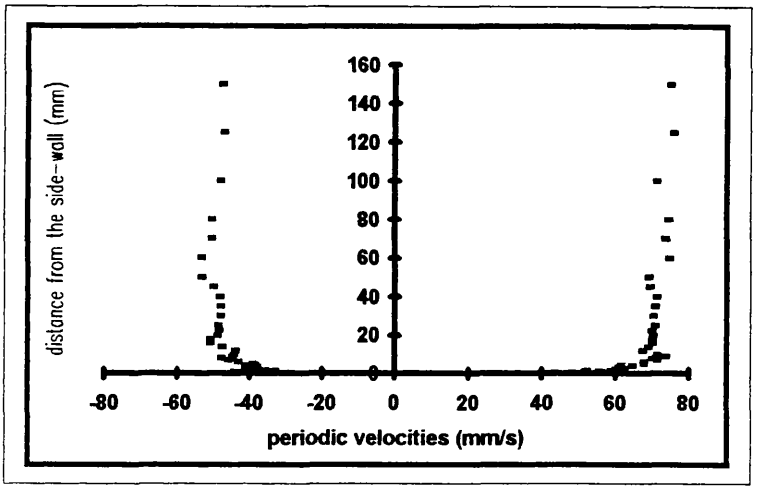

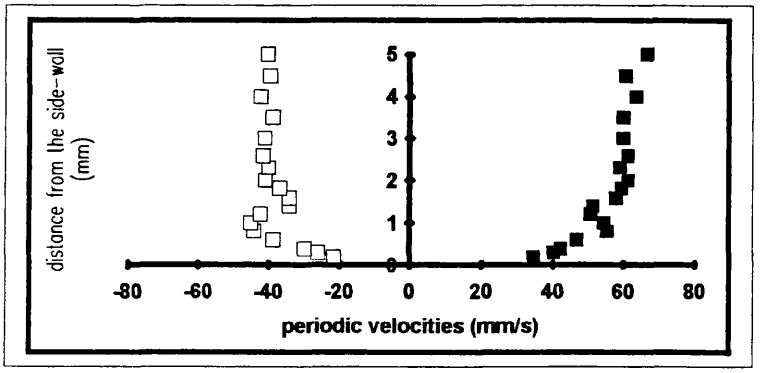

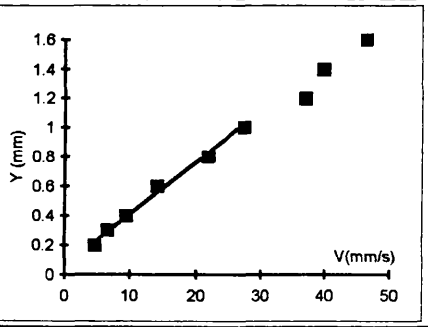

Slope of the inner layer :	28.25
kinematic viscosity	1.04
Wall shear stress over density:	29.24

TEST NO. : C-SSW20

Distance from the bed(mm):	20	Water Depth (mm):	300
Surface current before waves (mm/s):	0	Wave height (mm):	40
Head difference (mm):	0	Wave length(mm):	1700
Temperature (C) :	20	Wave period (s):	1.2

Distance from wall mm	Mean velocity mm/s	Periodic Velocities max mm/s	min mm/s
0.2	11	39	-33
0.3	8	46	-40
0.4	8	52	-46
0.6	9	60	-52
0.8	9	62	-54
1	7	62	-56
1.2	9	68	-55
1.4	9	70	-55
1.6	10	66	-54
1.8	11	65	-56
2	11	58	-59
2.3	9	51	-49
2.6	9	47	-44
3	9	52	-45
3.5	8	61	-51
4	7	59	-47
4.5	7	58	-49
5	6	68	-56
6	9	66	-52
7	9	66	-51
8	9	66	-51
9	9	65	-53
10	9	66	-60
12	11	65	-51
14	7	59	-43
16	5	57	-45
18	9	54	-41
20	12	63	-56
22.5	9	60	-49
25	7	59	-46
30	5	65	-53
35	6	66	-49
40	6	68	-53
45	8	67	-52
50	9	66	-51
60	7	66	-51
70	7	64	-49
80	6	62	-47
100	5	66	-49
125	6	67	-47
150	9	69	-56

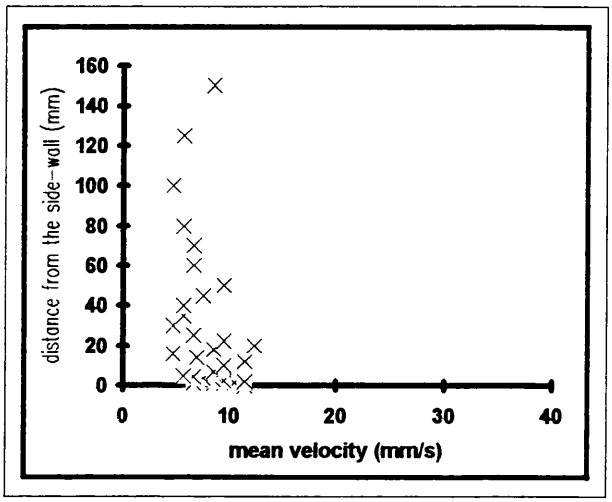

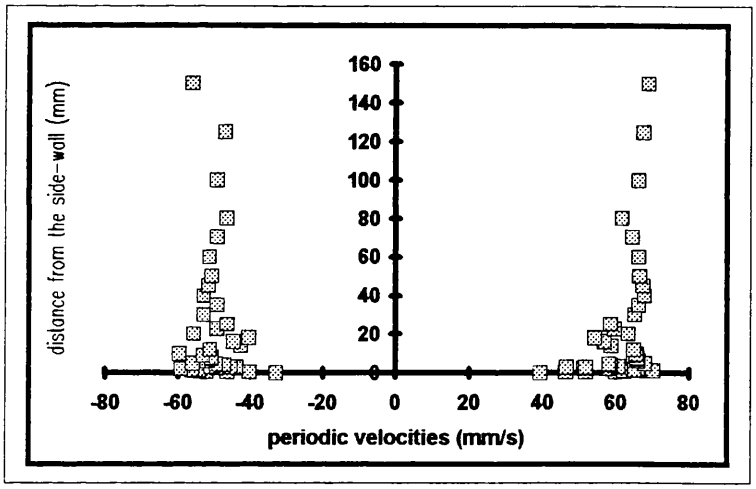

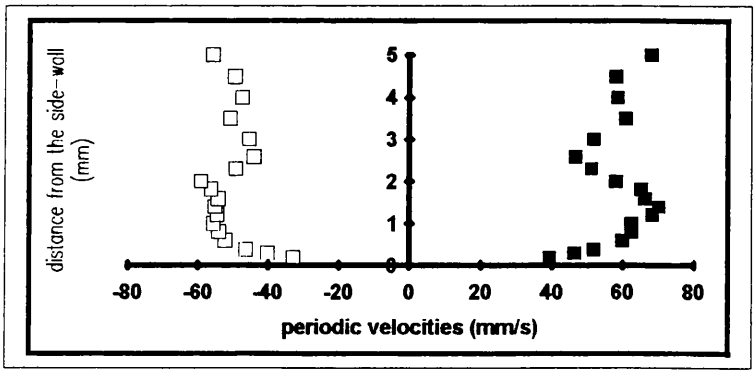

TEST NO. : **C-SSW150**

Distance from the bed(mm):	**150**	**Water Depth (mm):**	**300**
Surface current before waves (mm/s):	**0**	**Wave height (mm):**	**40**
Head difference (mm):	**0**	**Wave length(mm):**	**1700**
Temperature (C) :	**20**	**Wave period (s):**	**1.2**

Distance	Mean	Periodic Velocities	
from wall	velocity	max	min
mm	mm/s	mm/s	mm/s
0.2	8	61	-52
0.3	13	64	-55
0.4	12	71	-67
0.6	10	76	-69
0.8	9	80	-74
1	9	81	-71
1.2	9	83	-75
1.4	4	77	-70
1.6	9	74	-66
1.8	11	72	-65
2	14	70	-65
2.3	11	70	-66
2.6	10	73	-67
3	12	71	-65
3.5	10	72	-65
4	9	72	-66
4.5	9	72	-67
5	9	71	-66
6	8	70	-65
7	7	72	-66
8	6	74	-68
9	5	75	-69
10	4	75	-70
12	8	73	-71
14	7	74	-71
16	6	76	-72
18	5	77	-72
20	3	77	-70
22.5	3	78	-70
25	2	79	-70
30	1	77	-71
35	-2	76	-70
40	-3	75	-70
45	-2	74	-70
50	-2	76	-72
60	-2	76	-72
70	-3	76	-72
80	-4	74	-70
100	-5	77	-69
125	-8	75	-68
150	-10	76	-70

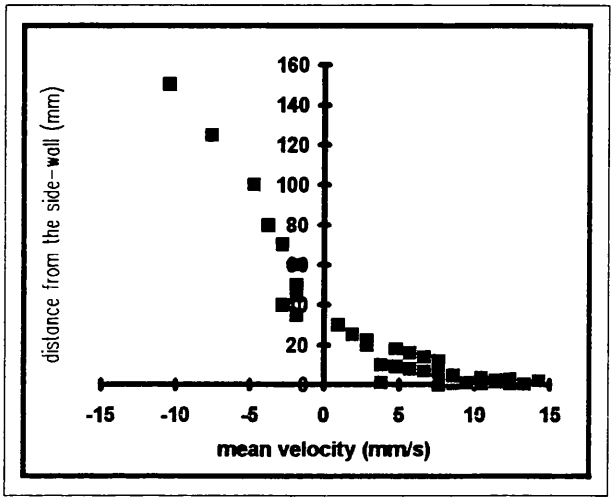

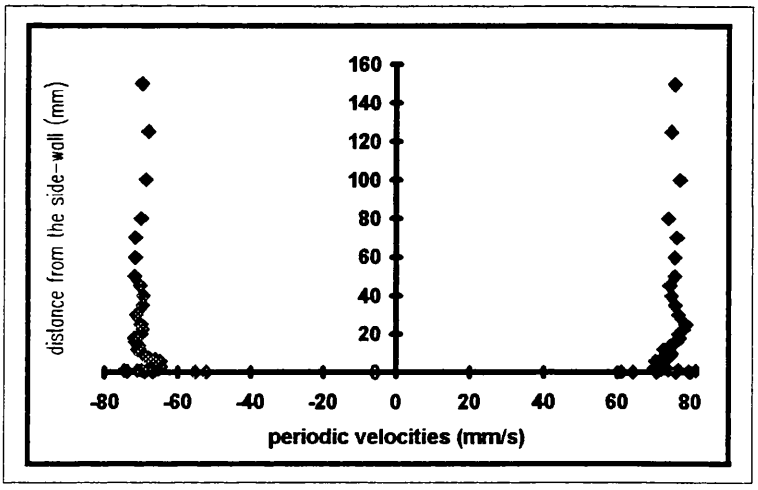

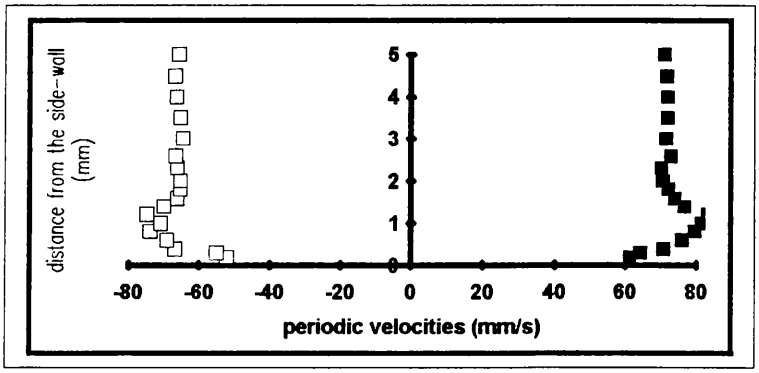

TEST NO. : C-SSWWC50

Distance from the bed(mm):	50	Water Depth (mm):	300
Surface current before waves (mm/s):		Wave height (mm):	39
Head difference (inch):	2.5	Wave length(mm):	
Temperature (C) :	20	Wave period (s):	1.2

Distance from wall mm	Mean velocity mm/s	Periodic Velocities max mm/s	min mm/s
0.2	2	49	-37
0.3	4	57	-45
0.4	4	64	-47
0.6	6	75	-56
0.8	9	76	-60
1	12	80	-65
1.2	13	79	-67
1.4	15	79	-66
1.6	16	75	-63
1.8	19	71	-61
2	20	67	-58
2.3	22	67	-54
2.6	23	66	-56
3	27	68	-57
3.5	28	73	-56
4	31	71	-53
4.5	31	72	-55
5	30	71	-54
6	30	68	-51
7	34	68	-57
8	38	72	-50
9	41	68	-54
10	41	71	-56
12	41	75	-58
14	41	73	-58
16	42	68	-61
18	43	66	-58
20	44	66	-60
22.5	45	66	-60
25	45	66	-59
30	46	70	-59
35	47	65	-58
40	47	63	-59
45	48	67	-57
50	47	70	-55
60	47	73	-51
70	48	73	-56
80	48	70	-54
100	47	70	-54
125	45	70	-58
150	45	69	-54

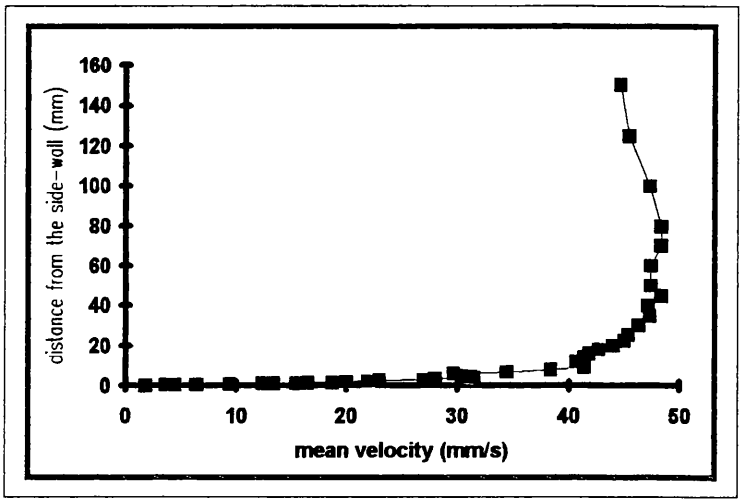

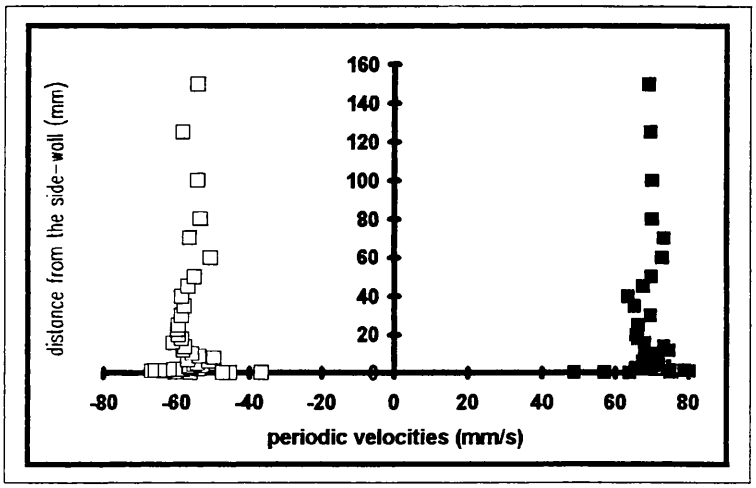

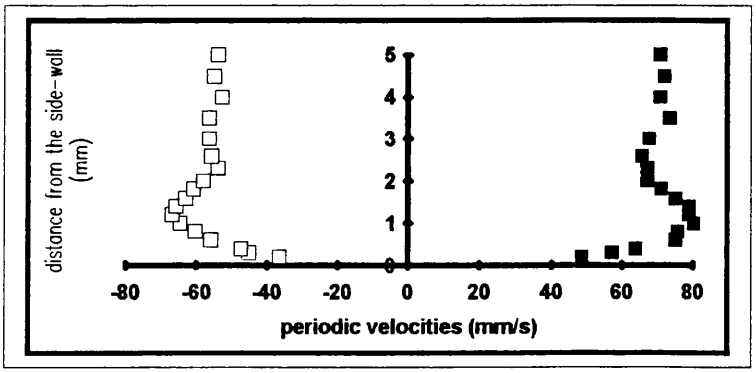

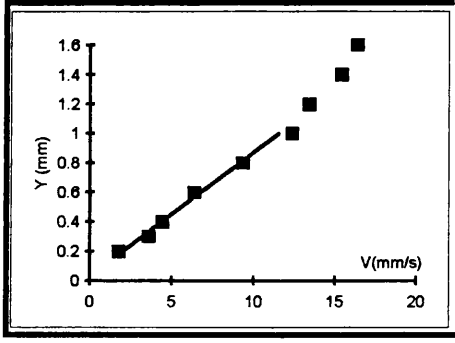

Slope of the inner layer :	11.92
kinematic viscosity	1.01
Wall shear stress over density:	12.04

TEST NO. : C-SSWWC150

Distance from the bed(mm):	150	Water Depth (mm):	300
Surface current before waves (mm/s):		Wave height (mm):	39
Head difference (inch):	2.5	Wave length(mm):	1800
Temperature (C) :	20	Wave period (s):	1.2

Distance from wall mm	Mean velocity mm/s	Periodic Velocities max mm/s	min mm/s
0.2	2	48	-36
0.3	3	57	-44
0.4	4	63	-46
0.6	6	74	-55
0.8	9	75	-59
1	12	80	-63
1.2	13	84	-67
1.4	15	85	-65
1.6	16	81	-69
1.8	18	76	-60
2	19	73	-57
2.3	21	61	-53
2.6	22	65	-55
3	26	67	-55
3.5	27	73	-55
4	30	70	-52
4.5	30	71	-54
5	29	70	-53
6	28	67	-50
7	33	68	-56
8	37	71	-49
9	39	68	-53
10	39	70	-55
12	39	74	-57
14	39	72	-57
16	40	67	-60
18	41	66	-57
20	43	65	-58
22.5	45	65	-59
25	43	66	-58
30	44	69	-57
35	45	65	-57
40	45	63	-57
45	46	67	-56
50	45	69	-54
60	45	72	-50
70	46	72	-55
80	46	69	-53
100	45	69	-53
125	43	69	-57
150	42	68	-53

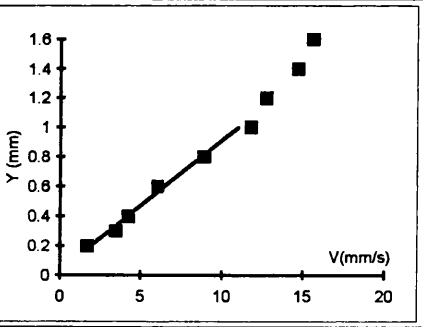

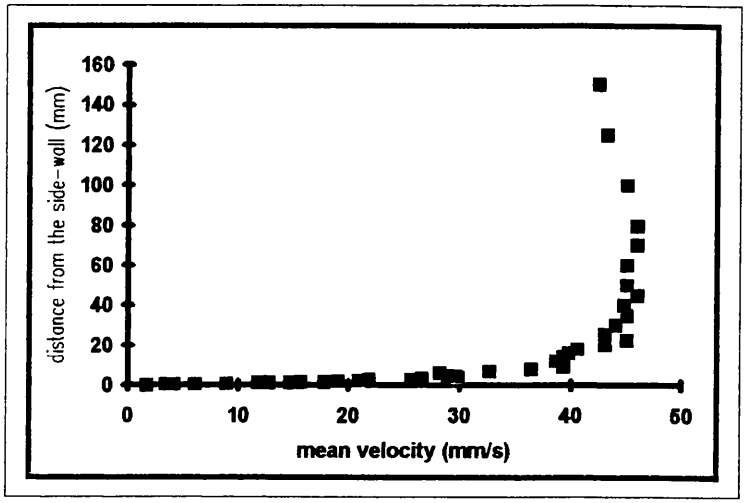

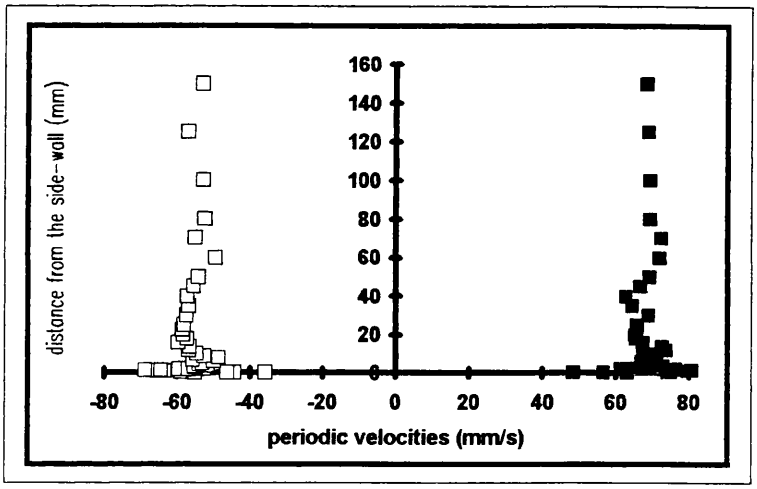

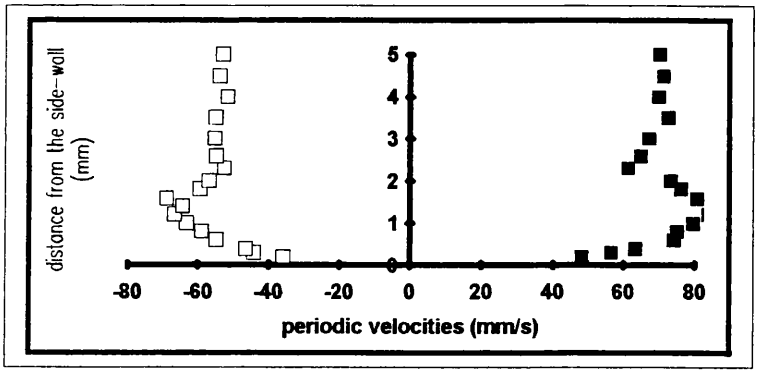

Slope of the inner layer :	11.34
kinematic viscosity	1.01
Wall shear stress over density:	11.46

TEST NO. : C-SSWMC20

Distance from the bed(mm):	20	Water Depth (mm):	300
Surface current before waves (mm/s):	-	Wave height (mm):	34
Head difference (inch):	8.4	Wave length(mm):	1830
Temperature (C) :	20	Wave period (s):	1.0

Distance from wall mm	Mean velocity mm/s	Periodic Velocities max mm/s	min mm/s
0.2	2	33	-29
0.3	4	39	-35
0.4	7	35	-32
0.6	9	53	-43
0.8	12	59	-47
1	15	57	-48
1.2	17	58	-52
1.4	18	57	-43
1.6	19	55	-46
1.8	19	59	-48
2	29	63	-46
2.3	28	61	-45
2.6	30	63	-46
3	31	61	-47
3.5	32	60	-37
4	33	44	-31
4.5	34	56	-26
5	35	53	-36
6	35	64	-35
7	40	58	-31
8	34	54	-35
9	37	59	-32
10	39	62	-36
12	40	58	-29
14	39	57	-30
16	39	55	-28
18	41	55	-29
20	42	56	-29
22.5	43	56	-30
25	45	58	-28
30	44	57	-26
35	48	59	-29
40	51	61	-32
45	57	63	-33
50	59	64	-34
60	62	64	-39
70	67	61	-33
80	70	60	-30
100	74	69	-41
125	73	67	-44
150	73	68	-38

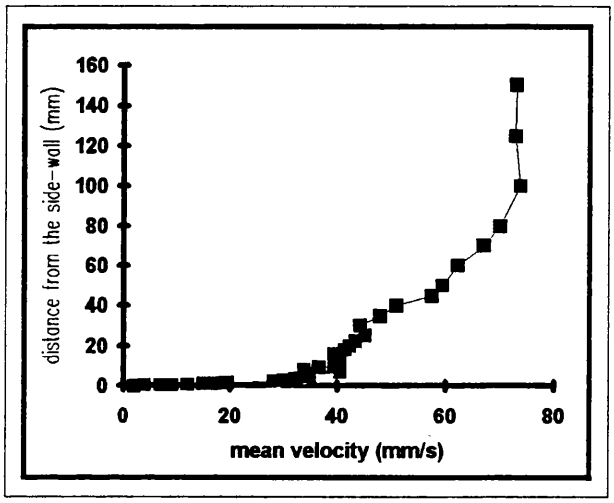

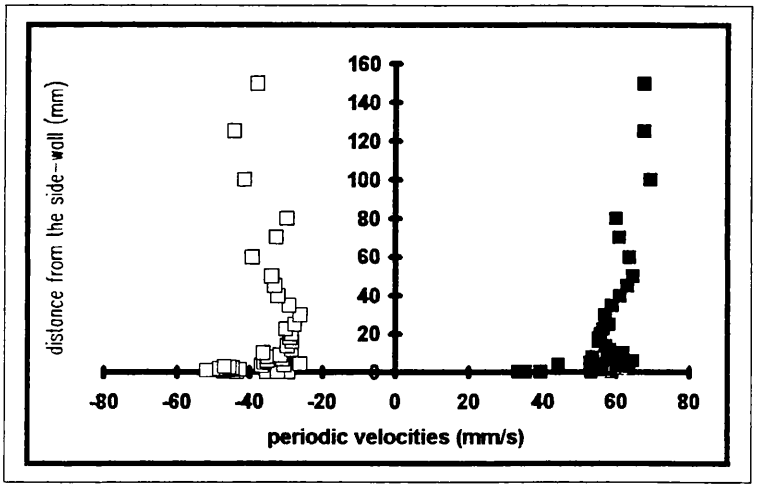

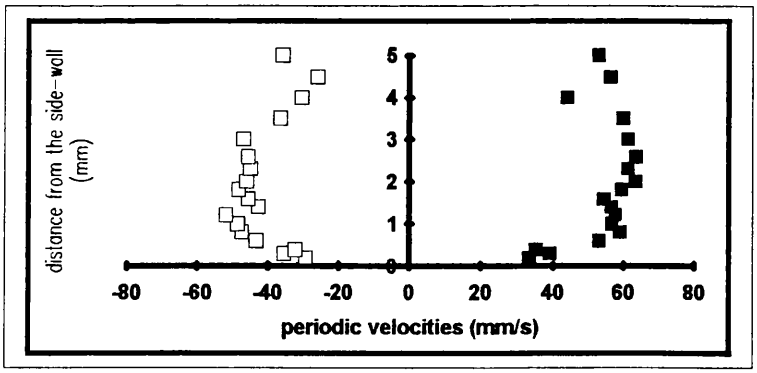

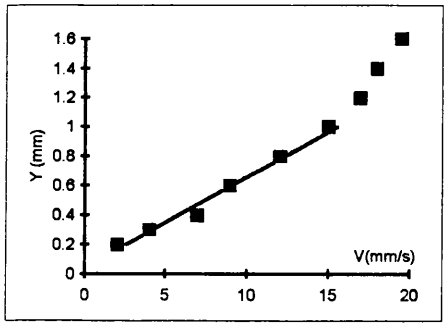

Slope of the inner layer :	16.21
kinematic viscosity	1.01
Wall shear stress over density:	16.37

TEST NO. : C-SSWMC50

Distance from the bed(mm):	50	Water Depth (mm):	299
Surface current before waves (mm/s):		Wave height (mm):	34
Head difference (inch):	8.4	Wave length(mm):	1818
Temperature (C) :	18	Wave period (s):	1.2

Distance from wall mm	Mean velocity mm/s	Periodic Velocities max mm/s	min mm/s
0.2	2	20	-8
0.3	4	31	-26
0.4	7	46	-39
0.6	11	57	-43
0.8	16	68	-54
1	21	71	-57
1.2	24	69	-53
1.4	27	74	-62
1.6	27	75	-60
1.8	31	67	-55
2	34	63	-49
2.3	37	65	-42
2.6	38	59	-45
3	39	63	-48
3.5	44	62	-44
4	44	64	-42
4.5	52	60	-37
5	56	62	-38
6	57	65	-38
7	60	65	-38
8	60	61	-37
9	61	65	-36
10	64	63	-34
12	65	70	-39
14	64	68	-39
16	62	69	-41
18	62	67	-41
20	62	64	-45
22.5	66	65	-40
25	70	64	-45
30	71	65	-43
35	73	69	-41
40	74	71	-38
45	75	69	-41
50	76	68	-43
60	79	70	-45
70	83	72	-40
80	85	69	-45
100	84	73	-43
125	83	71	-48
150	83	70	-47

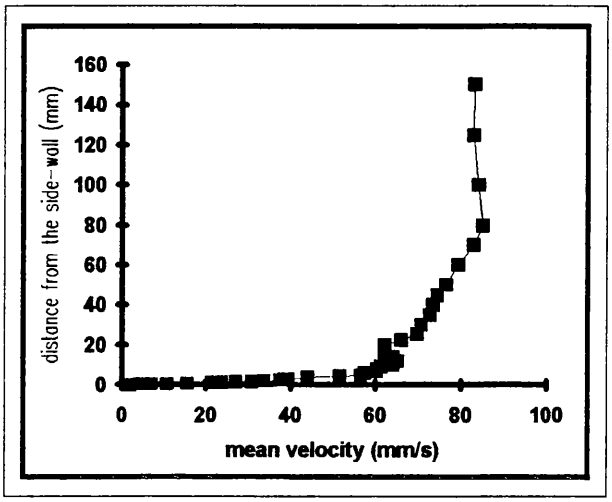

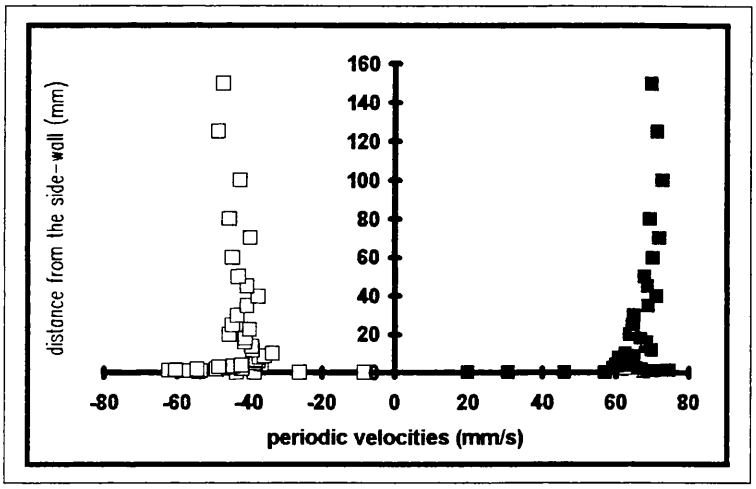

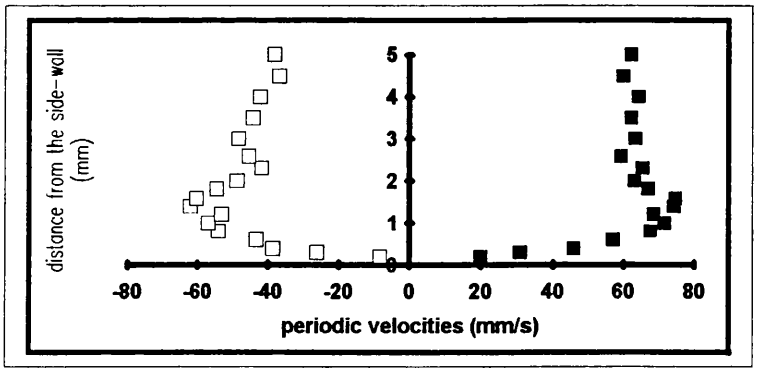

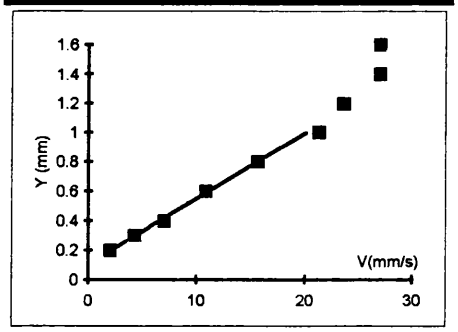

Slope of the inner layer :	22.50
kinematic viscosity	1.06
Wall shear stress over density:	23.87

TEST NO. : C-SSWMC150

Distance from the bed(mm):	150	Water Depth (mm):	298
Surface current before waves (mm/s):		Wave height (mm):	35
Head difference (inch):	8.2	Wave length(mm):	1820
Temperature (C) :	18	Wave period (s):	1.2

Distance from wall mm	Mean velocity mm/s	Periodic Velocities max mm/s	min mm/s
0.2	2	29	-23
0.3	7	31	-27
0.4	9	40	-29
0.6	11	38	-38
0.8	14	48	-45
1	19	56	-49
1.2	19	70	-56
1.4	20	74	-62
1.6	22	75	-59
1.8	23	70	-54
2	27	66	-47
2.3	32	59	-43
2.6	34	56	-36
3	38	60	-39
3.5	43	63	-46
4	49	70	-50
4.5	47	70	-46
5	53	67	-38
6	53	73	-45
7	63	66	-45
8	62	68	-39
9	65	67	-39
10	65	67	-38
12	66	69	-39
14	68	70	-42
16	69	67	-45
18	71	67	-42
20	72	67	-39
22.5	73	68	-39
25	74	72	-38
30	73	69	-44
35	76	69	-40
40	77	70	-39
45	78	70	-39
50	79	74	-38
60	77	74	-41
70	78	69	-39
80	77	67	-39
100	77	72	-40
125	75	67	-40
150	71	69	-41

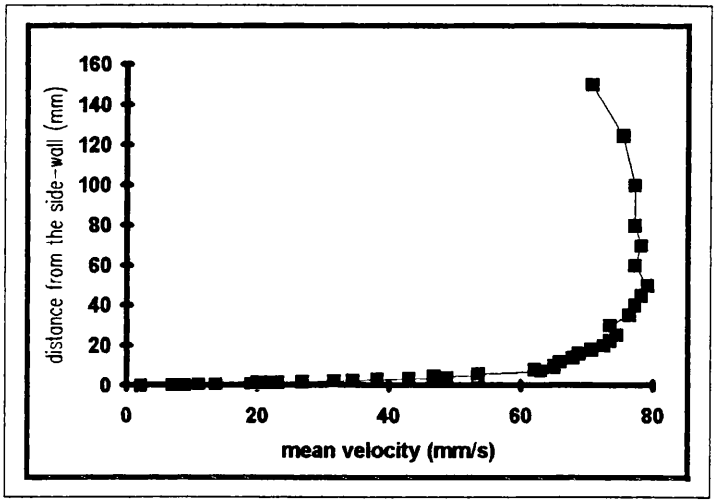

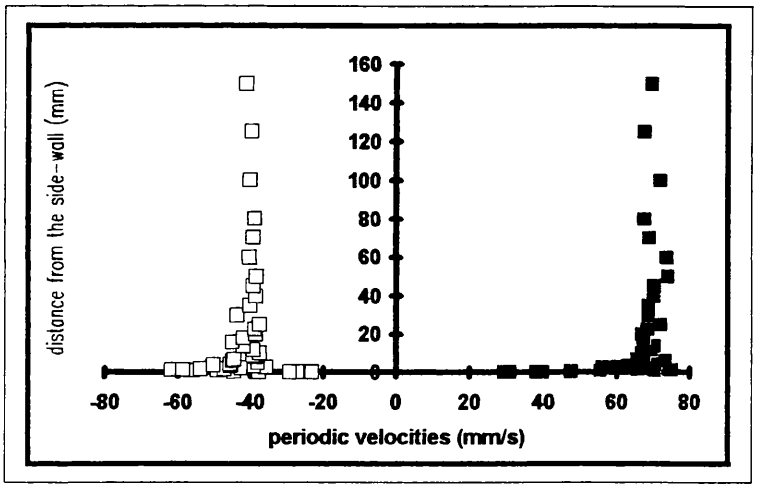

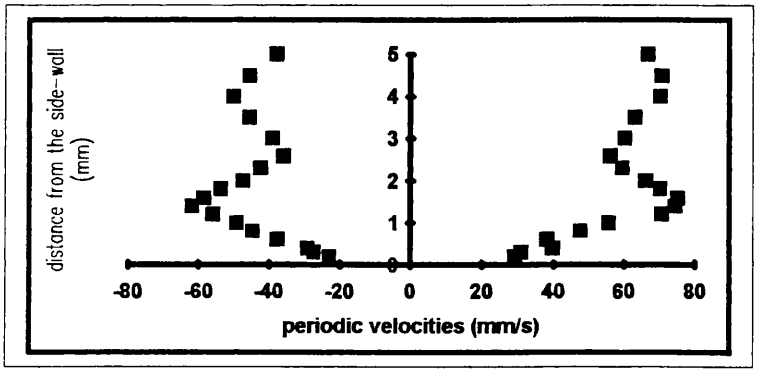

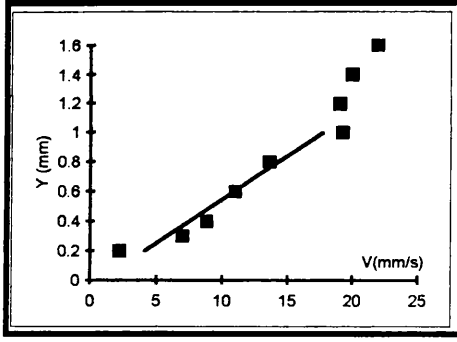

Slope of the inner layer :	16.98
kinematic viscosity	1.06
Wall shear stress over density:	18.02

TEST NO. : C-SSWSC20

Distance from the bed(mm):	20	Water Depth (mm):	300
Surface current before waves (mm/s):		Wave height (mm):	34
Head difference (inch):	25	Wave length(mm):	
Temperature (C) :	19	Wave period (s):	1.2

Distance from wall	Mean velocity	Periodic Velocities max	Periodic Velocities min
mm	mm/s	mm/s	mm/s
0.2	2	27	-23
0.3	3	26	-19
0.4	5	41	-31
0.6	12	51	-41
0.8	18	55	-44
1	25	62	-51
1.2	29	62	-49
1.4	32	63	-49
1.6	35	61	-49
1.8	41	65	-50
2	43	70	-48
2.3	51	64	-48
2.6	54	68	-50
3	52	70	-47
3.5	59	64	-44
4	60	63	-39
4.5	61	64	-40
5	65	62	-40
6	65	58	-42
7	70	61	-38
8	73	64	-43
9	67	70	-39
10	72	71	-39
12	77	66	-45
14	74	69	-44
16	74	65	-44
18	78	67	-47
20	81	72	-46
22.5	80	73	-45
25	88	69	-49
30	89	68	-44
35	90	71	-48
40	91	70	-47
45	92	68	-48
50	93	69	-48
60	98	72	-49
70	103	72	-52
80	106	73	-54
100	107	74	-53
125	111	74	-52
150	117	72	-53

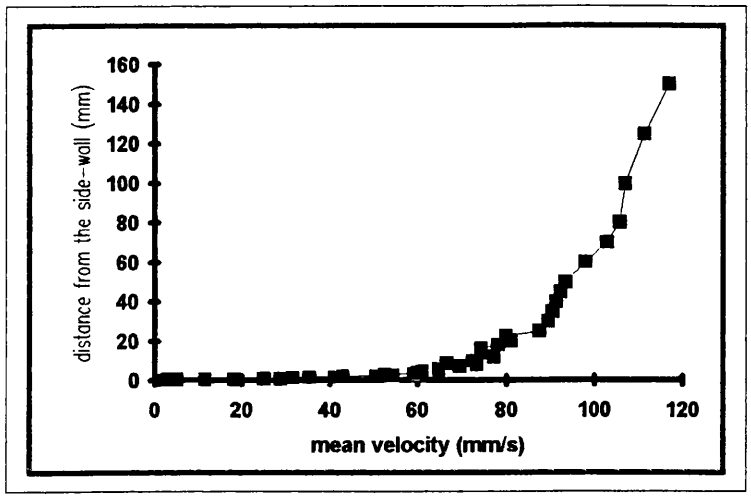

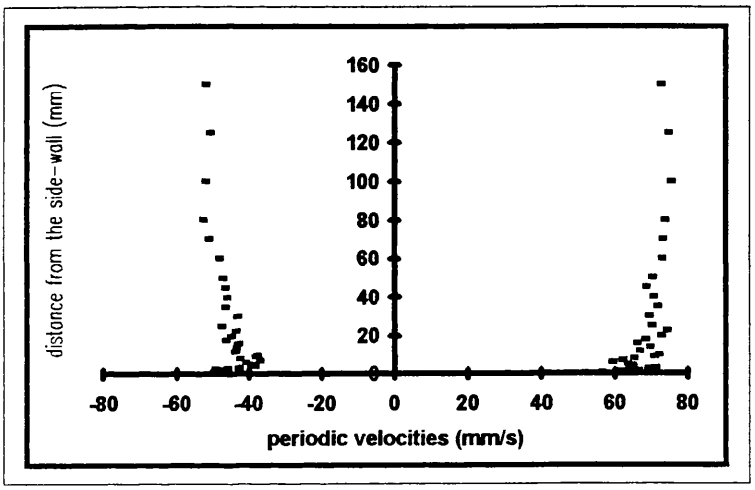

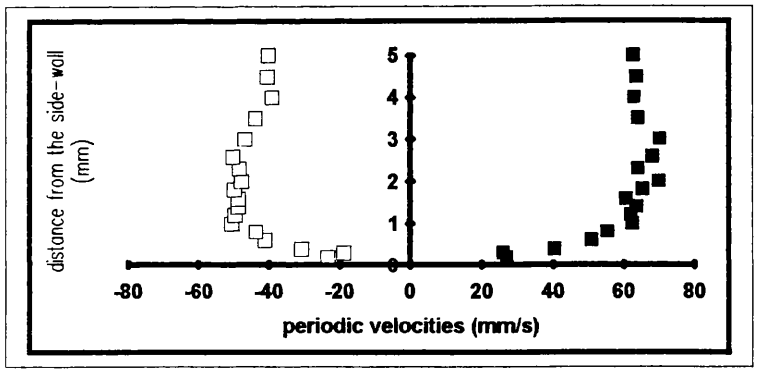

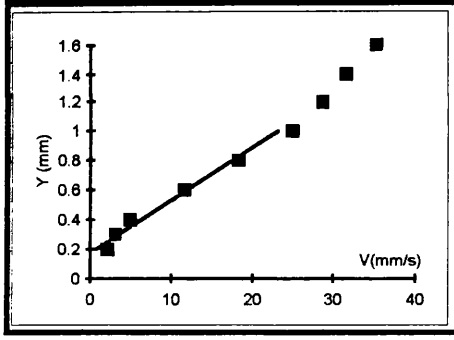

Slope of the inner layer :	28.00
kinematic viscosity	1.04
Wall shear stress over density:	28.98

TEST NO. : C-SSWSC50

Distance from the bed(mm):	50	Water Depth (mm):	300
Surface current before waves (mm/s):		Wave height (mm):	34.4
Head difference (inch):	24.9	Wave length(mm):	2030
Temperature (C) :	20	Wave period (s):	1.2

Distance from wall mm	Mean velocity mm/s	Periodic Velocities max mm/s	min mm/s
0.2	20	44	-40
0.3	21	49	-42
0.4	24	59	-47
0.6	34	68	-50
0.8	42	75	-54
1	48	75	-53
1.2	50	72	-58
1.4	52	73	-52
1.6	60	72	-54
1.8	61	66	-44
2	62	66	-44
2.3	69	70	-45
2.6	75	74	-47
3	77	67	-45
3.5	83	64	-45
4	85	59	-39
4.5	86	65	-42
5	89	63	-45
6	89	67	-49
7	91	72	-51
8	91	70	-54
9	96	76	-55
10	95	73	-51
12	96	74	-52
14	98	73	-52
16	100	72	-52
18	99	70	-48
20	98	70	-48
22.5	102	70	-49
25	104	74	-52
30	111	76	-50
35	111	74	-51
40	110	73	-52
45	113	74	-53
50	117	75	-54
60	120	73	-52
70	123	75	-56
80	131	77	-52
100	133	77	-53
125	135	77	-54
150	138	77	-54

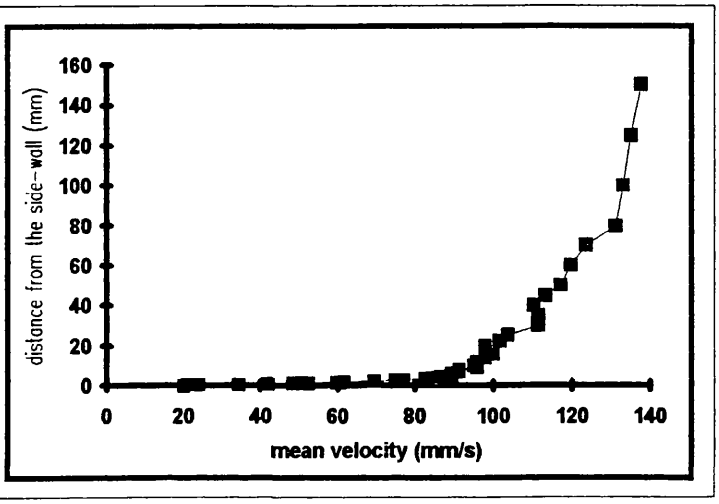

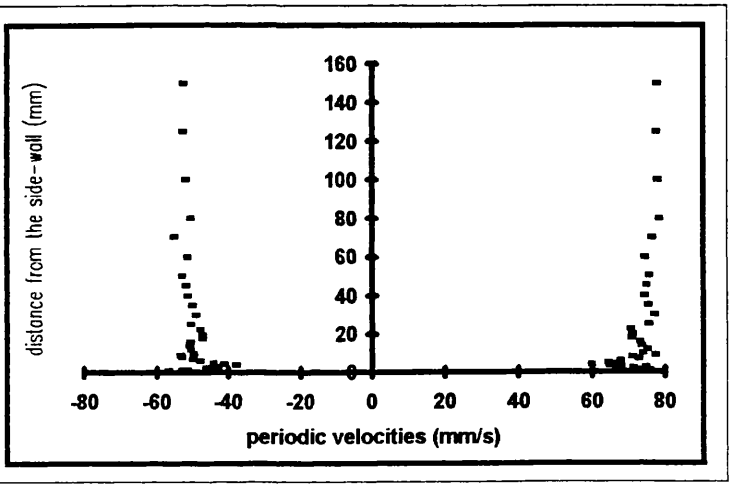

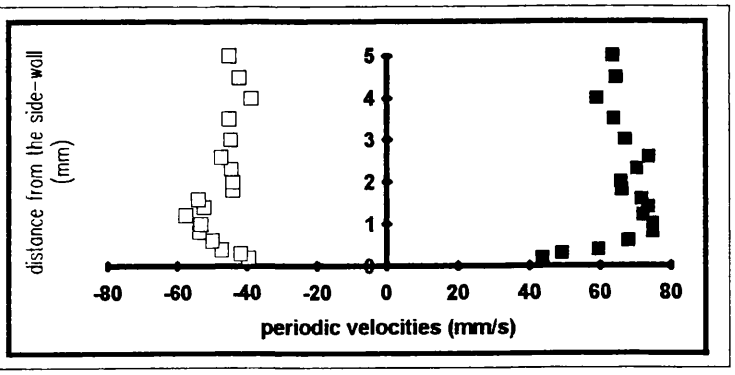

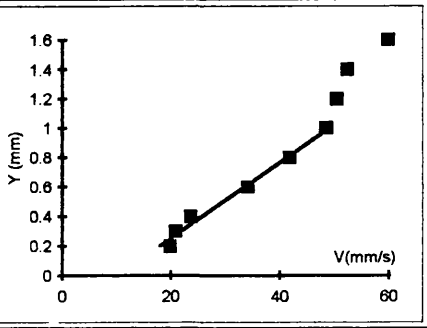

Slope of the inner layer :	38.97
kinematic viscosity	1.01
Wall shear stress over density:	39.37

TEST NO. : C-SSWSC150

Distance from the bed(mm):	150	Water Depth (mm):	300
Surface current before waves (mm/s):		Wave height (mm):	34.4
Head difference (inch):	25	Wave length(mm):	2030
Temperature (C) :	19	Wave period (s):	1.2

Distance from wall	Mean velocity	Periodic Velocities max	Periodic Velocities min
mm	mm/s	mm/s	mm/s
0.2	3	25	-11
0.3	6	31	-21
0.4	10	38	-31
0.6	15	50	-42
0.8	27	67	-48
1	35	77	-52
1.2	46	72	-45
1.4	51	71	-42
1.6	59	74	-43
1.8	60	68	-50
2	65	66	-49
2.3	68	66	-38
2.6	75	64	-42
3	78	69	-44
3.5	81	69	-43
4	82	70	-46
4.5	88	65	-51
5	94	78	-48
6	92	73	-49
7	100	74	-50
8	106	76	-53
9	108	77	-53
10	109	78	-52
12	112	74	-51
14	109	77	-51
16	109	76	-53
18	113	75	-57
20	119	77	-60
22.5	122	78	-57
25	124	79	-56
30	127	76	-59
35	128	76	-58
40	131	76	-58
45	132	77	-56
50	143	77	-55
60	136	79	-60
70	136	81	-62
80	135	80	-62
100	137	79	-57
125	135	77	-56
150	137	78	-57

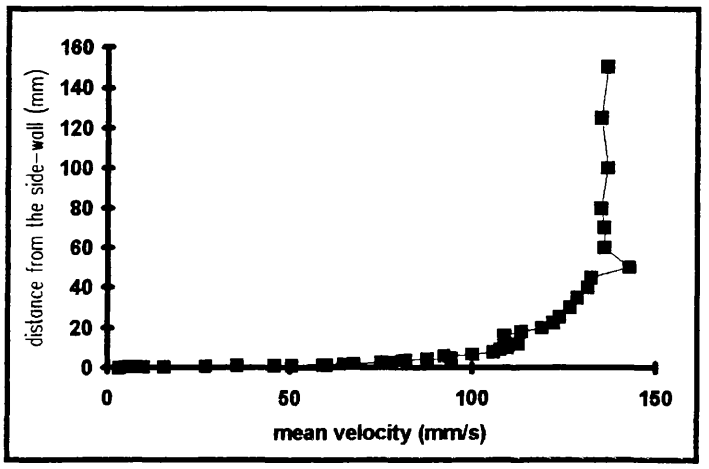

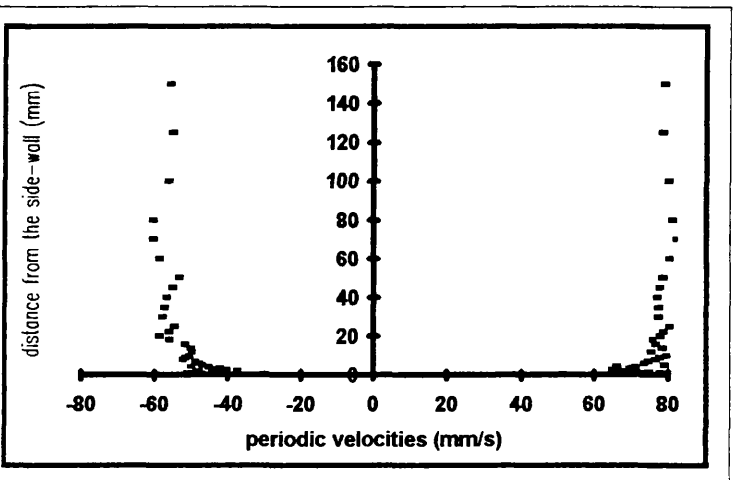

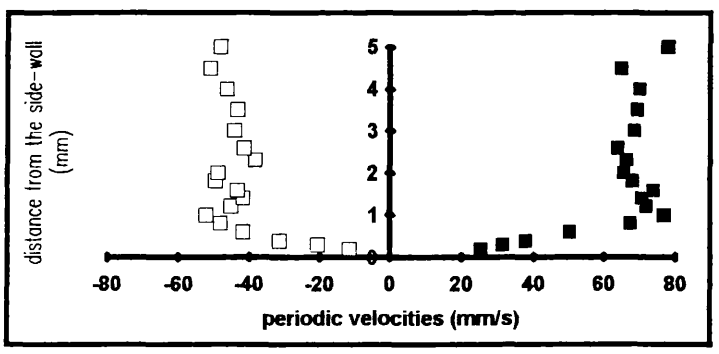

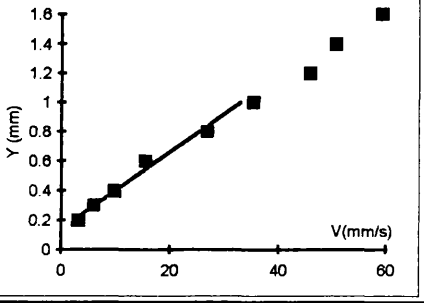

Slope of the inner layer :	38.56
kinematic viscosity	1.04
Wall shear stress over density:	39.91

TEST NO. : C-SWC 50/150

Distance from the bed(mm):		Water Depth (mm):	300
Surface current before waves (mm/s):		Wave height (mm):	0
Head difference (inch):	2.5	Wave length(mm):	0
Temperature (C) :	20	Wave period (s):	0.0

Distance from wall mm	C-SWC50 MEAN VELOCITY mm/s	C-SWC150 VELOCITY mm/s
0.2	2	1
0.3	3	2
0.4	3	4
0.6	6	7
0.8	7	9
1	9	10
1.2	9	11
1.4	10	13
1.6	11	14
1.8	13	13
2	11	11
2.3	12	13
2.6	15	15
3	19	16
3.5	21	18
4	20	20
4.5	21	19
5	22	17
6	22	16
7	23	18
8	24	20
9	25	24
10	26	28
12	27	26
14	28	29
16	31	31
18	34	35
20	33	41
22.5	35	42
25	36	44
30	37	46
35	37	46
40	37	45
45	37	46
50	38	47
60	40	49
70	42	49
80	44	49
100	45	49
125	46	49
150	46	48

Slope :	8.33	13.14
υ:	1.01	1.01
τ/ρ :	8.41	13.28

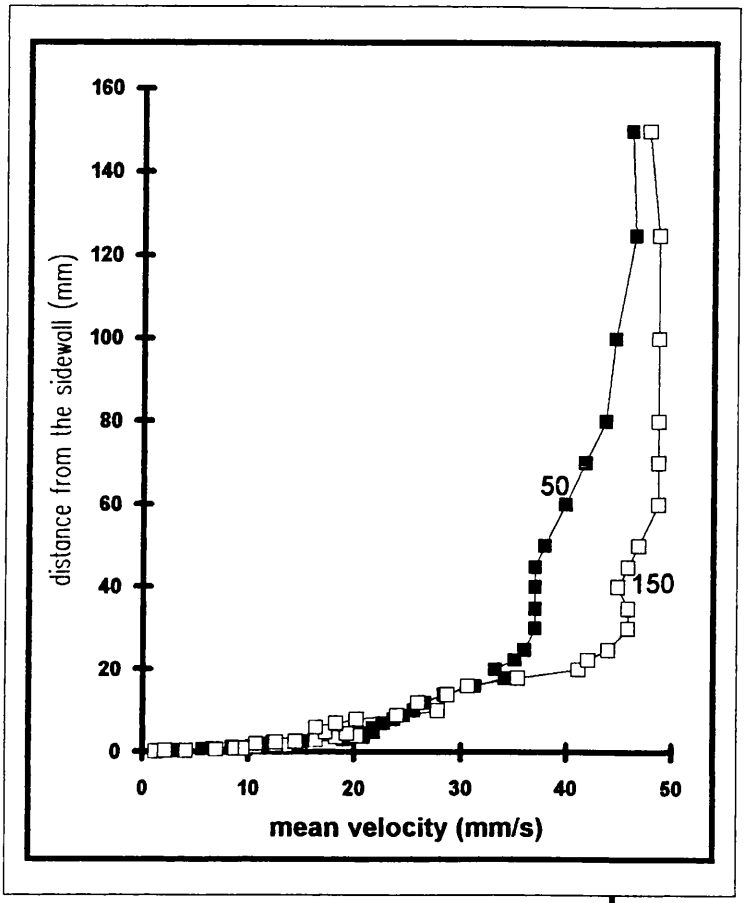

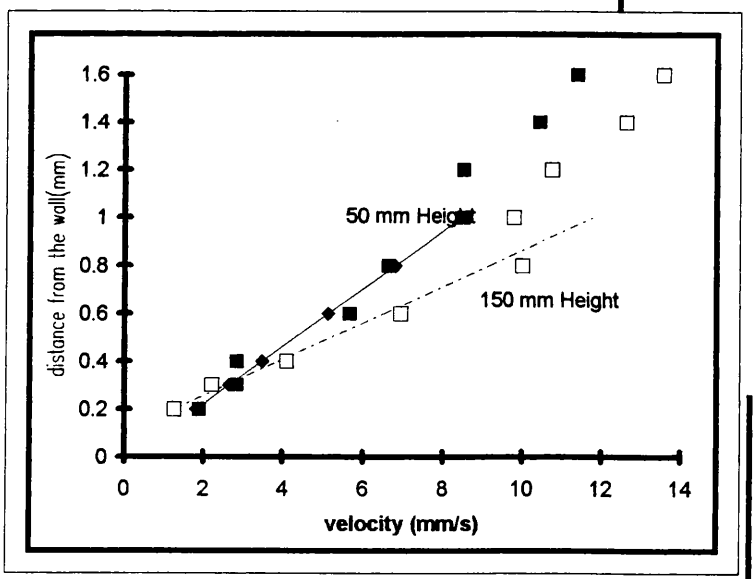

REFERENCES

Asano, T., Nakagowa, M., and Iwagaki, Y. (1986): Changes in Current Properties due to Wave Superimposing. J. Coastal Eng.: pp. 925-936.

Biesel, F. (1949): Calcul de l'amortissement d'une houle dans un liquide visquex de profondeur finie. La Houille Blanche, 4: pp. 630-634.

Brevik, I. (1981): Waves Superimposed on Currents, in Per Brunn (ed.), The Stability of Shores: Theory and Engineering. Elsevier, Amsterdam.

Brevik, I., and Aas, B. (1980): Flume Experiments on Waves and Currents I: Rippled Bed. Coastal Engineering, 3: pp. 149-177.

Brink-Kjaer, O., and Jonsson, I.G., (1976): Radiation Stress and Energy Flux in Waterwaves on a Shear Current. Prog. Rep. 36, Technical University of Denmark, pp. 27-32.

Carry, C. (1956): Cacul de lamoritssement d'une houle dans un liquide visqueux en profondeur finie. La Houille Blanche, 11: pp. 75-79.

Christoffersen, J.B., and Jonsson, I.G., (1985): Bed Friction and Dissipation in a Combined Current and Wave Motion. Ocean Engineering, 12: pp. 387-423.

Christoffersen, J.B. (1982): Current Depth Refraction of Dissipative Water Waves. Ph.D Thesis, Inst. Hydrodynamics, Technical University of Denmark.

Coffey, F.C., and Neilsen, P. (1986): The Influence of Waves on Current Profiles. Int. Proceedings of the 20th Conf. on Coastal Engineering. Taipei, ASCE, New York, pp. 82-96.

Collins., J.I. (1963): Inception of Turbulence at Bed Under Periodic Gravity Waves. Journal of Geophys. Res., Vol. 68, No. 21, pp. 6007 - 6014.

Davies, A.G., Soulsby, R.L., and King, H.L. (1988): A Numerical Model of the Combined Wave and Current Bottom Boundary Layer. J. Geophys. Res., 93: pp. 491-508.

Du Toit, C.G., and Sleath, J.F.A. (1981): Velocity Measurements Close to Rippled Beds in Oscillatory Flow. Journal of Fluid Mechanics, Vol. 112, pp. 71-96.

Fredsoe, J. (1984): The Turbulent Wave Boundary Layer Along a Vertical Wall. Prog. Rep. No. 61, I.H.H.E., Technical University of Denmark, pp. 21-33.

Grant, W.D., and Madsen, O.S. (1986): The Continental Shelf Bottom Boundary Layer. Ann. Rev. Fluid Mech., 18: 265-305.

Grant, W.D., and Mad sen, O.S. (1979): Combined Wave and Current Interaction with a Rough Bottom. J. Geophys. Res., 84: pp. 1797 - 1808.

Grosch, C.E. (1962): Laminar Boundary Layer Under a Wave. Phys. Fluids, 5: pp. 1163-1167.

Hino., M., Sawamoto, M. and Takasu, S. (1976): Experiment on Transition to Turbulence in an Oscillatory Pipe Flow. J. Fluid Mech. 75P: pp. 193-207.

Horikawa, K., and Watanabe, A. (1968): Laboratory Study on Oscillatory Boundary Layer Flow. Coastal Engineering Japan, Vol. 11, pp. 13-28.

Hunt, J. N. (1952): Viscous Damping of Waves over an Inclined Bed in a Channel of Finite Width. La Houille Blanche, 1952: pp. 836-842.

Isaacson, M. de St. Q. (1976): The Second Approximation to Mass Transport inCnoidal Waves. Journal of Fluid Mechanics, 78: pp 445 - 457.

Jensen, B.L.B., Sumer, M. and Fredsoe, J. (1988): Transition to Turbulence at High Reynolds Numbers in Oscillating Boundary Layer. Progress Report No. 66, Institute of Hydrodynamics and Hydraulic Engineering, Technical University of Denmark, Lyngby, pp. 3-15.

Jensson, R.J. (1989): Experimental and Theoretical Investigation in an Oscillatory Rough Turbulent Boundary Layer. Series Paper, No. 44. Inst. Hydrodynamic and Hydr. Eng. Technical University of Denmark, Lyngby, Denmark.

Jonsson, I.G. (1966): The Friction Factor for a Current with Superimposed Waves. Progress Report No. 11: Coastal Eng. Lab, Technical University of Denmark.

Jonsson, I.G., and Carlsen, N.A., (1976): Experimental and Theoretical Investigations in an Oscillatory Turbulent Boundary Layer. J. Hyd.. Res., 14: pp. 45-60.

Kamphuis, J.W. (1975): Friction Factors Under Oscillatory Waves. Proc. A.S.C.E. J. Waterways and Harbours Coastal Eng. Div., 101: pp. 135-144.

Kemp, P.H., and Simons, R.R. (1983): The Interaction of Waves and a Turbulent Current: Waves Propagating Against the Current. J. Fluid Mech., 130: pp. 73-89.

Kemp, P.H., and Simons, R.R. (1982): The Interaction Between Waves and a Turbulent Current: Waves Propagating with the Current. J. Fluid Mech., 116: pp. 227-

250.

Knight, D.W. (1981): Boundary shear in smooth and rough channels. Journal of the Hydraul. Div., Proc. ASCE, Vol. 107, No. HY7, July 1981.

Kyriacou, A. (1988): Wave Height Attenuation in the Presence of current. Ph.D. Thesis, University College London.

Lamb, H. (1932): Hydrodynamics. 6th ed. Cambridge, Cambridge University Press.

Lighthill, M.J. (1954): The Response of Laminar Skin Friction and Heat Transfer to Fluctuation in Stream Velocity. Proc. Royal Soc. Ser. A., 224: pp. 1-23.

Longuet-Higgins, M.S. (1953): Mass Transport in Water Waves. Phils. Trans. Roy. Soc., Ser. A, 245: pp. 63-84.

Myrhaug, D., and Slaattelid, O.H. (1990): A Rational Approach to Wave Current Friction Coefficient for Rough, Smooth and Transitional Turbulent Flow. Coastal Eng., 14: pp. 265-293.

Myrhaug, D., and Slaattelid, O.H. (1989): Combined Wave and Current Boundary Layer Model for Fixed Rough Seabeds. Ocean Eng., 162: pp. 119-142.

Myrhaug. D. (1989): A Rational Approach to Wave Friction Coefficients for Rough, Smooth and Transitional Turbulent Flow. Coastal Eng., 13: pp. 11-21.

Sarpkaya, T. (1955): Oscillatory Gravity Waves in Flowing Water. Trans. ASCE, 122: pp 564-.

Sheng, Y.P. (1986): Modelling Turbulent Bottom Boundary Layer Dynamics. Int. Proc. of the 20th Conf. on Coastal Eng. Taipei, pp. 1496-1508.

Simons, R.R., Grass, A.J., and Kyriacou, A. (1988): The Influence of Current on Wave Attenuation. Proc. 21st Int. Conf. Coastal Engineering, Spain.

Sleath, J.F.A. (1984): Sea Bed Mechanics. New York, NY: Wiley.

Sleath, J.F.A. (1970): Velocity Measurement Close to a Bed in a Wave Tank. Journal of Fluid Mechanics. Vol. 42, pp. 111-123.

Sleath, J.F.A. (1990): Seabed Boundary Layers. The Sea, Vol. 9, Part B. New York, NY: Wiley, pp. 693-726.

Sleath, J.F.A. (1968): The Effect of Waves on the Pressure in a Bed of Sand in a Water Channel and on the Velocity Distribution Above it. Ph.D. Thesis, Cambridge University.

Soulsby, R.L., Hamm, L., Klopman, G., Myrhaug, D., Simons, R.R., and Thomas,

G.P. (1993): Wave-current interaction within and outside the bottom boundary layer. Coastal Engineering, vol 21, pp 41-69

Stokes, G.G. (1851): On the Effect of the Internal Friction of Fluids on the Motion of Pendulums. Trans. Cambridge Philos. Soc., Vol. 9, pp. 20-21.

Tanaka, H. and Shuto, N. (1984): Friction Laws and Flow Regimes Under Wave and Current Motion. J. Hydraulic Res., 22: pp. 245-261.

Thomas, G.P., (1990): Wave-Current Interactions: An Experimental and Numerical Study. Part 2. Non-linear Waves. J. Fluid Mechanics, 216: pp. 506-536.

Thomas, G.P. (1981): Wave-Current Interaction: an Experimental and Numerical Study. Part 1, Linear Waves. J. Fluid Mechanics, 110: pp. 457-474.

Treloar, P.D., and Brebner, A. (1970): Energy Losses Under Wave Action. Proc. 10th Conference, Coastal Engineering, Chapter 16.

Van Dorn. W.G. (1966): Boundary Dissipation of Oscillatory Waves. Journal of Fluid Mechanics, 24: pp. 769-779.

Van Dorn, T. (1981): Experimental Investigation of the Near Bottom Velocities in Water Waves without and with a Current. Report M1423. Part 1, Delft Hyd. Lab.

Wang, C.Y. (1991): Exact Solution of the Steady State Navier-Stokes Equations. Ann. Rev. Fluid Mech., 23: pp. 150-173.

You, Z-J., Wilkinson, D.L., and Neilsen, P. (1991): Velocity Distributions of Waves and Currents in the Combined Flow. Coastal Engineering, 15: pp. 525-543.

Additional References

Cokelet (1977): Steep Gravity Waves in Water of Arbitrary Uniform Depth. Philos. Trans. Royal Society Ser. A. 286: 183-230

Dean (1970): Relative Validity of Water Wave Theories. Proc. A.S.C.E. J.waterw. Harbours Coastal Eng. Div. 96 (WW1): 105-119

Durst, F., Melling, A., and Whitelaw, J.H. (1976): Principles and Practice of Laser-Doppler Anemometry. London: Academic Press.

Hansen, J.B., Schiolten, P., and Svendsen, I.A. (1975): Laboratory Generation of Waves of Constant Form. Inst. of Hydrod. and Hydr. Eng. Tech. Univ. Denmark. Tech. Paper 9.

Hinze, J. (1975): Turbulence. 2nd Edition. New York: McGraw Hill.

Inman, D.L., and Bowen, A.J. (1963): Flume Experiments on Sand Transport by Waves and Currents. Proc. 8th Int. Conf. Coastal Engng., Mexico City, Vol. 2, Ch. 11, pp. 137-150.

Kajiura, K. (1968): A Model for the Bottom Boundary Layer in Water Waves. Bull. Earthquake Res. Inst., University of Tokyo, Vol. 46, pp. 75-123.

Le Mehaute, B. (1976): An Introduction to Hydrodynamics and Waves. Dusseldorf: Springer Verlag.

Longuet-Higgins, M.S. and Stewart, R.W. (1960): Changes in the Form of Short Gravity Waves on Long Waves and Tidal Currents. Journal of Fluid Mech., Vol. 8.

Machemehl, J.L., and Herbich, J.B. (1971): Non-steady Flow on Sloping Beach with Large Roughness Elements. IAHR Congress, Paris, Paper B22, 1971.

Madsen, O.S., Mei., C.C., and Savage, R.P. (1970): Evolution of Time Periodic Long Waves of Finite Amplitude. J. Fluid Mech., Vol. 44, Part 1.

Raven, P.W.J. (1977): Turbulent Boundary Layer Characteristics in Open Channel Flow over Fixed and Mobile Sand Beds. Ph.D. Thesis, University of London.

Shore Protection Manual (1984): US Army Coastal Engineering Research Centre, US Government Printing Office.

Stuart, R.J. (1984): Three Dimensional Characteristics of Coherent Flow Structures in a Turbulent Boundary Layer Over a Rough Surface. Ph.D. Thesis, University of London.

van Hoften, J.D.A., and Karaki, S. (1976): The Interaction of Gravity Waves and Turbulent Channel Flow. Tech. Rep., Dept. of Civil Eng., Colorado State University.